UNIVERSITY OF SOUTHAMPTON

FACULTY OF MEDICINE

Clinical and Experimental Sciences

NANOTOXICOLOGY:
Nanoparticle Interaction with Surfactant Proteins A and D

by

Zofi Amelia McKenzie

Thesis for the degree of Doctor of Philosophy

September 2013

UNIVERSITY OF SOUTHAMPTON

ABSTRACT

FACULTY OF YOUR MEDICINE

Thesis for the degree of Doctor of Philosophy

NANOTOXICOLOGY: NANOPARTICLE INTERACTION WITH SURFACTANT PROTEINS A AND D

Zofi Amelia McKenzie

Numerous epidemiological and toxicological studies have associated enhanced exposure to ambient air pollution with reduced resolution and increased incidence of respiratory infections. Surfactant Proteins A (SP-A) and SP-D are innate immune molecules within the lung and are important mediators in the resolution and clearance of microbial infections. They have also been implicated in the opsonisation and clearance of inorganic particulates *in vitro*. This study aimed to investigate the interaction of SP-A and SP-D with model 100nm unmodified (U-PS) and amine modified polystyrene (A-PS) nanoparticles. Firstly, it was hypothesised that the particle interaction with these proteins would alter particle clearance by macrophages and secondly that the sequestration of SP-A and SP-D by particles would result in a reduction in the anti-microbial function of these proteins. SP-A and SP-D were purified from the bronchoalveolar lavage fluid of subjects with alveolar proteinosis. Using absorption, turbidity, size and zeta potential measurements SP-A and SP-D were shown to interact with A-PS and U-PS particles and the extent of these interactions were dependent on the zeta potential of the particles. SP-A and SP-D altered the colloidal stability of the particles and this was related to the effect of each protein on the differential particle uptake by macrophages. *In vitro* influenza A virus (IAV) infection models were optimised using flow cytometry to detect surfactant protein mediated neutralisation of this virus at sub-maximal levels in cell lines representing cells found within the alveolus. These models were used to study the effect of U-PS and A-PS particles on surfactant protein mediated neutralisation of IAV. The results showed that nanoparticles can modulate *the vitro* function of SP-A and SP-D in a biphasic fashion in alveolar epithelial cells. However, this effect was dependent on a number of factors, including the particle, the protein and cell type under investigation. The identification of unlabelled lipids and nanoparticles *in vitro* by coherent anti-stokes raman scattering (CARS) was also be discussed.

Contents

List of tables

List of figures

DECLARATION OF AUTHORSHIP

I, Zofi Amelia McKenzie, declare that the thesis entitled

NANOTOXICOLOGY: Nanoparticle Interaction with Surfactant Proteins A and D

and the work presented in the thesis are both my own, and have been generated by me as the result of my own original research. I confirm that:

- this work was done mainly while in candidature for a research degree at this University;
- where any part of this thesis has previously been submitted for a degree or any other qualification at this University or any other institution, this has been clearly stated;
- where I have consulted the published work of others, this is always clearly attributed;
- where I have quoted from the work of others, the source is always given. With the exception of such quotations, this thesis is entirely my own work;
- I have acknowledged all main sources of help;
- where the thesis is based on work done by myself jointly with others, I have made clear exactly what was done by others and what I have contributed myself;
- parts of this work have been published as:

  Kendall, M. Ding, P. Mackay, R. M. Deb, R. McKenzie, Z. Kendall, K. Madsen, J. and Clark, H. *Surfactant protein D (SP-D) alters cellular uptake of particles and nanoparticles*. Nanotoxicology, 2013. 7(5): p. 963-73.

  McKenzie Z, Kendall M, Ding P, Townsend P, Mackay RM, Madsen J, and Clark HW. (2012) *Surfactant Protein D Interaction With Functionalised And Non-Functionalised Polystyrene Nanoparticles*. Am. J. Respir. Crit. Care Med. 185: A1992.

  Kotecha, S. Doull, I. Davies, P. McKenzie, Z. Madsen, J. Clark, H. and McGreal, E. (2013) *Functional heterogeneity of pulmonary surfactant protein-D in cystic fibrosis.* BBA - Molecular Basis of Disease. 1832(12): p2391-2400

Signed: ……..

Date:…….

Acknowledgements

This project was funded by the Medical Research Council through the Integrated Toxicology Training Partnership. I would like to thank Dr Andy Smith from the MRC for facilitating this scheme and providing excellent toxicology training throughout this degree.

I would like to thank my supervisor Howard Clark for his help and support. His guidance and encouragement during the last four years has proved to be invaluable. I would like to send a special note of thanks to Dr Jens Madsen, my supervisor, mentor and friend, for his tireless dedication, support and commitment to keeping the project and me on track. Without his guidance support, and proof reading this project would not have been possible.

I would also like to thank Dr Michaela Kendall for her help and advice during this project.

I thank Dr Jacqueline Pugh for her help and advice with the purification of viruses and for her assistance with the surfactant protein neutralisation assay. I would also like to thank her and Dr Rosie Mackay for their support, advice and friendship over the last four years.

I would like to thank Paul Townsend for providing SP-D and assistance with protein purification. I would like to thank Alastair Watson for his assistance with purifying and characterising surfactant proteins. I would also to acknowledge the help I received from Dr Mackay and Dr Madsen in the isolation of alveolar macrophages from mice.

I am thankful to Maurits de Planque for the use of his DLS and supplying the 200nm non fluorescent particles for the CARS study. I would also like to send my appreciation to Denny Jack for helping me in the clean room. I also

thank Dr Sumeet Mahajan for imaging and analysing the CARS samples in this project.

I would like to thank Mark Griffiths for supplying the BALF, Professor Terry Tetley and Andrew Thorley for the TT1 cells and Liku Tezera for the THP-1 cells.

I would like to thank Anton Page and Dave Johnson and the entire biomedical imaging unit for their continued assistance with electron and light microscopy. I would also like to thank Susan Wilson and Jon Ward from the histochemistry unit for their advice and Jane Warner for supplying conditioned medium.

I have spent countless hours in the FACS facility from which I would like to thank Richard Jewell and Carolann McGuire for their training, guidance and assistance in keeping the machines running.

I would like to thank Harry Whitwell and Katy Pike for helping me compile the thesis document.

On a personal note, I would like to thank the CFS service at the Royal Free Hospital for giving me the confidence to start a PhD in the first place.

Finally, I would like to thank my wonderful family. To my sisters, Zoe and Zara, who have always been there with support and encouragement: to my nephews, Douglas and Eddie, for managing to make me laugh whatever my mood: to my brother in law, Andrew, for his help and advice whenever I needed technical assistance with compiling this thesis; to my best friend Steph for always being there and finally to my parents, who have supported me financially, emotionally and sometimes physically through my various academic adventures I send my heartfelt appreciation and love.

Abbreviations

%NP+	percent nanoparticle positive
AKO	surfactant protein A knock out
ALRI	acute lower respiratory infection
AM	alveolar macrophages
ANOVA	analysis of variance
APC	allophycocyanin
A-PS	amine modified polystyrene
ARDS	acute respiratory distress syndrome
Asn	asparagine
Asp	aspartic acid
ATI	alveolar epithelial type I cell
ATII	alveolar epithelial type II cell
BAL	bronchoalveolar lavage
BALF	bronchoalveolar lavage fluid
BSA	bovine serum albumin
Ca	calcium
CARS	coherent anti-stokes raman scattering
CD	cluster of differentiation
CF	cystic fibrosis
CL	collectin
COPD	chronic obstructive pulmonary disorder
C-PS	carboxylated polystyrene
CRD	carbohydrate recognition domain
CV	column volume
Cys	cysteine
DCS	differential centrifugation sedimentation
DE	diesel exhaust

DEP	diesel exhaust particles
DKO	surfactant protein D knock out
DLS	dynamic light scatter
DMSO	dimethyl sulfoxide
DNA	deoxyribonucleic acid
DPPC	dipalmitoyl-phosphatidylcholine
E. coli	*Escherichia coli*
EDTA	ethylenediaminetetraacetic acid
ELISA	enzyme linked immunosorbent analysis
ENM	engineered nanomaterials
F protein	fusion glycoprotein
FACS	fluorescent activated cell sorting
FBS	foetal bovine serum
FFA	fluorescent focus assay
FFRA	fluorescent focus reduction assay
FFU	fluorescent foci units
FITC	fluorescein isothiocyanate
FSC	forward scatter
Glu	glutamic acid
Gly	glycine
GM-CSF	granulocyte-macrophage colony-stimulating factor
GNP	gold nanoparticle
GNR	gold nanorods
gp120	glycoprotein 120
HA	haemaglutinin
HAA	haemagglutination assay
HAI	haemagglutination inhibition
HAT	human airway trypsin-like protease
HAU	haemagglutination units

HI FBS	heat inactivated foetal bovine serum
HIA	haemagglutination inhibition assay
HIC	haemagglutination inhibitory concentration
HIV	human immunodeficiency virus
HRP	horse radish peroxidase
HRV	human rhinovirus
HSA	human serum albumin
IAV	influenza A virus
IC_{50}	inhibitory concentration causing a 50% reduction in infection
Ig	immunoglobulin
IL	interleukin
IP-10	interferon gamma induced protein-10
K. pneumonia	*Klebsiella pneumoniae*
kDa	kiloDalton
LAL	Limulus Amebocyte Lysate
LBP	lipopolysaccharide binding protein
LPS	lipopolysaccharide
LSD	least significant difference post hoc test
M. avium	*Mycobacterium avium*
M1/2	matrix protein 1/2
ManNAc	N-Acetyl-D-mannosamine
MBL	mannose-binding lectin
MDCK cells	Madin Darby canine kidney cells
Met	methionine
MFI	mean fluorescence intensity
mRNA	messenger ribonucleic acid
MTT	3-[4,5-dimethylthiazol-2-yl]-2,5 diphenyl tetrazolium bromide
MWCO	molecular weight cut off
MWM	molecular weight marker

NA	neuraminidase
NF κB	nuclear factor kappa B
nhSP-A	native human surfactant protein A
nhSP-D	native human surfactant protein D
NLRP3	nod like receptor 3
nm	nanometre
NP	nanoparticle
NS1/2	non-structural protein 1/2
NSCC	non small cell carcinoma
NSM	nano-sized material
NSP	nano-sized particle
OGP	n-octyl-B-D-glucopyranoside
PA	polymerase acid
PAP	pulmonary alveolar proteinosis
PB1/2	polymerase base protein 1/2
PBDM	peripheral blood derived monocytes
PBS	phosphate buffered saline
PDI	polydispersity index
PI	phosphidylcholine
PLGA	poly(lactic-co-glycolic acid)
PM	particulate matter
PM_{10}	particulate matter with aerodynamic diameter of ≤10μM
$PM_{2.5}$	particulate matter with aerodynamic diameter of ≤2.5μM
PMA	phorbol 12-myristate 13-acetate
Pro	proline
PS	polystyrene
pSP-D	porcine surfactant protein D
PVDF	polyvinylidene difluoride
RBC	red blood cells

RDS	respiratory distress syndrome
rfhSP-D	recombinant fragment of surfactant protein D
rLPS	rough lipopolysaccharide
RNA	ribonucleic acid
RPMI	Roswell Park Memorial Institute
RSP-A	rat surfactant protein A
RSV	respiratory syncytial virus
S. aureus	*Staphylococcus aureus*
S. pneumoniae	*Streptococcus pneumoniae*
SARS-CoV	severe acute respiratory syndrome coronavirus
SDS-PAGE	sodium dodecyl sulfate polyacrylamide gel electrophoresis
SF	serum free
sLPS	smooth lipopolysaccharide
SP-A	surfactant protein A
SP-A$^{-/-}$	surfactant protein A deficient
SP-D	surfactant protein D
SP-D$^{-/-}$	surfactant protein D deficient
SPIONS	supraparamagnetic iron nanoparticles
SSC	side scatter
TBS	tris buffered saline
TEM	transmission electron microscopy
Thr	threonine
TLR	toll like receptor
TMB	tetramethylbenzidine
TNF	tumour necrosis factor
TrPBS	0.3% triton in phosphate buffered saline
U-PS	unmodified polystyrene
UV	ultraviolet
VACV	Vaccinia virus

VARV	variola virus
VC	vehicle control
VD3	1,25-dihydroxyvitamin D3
vRNP	viral ribonucleoprotein
WT	wild type
ZP	zeta potential

Chapter 1: Introduction

Nanotoxicology is an evolving discipline aimed at identifying and attenuating the adverse effects of nano-sized materials (NSM). The need for this discipline has arisen due to the exponential rise in the manufacture and use of engineered nanomaterials (ENM) in the last decade. Nanotechnology is a rapidly developing and exciting area of scientific discovery with a vast array of possible applications and uses. These applications are summarised in Figure 1.1 and range from biomedical uses such as cancer diagnostics to using nanomaterials to decontaminate water and soil polluted with chemicals [1-3]. Forecasters predict that by 2015 the nanotechnology industry will be worth between US$1.1-2.5trillion and employ 2 million workers worldwide [4, 5]. There are now more than 1,300 products on the market which have been identified by their manufacturer as containing ENM. More than half of these marketed nano-products relate to health and fitness and there is also increasing interest in the use of nanomedicines for both diagnostic and therapeutic purposes [6]. However, the potential risk of these materials to consumers, workers and the environment is currently unclear.

Exposure to NSM is not a new phenomenon, throughout evolution humans have been exposed to nano-sized particles (NSP) from both biogenic and anthropogenic sources. However, over the last century the numbers of NSP that we are exposed to has risen dramatically due to anthropogenic emission sources such as diesel engines, power plants and other industrial processes [7]. Natural sources of NSM, including forest fires and volcanic eruptions, still contribute significantly to airborne NSM [8]. A European Scientific Committee on Emerging and Newly Identified Health Risks has stated that in every litre of air there are between 10^6 and 10^8 NSP [9]. As the average human airway processes eleven thousand litres of air every day this means that the airway is

exposed to around 10^{10} to 10^{12} NSP every single day. However, even this dose can be several times higher in those who are exposed to high NSP concentrations in the workplace [10, 11]. Inhaled particles deposit in the respiratory tract in a size dependent manner. Large 8-10μm particles deposit in the upper respiratory tract and are readily cleared by macrophages and the mucociliary escalator. However, particles with diameters of less than 1 μm can reach the alveolus of the lungs and may translocate throughout the organism [7, 12]. The lung is an attractive target site for drug delivery using nano-carriers for both pulmonary and systemic targets as it presents the largest surface area in the human body to come into direct contact with the environment and also has the potential to avoid first pass metabolism [13].

It is being increasingly accepted that the toxicity profile of NSM will be dependent on how they interact with biological molecules such as proteins and lipids and the affect that this interaction has on both particle toxicity and protein function. This thesis aims to study the interaction of model nanoparticles with two proteins, found primarily in the lung, that are responsible for maintaining a clean and sterile environment within the alveolar space. Furthermore, this thesis will examine how this interaction affects the ability of these proteins to neutralise viral challenge.

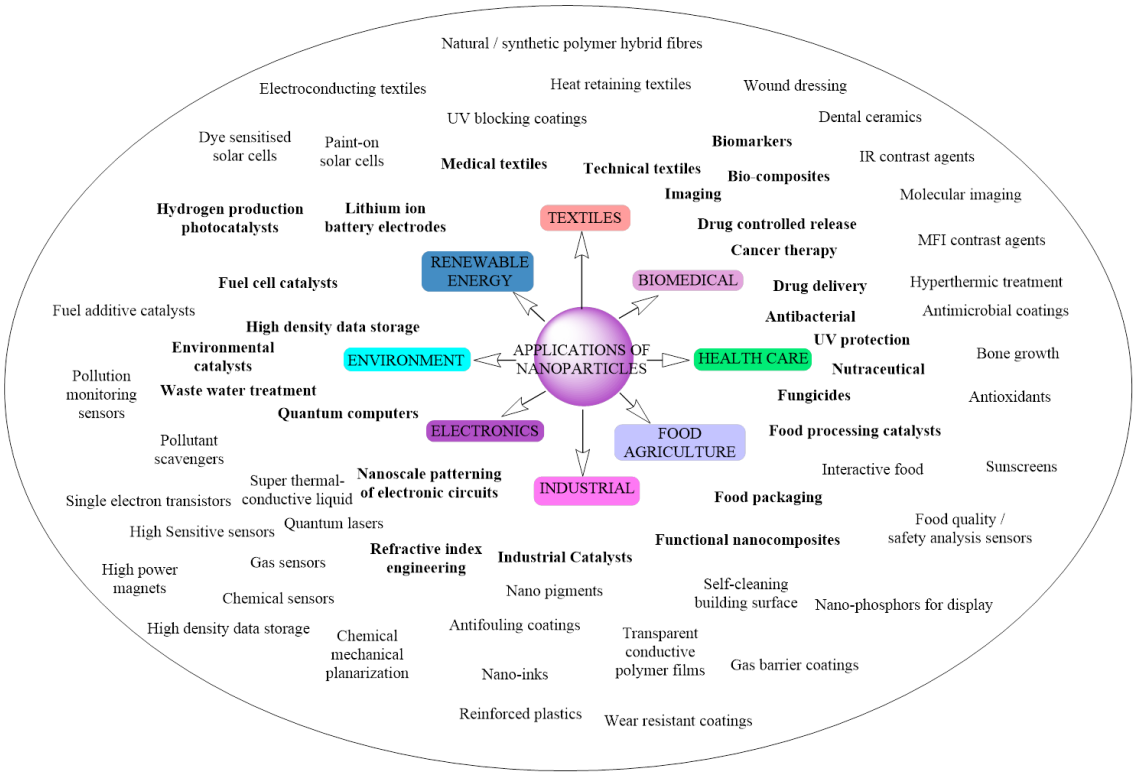

Figure 1.1: Applications of nanoparticles. Adapted from [14].

1.1. The alveolus

The human lung has an internal surface area of approximately 140m^2 with more than 95% of the surface area comprising of the alveolar epithelium [15, 16]. There are two types of alveolar epithelial cells; type I (ATI) and type II (ATII) epithelial cells. ATI cells are large thin squamous cells that comprise 94% of the alveolar surface area but only a third of the number of alveolar epithelial cells [16]. Although conventionally considered to be biologically inactive, simply providing the large surface area of the air-blood barrier required to facilitate gas exchange, recent evidence points to a role in maintaining lung liquid homeostasis [17]. ATI cells have been shown to be highly permeable to water and to play an important role in the high permeability to water between the airspace and the blood vessels in the alveolus [18]. Moreover, ATI cells have also been shown to actively transport ions and secrete factors that protect the alveolus from oxidant induced injury [19, 20]. The main function of ATII cells is

the generation, recycling and processing of pulmonary surfactant (see section 1.2). However, they are also involved in ion transport and act as progenitor cells to replace ATI cells following death or injury [21-23].

1.2. Pulmonary Surfactant

Pulmonary surfactant, produced by ATII cells, is a lipoprotein substance which lines the alveolar epithelium at the air liquid interface [24, 25]. Pulmonary surfactant performs two vital functions in the lung; reducing alveolar surface tension after exhalation and protecting the lung from microbial infection [26]. Four surfactant proteins (SP) have been identified and comprise 10% by weight of pulmonary surfactant. SP-B and SP-C are small lipophilic proteins, which are highly associated with surfactant lipids and are integral to maintaining surface tension within the alveolus [25]. SP-A and D are relatively hydrophilic proteins and belong to a c type (calcium dependent) lectin subfamily known as the collectins.

1.3. Collectins

Nine collectins have thus far been identified; these are mannose-binding lectin (MBL), conglutinin, surfactant protein A (SP-A), SP-D, collectin of 43kDa (CL-43), collectin of 46kDa (CL-46), collectin liver (CL-L1), collectin placenta (CL-P1), and collectin kidney (CL-K1 or CL-11) [27]. CL-P1 is unique among the identified collectins in that it is a transmembrane protein [28]. Conglutinin, CL-43 and CL-46 are only expressed in species within the *Bovidae* family[29, 30].

1.3.1. Collectin structure

Collectin monomers are characterised by their four structural domains; an amino terminus, a collagenous domain, a neck region and carbohydrate recognition domain (CRD). The collagenous domain is composed of repeated

Gly-Xaa-Yaa triplets where Xaa and Yaa represent any amino acids. The structure and assembly of SP-A and SP-D monomers and multimers are shown in Figure 1.2. Collectin trimers are generated through the formation of a triple coiled coil of the neck region of three monomers which mediates the formation of a collagen triple helix and disulphide bridges between the amino termini [31, 32]. The amino termini of the trimers then oligomerise to form cruciform shaped dodecamers (i.e. four trimers) and bouquet like octadecamers (i.e. six trimers) for SP-D and SP-A respectively [33]. SP-D can also form higher order oligomers called stellate multimers consisting of several dodecamers orientated in a wheel formation as shown Figure 1.2. The recombinant fragment of human SP-D (rfhSP-D) which has been used in this study contains a CRD, neck, and truncated collagenous domain containing eight Gly-Xaa-Yaa triplets. This rfhSP-D is unable to form the collagen triple helix or oligomerise to form supramultimeric structures [31, 34-36].

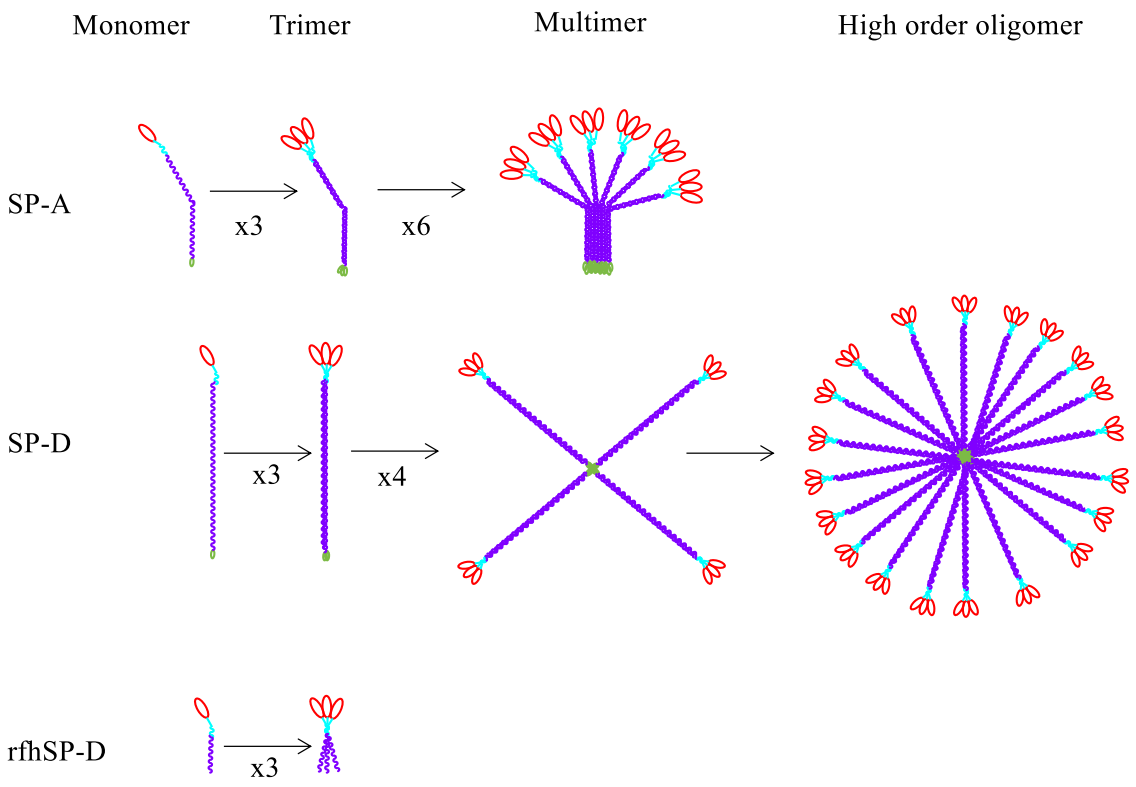

Figure 1.2: Structure and assembly of SP-A, SP-D and rfhSP-D. Collectin monomers consist of four structural domains; the carbohydrate recognition domain (red), alpha coiled neck region (blue), collagenous domain (purple) and amino terminus (green). The oligomerisation of SP-A trimers results in the formation of octadecamers. SP-D trimers oligomerise to form dodecamers and higher order oligomers such as stellate multimers. rfhSP-D trimers are unable to form supratrimeric oligomers [33, 35]. Not to scale.

1.3.1.1 Carbohydrate recognition domain

The carbohydrate recognition domain (CRD) of collectins contains four highly conserved cysteine residues which act to stabilise the globular structure of the CRD through the formation of two disulphide bridges (shown in yellow in Figure 1.3). The main structural CRD differences between SP-A and SP-D are the calcium binding sites, surface loops and electrostatic charge (see Figure 1.3).

The SP-D CRD contains a high affinity calcium binding or "primary" site and two auxiliary calcium sites. The auxiliary calcium binding sites are situated 8Å and 12Å from the primary site. At concentrations of calcium greater than 2mM a calcium ion situates within the trimeric axis and results in conformational changes in Glu232 residue and thereby alters the charge

distributions across the CRD surface. Crystallisation of the structure of rat SP-A shows one calcium bound to the primary site [37]. This means that for each trimeric subunit SP-D contains 10 calcium ions whereas SP-A contains 3 calcium ions. The structure of native human SP-A (nhSP-A) and nhSP-D have not been crystallised therefore the calcium sites in the CRD of rfhSP-D and rat SP-A are shown in Figure 1.3. The angle between the CRD and neck region is almost perpendicular in SP-A whereas in SP-D this angle is much greater (T versus Y orientations) [37]. Previous studies have indicated that the CRD domain of SP-A is much more hydrophobic than that of SP-D [37]; however, models of the electrostatic surface charges reveal that both proteins contain a large positively charged area within the cleft of the CRD (see Figure 1.3B).

Collectin carbohydrate recognition domains have different carbohydrate specificities depending on the collectin and species [38]. Collectins bind with greater affinity to the microbial associated ligands such as mannose and glucose compared to galactose or fructose which are more common in higher order species. SP-A and SP-D recognise equatorial 3′ and 4′ hydroxyl groups on polysaccharides [39]. Differences in the glycosylation patterns on microbial surfaces allows the collectins to distinguish self from non-self. Variations in the specificities and affinities of native human SP-A (nhSP-A) and nhSP-D to different carbohydrate residues widens the number of microbial targets for these two innate immune molecules. The relative carbohydrate specificities of nhSP-A and nhSP-D have been determined using mannan binding competition assays. For nhSP-A these were N-acetyl-mannosamine > L-fucose, maltose > glucose > mannose. Galactose, D-fucose, glucosamine, mannosamine, galactosamine, N-acetyl-glucosamine, and N-acetyl-galactosamine did not inhibit mannan binding to nhSP-A [40]. For nhSP-D the inhibitory potencies of carbohydrates were determined to be N-acetyl-mannosamine > maltose > glucose > mannose > myo-inositol > galactose > N-acetyl-glucosamine [41, 42]

The CRD of nhSP-A contains a partially sialylated asp at position 187 which plays an important role in the ability of SP-A to neutralise certain microbial pathogens such as influenza virus. Porcine SP-D (pSP-D) contains a terminal sialic acid residue in the CRD which is not present in SP-D from other species; pSP-D has been shown to have enhanced haemagglutination inhibition compared to human or rat SP-D against β sensitive influenza A strains [42].

1.3.1.2 Neck region

Trimerisation of SP-A and SP-D is mediated at the α helical coiled coil neck region [43]. The neck region of SP-A and SP-D contain heptad repeats with hydrophobic residues at positions a and d. The crystal structure of the neck region of rfhSP-D shows that that it makes eight helical turns [44]. Binding and crystallographic studies have suggested that SP-A contains an addition calcium binding site in an anionic section of the neck region [37]. This anionic patch is clearly evident on the electrostatic diagram of the neck and CRD region of SP-A (see Figure 1.3C)

1.3.1.3 Collagenous domain

The collagenous domain of nhSP-A consists of 23 Glycine-Xaa-Yaa triplets. A sequence disruption containing the Pro-Cys-Pro-Pro motif between the 13th and 14th triplet results in a disruption or bend in the tertiary structure of the collagen triple helix. The cysteine residue has been implicated in the formation of disulphide bridges between SP-A units and the stabilisation of the trimeric units [45]. The collagenous domain of SP-D is comprised of 59 uninterrupted Gly-X-Y triplets [46]. The collagenous domains of native SP-A and SP-D are rich in hydroxyproline residues, which are important in the stabilisation of the collagen triple helix. The collagenous domain of SP-D also contains 6 hydroxylated lysine residues which are potential sites for O-glycosylation [47]. Moreover, SP-D contains a site for N-linked glycosylation at Asn70 situated in

the collagenous domain [48]. This Asn-Gly-Ser glycosylation site is conserved across all SP-D characterised to date including porcine, human, rat and bovine SP-D [31]. In contrast to other collectins the collagenous domain of SP-A does not contain hydroxylated lysine residues [49-51].

1.3.1.4 Amino terminus

Two cysteine residues at positions 15 and 20 are contained within the SP-D amino terminus whereas SP-A contains one cysteine residue at position 6 of the mature protein. The cysteine residues within the SP-A and SP-D terminus have been shown to play vital roles in the formation of supratrimeric oligomers, when the SP-D cysteine residues at positions 15 and 20 are mutated or nitrosylated SP-D is expressed solely as trimeric subunits [52-54].

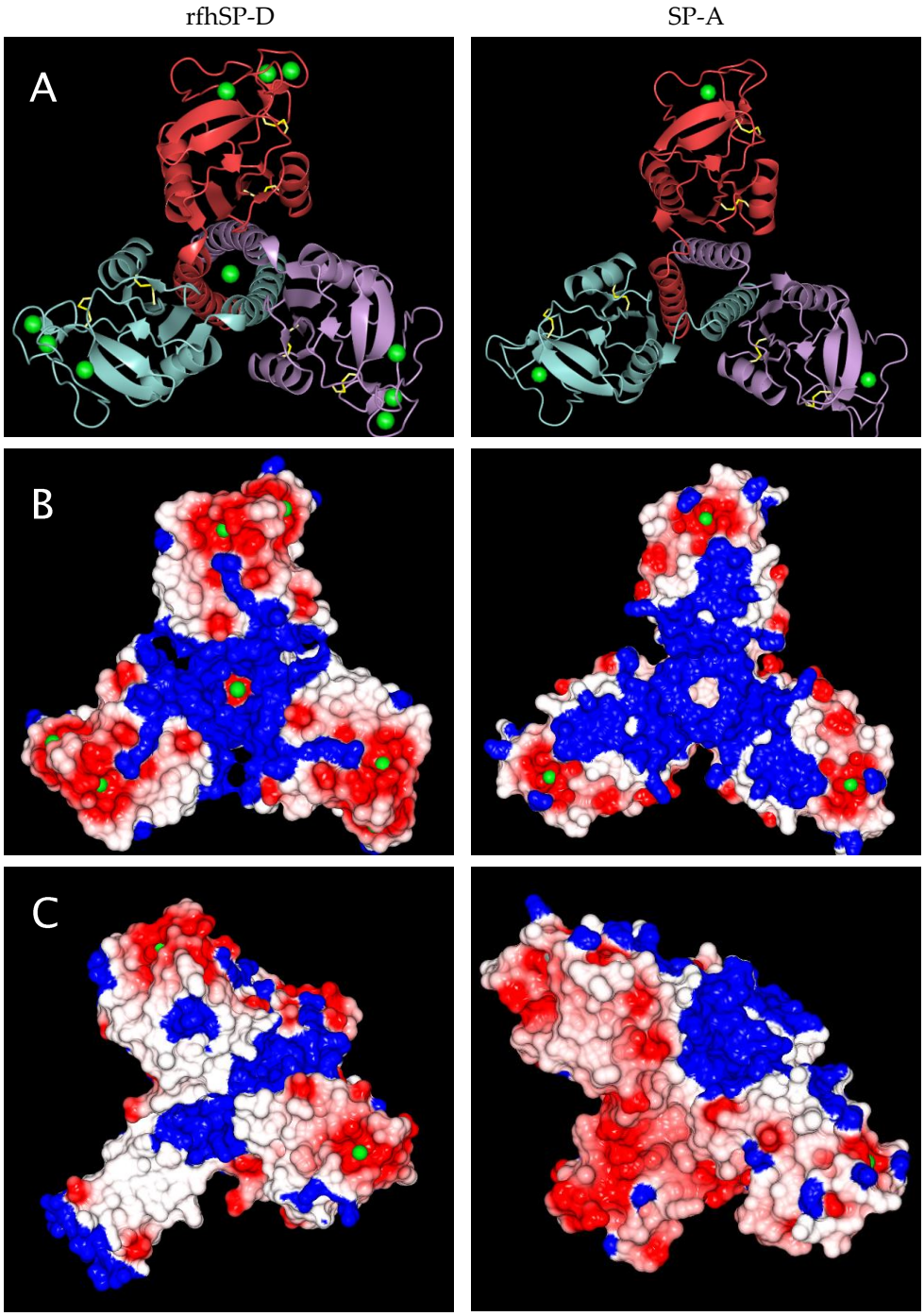

Figure 1.3: Electrostatic potentials and structure of a recombinant fragment of human SP-D and a neck CRD fragment of rat SP-A. (**A**) Ribbon diagrams of the CRD of rfhSP-D (left panel) and rat SP-A (right panel). Calcium ions are shown as green spheres and disulphide bridges are coloured yellow. Each monomeric subunit is coloured separately. (**B**) Electrostatic potentials of the CRD and (**C**) CRD, neck and collagen domain of rfhSP-D and rat SP-A. Positive charges are shown in blue and negative charges in red. Calcium ions are coloured green. Pictures created using RasMol software with 3PAQ and 1PW9 PDB files for SP-A and rfhSP-D respectively.

1.3.2. Genetics of SP-A and SP-D

SP-A and SP-D genes are clustered on the long arm of chromosome 10q22-23 [55]. The SP-A locus consists of two functional genes (SP-A1 and SP-A2) flanking a non-functional pseudogene [56]. More than 30 variants of SP-A1 and SP-A2 have been described with four SP-A1 alleles and six SP-A2 alleles reported to occur in more than 1% of the population (i.e. polymorphic) [57]. The major differences between SP-A1 and SP-A2 are located at residues 46, 53, 61 and 65 corresponding to the 13th, 14th, 17th and 18th Gly-Xaa-Yaa triplet of the collagen like domain. SP-A1 contains a cysteine residue at position 65, which may account for the enhanced thermal stability of SP-A1 compared to SP-A2 [58]. Originally, it was suggested that SP-A consisted of heterotrimeric units constructed of two SP-A1 and one SP-A2 monomeric subunits [59]. However, more recent evidence suggests that the proportions of SP-A1 and SP-A2 are determined by a number of factors including existing pulmonary disorders, age and changes to the lung microenvironment [51, 60]. SP-A2 has been shown to bind a wider variety of carbohydrate moieties with greater affinity than SP-A1 [61]. Both SP-A1 and SP-A2 are able to bind rough LPS however, only the latter induces LPS aggregation [62]. SP-A2 has also been shown to have a greater opsonic effect on *Pseudomonas aeruginosa* than SP-A1 [63]. The reasons for the enhanced activity of the SP-A2 gene product remain unclear.

Three polymorphisms in the SP-D gene have been identified at residues 11 (Met^{11}Thr), 160 (Ala^{160}Thr), and 270 (Ser^{270}Thr). The Met^{11}Thr residue is situated within the amino terminus of SP-D and Thr/Thr11 variants result in a loss of supratrimerisation of the native protein. The polymorphisms at the other sites do not alter the supratrimeric structure of the protein [64].

1.3.3. SP-A and SP-D extrapulmonary expression

SP-A and SP-D are mainly located on the luminal surface of the pulmonary epithelium; however, both proteins have been localised to a number of extrapulmonary sites. SP-A has been found in the submucosal gland of human nasal mucosa, in skin, in the intestinal epithelium and vaginal epithelium [65-68]. SP-A mRNA expression has also been detected at various extrapulmonary sites including the prostate and pancreas [66]. SP-D mRNA is expressed in a number of sites including the trachea, brain, testis, salivary gland, intestine, placenta, prostate, kidney and pancreas. SP-D protein expression has also been localised to exocrine salivary and sweat glands as well as the ductiles of the pancreas and small bile. Moreover, SP-D has been localised within epithelial cells in skin, the oesophagus, uterus bladder, kidney collecting ducts, nasal mucosa and urinary bladder [68-70]. SP-D has also been localised to the cervix, vagina, uterus and oviduct of the murine and human genitourinary tract [70, 71].

1.3.4. SP-A and SP-D in Health and Disease

The pulmonary collectins play an integral role in the innate immune defence of the lung; they are pattern recognition molecules and are able to protect the lung from infection through a variety of mechanisms. They recognise and bind specific carbohydrate moieties on the surface of micro-organisms and can act to neutralise microbial challenge through their agglutination and opsonisation [34, 72-74]. The multifaceted functions of SP-A and SP-D are outlined below.

1.3.4.1 SP-A and SP-D in viral infections

Surfactant Proteins A and D have been shown to mediate the neutralisation and/or opsonisation of a number of viruses. The most

characterised are the interactions of SP-A and SP-D with influenza A virus and respiratory syncytial virus. The surfactant protein mediated neutralisation of IAV is described in detail in section 1.4.3.

1.3.4.1.1. Respiratory Syncytial Virus

Respiratory syncytial virus (RSV) belongs to the paramyxoviridae family of viruses and is an enveloped negative sense RNA virus. RSV contains two surface glycoproteins called the fusion (F) and G glycoproteins [75]. RSV has been reported to infect up to 80% of children in first year of life and is the most common cause of severe respiratory disorders in infants [76]. Approximately 70% of acute bronchiolitis cases are caused by RSV and it accounts for a significant proportion of infant hospitalisations [77, 78].

SP-A and SP-D have been shown to bind to the G protein of RSV in a calcium dependent manner [79, 80]. SP-A has also been shown to bind to the F protein of RSV; however, in this study SP-A and SP-D did not bind to RSV G protein [81]. SP-A and a recombinant form of SP-D have been shown to be able inhibit RSV infection both *in vitro* and *in vivo* [80-82]. Both collectins have been shown to be opsonins for RSV. SP-A enhances RSV uptake by peripheral blood monocytes (PBMC) and the U937 macrophage cell line, whereas SP-D has been shown to enhance RSV uptake by alveolar macrophages and neutrophils [79]. The reduced phagocytosis of RSV by the alveolar macrophages of SP-D$^{-/-}$ compared to wild type mice has also been reported [83].

SP-A and SP-D increase the generation of oxygen radicals by phagocytes infected with RSV. Moreover, infiltration of polymorphonuclear leukocytes were elevated in both SP-A and SP-D deficient mice following RSV infection compared to wild type controls [82, 83]. High serum levels of SP-D have been shown to be a biomarker of lung injury during RSV induced bronchiolitis [84]. Reduced levels of lung SP-A and SP-D in infants have also been associated with

severe RSV infection and polymorphisms in SP-A and SP-D have been linked to enhanced susceptibility to RSV infections [85-87].

1.3.4.1.2. Human Immunodeficiency Virus

The identification of SP-A and SP-D in vaginal fluid and the female genitourinary tract has led to investigations into the immunomodulatory role of these collectins in sexually transmitted infections such as human immunodeficiency virus (HIV). SP-A and SP-D bind in a calcium dependent manner to gp120, the glycosylated envelope protein on HIV [88-90]. The binding of SP-D to gp120 has been shown to be dependent on gp120 glycosylation [90]. SP-A and SP-D inhibit the direct infection of CD4+ T cells by inhibiting the interaction of gp120 with CD4. However, they also enhance the phagocytosis of HIV by immature dendritic cells thereby increasing DC transfer of HIV to CD4+ T cells. This implies that SP-A and SP-D have dual immunomodulatory roles in HIV infection [88]. Moreover, SP-A levels in the lungs are elevated in individuals with HIV which has been shown to enhance the susceptibility of HIV infected individuals to Mycobacterium tuberculosis through increasing the attachment of this bacterium to alveolar macrophages [91, 92]

1.3.4.1.3. Other viruses

SP-D has been shown to bind human rhinovirus (HRV) and this binding was shown to be calcium dependent and inhibited in the presence of saccharide ligands. However, SP-A did not bind to HRV in this study and the effect of SP-D on HRV infections remains unclear [93]. SP-D has also been shown to bind and inhibit the infection of Vaccinia virus (VACV), a prototype for the variola virus (VARV) which is the causative agent of smallpox [94]. SP-D binds to the glycosylated protein (S protein) on the surface of severe acute respiratory

syndrome coronavirus (SARS-CoV) in a calcium dependent manner [95]. SP-A has also been shown to be an opsonin for herpes simplex virus [96].

1.3.4.2 SP-A and SP-D in bacterial infections

The bacterial ligand lipopolysaccharide (LPS) on the surface of gram negative bacteria is a potent inducer of inflammatory mediators such as tumour necrosis factor alpha (TNFα), interleukin (IL) 1α, IL-1β, IL-6, IL-8 and IL-10 [97, 98]. The over-expression of these cytokines, especially TNFα, has been linked with the pathogenesis of many diseases including acute respiratory distress syndrome (ARDS) and sepsis [99]. There are two forms of LPS; smooth (s) LPS contains an o antigen, core oligosaccharides and lipid A component; whereas rough (r) LPS lacks the o antigen and part of the core oligosaccharide domain (see Figure 1.4). The interaction of LPS with the CD14 receptor on monocyte derived cells is an essential part of the cell response to LPS [100]. LPS binding protein (LBP) binds LPS and triggers LPS interaction with the CD14 receptor; this results in the homodimerisation of toll like receptor (TLR) 4, the formation of MD2-TLR4 complexes and the activation of the NF-κB signalling pathway. Both SP-A and SP-D have been shown to modulate LPS stimulation of macrophage like cells through modulation of this CD14-LPS interaction. However, the mechanism and effects of these collectins on LPS stimulation differ (see Figure 1.5). SP-A binds to the lipid A component and SP-D binds to the core oligosaccharides of rLPS through their CRD and this interaction is dependent on the lectin activity of these proteins as the interactions are inhibited by the presence of mannose or EDTA [34, 101-103]. These collectins are unable to bind to these components of sLPS due to the presence of o antigen. SP-D binds to CD14 through its CRD and therefore prevents LPS binding to this membrane receptor. SP-A binding to the CD14 receptor is not lectin dependent and occurs through the neck region. Although SP-A inhibits the binding of sLPS to CD14, the formation of CD14-SP-A-rLPS complexes may

enhance the cellular response to rLPS [101, 104]. However, this latter point has been disputed in some papers [105, 106].

The extent of SP-D binding to bacterial LPS has been shown to influence the aggregation of bacteria. SP-D induced gross macroscopic aggregation of rLPS containing bacteria; whereas SP-D only induced microscopic aggregation of bacteria with smooth LPS [107, 108]. SP-D also enhances the uptake and killing of bacteria by providing a bridge between collectin receptors on the surface of these cells and bacterial ligands. rfhSP-D has also been shown to enhance uptake of the gram negative *Haemophilus influenzae* bacteria by macrophages [109].

These collectins can also bind to and activate macrophages, independent of microbial binding, resulting in enhanced phagocytosis and reactive oxygen species mediated destruction of micro-organisms [110]. SP-A and SP-D have been shown to permeabilise gram negative bacteria membranes and this permeability was dependent on the presence of rLPS in the bacterial membrane [111-113]. SP-A and SP-D have also been shown to bind in a calcium dependent manner to *Mycobacterium avium* and this binding resulted in a reduction in the metabolic rate of the mycobacteria. SP-D was also shown to aggregate and opsonise *M. avium* by macrophages [114].

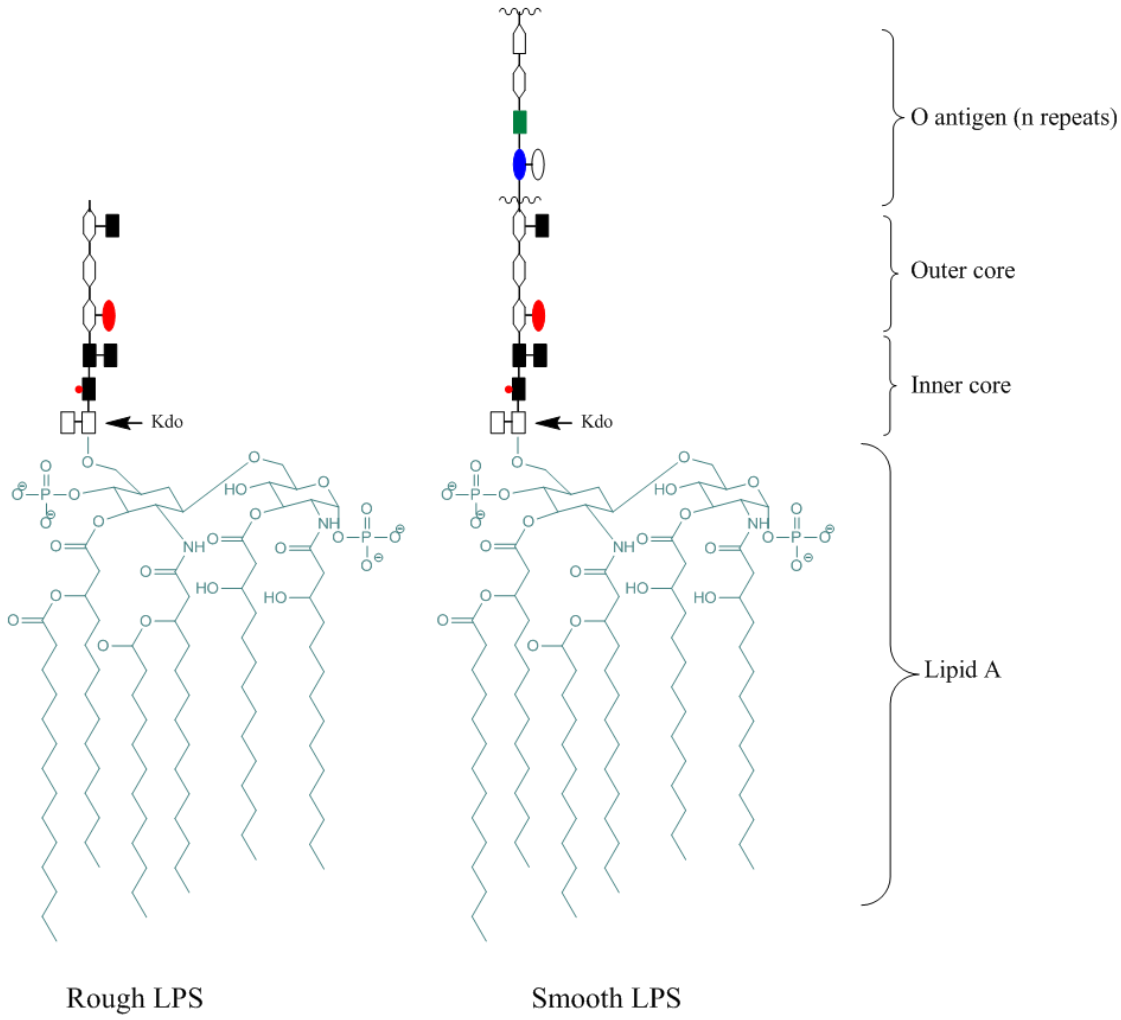

Figure 1.4: Structure of rough and smooth LPS. Smooth LPS consists of repeating units of o antigen, core oligosaccharides (outer and inner core) and lipid A (endotoxin) components. Rough LPS lacks the o antigen domain and Ra Rb, Rc, Rd, and Re mutants contain progressively shorter core oligosaccharide domains. The core oligosaccharides are non-repeating oligosaccharide units which differ between LPS subtypes except for the Kdo (2-keto-3-deoxyoctulosonic acid) residue which is conserved across all identified LPS subtypes. Figure adapted from [115, 116] and drawn using ChemDraw v12.

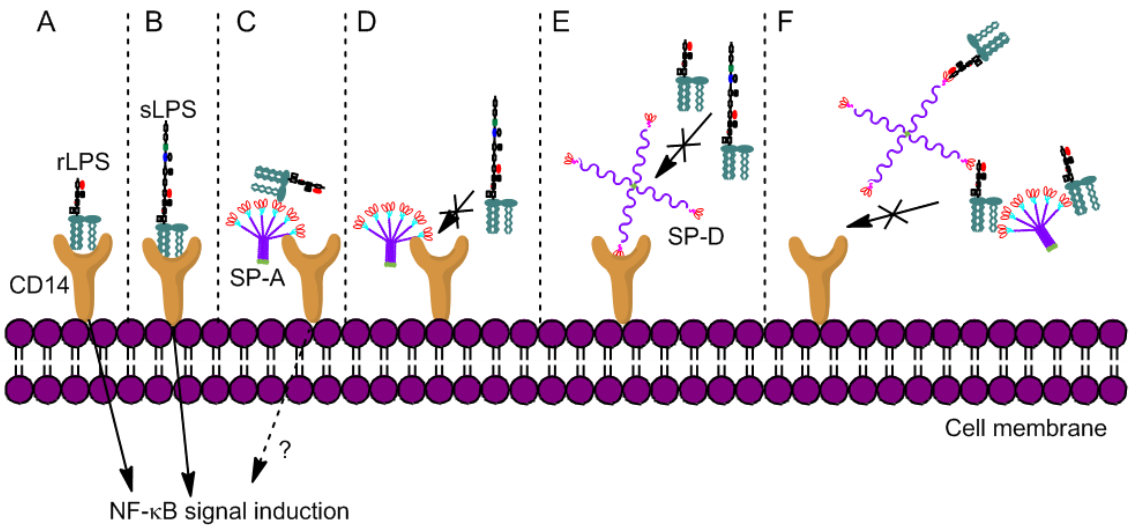

Figure 1.5: SP-A and SP-D modulate the interaction of sLPS and rLPS with CD14; Interaction of **A**. rough LPS (rLPS) and **B**. smooth LPS (sLPS) with CD14 receptor results in the activation of the NF-κB signalling. **C.** Formation of SP-A –CD14-rLPS complex may result in NF-κB signalling. **D**. SP-A association with CD14 prevents sLPS binding to this receptor. **E.** SP-D interacts with CD14 via its CRD region preventing the association of both types of LPS with CD14**. F**. SP-A and SP-D may also bind to rLPS, resulting in LPS aggregation and preventing rLPS association with CD14. Adapted from [101, 104]

1.3.4.3 SP-A and SP-D in the allergic response

SP-A and SP-D have been shown to protect against allergic challenge through a variety of mechanisms. In mice, SP-A and SP-D have been shown to supress allergen specific IgE production, reduce eosinophilia, and result in a shift from a Th2 response towards a Th1 response [117, 118]. SP-D deficient mice demonstrated an exacerbated allergic response and this response was attenuated with the administration of exogenous SP-D [119]. Moreover, in wild type mice and rats allergic sensitisation with ovalbumin has been associated with an increase in the expression of SP-A and SP-D [119-121]. Interestingly, in humans allergen challenge has been shown to result in SP-D cross-linking and perturb the supratrimeric structure of SP-D. In asthmatics the formation of this cross-linked SP-D was shown to enhance the pro-inflammatory response to allergen challenge [122]. Moreover, exogenous SP-D has been reported to enhance the apoptosis and clearance of eosinophil from allergic but not healthy individuals [123].

SP-D has been shown to aggregate and opsonise pollen-allergen granules. This effect was dependent on calcium and the supratrimeric structure of the protein [124]. Although the opsonisation and aggregation of allergen is dependent on the supratrimeric SP-D structure, rfhSP-D has been shown to reduce the Th2 response, reduce eosinophilia and reduce nitric oxide production by alveolar macrophages from sensitised wild type mice [125]. The Thr^{11}Thr SP-D polymorphism has been associated in a Chinese population with the development of allergic rhinitis [126]. Single nucleotide polymorphisms in SP-A2 have also been associated with allergic bronchopulmonary aspergillosis and bronchial asthma with rhinitis [127].

1.3.4.4 SP-A and SP-D in apoptotic cell clearance

During apoptosis DNA fragments and is presented on the cell surface. SP-A and SP-D have been shown to bind DNA and RNA through both their CRD and collagenous domain. The CRD mediated binding to nucleic acids was shown to be calcium dependent [128, 129]. SP-A and SP-D can both enhance apoptotic cell clearance *in vitro* however, *in vivo* only SP-D has been shown to enhance apoptotic cell phagocytosis [130, 131].

1.3.4.5 SP-A and SP-D in surfactant homeostasis and structure

The importance of SP-D in the homeostasis of pulmonary surfactant became strikingly evident following the characterisation of the phenotype of the SP-D deficient mouse. SP-D null mice develop a progressive emphysema like phenotype characterised by an accumulation of surfactant phospholipids, inflammation, hyperplastic ATII cells containing enlarged laminar bodies, and increased numbers of alveolar macrophages. By 24 weeks of age SP-D$^{-/-}$ mice have a 10 fold increase in the number of alveolar macrophages compared to their wild type counterparts, a high proportion of these macrophages being

foamy in appearance [132]. The administration of a recombinant fragment of SP-D containing a truncated collagenous domain can partially correct this emphysema like phenotype, this correction is dependent on the truncated collagenous domain as a SP-D fragment lacking this region does not correct morphological changes [133, 134].

Laminar bodies are specialised organelles in ATII cells in which pulmonary surfactant is packaged and stored before excretion by exocytosis [135, 136]. The secretion of laminar bodies from ATII cells into the alveolar space results in the formation of tubular myelin, a highly organised square lattice of surfactant lipids. SP-A has been shown to be important in the formation of these surface active structures and has been co-localised to the corners of the tubular myelin lattice [137]. SP-A deficient mice have been shown to have normal pulmonary function and surfactant homeostasis but are unable to form tubular myelin structures [138].

1.3.4.6 SP-A and SP-D in disease

Polymorphisms and aberrant levels of SP-A or SP-D have been linked to the pathogenesis of a number of diseases. However, no disease has yet been identified to directly result from a deficiency or mutation of either protein. Damage to the alveolar epithelium can lead to increased translocation of SP-A and SP-D into the systemic circulation [139]. This can lead to enhanced levels of surfactant proteins in serum and a concomitant reduction of the protein within the alveolar air space. Enhanced SP-A and/or SP-D serum concentrations have been shown to be predicative biomarkers for lung injury from a number of diseases and causes. Increased serum concentrations of SP-A have been associated with lung injury from smoking, COPD, pulmonary thromboembolism, and acute respiratory distress syndrome [140, 141]. Enhanced serum SP-D has been reported to be associated with idiopathic

pulmonary fibrosis, interstitial pneumonia, pulmonary alveolar proteinosis and cystic fibrosis. Increased serum SP-D in these disorders negatively correlate with disease severity and/or lung function [142-144]. Enhanced SP-A and SP-D levels have been shown to correlate with the incidence and severity of paediatric interstitial lung disease, idiopathic pulmonary fibrosis, and COPD [145-150]. Reduced SP-A and SP-D has also been reported in the BALF of smokers compared to non-smokers [151, 152]. In one study, both SP-A and SP-D expression was lower in the BALF of cystic fibrosis subjects compared to healthy controls [153]; however in a second study a reduction in SP-A but not SP-D was observed in BALF of cystic fibrosis subjects [154]. This difference may be due to variations in the study populations. Furthermore, proteolytic enzymes present in cystic fibrosis have been shown to degrade SP-D [155]. Children with gastrointestinal flux show reduced levels of higher order SP-A and SP-D oligomers and are at increased risk of recurrent pulmonary infections [156]. Sarcodosis and silicosis has been shown to be associated with increased SP-D levels in BALF [157, 158].

Interestingly, the Thr11 polymorphism has been linked in a number of studies to an increased risk of COPD whereas a reduced serum concentration of SP-D has also been associated with this polymorphism [147, 159, 160]. The $Met^{11}Thr$ SP-D polymorphism has also been shown to be associated with differential risk of pre-term birth. Individuals homozygous for methionine at position 11 were shown to be associated with increased risk of preterm birth whereas a reduction in the incidence of preterm birth was observed for $Thr^{11}Thr$. This differential polymorphic effect was observed for the foetus but not the mother in both instances [161].

An SP-A2 polymorphism within the CRD domain results in increased incidence and mortality from meningococcal disease whereas a SP-A1 polymorphism has been linked to an increased risk of idiopathic pulmonary

fibrosis [162, 163]. Abhorrent SP-A expression has been shown to be associated with a number of lung cancers. Deletions in the expression of SP-A mRNA in non small cell carcinoma (NSCC) tumours and surrounding cells have been shown to be a indicator for a poor prognosis and enhanced relapse [164]. SP-A1 and SP-A2 polymorphisms have also been associated with enhanced risk of NSCC and lung adenocarcinoma [165]. SP-A has also been shown to be a useful biomarker for lung adenocarcinomas compared to other lung cancers such as mesothelioma [166]. Furthermore, a four fold increase in the SP-A levels in BALF has been reported in children with various malignancies compared to healthy controls [167].

SP-A and SP-D polymorphisms have been implicated in the success of lung transplants. Donor lung grafts which express low SP-A mRNA expression prior to transplantation show reduced survival following transplantation. The level of SP-A expression has been linked to certain SP-A polymorphisms [168]. Lung donors possessing the $Thr^{11}Thr$ SP-D polymorphism have also been shown to result in reduced survival following transplantation [169]. High serum SP-D levels in lung transplant recipients has been shown to be strongly associated with mortality [170]. In a murine study, SP-A has been shown to protect against gastrointestinal graft versus host disease following bone marrow transplantation [171].

1.4. Influenza A virus

Influenza viruses belongs the Orthomyxoviridae family of viruses which consist of influenza A, B and C as well as Thogotovirus and Isavirus [172]. According to the World Health Organisation influenza infects up to 15% of the world's population, causing severe morbidity in 3-5million people and mortality in up to 500,000 people in non-pandemic years; however, these figures increase exponentially during pandemics [173]. In the years between

1999 and 2009 it was estimated that the annual mortality rate in England and Wales from seasonal influenza was between 7,000 and 25,000 [174]. Influenza A virus (IAV) is the most common and pathogenic of these viruses within the human population [175].

1.4.1. Influenza virion structure

IAV is a lipid enveloped negative sense RNA virus; its genome consists of eight segmented single stranded RNAs of different lengths which encode ten viral proteins [172]. The structure of a typical spherical influenza A viron is shown in Figure 1.6A. These proteins are nucleoprotein, polymerase base protein 1 (PB1), PB2, polymerase acid (PA), haemaglutinin (HA), neuraminidase (NA), matrix protein 1 (M1), M2, non-structural protein 1 (NS1) and NS2 [176, 177]. Each of the eight viral RNA strands are encapsulated in nucleoprotein and associated with a polymerase trimer, consisting of PB1, PB2 and PA, to form viral ribonucleoprotein (vRNP) complexes. The 8 vRNP are encapsulated within a host derived lipid envelope in which the inner leaflet of the membrane is associated with a layer of M1 protein. The M1 protein confers structural integrity to the virion. HA and NA are the two major glycoproteins on the surface of the virus and are expressed as trimers and tetramers respectively [178]. IAV are classified according to the subtypes of HA and NA they express on their surface; seventeen HA (H1-17) and ten NA (N1-10) subtypes have been described however, not all IAV subtypes are infectious to humans [179]. These proteins also determine the virulence and species specificity of IAVs. IAV are usually spherical particles with a diameter ranging from 80-120nm; however, fibrous influenza A virons have also been described [180].

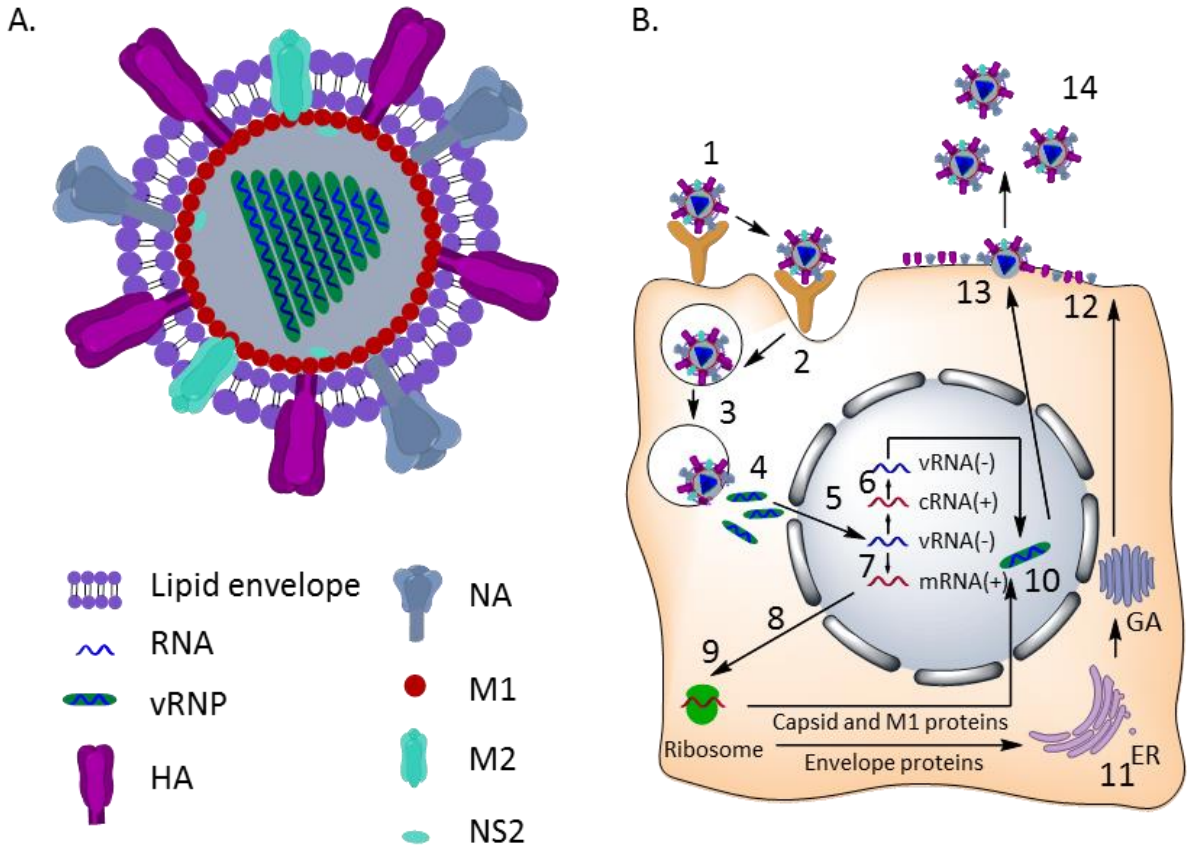

Figure 1.6: Influenza A Virus; A. Influenza A viron structure and B. replication cycle in epithelial cells; 1. Attachment of viral HA to sialic acid receptor; 2. endocytosis of virus-receptor complex; 3. fusion of endosomal and viral membranes; 4. release of vRNP into the cytoplasm 5. transport of vRNP into the nucleus; 6. replication of vRNA(-) to cRNA (+) and then progeny vRNA(-); 7. transcription of vRNA(-) to vmRNA (+); 8. transport of vmRNA to ribosome 9. translation of viral proteins and translocation of capsid and M1 proteins to nucleus; 10. formation of M1-vRNP complexes; 11. glycosylation of envelope proteins in the endoplasmic reticulum and transport to the golgi apparatus; 12. incorporation of envelope proteins into the apical plasma membrane; 13. virus assembly and budding; 14. progeny virion release. Abbreviations; ER endoplasmic reticulum; GA: golgi apparatus; HA haemaglutinin; M1 matrix protein 1; M2 matrix protein 2; NA neuraminidase; NS2 non-structural protein 2; RNA ribonucleic acid; Adapted from A. [172] and B. [181]. Drawn with ChemDraw Ultra v12.

1.4.2. IAV Replication

The main site of viral replication occurs in the epithelial cells lining the respiratory tract and is summarised in Figure 1.6B. The IAV infection cycle begins with the attachment of viral HA to sialic acid containing receptors on the surface of these cells. HA binds to terminal sialic acid residues which are linked through either a α(2-6) or α(2-3) linkage to a penultimate galactose residue (see Figure 1.7). The specificity of the HA to these residues determines the species infectivity of the virus as birds express solely the α(2-3) whereas humans express the α(2-6) linkage. Pigs are an important species in IAV re-assortment as they express equal amounts of both of these sialic acid linkages [182]. Following attachment of HA to cell receptors, the receptor-virus complex is internalised by endocytosis. The major route of virus entry is generally attributed to clathrin dependent mechanisms; however, non-clathrin non-caveolae endocytosis has also been described [178]. During clathrin mediated endocytosis, HA binding to surface receptors causes the recruitment of clathrin to the basolateral surface and an invagination of the plasma membrane [178, 183]. The internalised vesicle fuses with endosomes causing a reduction in the pH inside the vesicle. This acidic pH triggers the transportation of protons through the M2 membrane proton channel and conformational changes to the HA glycoprotein [177, 184]. These lead to the fusion of the endosomal and viral membrane through the HA fusion peptide and release of vRNP into the cell cytoplasm. Nuclear translocation signals encoded within the nucleoprotein cause the transportation of the vRNP into the nucleus of the host cell. The dissociation of the vRNP from M1 is an essential process in viral replication as vRNP cannot transport through nuclear pores whilst in association with M1 [177]. The negative sense vRNA is transcribed to viral mRNA which is translocated to ribosomes in the cytoplasm for translation and production of viral proteins. Complementary RNA is also generated at this stage which in

turn provides a template for the production of progeny vRNA. Newly synthesised viral capsid (PB1, PB2, PA, NP and NS2) proteins are translocated into the nucleus and packaged to form the vRNP. M1 protein is also transported into the nucleus at this stage and associates with the vRNP, triggering nuclear export of the M1-vRNP complex. HA, NA, and M2 are glycoyslated in the endoplasmic reticulum transported to the golgi apparatus and then to the apical surface where they are incorporated into the plasma membrane through their association with lipid rafts [185, 186]. The HA mediates the association of the M1 protein of the M1-vRNP complex to the lipid membrane [187]. NA triggers the release of progeny virons into the airway lumen by cleaving the cell associated sialic acid residues bound to viral HA. HA is produced and incorporated into the apical plasma membrane as a homotrimer. Each HA monomer consists of the two subunits HA1 and HA2 joined by a disulfide bridge [188]. In order for HA mediated fusion of the endosomal and viral membranes to occur the HA must be cleaved between HA1 and HA2 by proteases (e.g. human airway trypsin-like protease (HAT)) of the respiratory tract [189]. This usually occurs either shortly after HA incorporation into the apical host membrane or after virion release into the airway.

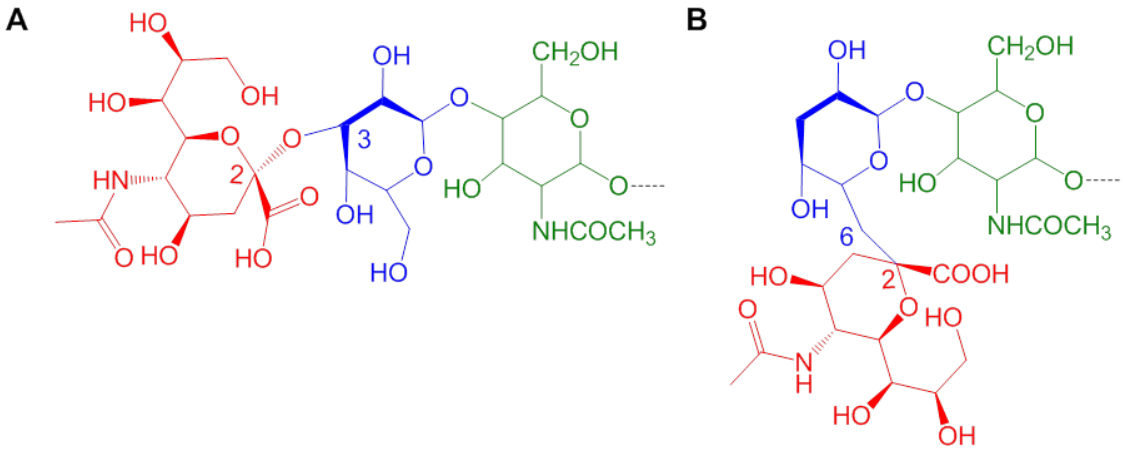

Figure 1.7: Structures of terminal sialic acid residues. Sialic acid residues (red) linked thorough A. α(2,3) and B. α(2,6) linkages to penultimate galactose residues (blue). Dashed line represents link to trimannosyl core. Adapted from [182]. Drawn with ChemDraw Ultra v12.

1.4.3. SP-A and SP-D neutralisation of IAV

The innate immune response to influenza infection is a multifaceted response involving both cell and soluble mediators [190]. Both SP-A and SP-D form a vital part of the defence against IAV infection; however, the mechanisms behind these inhibitions differ. IAV HA binds to the partially sialyated asparagine 187 residue in the CRD of human SP-A. This interaction causes IAV neutralisation by occupying the HA binding sites and thus preventing their interaction with sialic acid receptors. The SP-A mediated inhibition of IAV is not dependent on the presence of calcium and is not antagonised by mannan [182, 190, 191]. The interaction of SP-D with IAV occurs through binding to glycosylation sites on HA and NA; SP-D is classified as a β type inhibitor of influenza as this interaction is calcium dependent and SP-D is heat labile and resistant to degradation by NA. Glycosylation of the collectin binding site at the asparagine residue at codon 165 of H3 is essential for β inhibitor sensitivity [192, 193]. Wild type and SP-A knockout mice, who have normal SP-D levels, infected with IAV strains lacking this glycosylation site (i.e. β inhibitor resistant influenza strain) have increased morbidity and mortality than those infected

with strains which are sensitive to β inhibitors [194, 195]. SP-D also inhibits NA activity causing a reduction of progeny virion release from the budding site [190]. In β inhibitor sensitive strains, SP-D is more effective at neutralising IAV infection than SP-A; however, SP-A is more effective at neutralising deglycosylated IAV strains than SP-D [196]. SP-A has also been shown to be an opsonin to IAV in rat macrophages whereas, SP-D opsonises IAV uptake by neutrophils [197, 198].

1.4.4. Factors effecting IAV susceptibility and severity

There are many factors which influence an individuals susceptibility and resulting severity of influenza infection. These include age, lifestyle, pre-existing health conditions, and environmental exposure to certain substances [199-205]. Subjects at particular risk of infection include young children, the elderly and those with pre-existing respiratory conditions such as asthma and COPD [203, 206, 207]. A number of other environmental or lifestyle factors have also been identified to modulate susceptibility to influenza infection. Smokers have been identified as a group at increased risk of influenza infection in both epidemiological and toxicological studies. Smokers are several fold more likely to develop influenza infections and these infections tend to more severe than in non-smokers [204, 205]. Mice exposed to cigarette smoke prior to influenza infection show an exaggerated inflammatory response, increased viral replication, a reduction in body weight and enhanced mortality compared to non-cigarette exposed mice [208-210]. The production of the interferon gamma induced protein-10 (IP-10) is a well documented response to IAV infection in both *in vitro* and *in vivo* models and is an important step for the successful resolution of IAV infections. [205]. Pre-exposure to cigarette smoke reduces the production of IP-10 following IAV infection [204, 205]. Moreover, this inhibition can be antagonised when co-treated with antioxidants; suggesting that the

suppression of these antiviral immune responses are in part caused by the oxidant activities of cigarette smoke [204]. Exposure to high concentrations of diesel exhaust (DE) and diesel exhaust particles (DEP) is also a risk factor for influenza infection. Studies have shown that mice exposed to DE show enhanced viral replication, and an exaggerated inflammatory response to influenza than non-DE exposed mice [199-202]. This may be due to an up-regulation of the Th2 cytokine IL-4 by DE as this cytokine has been shown to inhibit viral clearance in the lung [200]. However, reduced levels of SP-A and SP-D have also been reported in mice co-exposed to DE and IAV [199].

1.5. Particle exposure and respiratory infections

Most of the evidence surrounding the enhanced susceptibility to respiratory infections following particulate exposure relates to ambient particulate matter rather than engineered nanoparticles. However, these studies serve as useful guides to understand the potential toxicological issues which may be faced following exposure to NSP.

1.5.1. Epidemiological evidence

Numerous epidemiological studies have associated increased exposure to airborne particulate matter (PM) to enhanced morbidity and mortality from cardiopulmonary causes [211-214]. One of the adverse respiratory outcomes following exposure to high PM levels is increased incidence and severity of respiratory infections [215]. This is of particular concern in young children and the elderly [216, 217]. Pre-natal exposure to $PM_{2.5}$ has been shown to increase the incidence of recurrent pneumonia and acute bronchitis in children in a concentration dependent manner. Moreover, the incidences of these pulmonary infections following exposure to $PM_{2.5}$ was much higher in children with asthma [218]. In children less than 1 year, every hour of exposure to indoor

$PM_{2.5}$ above 100μg/m^3 led to a 7% increase in the risk of acute lower respiratory infection (ALRI); however, this risk was not found in children of 1-2 years [219]. These indoor exposures concentrations are common in developing countries where ALRI accounts for around 1 in 5 of the deaths of children under 5 [220]. Pre-exposure to >33.3 μg/m^3 PM_{10} has also been shown to delay the resolution of respiratory tract infections by around 20% in healthy infants [215].

1.5.2. Toxicological evidence

As discussed in section 1.4.4, DEP and DE have also been shown to enhance and exacerbate IAV infections in mice [199-202]. Pre-exposure to DE and DEP has also been shown to increase RSV infection and viral induced lung inflammation in mice *in vivo*. Interestingly, this study also showed a reduction in SP-A expression during RSV infection following exposure to DE [221]. In another study the exposure of mice to DEP for 6 months prior to IAV infection resulted in an increased incidence of infection but did not alter mortality in IAV exposed mice [222]. Conversely, prior exposure to high acute doses of ultrafine carbon black has been shown to protect against Streptococcus pneumonia induced mortality in mice [223]. Prior exposure to $PM_{2.5}$ also resulted in changes to the resolution kinetics of rats exposed to S. pneumoniae; at 24 hours post infection bacterial burdens were enhanced in the lungs of PM exposed rats whereas at later time points bacterial burdens were reduced in these rats [224].

1.6. Cationic nanoparticles; applications and toxicity

In the current study amine modified polystyrene nanoparticles are used as a model cationic particle. Cationic particles have been investigated for use in a number of biomedical applications for diagnostic and therapeutic purposes. Cationic supraparamagnetic iron nanoparticles (SPIONS) have been investigated for use as contrast agents for magnetic resonance imaging (MRI)

[225]. Cationic particles have also been investigated as vectors to deliver drugs to tumour target sites and as vectors for gene delivery [226-230]. Moreover, cationic gold nanoparticles coupled to single walled carbon nanotubes have been used to detect nucleic acid (e.g. DNA) and non-nucleic acid targets (e.g. cocaine) in situ [231].

Although there has been little peer reviewed research on the subject, a number of patents have been granted regarding the use of cationic particles in personal health care products ranging from sun screen to hair dye products [232-236]. Polycationic components of paint have been linked to the development of Ardystil syndrome, a condition in textile paint sprayers characterised by acute pulmonary oedema and severe respiratory disease [237-239].

Cationic nanoparticles have been shown to be internalised by cells to a greater extent than their anionic counterparts. This is due to the binding of the cationic particles to anionic components of the lipid cell membrane [240]. However, enhanced cytotoxicity has also been reported in a number of studies [241]. Cationic particles have been shown to cause localised membrane disruption in rat cardio myocytes and 'holes' in the membranes of human alveolar epithelial cells [242, 243]. Amine particles have been shown to accumulate in the lysosomes of cells. At the acidic pH of the lysosome the amine functional groups can act as a proton sponge , lead to increased proton pump activity, result in lysosomal swelling and eventually rupture. Although carboxylated particles have also been shown to accumulate within the lysosome, this accumulation is not associated with lysosomal swelling [244]. Amine modified polystyrene particles have also been shown to activate the Nod like receptor 3 (NLRP3) inflammasome in macrophages which resulted in the up-regulation of IL-1β. This activation was shown to be dependent on the generation of reactive oxygen species and was not observed for unmodified or

carboxylated polystyrene particles[245]. Amine modified polystyrene particles have also been shown to have enhanced pro-inflammatory potential in intratracheally instilled mice compared to unmodified or carboxylated nanoparticles [246].

1.7. Nano-bio interface and the protein corona

The 'nano-bio' interface is the site at which nanosized materials interact with biological substrates such as proteins, lipids, DNA and organelles. The interactions which occur at the nano-bio interface are dynamic and NSM surface characteristics play pivotal roles in determining the strength and extent of these interactions; these characteristics include but are not limited to chemical composition, functionalization, shape, curvature, and the hydrophobicity/hydrophilicity of the material surface [247]. In biological fluids proteins coat the surface of the nanoparticle forming a multi-layered protein corona. The corona consists of an inner layer of proteins strongly associated to the particle surface and an outer layer of weakly associated proteins. The strongly associated proteins form the "hard" corona and are often described as being irreversibly bound to the particle core [248, 249]. Proteins of the "soft" corona are weakly associated and are rapidly exchanged with bio-molecules from the surrounding medium [250, 251]. The protein corona is degraded in the lysosomes; in the case of cationic particles such as amine functionalised polystyrene, the degradation of the protein corona leads to exposure of the protonated cationic groups and lysosomal escape following rupture of the lysosomal membrane [244].

1.7.1. Nano-bio interactions effect on protein function

Interactions of nanomaterials with proteins can induce protein conformational changes and effect protein function [250, 252, 253]. Serum

albumins from bovine (BSA) and humans (HSA) have been extensively studied for their ability to associate with a range of nanoparticles [254, 255]. BSA has been shown to associate with both gold nanoparticles (GNP) and gold nanorods (GNR) however, the chemistry behind these associations differ. The thermodynamic profiles of the association between BSA and GNR or GNP vary. The BSA-GNR interaction is an endothermic reaction whereas the latter interaction is exothermic. Moreover, the binding affinity of BSA to GNR is around 100x greater and results in a substantial reduction in protein function compared to the interaction with GNP [254].

1.7.1.1 Nanoparticle interaction with components of pulmonary surfactant

Once in the alveolus the particles deposit onto the air-liquid interface of the epithelium and are displaced into the surfactant hydrophase through wetting forces [256]. A number of studies have investigated the acellular interactions between components of pulmonary surfactant and NSM. These studies have demonstrated that both surfactant phospholipids and proteins can interact with these materials and that this interaction can affect the properties of both NSM and the biological molecules. The addition of titanium dioxide, polystyrene, or gold NSP to surfactant alters surfactant ultrastructure *in vivo* and perturbs the surface tension lowing properties of surfactant phospholipids *in vitro* [257, 258]. Dipalmitoyl-phosphatidylcholine (DPPC) is the most abundant component, comprising up to 70% by weight of pulmonary surfactant [259]. DPPC has been shown to interact with NSP and micro-particles and this interaction has been shown to be dependent on both particle concentration and surface chemistry [260-262]. Moreover, the interaction of poly(lactic-co-glycolic acid) (PLGA) micro-particles with DPPC has been shown to reduce particle uptake by alveolar macrophages [261].

1.7.1.1.1. Particle interaction with SP-A and SP-D

The interaction of surfactant proteins with NSM has also been reported. Salvador-Morales et al. (2007) reported that SP-A and SP-D bind to functional groups, generated from impurities during synthesis, on the surface of carbon nanotubes. This binding was mediated by the CRD domain of the proteins and was dependent on the presence of calcium. Furthermore, SP-A and SP-D were unable to bind bare (i.e. non-functionalised) carbon nanotube surfaces [263]. SP-A has been shown to enhance the uptake of titanium dioxide particles (size undisclosed) and 1μm latex beads by rat alveolar macrophages. In this study, surfactant lipids and IgG enhanced titanium dioxide particle uptake to a similar extent to SP-A. The pre-treatment of macrophages with SP-A also resulted in enhanced uptake of unopsonised titanium dioxide [264]. Metal oxide nanoparticles incubated in BAL have been shown to absorb SP-A; the extent of this interaction was shown to be dependent on the particle surface chemistry [265]. The interaction between magnetite particles possessing different polymer coatings with SP-A and SP-D has also been investigated. These studies have shown that both SP-A and SP-D enhance the uptake by macrophages of magnetite particles with hydrophobic and hydrophilic surface coatings. However, SP-D enhanced the uptake of hydrophilic nanoparticles to a greater extent than SP-A; whereas for hydrophobic particles the reverse was true [266, 267]. The effect of SP-A and SP-D on the uptake of polymer coated magnetite particles was negated following pre-incubation with surfactant lipids [267]. This is consistent with other work which showed that surfactant protein related amino acids associate with $PM_{2.5}$ incubated in bronchoalveolar lavage fluid; however, this study also showed that $PM_{2.5}$ associates most strongly with the surfactant lipid DPPC [262]. Furthermore, in an *in vivo* study the systemic bio-distribution of gold nanoparticles was shown to be slightly but not significantly reduced following pre-incubation with exogenous SP-D [268]. The effect of

particle interaction with nanoparticles on the function of SP-A and SP-D has yet to be investigated.

1.8. Study aims and hypothesis

The overarching hypothesis of this study was that nanoparticles can sequester surfactant proteins A and D in the alveolus and that this sequestration will lead to altered particle clearance by immune cells (see Figure 1.8). Furthermore, it is hypothesised that the association of particles with SP-A and SP-D will lead to a deficiency in these surfactant proteins and enhance susceptibility to infection.

The aims of this study were as follows;

1) To investigate the absorption of SP-A, SP-D and rfhSP-D to polystyrene nanoparticles with different surface modifications and charges;

2) To determine the effect of this interaction on particle aggregation;

3) To examine the effect of the interaction of protein and particle on the uptake by a macrophage-like cell line and alveolar macrophages from wild type, SP-A deficient and SP-D deficient mice;

4) To develop *in vitro* infection assays capable of determining the effect of nanoparticles on SP-A and SP-D function;

5) To investigate the use of coherent anti-stokes raman spectroscopy to detect unlabelled lipids and nanoparticles *in vitro*.

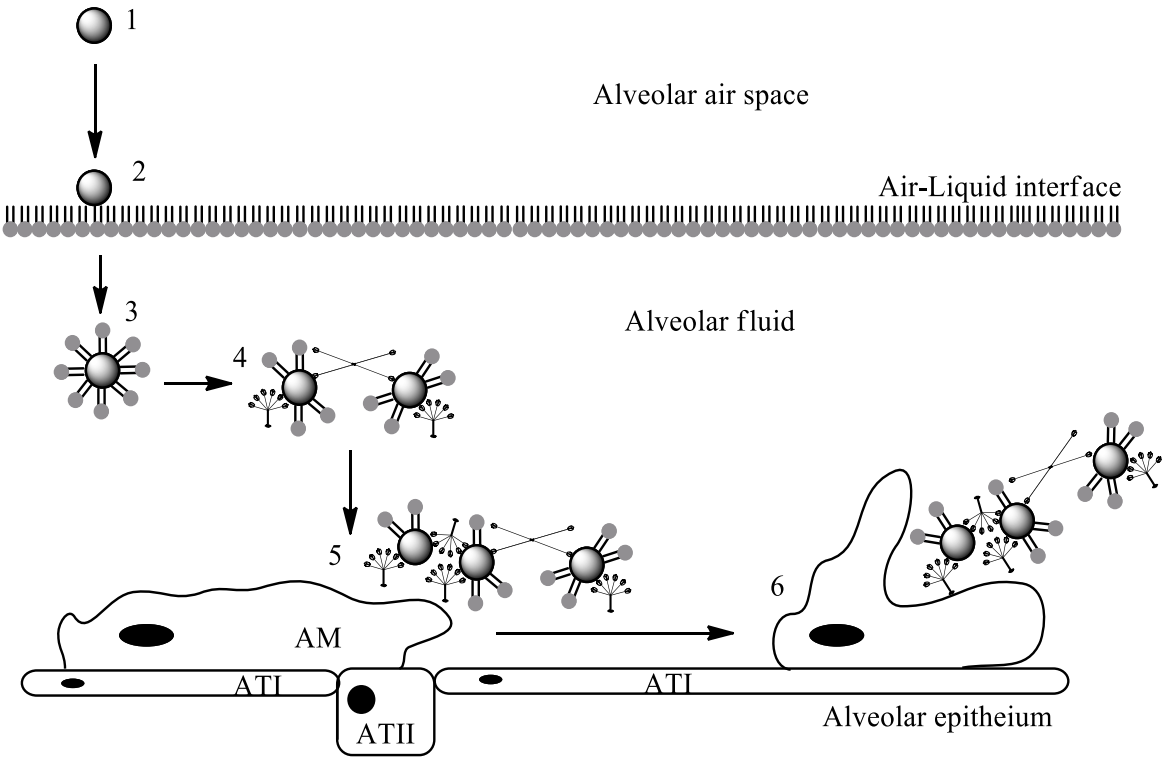

Figure 1.8: Hypothesised particle interaction with surfactant proteins in the alveolar lining fluid: Inhaled particles enter the alveolar space (1) and deposit onto the air-liquid interface of the alveolus (2). The particles are then displaced into the fluid phase through wetting forces, resulting in the formation of a lipid corona (3). The bio corona is then modified through the incorporation of Surfactant Proteins, resulting in particle agglomeration (4). Particle agglomerates are recognised by alveolar macrophages (5) and phagocytosed (6). Abbreviations: ATI; alveolar epithelial type I cells, ATII alveolar epithelial type II cells. Adapted from [269].

Chapter 2: Purification of Surfactant Proteins A and D

2.1. Introduction

This chapter outlines the expression and purification of a recombinant fragment of SP-D (rfhSP-D) as well as the purification of native human surfactant protein A (nhSP-A) and nhSP-D from bronchoalveolar lavage fluid (BALF). The purification of nhSP-D using two different affinity resins were compared using yield, purity and endotoxin levels as measurement markers. Purified proteins were characterised by SDS PAGE and western blot analysis.

2.2. Methods

2.2.1. Expression of rfhSP-D in Escherichia coli

rfhSP-D was expressed and purified as described in [270]. *Escherichia coli* (*E. coli*) bacteria (BL21 DE3 containing pALMI-53) containing a rfhSP-D kanamycin resistant plasmid was incubated overnight at 37°C on fresh sterile LB agar (Sigma, Dorset, UK) containing 25µg/mL Kanamycin monosulphate (Sigma, UK). Sterile LB broth (Sigma, UK) containing 25µg/mL Kanamycin monosulphate was inoculated with a single colony from this culture and incubated overnight whilst shaking at 220rpm at 37°C. Magic Media Component A (Invitrogen, UK) was dissolved in 950mL mQ water, autoclaved and then Magic Media Component B (50mL) with 25µg/mL Kanamycin monosulphate was added to a 2L baffle flask. This was then divided into two sterile baffle flasks and the bacterial culture was split between these two flasks. The bacterial cultures were then incubated for 22 hours at 37°C whilst stirring. The cells were harvested by centrifugation at 2700g for 20 minutes at 4°C and the cell pellet was re-suspended in 6mL of Bugbuster master mix (Novagen, Merck Chemicals Ltd. Nottingham, UK) per gram of bacterial cell pellet.

Complete protease inhibitor cocktail (Roche Diagnostics Ltd, West Sussex, UK) was added to the resuspended pellet which was then rotated for 20 minutes to lyse the cells and then centrifuged at 16,000g for 20 minutes. The pellet was resuspended in Bugbuster mastermix (60mL/g) and rotated for 10 minutes to mix. The mixture was then centrifuged again at 16,000g for 20 minutes and the pellet was resuspended in solubilisation buffer consisting of 20mM Tris, 150mM NaCl, 5mM $CaCl_2$, 5% v/v glycerol, 8M urea (pH 7.4) to achieve a 10mg/mL protein concentration. The sample was then mixed at 4°C for 1 hour and then centrifuged at 9,000g for 20 minutes. The supernatant was dialysed in Snakeskin Pleated dialysis tubing (Thermo Scientific, UK) against solubilisation buffer containing 4M urea overnight at 4°C. Buffers were exchanged every 24 hours using decreasing concentrations of urea (2M, 1M then 0M). The sample was then dialysed against fresh solubilisation buffer without glycerol or urea and this was changed every 2 hours. The dialysate was centrifuged at 9,000g for 15 minutes, the supernatant recovered and stored in 50mL aliquots at -20°C until needed.

2.2.2. Purification of rfhSP-D

Protein purification was performed using fast performance liquid chromatography on an Akta 900 (Amersham BioSciences). A N-Acetyl-D-mannosamine (ManNAc) sepharose (20mL) column was equilibrated with 20mM Tris, 150mM NaCl, 5mM $CaCl_2$ at pH7.4 (running buffer). The column was then loaded with one 50mL aliquot of the expressed protein (see *expression of rfhSP-D*) in running buffer. Following loading, the column was washed (3 column volumes (CV)) with a high salt buffer containing 20mM Tris, 1M NaCl, 5mM $CaCl_2$ at pH7.4; then with running buffer (3CV). Protein was eluted with 20mM Tris, 150mM NaCl, 10mM EDTA at pH 7.4 (EDTA buffer). This protein was collected in 2mL fractions and these fractions were loaded onto a Superdex

200 100mL column, for size chromatography, equilibrated with EDTA buffer. Fractions (1mL) were taken and those containing protein were pooled and concentrated to 4mg/mL with Amicon Ultra filters (30,000 MWCO; Millipore, Watford, UK). A polymixin B 20mL column (Pierce, ThermoScientific, UK) was equilibrated in calcium free PBS (3CV; PAA laboratories Ltd, Somerset, UK) and the protein was then loaded and eluted from the column in this PBS. The column was then serially washed with three CV of Limulus Amoebocyte Lysate (LAL) Reagent water (Lonza Biologics Plc, Berkshire, UK), 1% sodium deoxycholate, then LAL water to remove bound endotoxin and protein from the column. The column was then equilibrated in 20% ethanol for storage. Eluted protein was collected, pooled and aliquoted before being frozen at -20°C until needed. The optical densities of the protein samples at 280nm were measured before and after each purification step.

2.2.3. Purification of Surfactant Proteins from BALF

nhSP-A and nhSP-D were purified from the bronchoalveolar lavage fluid (BALF) of subjects with alveolar proteinosis. The Respiratory Biomedical Unit Heads of Corsortia (NRS reference 10/H0504/9) approved the use of BALF, for the purification of surfactant proteins. Lavage was brought to 10mM EDTA and 20mM Tris and adjusted to pH7.4 using concentrated hydrochloric acid. The BALF was then centrifuged at 10,000g for 45 minutes at 4°C. The supernatant was decanted and frozen for nhSP-D purification as described in section 2.2.3.2. The pellet was kept for the purification of nhSP-A as described in section 2.2.3.1.

2.2.3.1 Purification of nhSP-A from BALF

SP-A was purified from the bronchoalveolar lavage pellets of alveolar proteinosis subjects using a protocol provided by Wright, JR [271]. Aliquots of surfactant pellet (see section 2.2.3) were injected into a 50x excess of 1-butanol

(Sigma, UK) to delipidiate the sample and allowed to stir for 1 hour at room temperature. The solution was then centrifuged at 134,000g for 30 minutes at 4°C. The supernatant was removed and the pellet resuspended in butanol. The solution was then centrifuged again at 134,000g for 30 minutes at 4°C. The pellets were then dried under nitrogen to remove the butanol and resuspended in 20mM n-octyl-B-D-glucopyranoside (OGP), 150 mM NaCl, and 5 mM Tris at pH 7.4 (OGP buffer). The suspension was centrifuged at 134,000g for 30 minutes at 4°C and the pellets were re-suspended in OGP buffer then centrifuged again at 134,000g for 30 minutes at 4°C. The pellet was then re-suspended in 5mL of 5mM Tris and 0.141g of OGP was added to the solution and rotated at room temperature for 30 minutes. Polymixin B beads were added to the mixture to remove endotoxin and the solution was dialysed (10,000MWCO, Thermo Scientific, UK) against four 12 hour changes of 5mM Tris. The polymixin B beads were removed from the preparation by centrifuging for 10 minutes at 10,000g. The sample was then centrifuged at 134,000g for 60 minutes and the SP-A containing supernatant was sterile filtered using a 0.22μm filter. The SP-A was then aliquoted and stored at -20°C until needed. SP-A in the preparation was confirmed using SDS PAGE and western blot analysis.

2.2.3.2 *Purification of nhSP-D from BALF*

nhSP-D from subjects with alveolar proteinosis was purified as previously described [272]. Affinity resin (15mL of maltose agarose or ManNAc sepaharose as described in text) was regenerated in 20mM Tris, I50mM NaCl and 50mM EDTA, pH7.4. Following regeneration the column was re-equilibrated in running buffer (see section 2.2.3). The lavage was defrosted and brought to 20mM $CaCl_2$ (Sigma, UK). The pH of the lavage was maintained between 6.5-8.0 with concentrated sodium hydroxide during calcium addition and brought to pH7.4 after the final calcium was added. The equilibrated affinity resin was added to the lavage and allowed to mix overnight at 4°C. The

lavage was passed through a grade 1 sintered funnel under vacuum and the resin recovered using running buffer. The resin was packed into an affinity column and connected to the Akta 900 (Amersham BioSciences). The slurry was packed down in the running buffer and washed with this buffer until a stable baseline was reached. The column was then washed with 1.5CV of high salt buffer before being re-equilibrated in running buffer (1.5CV). The nhSP-D was eluted with 2CV 20mM Tris, 150mM NaCl and 50mM MnCl2 (pH7.4). The eluted peak was pooled and buffer exchanged into EDTA buffer then concentrated to ~1mg/mL with a Amicon 30k molecular weight cut off (MWCO) concentrator (Millipore, Fisher, UK). The affinity resin was washed with EDTA buffer (2CV) to clean the column. The Superose 6 (120mL; unless otherwise stated) column was equilibrated with 1.5CV EDTA buffer and the concentrated protein was loaded onto the column. The gel filtration column was run with EDTA buffer for 2CV to elute the protein. Fractions (0.5mL) were collected and frozen for analysis by ELISA, SDS PAGE and western blot. Following verification, the nhSP-D peak fractions were pooled and concentrated using a Amicon 30kMWCO concentrator. The nhSP-D was mixed with polymixin B beads for 1 hour at room temperature then centrifuged at 300g for 5 minutes to remove the beads. nhSP-D was aliquoted into 20µl aliquots and frozen at -20°C for later use.

2.2.4. nhSP-D ELISA

SP-D ELISA protocol was adapted from [273].The rabbit polyclonal anti-human rfhSP-D (capture) antibody was diluted 1000 times in carbonate buffer (pH9.6; Sigma, UK) to a concentration of 1.6µg/mL and 100µl was added to each well of a 96 well Maxisorp plate (Nunc, Fisher Scientific, UK). The plate was sealed with parafilm and incubated overnight at 4°C. The plate was washed four times in TBS, 5mM $CaCl_2$, 0.05% Tween20 (wash buffer) and then

each well was incubated in 200µl wash buffer for 15 minutes at room temperature to block unbound sites. The plate was then washed once more with wash buffer then 100µL of sample or standard was added. Recombinant full length SP-D was kindly provided by Dr Jens Madsen for the ELISA standard. The plate was incubated overnight at 4°C then washed four times in wash buffer. The wells were then incubated with 100µL detection antibody (0.5µg/mL biotinylated monoclonal mouse anti-human SP-D antibody, Hyb 246-04) in wash buffer for 1 hour at room temperature. The plate was then washed four times in wash buffer then incubated for 1 hour with 100 µL/well of 33ng/mL Streptavidin-HRP (Sigma, UK) in wash buffer. The plate was washed again four times in wash buffer then 100 µL/well of TMB (3,3′,5,5′-tetramethylbenzidine**)** substrate was added and incubated for 30 minutes at room temperature. The reaction was stopped by adding 50 µL/well of 0.5 M H_2SO_4. The absorbance was read at 450nm using a Molecular Devices SpectraMax 340pc plate reader**.**

2.2.5. Sodium Dodecyl Sulfate Polyacrylamide Gel Electrophoresis

SDS PAGE was conducted using NuPAGE 4-12% Bis-Tris gels (unless otherwise stated) with MES buffer as recommended by the manufacturer (Invitrogen, Paisley, UK). Samples for reduced gels were prepared by adding 13.5µL of sample in milliQ water to 5µL of (4x) NuPAGE LDS sample buffer and 2µL of (10x) reducing agent. Gels were run at 200mV for 35 minutes and stained using simply blue or silver or transferred onto western blot membranes.

2.2.5.1 Simply blue staining

Immediately following electrophoresis, gels were removed from their casing and rinsed twice with milliQ water. Fresh milliQ water (100mL) was added, then the gel was microwaved for 1 minute on medium high and placed on a rotary shaker for a further minute. This wash step was repeated twice

more with fresh milliQ water at each step. The gel was then immersed in 20mL of Simply Blue Safe stain (Invitrogen, UK), covered with parafilm and placed on a rotary shaker overnight. The gel was destained using milliQ water (3 washes of 1 hour each) on a rotary shaker.

2.2.5.2 Silver staining

Silver staining was conducted as recommended by the manufacturer (BioRad, Hemel Hempstead, UK) Immediately after electrophoresis was complete the gels were placed in fixative solution containing 40% methanol and 10% acetic acid (v/v) and incubated for at least 60 minutes. The fixative was then removed and replaced with 200mL of 10% ethanol with 5% acetic acid (v/v) and incubated for a further 30 minutes. The gel was then incubated for a further 30 minutes in fresh 10% ethanol, 5% acetic acid and then for 10 minutes in oxidiser. The gel was washed three times for 10 minutes per wash in milliQ water or until all the yellow colour was removed. The gel was then incubated for 30 minutes in silver reagent (200mL) then washed briefly for 2 minutes in milliQ water. The gel was placed in developer for 30 seconds then replaced twice with fresh developer and incubated for a further 5 minutes for each incubation. The reaction was stopped using 5% acetic acid (v/v).

2.2.5.3 Western blot

Western blots for SP-A and SP-D were conducted as recommended by the manufacturer (Invitrogen, UK). Gels were transferred onto PVDF membranes using an iBlot (Invitrogen, UK). Following transfer, PVDF membranes were washed twice with water and then incubated overnight at room temperature in 5% milk in TBS containing 0.1% tween (blocking buffer) to block non-specific staining. The membranes were then washed three times in TBS with 0.1% tween for 5 minutes per wash on a rotary shaker. The membranes were then incubated with primary antibody in blocking buffer for 1

hour at 37°C. For nhSP-A specific western blots a polyclonal rabbit nhSP-A specific antibody (Rb 96/17792) at a dilution of 1 in 1000 was used. For both rfhSP-D and nhSP-D western blots a polyclonal rabbit antibody raised against rfhSP-D was used at a concentration of 1.6 μg/mL. The primary antibody was removed and the membrane washed three times in TBS with 0.1% tween as previously described. The membrane was then incubated with 2mL secondary anti-rabbit antibody conjugated to alkaline phosphatase (Invitrogen, UK) for 30 minutes at 37°C. The membrane was then washed three times in TBS with 0.1% tween as described previously and then the membrane was placed onto a 1mL aliquot of AP- chemiluminescent substrate (Novex, Invitrogen, UK) and incubated for 5 minutes. The membrane was then sandwiched with plastic in a film cassette and in the dark, a photographic film was placed onto the plastic covered membrane. The film was exposed to the membrane for 5-15 minutes in the closed cassette then placed in photographic developer. The film was washed in water then placed in photographic fixer for 20 seconds. The film was washed again in water then dried.

2.2.6. Limulus Amoebocyte Lysate assay

Endotoxin concentrations in purified protein samples were determined using the Limulus Amebocyte Lysate (LAL) chromogenic assay (Lonza, UK) and conducted as described by the manufacturer. Briefly, sample and standards (50μL) diluted in LAL free water (Lonza, UK) were aliquoted into a 96 well plate which were incubated in Limulus Amebocyte Lysate (50μL) at 37°C for 10 minutes. Aliquots (50μL) of chromogenic lyophilized substrate were added to each well and incubated for 6 minutes at 37°C, the reaction was then stopped using 10% Sodium dodecyl sulphate in LAL water (100μL/well). A Molecular Devices SpectraMax 340pc plate reader was used to determine the absorbance of each sample at 405nm. A four point 2 fold serially diluted standard curve

with a top concentration of 1 endotoxin unit/mL was used. Each sample was prepared in duplicate.

2.2.7. Transmission Electron Microscopy

SP-D samples (5μL) were placed on formvar-carbon coated grids and left for 1 hour. Any residual liquid was removed using tissue paper then the samples were negatively stained with 5μL uranyl acetate for 10 seconds. The samples were then analysed using a Technai12 Transmission Electron Microscope (FEI, Eindhoven, The Netherlands).

2.3. Results

2.3.1. Expression and purification of rfhSP-D

A recombinant fragment of surfactant protein D (rfhSP-D) was expressed in *E. coli* as previously described [270]. Successful induction with magic media was confirmed using SDS PAGE (see Figure 2.2A). Protein folding was conducted using a urea gradient and was then purified using affinity chromatography and gel filtration. Table 2.1 shows the total amount of protein at each stage of the purification process. Prior to affinity chromatography there was approximately 76.2mg of protein, this will include incorrectly folded protein, rfhSP-D without lectin activity, and some bacteria associated proteins as well. Expressed protein was flowed through a ManNAc sepharose affinity column in the presence of calcium. Protein which was unable to bind to the carbohydrate based column in the presence of calcium was eluted and discarded at this step (see Figure 2.1A; peak 1). A high salt wash was conducted to elute protein (Figure 2.1A; peak 2) which was non-specifically bound to the column matrix. The final EDTA wash eluted protein which was bound in a calcium dependent manner to the sugar based column (Figure 2.1A peak 3).

This peak was pooled and purified using gel filtration. Gel filtration separates protein on the basis of size. Following affinity chromatography approximately 20.3mg of protein remained, this includes protein which binds the ManNAc in a calcium dependent manner but may include other oligomeric forms (see Table 2.1). Figure 2.1B shows a typical gel filtration chromatogram. The main peak at an elution volume of around 70mL was collected as indicated in Figure 2.1B, the shoulder of this peak was not collected. Following gel filtration there was approximately 11.2 mg protein which was correctly folded, with a uniform size distribution and a functional lectin domain. However, as the protein was expressed in a bacterial system, it is prone to high levels of endotoxin contamination and it is therefore important to reduce this contamination. The rfhSP-D was flowed through a polymixin B containing detoxigel column to remove endotoxin contamination and yielded a total amount of 8.4mg of rfhSP-D in the final preparation. The endotoxin concentration of the final preparation was determined using the Limulus Amebocyte Lysate (LAL) assay to be 0.105 ng/μg rfhSP-D. rfhSP-D was either expressed and purified by ZM/JPT or by GlaxoSmithKline. A rfhSP-D western blot confirmed the identity of the expressed protein (Figure 2.2C).

Purification step	**OD280**	**Volume of protein (mL)**	**Total protein mg**
Pre-affinity	1.523	50	76.2
Post affinity	1.267	16	20.3
Post Superdex	0.312	36	11.2
Post Detoxigel	0.985	8.5	8.4

Table 2.1: rfhSP-D protein loss during purification.

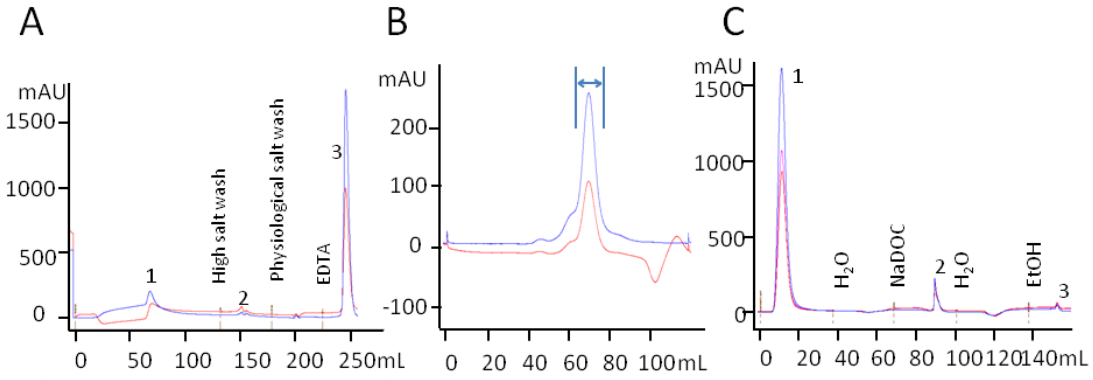

Figure 2.1: Purification of rfhSP-D. Representative chromatograms from **A**. Affinity, **B** Size exclusion and **C**. Detoxigel columns. Chromatograms represent intensity of signal in milliabsorbance units (mAU) against volume of buffer flowed through column (mL). Blue, red and pink lines represent absorption at 280nm, 254nm and 259nm respectively. Note different scales in chromatograms. Expression and purification of rfhSP-D was conducted by Zofi McKenzie and Paul Townsend during MRes.

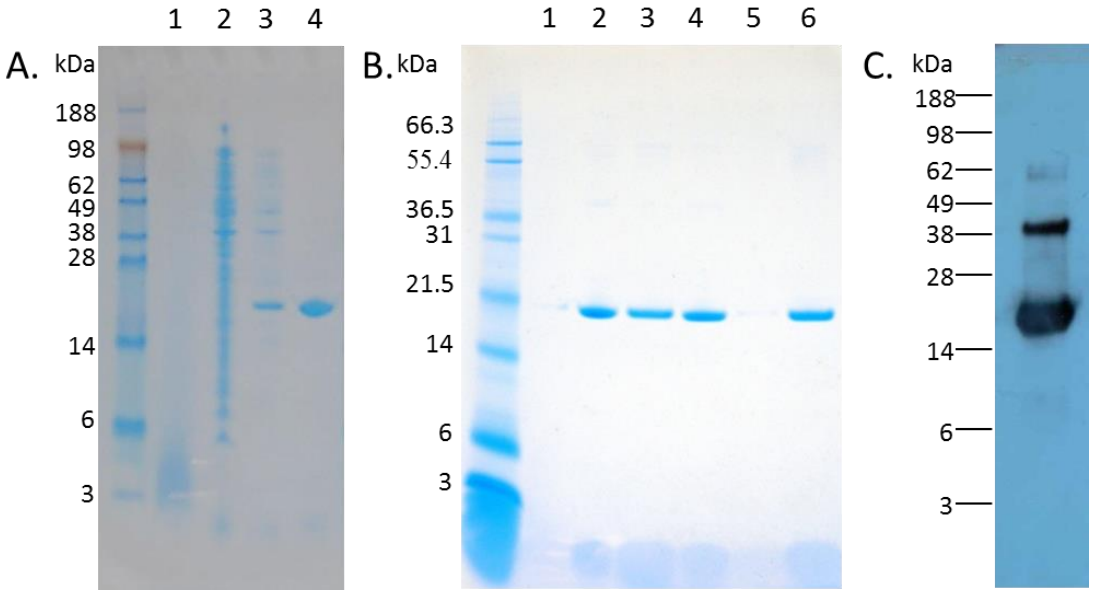

Figure 2.2: Expression and Purification of rfhSP-D. A. Induction of rfhSP-D; Lane numbers; **1.** Negative control; **2.** Bacteria lysate pre-induction; **3.** Bacteria lysate post-induction; **4.** rfhSP-D control (1µg/mL) **B.** Purification of rfhSP-D; Lane numbers; **1.** Blank **2.** Post affinity **3.** Post gel filtration **4.** Post detoxigel **5.** Blank **6.** rfhSP-D control. Amount of rfhSP-D loaded per well normalised to 1µg as determined by optical density at 280nm. **C.** Western blot for rfhSP-D.

2.3.2. Purification of nhSP-A

nhSP-A was purified as previously described from the bronchoalveolar lavage of subjects with alveolar proteinosis [271, 274]. Lipid was extracted from the 10,000g nhSP-A containing pellet of BALF using butanol. OGP (n-octyl-B-D-glucopyranoside) is a non-ionic detergent used to solubilise lipid bound proteins. The butanol insoluble protein containing pellet was solubilised using low concentrations of OGP and the soluble fraction was removed by centrifugation. A high concentration of OGP was then used to solubilise the nhSP-A and then the OGP was removed using dialysis. The insoluble fraction was removed using centrifugation and the nhSP-A containing supernatant was frozen in aliquots. Endotoxin content was assessed by LAL assay to be <0.1 ng/μg of nhSP-A. Purified preparations of nhSP-A contained two bands at around 33kDa and 56kDa on reduced SDS PAGE (see Figure 2.3). This is consistent with previous literature and with western blots for nhSP-A (see Figure 2.6). Western blot analysis of nhSP-A samples also showed that nhSP-A samples did not contain detectable nhSP-D.

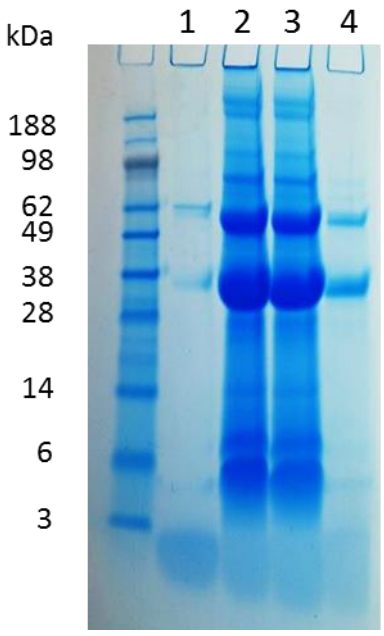

Figure 2.3: Purification of nhSP-A; Simply blue stained reduced SDS PAGE gel of **1.** nhSP-A control; **2.** BALF pellet; **3.** Post dialysis sample **4.** Purified SP-A sample. Gel was run under reducing conditions by Z. McKenzie and J. Pugh

2.3.3. Purification of nhSP-D

nhSP-D was purified from the bronchoalveolar lavage of subjects with alveolar proteinosis. The superose 6 chromatograph shows the elution of two peaks following affinity chromatography with ManNAc Sepharose (see Figure 2.4A). The first peak with an elution volume of 31mL corresponds to a protein mass of approximately 1.7mDa as determined by gel chromatography standards (data not shown). As this peak is eluted near the void volume of the column, this is only an approximate molecular mass. The second peak is eluted at 43mL which corresponds to ~800kDa. The SDS PAGE gel shows a 49kDa band corresponding to the molecular mass of monomeric control SP-D in both the 800kDa and 1.7mDa peaks. However, the 800kDa peak also shows bands at ~36kDa and 56kDa corresponding to those of SP-A (see Figure 2.4B).

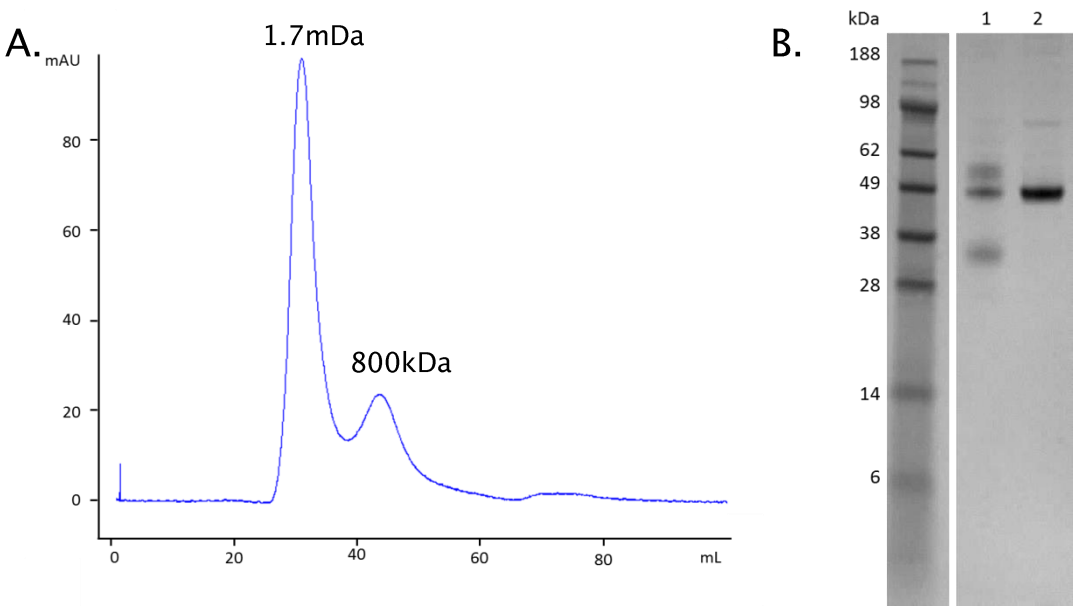

Figure 2.4: SP-D purification. A. Superose 6 (80mL) size exclusion chromatograph of nhSP-D. Line represents emission at 280nm. Chromatograph and molecular weight quantification from purification conducted by Paul Townsend**. B.** 12% Bis-Tris SDS PAGE of **1**) 800kDa SP-D and **2**) 1.7mDa SP-D under reducing conditions.

2.3.3.1 Maltose verses ManNAc purification

Previous studies have used maltose as the affinity resin for the purification of nhSP-D from lavage fluid. However, ManNAc has a greater binding efficiency to nhSP-D than maltose and preliminary experiments using ManNAc resin showed high nhSP-D yields and an extra peak at around 800kDa containing SP-D [41]. Therefore, the effectiveness of both these resins was directly compared for purifying nhSP-D. A 3L aliquot of BALF from an alveolar proteinosis subject was divided equally into two and 15mL of ManNAc or maltose resin was added. Gel chromatographs following maltose and ManNAc affinity chromatography confirm that purifying nhSP-D with ManNAc results in the elution of two peaks (see Figure 2.5).

The absorbance measured at 280nm shows the total protein eluted. Therefore, the SP-D was localised in alternate fractions using an ELISA for nhSP-D. The results, shown in Figure 2.5, show that the main peak eluted correspond with fractions containing large amounts of nhSP-D. Both the

absorbance readings from the chromatographs and the SP-D concentrations from the ELISA show greater concentrations of protein in the ManNAc compared to the maltose fractions. In the ManNAc chromatogram a small peak is observed following the elution of the main peak. However, this peak contained only minimal SP-D amounts as determined by ELISA and therefore was not further analysed in this experiment. The purity of the 1.7mDa peak from the two preparations were characterised by SDS PAGE using Simply blue and silver staining. The gels, shown in Figure 2.6A and B, show a main 49kDa band in both maltose and ManNAc purified nhSP-D consistent with the nhSP-D control. nhSP-A was not detectable in either preparation by Simply blue or silver staining. Western blots for nhSP-A and nhSP-D were used to confirm the 49kDa band as SP-D and the presence of SP-A in the samples. The SP-D western blot, shown in Figure 2.6C shows that the 49kDa band is nhSP-D, a higher band at ~96kDa is also visible constant with dimeric SP-D. In the SP-A western blot (Figure 2.6C) faint bands corresponding to the molecular weights of the SP-A monomer (36kDa) and dimer (56kDa) can be observed in both maltose and ManNAc preparations. There was a similar amount of SP-A detected by western blots between these preparations. Table 2.2 shows that ManNAc purified nhSP-D resulted in a higher yield and lower endotoxin concentrations than in the maltose purified SP-D. Therefore, ManNAc purified SP-D was used in the cell studies. In order to determine the oligomeric form of the 1.7mDa peak, samples were subjected to transmission electron microscopy. Figure 2.7 shows that this peak consists of both dodecamers and higher order oligomers.

	Yield	Endotoxin
Maltose	100 µg	>0.050 ng/µg
ManNAc	400 µg	0.015 ng/µg

Table 2.2: Comparison of SP-D yield and endotoxin concentrations between ManNAc and Maltose purifications

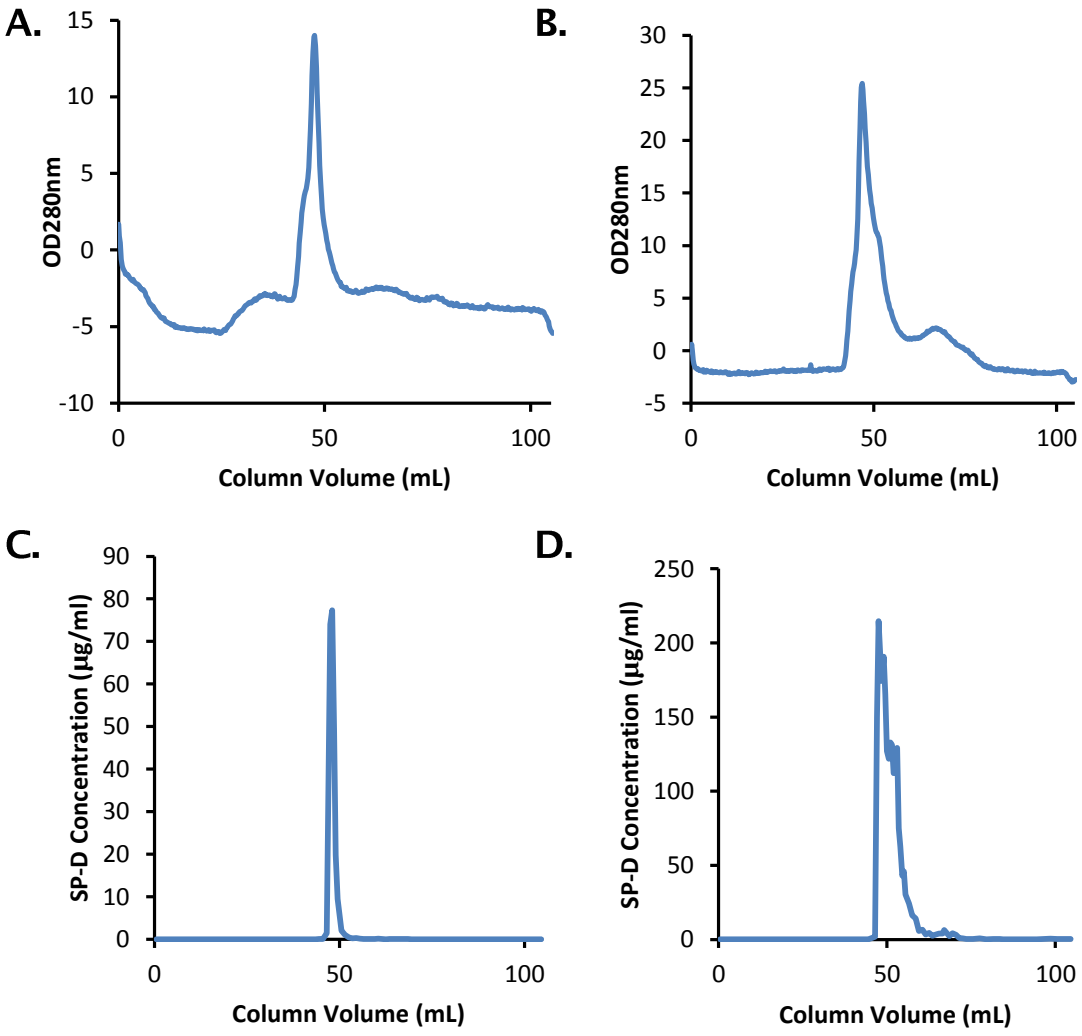

Figure 2.5: SP-D purification by Maltose and ManNAc affinity chromatography. Chromatograms from Superose 6 (120mL) gel filtration of **A.** Maltose and **B.** ManNAc purified lavage fluid. Concentrations of SP-D from Superose 6 fractions of **C.** Maltose and **D.** ManNAc purified lavage fluid. Note different scales between Maltose and ManNAc chromatograms. Purification and characterisation of nhSP-D conducted by Zofi McKenzie and Alastair Watson.

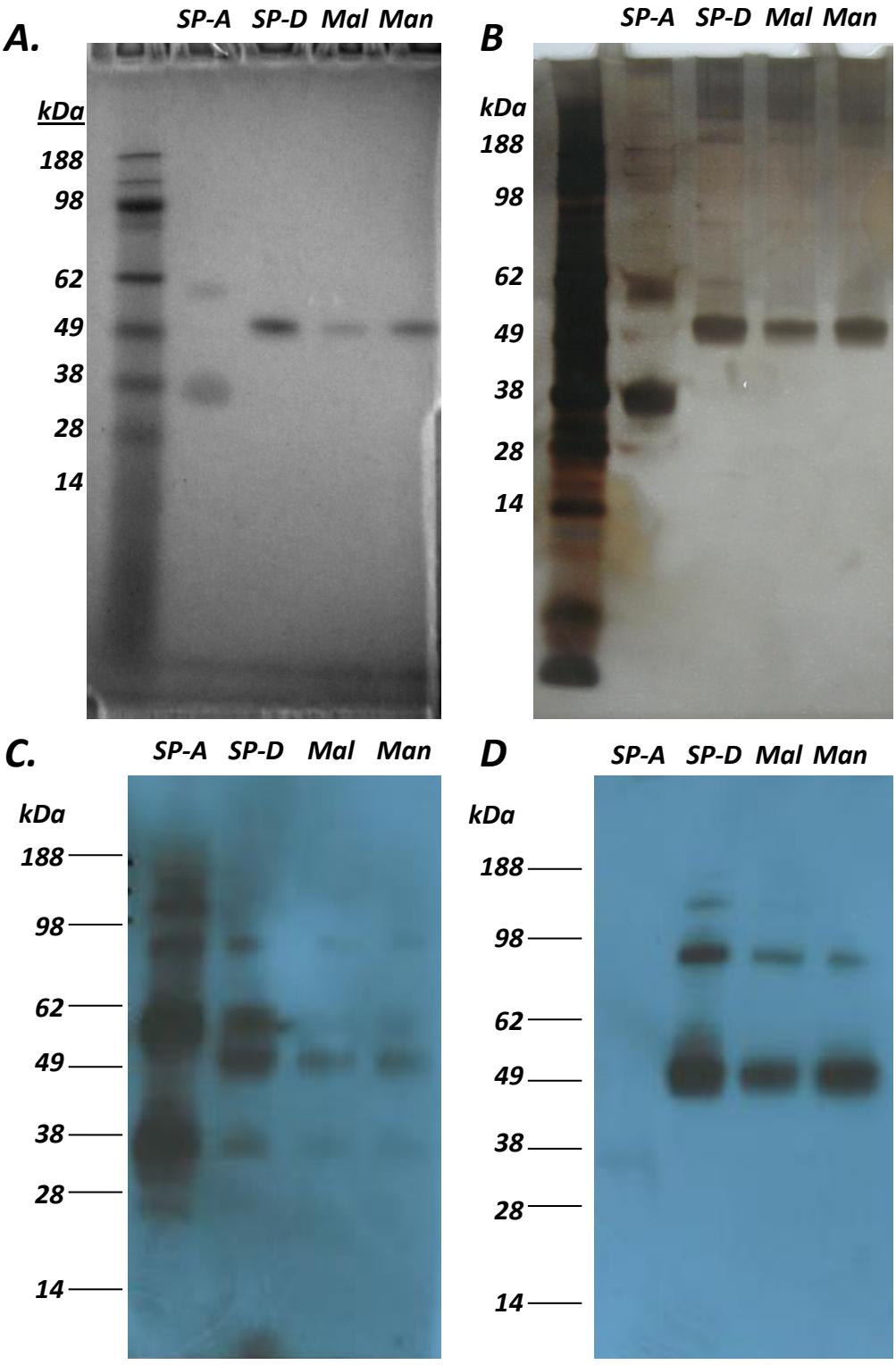

Figure 2.6: SP-D (1.7mDa) Purification by Maltose (Mal) and ManNAc (Man). **A.** Simply blue; **B.** Silver stain and western blots for **C.** SP-A western blots and **D.** SP-D western blots. All samples were analysed under reducing conditions. Purification and characterisation of nhSP-D conducted by Zofi McKenzie and Alastair Watson.

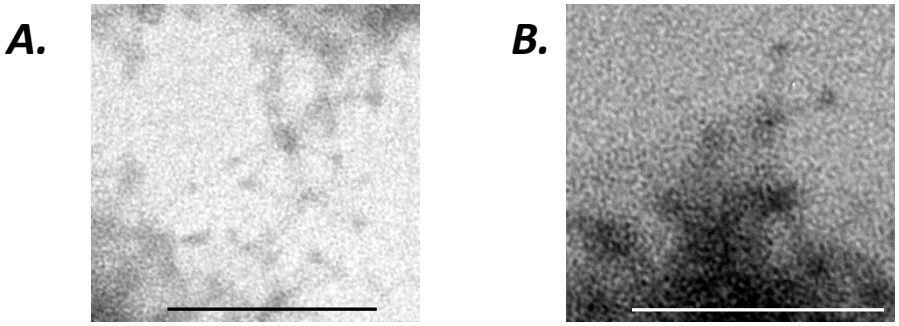

Figure 2.7: Transmission electron micrographs of 1.7mDa nhSP-D: A. Multimeric SP-D and **B.** Dodecameric SP-D following negative staining using uranyl acetate. Scale bars represent 200nm. Purification and characterisation of nhSP-D conducted by Zofi McKenzie and Alastair Watson.

2.4. Discussion

Pulmonary alveolar proteinosis (PAP) is a disorder characterised by the excess accumulation of surfactant proteins and lipids within the alveolar air spaces resulting in a reduction in gaseous exchange [275]. PAP is a rare disorder with a prevalence of 0.1 per 100,000 people; more than 90% of PAP cases are classified as an autoimmune disorder with the presence of autoantibodies against granulocyte-macrophage colony-stimulating factor (GM-CSF). The increase in SP-A and SP-D concentrations in BALF between healthy and PAP subjects has been estimated to be 100 fold and 50 fold respectively [276]. In most instances, treatment for PAP is whole lung lavage, in the absence of which subjects with PAP can suffer from respiratory failure [277]. The therapeutic lavage from subjects with PAP was used in this study to purify surfactant proteins A and D for *in vitro* experimentation. The use of this lavage has a number of advantages including, having increased concentrations of surfactant proteins and the fact that as the subjects are undergoing lavage for therapeutic purposes the lavage would otherwise go to clinical waste. However, as far as the author is aware there have been no studies on the functional differences of SP-D between healthy subjects and those with PAP.

nhSP-D usually runs at 43kDa under reducing conditions in SDS PAGE [278]. However, in this study nhSP-D migrated at a molecular weight corresponding to around 49-50kDa. The identification of this protein as nhSP-D was confirmed using western blot analysis and by ELISA. In one study nhSP-D was reported to migrate at around 50kDa due to differences in the o-glycosylation of the amino terminus. This change in glycosylation reportedly inhibited the formation of dodecamers or higher order multimers and was not eluted in the high molecular weight SP-D fraction following gel filtration [279]. As the SP-D characterised in the current study was eluted at high molecular weight (approximately 1.7mDa) and was shown to consist of multimeric SP-D by TEM it is more likely that the difference in the monomeric molecular weight of nhSP-D is due to differences in the SDS PAGE buffer system. This is supported by the migration of nhSP-D at around 49-50kDa in studies using a similar experimental setup (i.e. MES buffer system or NuPAGE Bis-Tris gels) [122, 280].

In this study the use of ManNAc and maltose affinity resins were compared and showed that ManNAc resulted in an increased yield and reduced endotoxin contamination compared to the maltose resin. Moreover, the purity of the SP-D as determined by silver staining and western blot were similar between these preparations. It was therefore decided to use the ManNAc purified SP-D in cell studies. The differences in the yield and endotoxin content may be due to the age of the affinity resins; however, this would have to be investigated further. An additional peak at approximately 800kDa is observed following ManNAc purification. This is likely due to the higher affinity of SP-D to ManNAc as compared to maltose [41]. In previous studies the purification of nhSP-D from amniotic fluid showed two peaks by gel filtration, one eluting close to blue dextran (2mDa) and the second slightly before thyroglobulin (670kDa). These peaks consisted of multimers and

dodecamers in the first peak and mainly of trimeric subunits in the second peak as shown by atomic force microscopy [64, 281]. Therefore, the peaks in the current study are likely to consist of these oligomeric SP-D forms. Both SP-A and SP-D have a high affinity to the ManNAc and maltose resins. Therefore, the co-extraction of SP-A at this step is not surprising. However, the co-elution of SP-A and SP-D at the same molecular weight using gel filtration was unexpected. This may be due to the difficulties in separating high molecular weight proteins with a high resolution. SP-A was purified using a lipid extraction method and resulted in no SP-D being detected in the SP-A preparation by western blot. This is due to the majority of the SP-D in BAL being retained in the supernatant following the first centrifugation step.

Respiratory distress syndrome (RDS) is the most prevalent pulmonary condition in premature neonates with 40% of infants born at 30 week gestation being diagnosed with this condition [282]. One of the predominant features of RDS is a deficiency of pulmonary surfactant; surfactant replacement therapy is the gold standard of treatment and results in reduced mortality [283]. Surfactant replacement therapy consists of either natural surfactant from porcine or bovine origin or synthetic surfactant. Natural surfactant is usually preferred as it contains surfactant proteins B and C and shows improved outcomes and survival in neonates with RDS compared to their synthetic counterparts [284-286]. Synthetic surfactant initially did not contain these surfactant proteins; however, recent improvements in their formulations have shown that the addition of SP-B and SP-C may improve their efficacy [287]. At present, SP-A and SP-D are absent from both natural and synthetic surfactant replacement therapies as these proteins are removed in the isolation and purification of natural surfactant due to their hydrophilic properties. Due to their now well established roles in innate immunity and controlling lung inflammation it has been hypothesised that surfactant replacement could be

improved with the addition of these natural surfactant components [288]. Moreover, exogenous SP-A or SP-D could be used as a therapeutic agent to combat other respiratory conditions and infections. For therapeutic purposes, a recombinant fragment is preferable to isolating natural collectins for a number of reasons. Firstly, the amount of protein that can be isolated is a principle disadvantage in using natural collectins. Secondly, the formulation of natural collectins is not consistent enough for therapeutic use. In this chapter a recombinant fragment of SP-D was expressed in *E. coli* and purified using affinity chromatography and gel filtration as described previously [270]. The benefits of *E. coli* as an expression system are that the protein can be expressed in large quantities and produces a consistent formulation which would be required for therapeutic purposes. However, full length SP-D cannot be expressed in this system as bacteria are unable to process the hydroxyproline required for the stabilisation of the collagen triple helix. Therefore, a fragment of SP-D containing a truncated collagenous domain with eight glycine-X-Y triplets was used in the current study. This rfhSP-D has been shown to partially correct the emphysema like phenotype of SP-D deficient mice [134]. It has also been shown to down regulate the allergic response to common house dust mite and *Aspergillus fumigatus* allergens in sensitised mice [289, 290]. The purpose of purifying this protein was firstly to study the effect of rfhSP-D in a number of *in vitro* assays and secondly to examine the effect of rfhSP-D binding to nanoparticles on particle uptake and protein function.

Chapter 3: Nanoparticle Interaction with SP-A and SP-D

3.1. Introduction

Nanoparticles have previously been reported to interact with components of pulmonary surfactant and this interaction has been reported to alter nanoparticle uptake *in vitro* [265, 267, 291]. In this chapter the association of SP-A, SP-D and rfhSP-D with polystyrene nanoparticles with different surface modifications was investigated. Furthermore, the effect of this interaction on particle aggregation and uptake into macrophages was investigated.

3.2. Methods

3.2.1. Particles

Fluoresbrite carboxylate modified and unmodified 100nm and 200nm polystyrene (PS) particles were purchased from Polysciences (Park Scientific, Northampton, UK). Fluorescent red 200nm amine particles were purchased from Invitrogen (Paisley, UK) and fluorescent orange 100nm amino particles were purchased from Sigma (Poole, UK). 3μm particles (amine and unmodified) were purchased from Polysciences (Park Scientific, UK). The term "unmodified" particle refers to non-functionalised polystyrene particles. The surface area concentration was determined by calculating the surface area of each particle (see Equation 1) and the number of particles per mL (see Equation 2) as recommended by the manufacturers;

$$\text{Surface area (cm}^2\text{)} = 4 \times \pi \times \text{radius}^2 \text{ (cm)}$$

Equation 1

$$\text{Particle Number /mL} = (6 \times \text{concentration (g/mL)} \times 10^{12}) / \text{density of polymer} \times \pi \times \text{diameter}^3$$

Equation 2

3.2.2. Nanoparticle Characterisation

3.2.2.1 Dynamic Light Scatter (DLS)

The hydrodynamic diameter and zeta potential of the 100nm polystyrene particles in calcium/magnesium free PBS was determined using a Zetasizer Nano ZS (Malvern, UK). Each measurement was taken in triplicate. The effect of proteins on size distribution were investigated in TBS with 5mM $CaCl_2$ or 5mM ethylenediaminetetraacetic acid (EDTA).

3.2.3. Proteins

nhSP-A, nhSP-D and rfhSP-D were purified as described in Chapter 2. In this chapter nhSP-D refers to the 1.7mDa SP-D oligomer. Bovine serum albumin (BSA, Sigma, UK) was used as a negative control in the cell uptake experiments. A concentrated stock of 2mg/mL BSA was prepared in PBS (PAA laboratories, UK) and sterile filtered using a 0.22μm syringe filter before use.

3.2.4. Protein adsorption to particles

Various concentrations of nanoparticles of different sizes were incubated with rfhSP-D (10μg/mL; unless otherwise stated) in low bind tubes (Eppendorf, Fisher Scientific, Loughborough, UK). Particle-protein suspensions were rotated for different time points and at different temperatures as indicated in the text. In order to investigate the role of calcium in the absorption of rfhSP-D to nanoparticles, experiments were conducted either in calcium and magnesium containing PBS or calcium/magnesium free PBS (PAA, Yeovil, UK) containing 5mM EDTA as indicated in the text. Following incubation, samples were

washed three times in the same buffer in which they were incubated. Wash steps were conducted by centrifuging the solution at 18,000g for 30 minutes, removing the supernatant and then re-suspending the pellet. Tubes containing 10μg/mL of rfhSP-D in PBS were prepared per experiment and were washed as per samples; these tubes are referred to as "washed tubes". Pellets were transferred to new tubes after the first and last wash. The absorption of nhSP-A and nhSP-D to A-PS, C-PS and U-PS was also examined in tris buffered saline (20mM Tris, 150mM sodium chloride, pH7.4) containing 5mM $CaCl_2$ or 5mM EDTA. These samples were incubated at 37°C for 24 hours then washed as described above. Samples were analysed by SDS PAGE as described in Chapter 2. Non-reduced samples were run by substituting the reducing agent for milliQ water. For the pH experiments, the pH of PBS containing 5mM EDTA was adjusted using sodium hydroxide/hydrogen chloride.

3.2.5. Spectrophotometry

The turbidity of particle-protein suspensions was analysed by measuring the percent transmittance of NP-SP-A solutions at 350nm using a spectrophotometer. Non-fluorescent A-PS, C-PS and U-PS 100nm particles (Polysciences, UK) were prepared in TBS with 5mM $CaCl_2$ or 5mM EDTA at a concentration of 10cm^2/mL. nhSP-A (5μg/mL) was added to the particle suspensions, the samples gently agitated and then the transmittance recorded at 5 second intervals for 10 minutes.

3.2.6. Transmission Electron Microscopy (TEM)

Particles (50cm^2/mL) were incubated whilst rotating with rfhSP-D (10μg/mL) for 2 hours at room temperature. Aliquots (5μL) were then placed on formvar-carbon coated TEM grids and after 1 minute the fluid was gently blotted off using tissue paper. The particles were then negatively stained using

ammonium molybdate (10 seconds) and analysed using a Technai12 Transmission Electron Microscope (FEI, Eindhoven, The Netherlands).

3.2.7. Cell culture

A549 cells were grown in Roswell Park Memorial Institute 1640 (RPMI-1640) medium supplemented with 10% foetal bovine serum (FBS; Sigma, UK), 100units/mL penicillin and 100μg/mL streptomycin (complete RPMI). Cells were routinely sub-cultured every 2-3 days using 0.25% trypsin and 0.038% EDTA. RAW264.7 cells were cultured in RPMI -1640 containing 10% heat inactivated FBS, 100units/mL penicillin and 100μg/mL streptomycin. and were sub cultured every 1-2 days using a cell scraper (Fisher Scientific, UK). Cell culture materials were purchased from Invitrogen (Paisley, UK) unless otherwise stated.

3.2.8. Immunofluorescent co-localisation assay for rfhSP-D

A549 cells ($4x10^5$) were plated in 24 well plates in complete RPMI and incubated overnight at 37°C 5% CO_2. The cells were washed and then incubated for 1 hour in SF medium containing 0, 1, 5, 10, or 25cm^2/mL of 200nm particles and 0, 1, 5, and 10μg/mL rfhSP-D. The particle solution was then removed; the cells washed three times in PBS and fixed for 1 hour in 1% formaldehyde. The cell membranes were permeabilised using 0.3% triton X-100 (TrPBS, Sigma, UK) in PBS before incubation for 1 hour at RT with a rabbit anti-rfhSP-D antibody (1.61μg/mL) in TrPBS and then for a further hour with an anti-rabbit IgG secondary antibody (667ng/mL in TrPBS) coupled to Alexa488 fluorophore. 4',6-diamidino-2-phenylindole (DAPI) was used as a DNA counter stain. Cells were visualised using a fluorescent microscope with fluorescein isothiocyanates (FITC), rhodamine and UV filters.

3.2.9. Flow cytometry

3.2.9.1 NP uptake in RAW264.7 cells

Aliquots of 100nm A-PS or U-PS particles (10µl/well) were mixed with proteins (10µl/well) at 5 times the final concentration in TBS containing 5mM calcium for 1 hour at 37°C in 96 well round bottom plates. RAW264.7 cells were washed three times in SF RPMI and dissociated from culture flasks using a cell scraper. Cells were suspended in SF RPMI at a concentration of $1.67x10^6$ cells/mL and 30µl aliquots were added to each well yielding a final particle concentration of $3.75cm^2$/mL. The cells were incubated for 1 hour at 37°C in a humidified atmosphere. The cells were washed once in 1mL PBS and centrifuged at 400g for 10 minutes to remove excess particles. The cells were resuspended in 40µl PBS and kept on ice prior to analysis. Trypan blue was added to the cells immediately before the analysis of 5000 cells per sample using flow cytometry (BD FACS Aria).

3.2.9.2 NP uptake in alveolar macrophages

Fluorescent amine modified (Sigma) or fluorescent unmodified polystyrene (Polysciences) nanoparticles with a nominal size of 100nm were used to determine nanoparticle uptake in alveolar macrophages. Alveolar macrophages were isolated from C57/B6 wild type, SP-A deficient and SP-D deficient mice as described previously [291]. Alveolar macrophages were isolated with the assistance of Dr Jens Madsen and Dr R. Mackay. NP ($0.2cm^2$) were pre-incubated for 90 minutes at 37°C, 5% CO_2 with 0.5µg nhSP-A in Tris buffered saline containing 5mM calcium (pH7.4). Alveolar macrophages (17,000/sample) in serum free phenol red free RPMI (Invitrogen) were added to the SP-A/NP preparation and incubated for a further 90 minutes at 37°C, 5% CO^2. Cells were washed with PBS with 1% BSA and 5mM EDTA (FACs buffer) and centrifuged at 400g for 10 minutes to remove excess particles. The cells

were then re-suspended in FACS buffer and kept on ice to prevent further phagocytosis. Trypan blue (0.4%; Sigma, UK) was added immediately before analysis to quench the fluorescence of extracellular NP. The cells were analysed (5000/sample) using flow cytometry (BD FACS Aria). Viability of AM following A-PS treatment was determined to be >90% using a trypan blue exclusion assay.

3.2.10. MTT assay

The MTT assay was based on a previously described protocol [292]. RAW264.7 cells were plated at a density of $1.5x10^4$ cells per well in a Nunclon 96 well plate (Fisher, UK) and incubated for 24 hours. The cells were then washed twice in SF RPMI. A-PS and U-PS (100nm) particles were prepared in TBS with 5mM calcium at 2.5 times the final concentration. The particles were then diluted in SF RPMI to the final concentration and the particle solution was added to the cells. The cells were then incubated for 1 or 24 hours at 37°C and 5% CO_2 in a humidified atmosphere. MTT (3-[4,5-dimethylthiazol-2-yl]-2,5 diphenyl tetrazolium bromide; Sigma, UK) solution was prepared by dissolving the tetrazolium salt in PBS to a concentration of 0.5mg/mL and passing through a 0.22µm sterile filter. The culture supernatant was removed and replaced with 50µl MTT solution and incubated for 4 hours at 37°C. Following this incubation the MTT solution was carefully removed and acidified isopropanol (0.1M hydrochloric acid in isopropanol) added to the cells. The plates were sealed with parafilm, gently agitated and incubated for at least an hour in the dark. The samples were then transferred to eppendorf tubes and centrifuged at 14,000g for 20 minutes as described previously [243]. Following centrifugation the samples were placed in a fresh 96 well plate and the absorbance read at 570nm using Molecular Devices SpectraMax 340pc plate reader.

3.2.11. Clonogenic assay

RAW264.7 cells were plated at a density of 500 cells per well in a Nunclon 6 well plate (Fisher Scientific, UK) in 3mL of growth medium. The cells were incubated for 24 hours at 37°C and 5% CO2 in a humidified atmosphere. Particles were prepared as described in section 3.2.10 and incubated with the cells for 24 hours. The particles were gently removed and replaced with 3mL fresh growth medium. The cells were then incubated undisturbed for 7 days at 37°C 5% CO_2. The medium was then removed, replaced with crystal violet staining solution (0.13% crystal violet, 5% formaldehyde, 5% ethanol in PBS) and incubated for 20 minutes in the dark. This solution was removed and excess stain was washed away with water. Colonies containing >50 cells were counted and the number of colonies in each treatment was normalised to the particle free control.

3.3. Results

3.3.1. Nanoparticle characterisation in PBS

3.3.1.1 Dynamic Light Scatter

The hydrodynamic diameter and zeta potential of the 100nm polystyrene particles was determined using dynamic light scattering (DLS) analysis (see Table 3.1). The results show that the diameter of the particles determined by DLS concurred with those reported by the manufacturer. The three 100nm polystyrene types were monodisperse in calcium free PBS. The carboxyl modified (C-PS) and unmodified (U-PS) particles both have one strong peak with z averages of 102.7nm and 116.2nm respectively; these peaks had narrow widths and low polydispersity indices (PDI) which are good indicators of a monodispersed sample. The zeta potential of both of these particles were also

highly negative which is indicative of non-aggregating particles. The amine modified polystyrene (A-PS) particles had a z average of 109.9nm and a positive zeta potential of 36.8mV; the width of the peak was broader and its subsequent intensity was less than the C-PS and U-PS particles. The PDI of the A-PS particles was also greater and their zeta potential was closer to zero than the other types of particles; however, the PDI of the A-PS particles was still within acceptable limits (<0.2) for monodispersed sample measurements. The results for the A-PS particles indicate that they are monodispersed but may have a greater propensity to aggregate than the C-PS or U-PS 100nm particles.

Particle	Nominal size	Reported size§	Z average* (nm)	PDI*	ZP* (mV)
U- PS	100nm	111nm	116.2 (±0.5508)	0.012 (±0.005)	-74.7 (±3.77)
C-PS	100nm	114nm	102.7 (±1.323)	0.006 (±0.004)	-69.6 (±6.76)
A-PS	100nm	100nm	109.9 (±4.813)	0.121 (±0.009)	+36.8 (±1.17)

Table 3.1. Characteristics of 100nm polystyrene particles
Abbreviations; PDI polydispersity index; ZP zeta potential; PS polystyrene
*Data represents mean (±standard deviation) of 3 measurements determined by DLS in PBS
§ diameter reported by manufacturer

3.3.2. Protein-Particle Interaction

3.3.2.1 rfhSP-D interaction with NP

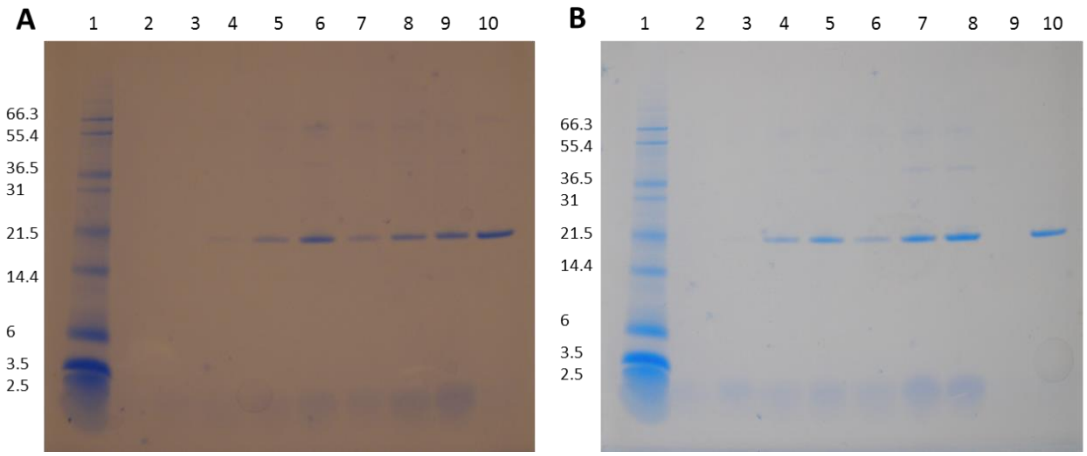

Figure 3.1. Effect of calcium on the adsorption of rfhSP-D to 3µm PS particles. Reduced SDS PAGE gels of A-PS and U-PS particles incubated with 5µg/mL rfhSP-D in the presence of **A**. EDTA and **B.** Calcium for 24 hours at 37°C. Lanes in **A**. represent **1**. Molecular weight marker; **2**. Blank; **3**. Washed tube; **4**. 1cm²/mL U-PS; **5**. 5cm²/mL U-PS; **6**. 10cm²/mL U-PS**; 7**. 1cm²/mL A-PS; **8**. 5cm²/mL A-PS; **9.** 10cm²/mL A-PS; **10.** 1µg rfhSP-D. Lanes in **B**. represent **1.** Molecular weight marker; **2.** Washed tube; **3**. 1cm²/mL U-PS; **4.** 5cm²/mL U-PS; **5**. 10cm²/mL U-PS; **6**. 1cm²/mL A-PS**; 7.** 5cm²/mL A-PS**; 8**. 10cm²/mL A-PS; **9.** blank; **10**. 1µg rfhSP-D

The first experiments that were carried out to investigate the interaction between rfhSP-D and particles showed that a significant amount of protein bound to the tube and rendered the results invalid (data not shown). The experimental protocol was adapted first through removing the pellet after each wash step into a clean tube and finally by using a low bind tube. In order to investigate whether the interaction of rfhSP-D with particles was mediated through calcium dependent binding of the CRD 3µm particles were incubated with rfhSP-D in the presence of calcium or EDTA. Figure 3.1 shows that similar levels of rfhSP-D adsorbs to 3µm PS particles in the presence or absence of calcium; this indicates that this is a calcium independent interaction and suggests that the protein-particle interaction is electrostatic. The amount of rfhSP-D binding to both 3µm A-PS and U-PS particles was dependent on the concentration of particles added, minimal absorption occurred at 1cm²/mL.

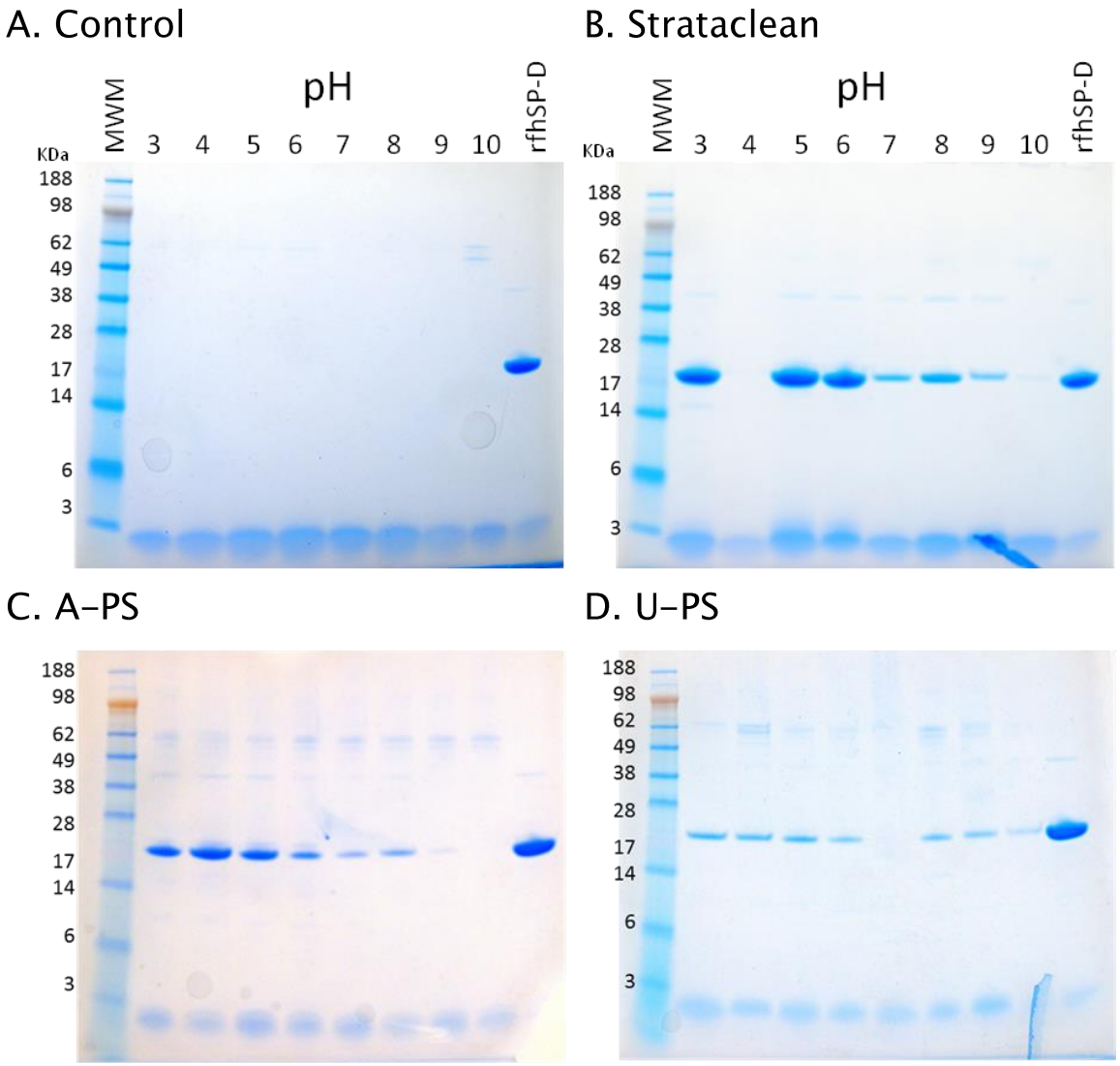

Figure 3.2. pH dependency of rfhSP-D association with PS particles; Reduced SDS PAGE gels of rfhSP-D (5µg/mL) association with 3µm PS particles (5cm²/mL) incubated in PBS at varying pH for 24 hours at 37°C. **A**. Controls (rfhSP-D incubated without particles); **B**. Strataclean; **C**. A-PS; **D**. U-PS. Each gel contains internal standard lanes of molecular weight markers (MWM) and 5µg rfhSP-D; Note that the pellet was lost on the pH4 strataclean gel.

In order to investigate the electrostatic potential of this interaction A-PS and U-PS 3µm PS particles were incubated with rfhSP-D in buffers adjusted to pHs between 3 and 10. Strataclean, a slurry of hydroxylated silica particles used to concentrate proteins in solution was used as a control. Figure 3.2 shows that decreasing the pH increases the amount of rfhSP-D associated with A-PS particles and strataclean. At pHs above 8 there is little/no rfhSP-D associating with A-PS particles. Maximal association of rfhSP-D with 3 µm A-PS particles

occurred at pH4. The U-PS particles show little or no association at pH7 but at both higher and lower pH small amounts of protein association is evident. Control samples were run in parallel to these experiments by incubating rfhSP-D in the absence of particles under the same conditions. These show small amounts of two high molecular weight proteins in the pH10 treatment.

The adsorption of rfhSP-D onto smaller particles was then investigated. A preliminary experiment using 100-1000nm COOH particles showed that the protocol used for the 3μm particles needed to be developed further to investigate particles with diameters of less than 500nm; the centrifugal force used to pellet the larger particles proved insufficient to remove these micro- and nanoparticles from solution (data not shown).

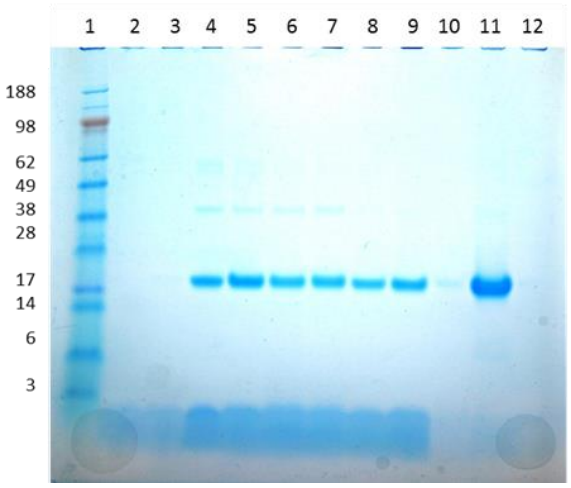

Figure 3.3. Calcium dependent binding of rfhSP-D to 100nm. Reduced SDS PAGE of adsorption of 100nm polystyrene particles (50cm2/mL) to rfhSP-D (10μg/mL). **1**. Molecular weight marker; **2**. No Particles (Ca); **3**.No Particles (EDTA) **4**. A-PS (Ca); **5**. A-PS (EDTA); **6**. C-PS (Ca); **7**. C-PS (EDTA); **8**. U-PS (Ca); **9**. U-PS (EDTA); **10**. Blank; **11**. 5μg rfhSP-D; **12**. Blank

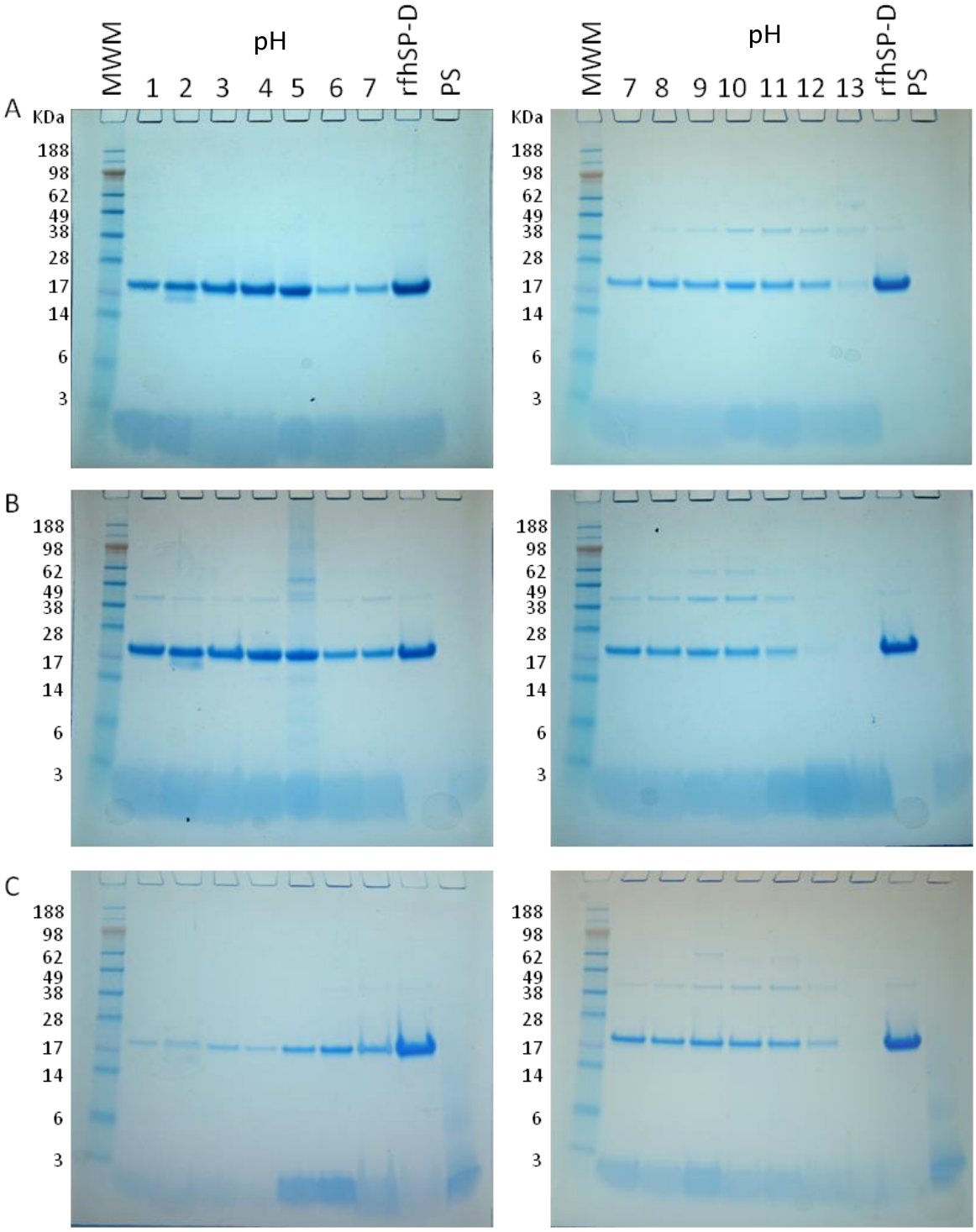

Figure 3.4. pH dependency of the adsorption of rfhSP-D to 100nm polystyrene particles. Reduced SDS gels of rfhSP-D (10µg/mL) adsorbed to 50cm²/mL of **A**. U-PS; **B**. C-PS and **C**. A-PS 100nm polystyrene particles in PBS containing 5mM EDTA adjusted to pH1-13 (1 hour at RT). Each gel contains internal control lanes of molecular weight markers (MWM), 5µg rfhSP-D and 25cm² of respective particles (PS).

After optimisation the effect of calcium and pH on rfhSP-D adsorption to 100nm particles was investigated. Figure 3.3 shows that rfhSP-D adsorption to 100nm U-PS, C-PS and A-PS particles occurs in the absence of calcium. In fact, in all three cases adsorption of rfhSP-D was slightly enhanced in the presence of EDTA. The effect of pH on the adsorption of rfhSP-D to these 100nm particles was also assessed. The results show that optimal adsorption of rfhSP-D to U-PS or C-PS particles occurs between pH1 and 5 (Figure 3.4A and B). In contrast optimum adsorption occurred between pH6 and 10 for the A-PS 100nm particles. The pH adsorption profiles for the 100nm particles correlate with their zeta potentials (see Table 3.1).

TEM has also been used to identify rfhSP-D association with nanoparticles. U-PS 100nm polystyrene particles were incubated in the presence or absence of rfhSP-D and these samples were analysed by TEM. The micrographs, shown in Figure 3.5, show a corona around the particles incubated with rfhSP-D. This corona appears to double the size of the particle which suggests that the rfhSP-D may be forming multiple layers around the particle.

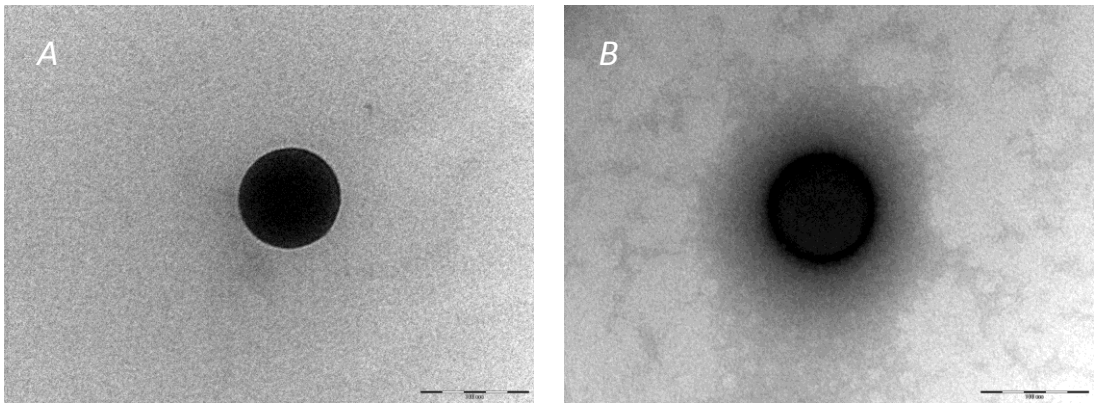

Figure 3.5. TEM micrographs of 100nm U-PS polystyrene particles (50cm²/mL) in the absence (A) or presence of rfhSP-D (10µg/mL) in PBS containing 5mM EDTA (2 hours at RT). Scale bar represents 100nm.

Reduced SDS PAGE of rfhSP-D incubated with 200nm particles (24 hours) resulted in the formation of bands corresponding to the monomeric, dimeric and trimeric forms of rfhSP-D at around 20, 40 and 60kDa respectively. Moreover, bands representing proteins with a higher molecular mass were also evident (see Figure 3.6). These bands were not present in the control samples (Lane 2 and 10) or with particles alone (data not shown). This suggests that the particles cause a fundamental change in the structure of the protein leading to the formation of higher order oligomers. This interaction was investigated further by incubating these 200nm particles for different lengths of time and resolving this interaction with both reduced and non-reduced SDS PAGE (Figure 3.7). The 200nm A-PS particles consistently associated with less rfhSP-D than either U-PS or C-PS particles at each time point. The intensity of the monomeric band was relatively stable between time points; this indicates that the interaction is a rapid process with the particles reaching maximal protein saturation within 1 minute and lasting up to 19 days (4°C). The higher order oligomers were less evident on the earliest time point and these bands increased in intensity in a time dependent manner. This indicates that the formation of the oligomers occurs after protein-particle association.

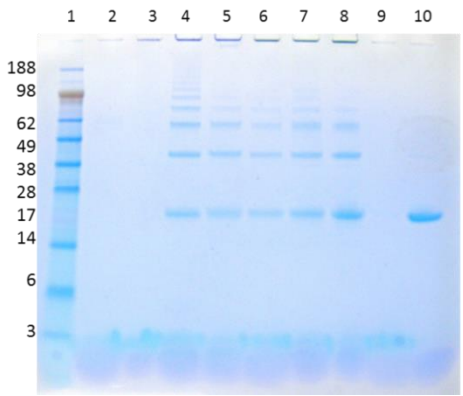

Figure 3.6. Absorption of rfhSP-D to 200nm PS: Particle association with rfhSP-D after incubation at 37°C. Reduced 12% Bis-Tris SDS PAGE gel. Lanes numbers represent **1.** Molecular weight marker; **2**. Washed tube; **3**. 25cm²/mL A-PS; **4.** 50cm²/mL A-PS; **5.** 100cm²/mL A-PS; **6.** 25cm²/mL C-PS; **7.** 50cm²/mL C-PS**; 8.** 100cm²/mL C-PS; **9.** Blank; **10.** 5µg rfhSP-D.

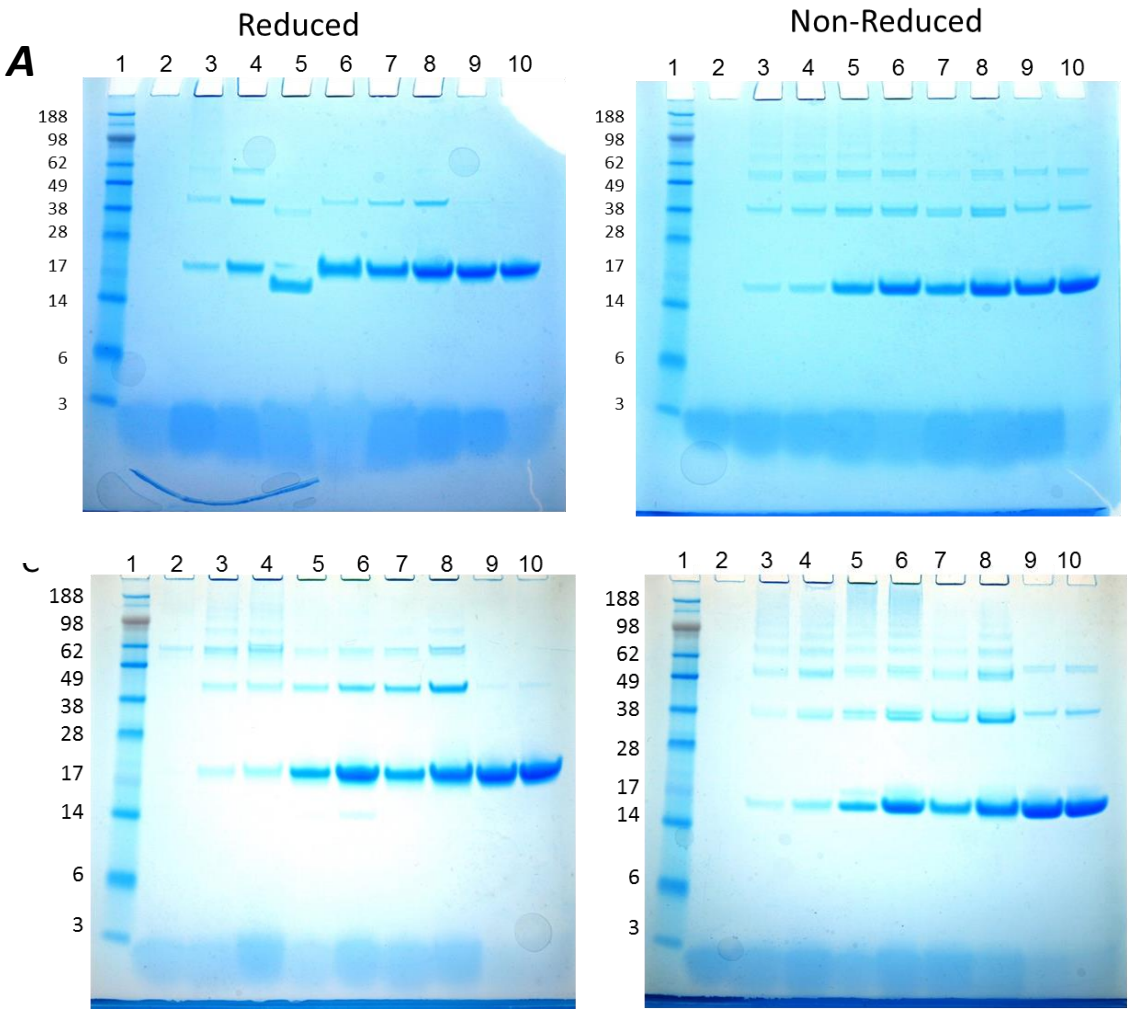

Figure 3.7. Time dependency of the absorption of rfhSP-D to 200nm PS: Particle association with rfhSP-D (10µg/mL) after **A**. less than 1 minute; and **B**. 19 days at 4°C. 12% Bis-Tris SDS PAGE gels were run under reducing (left) and non-reducing (right) conditions. Note the differences in loading order. Lanes numbers. represent **1.** Molecular weight marker; **2**. Washed tube; **3**. 25cm²/mL A-PS; **4.** 50cm²/mL A-PS; **5**. 25cm²/mL C-PS; **6**. 50cm²/mL C-PS; **7.** 25cm²/mL U-PS; **8**. 50m²/mL U-PS; **9**. Strataclean **10**. 5µg rfhSP-D.

3.3.2.1.1. Co-localisation of rfhSP-D and particles in A549 cells

The immunofluorescent co-localisation assay was used to determine whether rfhSP-D co-localises with particles in the epithelial A549 cell. A549 cells were originally derived from a lung carcinoma [293] and are often used as a model for type II alveolar epithelial cells to study the impact of particles on pulmonary epithelial cells [294-296]. Interestingly, rfhSP-D could not be detected in the cells when the 200nm A-PS particles were not present and increases in the concentration of particles resulted in dose dependent increases

in the amount of rfhSP-D observed (see Figure 3.8). Moreover, based on these immunofluorescent pictures, there also appeared to be increases in the amount of particles associating with the cells with increasing concentrations of rfhSP-D. This was particularly evident in the highest studied concentration of both particle and protein (25cm^2/mL and 10µg/mL respectively). There was no unspecific binding of the secondary antibody to the cells, protein or particles (data not shown). The distinct areas of particles within the cells in the fluorescent micrographs indicate that the fluorescent dye has remained encapsulated within the particles.

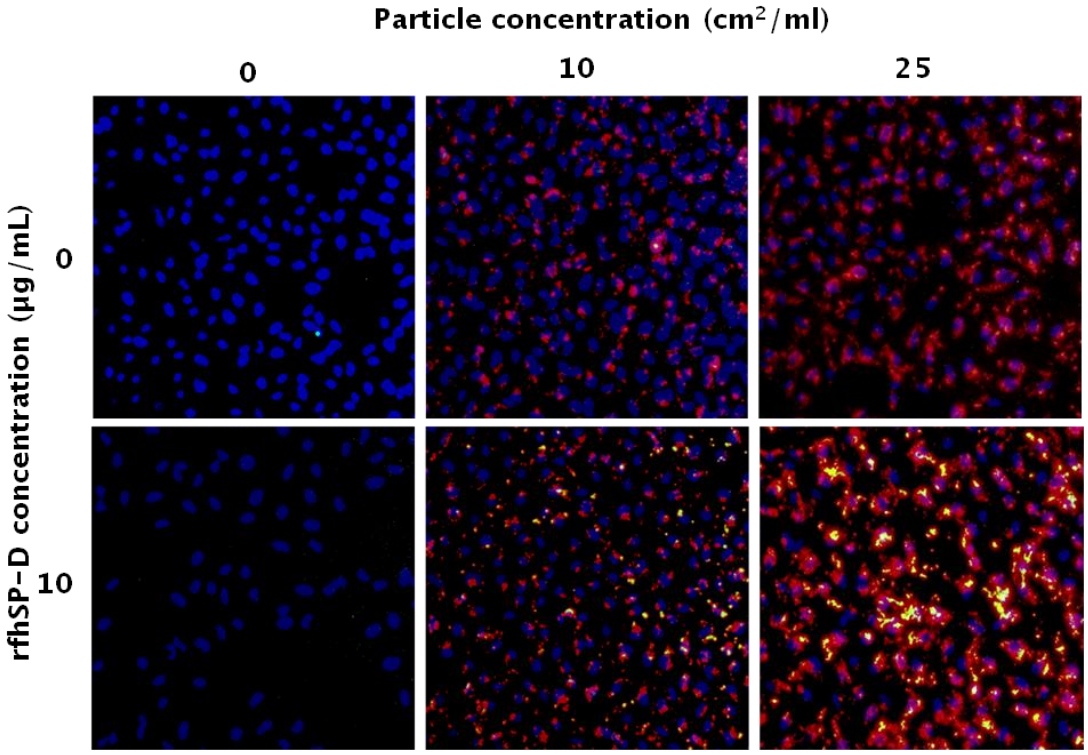

Figure 3.8. Immunofluorescent co-localisation of rfhSP-D and 200nm particles with A549 cells; A549 cells treated with 0, 10 or 25cm^2/mL of 200nm A-PS particles (red) in the presence or absence of 10µg/mL rfhSP-D (green). Fluorescent images represent overlay of UV, rhodamine and FITC images taken at x200 magnification. Reproduced with permission from [291] (Licence number: 3235320787551).

3.3.2.2 Native SP-A and SP-D absorption to NP

The absorption of nhSP-A and nhSP-D to 100nm A-PS, C-PS and U-PS were also studied. Particles were incubated with 5μg/mL of either protein in TBS with 5mM calcium or 5mM EDTA then washed three times in the relevant buffer. The results, presented in Figure 3.9A, show that nhSP-A associates more strongly with the C-PS and U-PS particles compared to the A-PS particles. Moreover, in each of these particles the presence of calcium enhances the amount of protein recovered (better retrieval due to aggregation?). The amount of nhSP-A recovered from the A-PS particles was only slightly increased compared to the background control. Figure 3.9B shows that SP-D associates most strongly with each particle type in the presence of EDTA rather than calcium. nhSP-D associated with U-PS >C-PS >A-PS. In the presence of EDTA bands at 62kDa and 100kDa are apparent which are not evident in the other treatments.

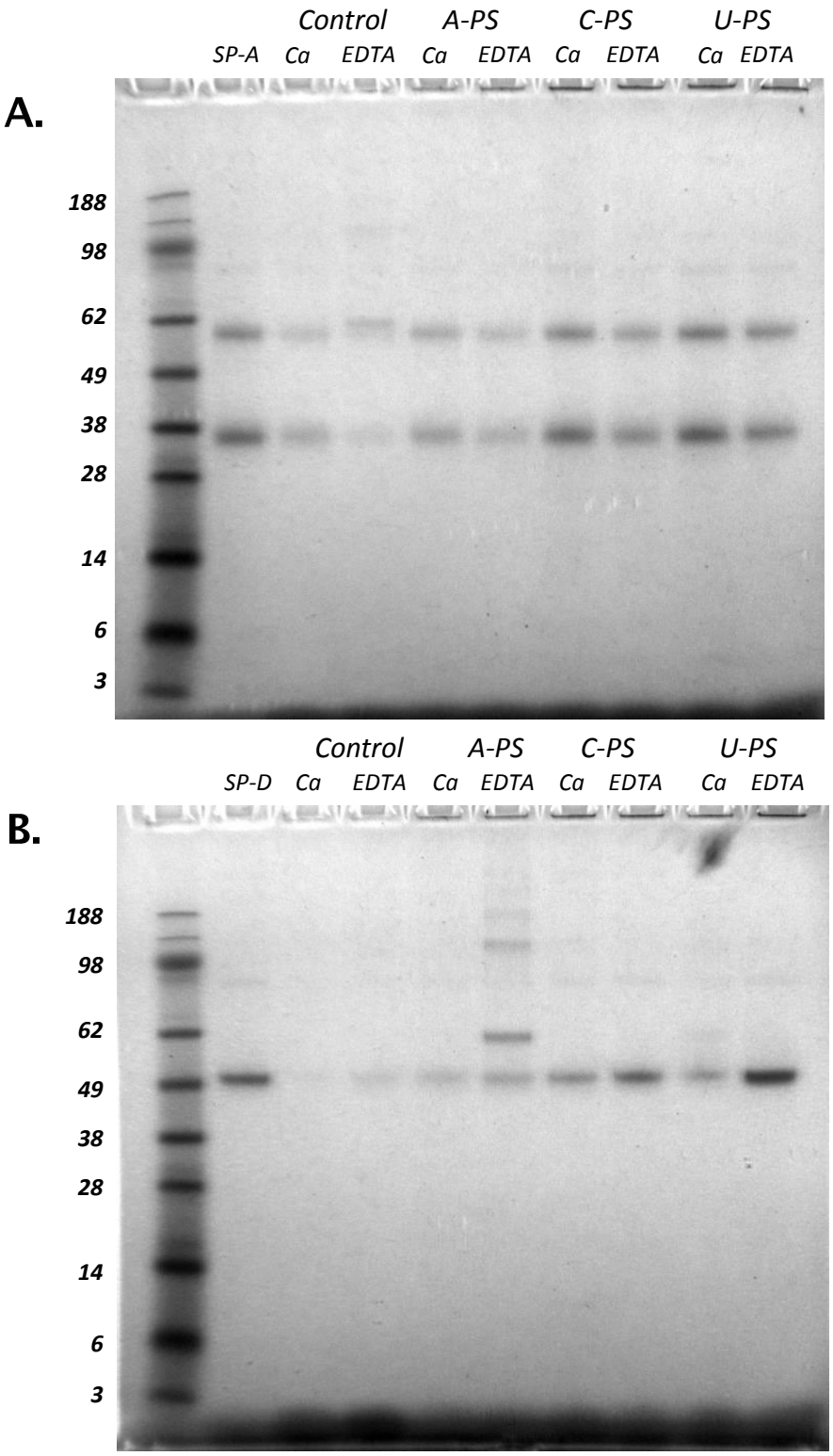

Figure 3.9. Native Surfactant Protein absorption to 100nm NP; Absorption of 5μg/mL A. nhSP-A and B. nhSP-D to 10cm²/mL 100nm particles for 24 hours in TBS containing 5mM calcium (Ca) or 5mM EDTA (EDTA). SP-A/D denotes positive control of 5μg of respective protein. Calcium and EDTA "control" samples represent protein incubation in the absence of added nanoparticles.

3.3.3. Characterisation of NP and protein aggregation

The ability of SP-A, SP-D and rfhSP-D to aggregate the U-PS particles was evaluated using DLS. The results show that the incubation of U-PS particles with SP-A results in a rapid and large increase in the Z average of the particles in the presence of calcium (see Figure 3.10A). This increase continued up to the 1 hour measurement time studied where a 13.5 fold increase in particle size was observed. In the presence of EDTA rather than calcium the size distribution increased by 14.8% over the same period. The incubation of U-PS with SP-D in the presence of calcium also resulted in an increase in the Z average of the particles (see Figure 3.10B). This 51.4% increase was much less pronounced than the change induced by SP-A in the presence of calcium. In the presence of EDTA, SP-D increased U-PS particle size by 11.6%. The incubation of U-PS particles with rfhSP-D resulted in a gradual increase in particle size over 1 hour this culminated in a 3% increase in EDTA and 5.5% increase in calcium over the hour (see Figure 3.10C). The incubation of U-PS with BSA also resulted in small 3.7% and 4.9% increases in particle size in TBS with EDTA and calcium respectively over 1 hour (see Figure 3.10D). In the presence of calcium the degree of change following protein incubation was SP-A>SP-D>rfhSP-D>BSA. C-PS particles showed a similar propensity to aggregate in a calcium enhanced fashion when incubated with SP-A (data not shown).

The ability of these proteins to alter A-PS particle size in the presence of calcium was also evaluated using DLS (see Figure 3.11). The incubation of A-PS with SP-A resulted in a rapid increase in the size distribution. This increase stabilised at around 10 minutes with 2.2 fold increase in particle size. SP-D also resulted in an increase of A-PS particle size which although was initially more gradual than the increase induced by SP-A culminated in a greater 2.9 fold increase at 1 hour.

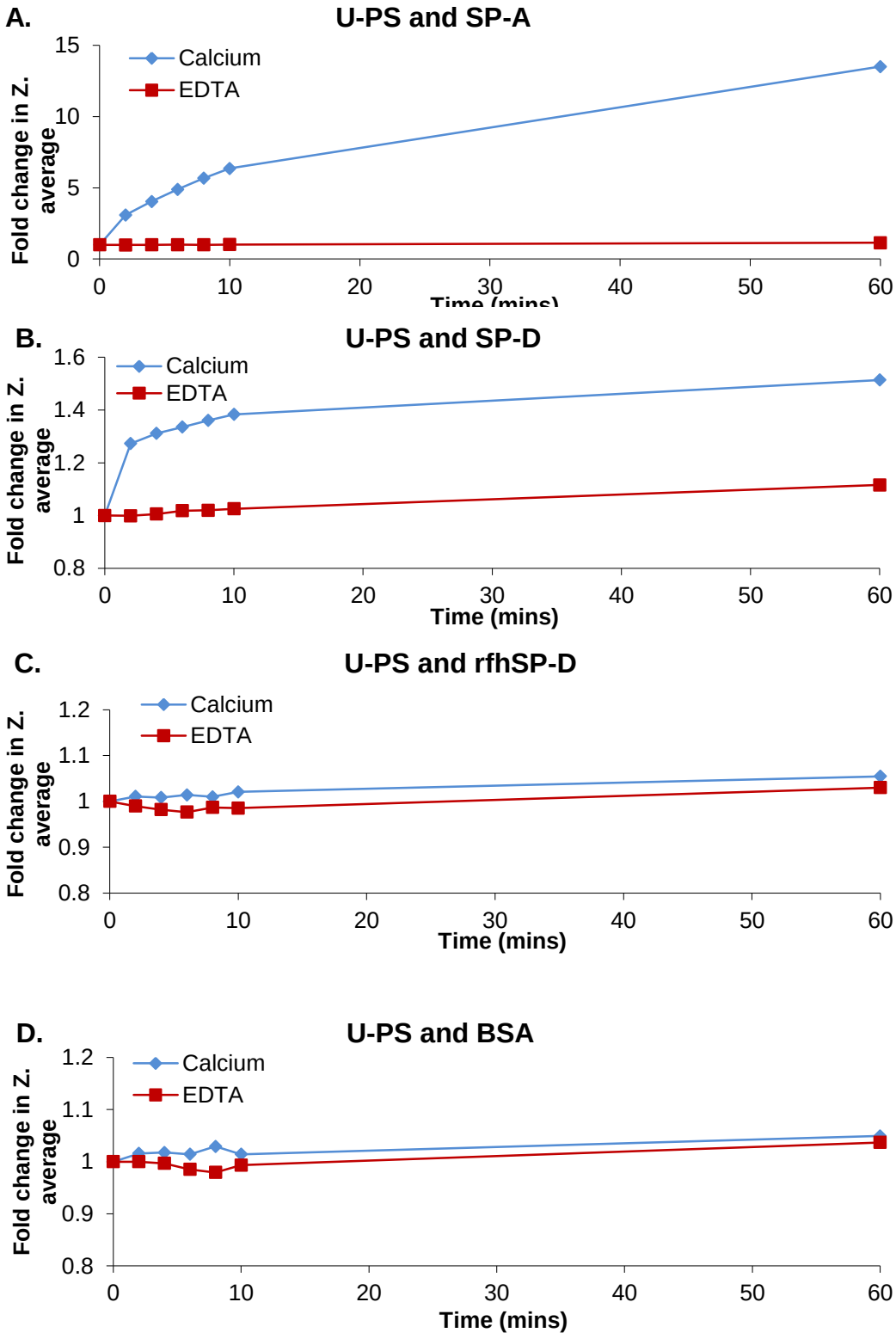

Figure 3.10. Effect of proteins on the size of 100nm U-PS over time in TBS with 5mM Ca or 5mM EDTA. SP-A data representative from three similar experiments. BSA and rfhSP-D data representative data from two similar experiments. SP-D data from one experiment.

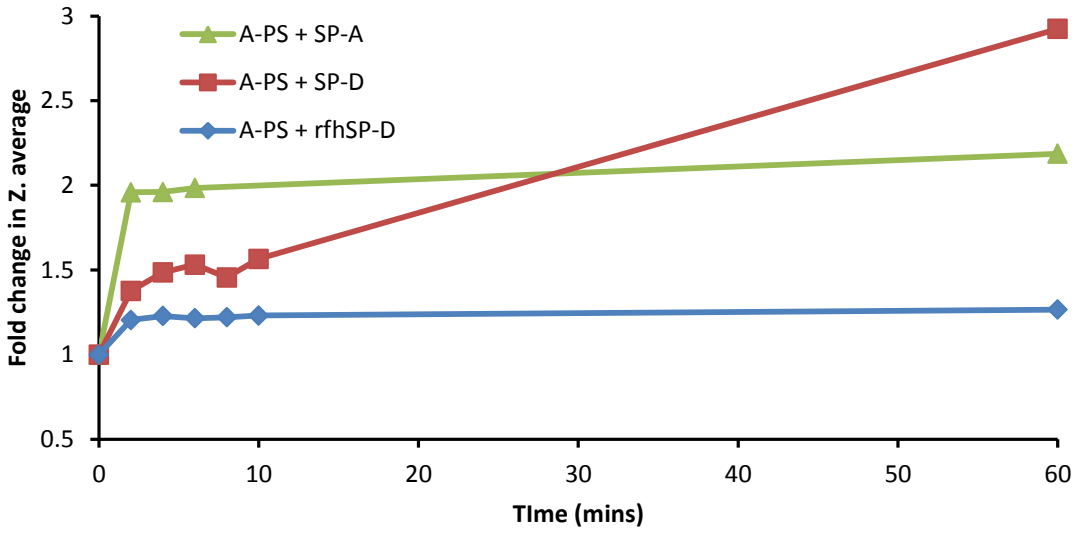

Figure 3.11. Effect of proteins on A-PS size distribution in TBS with 5mM calcium. SP-A data representative from three similar experiments. SP-D and rfhSP-D data representative data from two similar experiments.

The particle sizes of A-PS and U-PS particles following incubation with SP-A in water with and without 5mM Ca^{2+} was also determined by DLS (see Table 3.2). The incubation of 100nm A-PS particles with SP-A for 24 hours resulted in a 49.1% increase in particle size in the absence of calcium but a 4.1fold increase in the presence of calcium. The incubation of U-PS particles with SP-A resulted in a 5.7 fold increase in particle size after 24 hours in calcium but only a 1% increase in the absence of calcium.

	Size (nm)			
	No calcium		5mM Ca^{2+}	
NP	**d2(nm)**	**Δd(%)**	**d2(nm)**	**Δd(%)**
A-PS	100.6	49.1	96.0	405.5
A-PS + SP-A	150.0		389.3	
U-PS	120.8	1.0	117.3	574.7
U-PS + SP-A	122.0		674.1	

Table 3.2. Size of particles (2.5cm^2/mL) before and after mixing with 10μg/mL nhSP-A in milliQ water with or without 5mM calcium, Δd = (d(t)/d(t=0)).

The percent transmittance at 350nm was also measured immediately following the addition of SP-A to A-PS, C-PS and U-PS suspensions. The relative transmittance at this wavelength has previously been used to measure the surfactant protein mediated aggregation of viral particles such as IAV. A reduction of the relative transmittance at this wavelength was consistent with enhanced aggregation/turbidity of the surfactant protein/IAV suspensions [297]. It was therefore used to assess the aggregation of NP in TBS with Ca^{2+} or EDTA following the addition of SP-A. Importantly, unlike with DLS the relative transmittance did not change following the addition of SP-A to either Calcium or EDTA containing buffers (see Figure 3.12A). In calcium and EDTA buffers the addition of SP-A to A-PS resulted in a small reduction in the relative transmittance of approximately 2.5% (see Figure 3.12B). The degree of C-PS and U-PS aggregation was greatest in calcium containing rather than EDTA buffers;

although a reduction of transmittance was observed for both C-PS and U-PS in TBS with EDTA following the addition of SP-A. The degree of SP-A induced aggregation in the presence of calcium was greatest for the U-PS particles followed by C-PS then A-PS particles. In order to determine whether SP-A was associating with the A-PS particles the zeta potential of A-PS particles was measured in TBS with calcium before and after the addition of SP-A. The results, in Table 3.3, show that the positively charged A-PS particles adopt a negative zeta potential following incubation with SP-A. Similar results were observed following the addition of SP-A to A-PS particles in milliQ water with or without 5mM $CaCl_2$ (data not shown). Interestingly, A-PS in TBS with calcium also adopt a slight negative charge immediately following the addition of BSA.

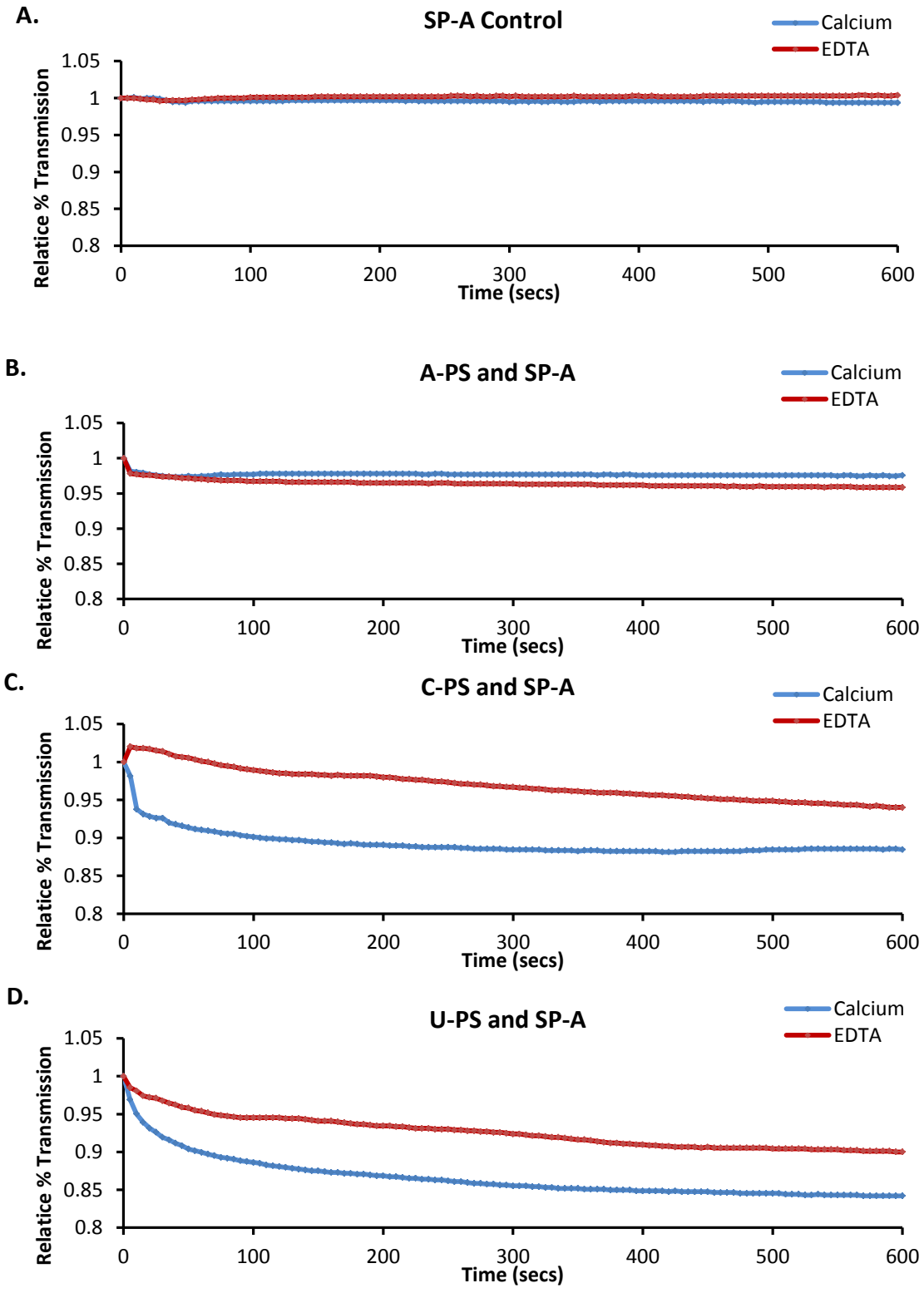

Figure 3.12. Turbidity of NP and SP-A in TBS with Calcium or EDTA.
Spectrophotometry of NP and SP-A preparations measured at OD350nm; Data representative of three similar independent experiments using non-fluorescent particles.

	Zeta potential
A-PS	20.4
A-PS+SP-A	-14.9
A-PS+BSA	-6.8

Table 3.3: The zeta potential of A-PS particles following the addition of SP-A (5µg/mL) or BSA (5µg/mL) in TBS with 5mM calcium.

In order to visualise SP-A induced particle aggregation fluorescent 100nm U-PS particles were incubated for 1 hour at 37°C with SP-A in PBS with or without calcium then placed on microscopy slides and photomicrographs taken using a fluorescent microscope. The micrographs show that the U-PS particles remained stable either in the presence or absence of calcium (see Figure 3.13A and B). The incubation of U-PS particles with SP-A in the absence of calcium resulted in a small degree of particle aggregation (see Figure 3.13C); however, this aggregation was greatly enhanced in the presence of 2mM calcium and SP-A. Micrographs with U-PS and BSA showed similar dispersal to the U-PS alone (data not shown). Similar results were also observed for C-PS particles and SP-A or BSA with and without calcium and in TBS buffer with calcium or EDTA (data not shown).

In order to visualise the effect of SP-A on A-PS aggregation, fluorescent 100nm A-PS particles were incubated in TBS with calcium with and without SP-A. These experiments were conducted at 37°C to mimic the physiological conditions of the *in vitro* experiments. The results showed that the A-PS particles underwent self-agglomeration in physiological conditions (Figure 3.14A) and that the addition of SP-A inhibited this agglomeration (Figure 3.14B). The addition of BSA did not appear to limit the self-agglomeration of A-PS particles (data not shown).

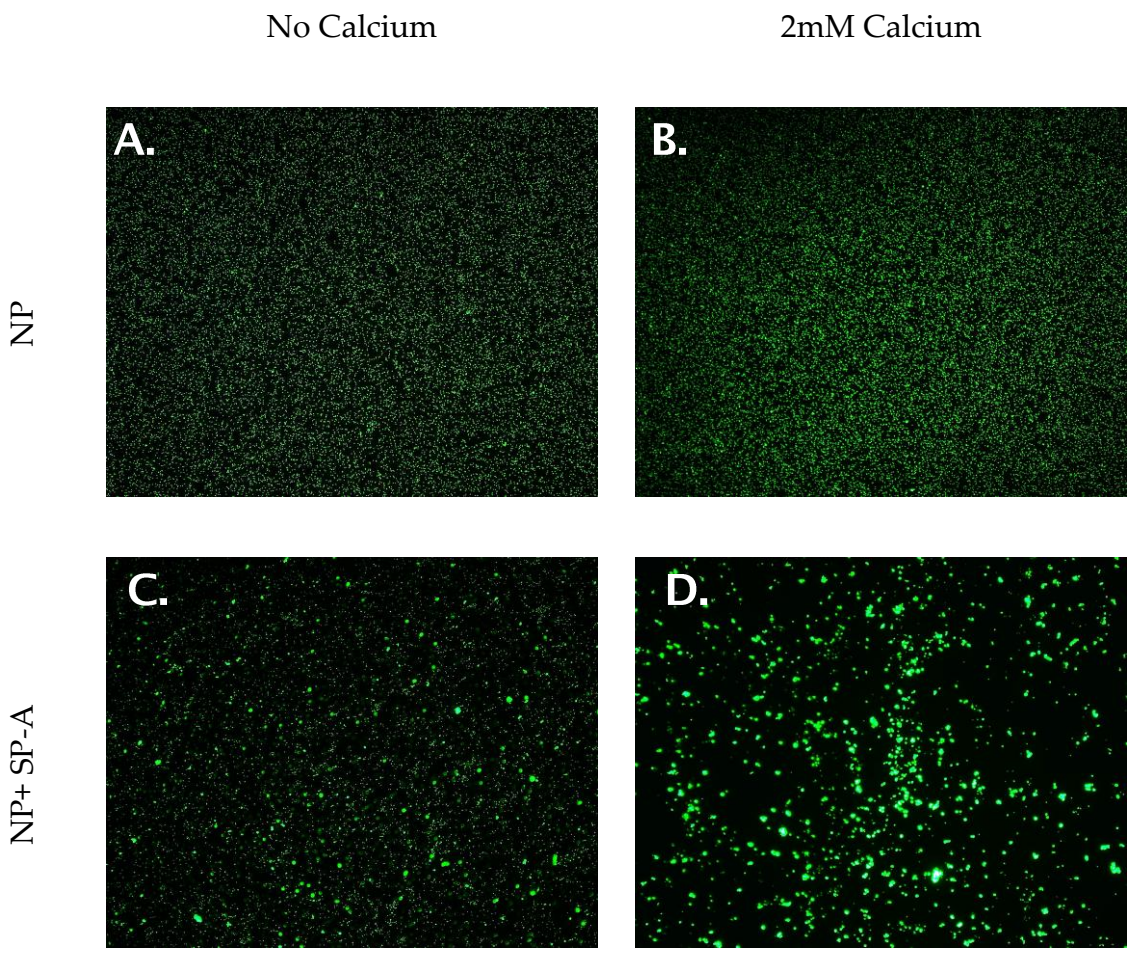

Figure 3.13. Aggregation of U-PS by nhSP-A is enhanced in the presence of calcium. The effect of SP-A (10μg/mL) in the presence and absence of calcium (2mM) in PBS on the aggregation of 100nm U-PS particles (3.8cm2/mL) was evaluated using fluorescent microscopy. U-PS were incubated for 1 hour at 37°C before being mounted onto slides for microscopy. Pictures were taken at x400 magnification.

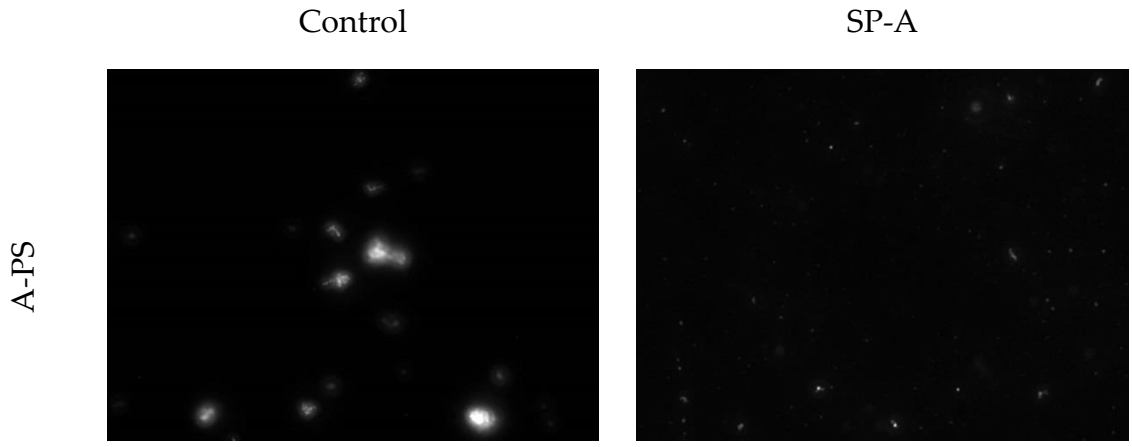

Figure 3.14: Effect of nhSP-A on the aggregation of A-PS particles; A-PS were incubated for 1 hour in TBS with 5mM calcium at 37°C before being mounted onto slides for microscopy. Pictures were taken at x400 magnification.

3.3.4. Effect of Surfactant Proteins on NP uptake

3.3.4.1 NP characterisation

	A-PS	**U-PS**
mQH_2O	106.9 ± 2.3	120.8 ± 0.6
TBS + 5 mM Ca	100.9 ± 0.6	123.9 ± 2.0
SF RPMI	124.8 ± 8.0	123.9 ± 1.3

Table 3.4: Size characterisation of A-PS and U-PS particles in different media. Data represents mean of 3 measurements ± Stdev taken at room temperature.

The size measurements of A-PS and U-PS particles in milliQ water, TBS with calcium and SF RPMI at room temperature are shown in Table 3.4. The results show that the size distribution of U-PS particles increase slightly in both TBS and SF RPMI buffers compared to in water which may be due to ions surrounding the particle and thus increasing the hydrodynamic diameter. Interestingly, the hydrodynamic diameter of the A-PS particles was slightly larger in water compared to TBS buffer. A-PS particles appeared to remain relatively monodispersed in SF RPMI and TBS with calcium at room temperature.

3.3.4.2 Effect of nhSP-A on NP uptake in RAW264.7 cells

The effect of nhSP-A absorption on the uptake of A-PS and U-PS particles by RAW264.7 was analysed (see Figure 3.15 and Figure 3.16). Trypan blue was used to quench the fluorescence from extracellular nanoparticles. Two measures of NP uptake were compared following A-PS or U-PS incubation with SP-A (see Figure 3.16A and B). The results show that nhSP-A at a concentration of 20μg/mL resulted in a significant 96.9% increase in U-PS uptake as measured by the number of particles per cell (MFI; p=0.028 t test). However, there was also a concomitant significant 11.9% reduction in the number of cells (%) containing nanoparticles following U-PS incubation with SP-A (p=0.045; t test). Bovine serum albumin (BSA) was used as a non-specific protein control; BSA resulted in a 3.8% increase in MFI and 1.6% decrease in the percent of NP containing cells. Both these differences were not statistically significant with associated p values of 0.440 and 0.341 respectively (t test). The effect of foetal bovine serum (FBS) on U-PS uptake was also examined. FBS resulted in 56.1% and 62.4% reductions in the %NP+ and MFI respectively. These reductions were highly statistically significant with associated p values of 0.006 and 0.001 respectively (t test).

Pre-incubation with nhSP-A resulted in 87.7% and 91.5% reductions in A-PS uptake as measured by the %NP+ cells and MFI. These reductions were highly statistically significant with associated p values of <0.001. Pre-incubation of A-PS with BSA resulted in 13.0% and 9.1% respective increases in %NP+ and MFI respectively. However, these increases were not statistically significant with associated p values of 0.378 and 0.326 respectively (t test). Pre-incubation of A-PS with FBS resulted in 2.4 and 2.2 fold increases in NP+ and MFI respectively. However, these increases did not reach statistical significance with associated p values of 0.189 and 0.290 respectively (t test).

Later experiments therefore used MFI to examine the effect of SP-A on NP uptake. nhSP-A resulted in a dose dependent increase in the number of U-PS particles taken up per cell (i.e. MFI). This increase started at a SP-A concentration of 2.5μg/mL and became significant ≥10μg/mL ($p<0.050$; ANOVA with LSD post hoc). On the other hand, the pre-incubation of nhSP-A with A-PS resulted in a dose dependent reduction in A-PS uptake by RAW264.7 cells. This reduction was evident at the lowest concentration of nhSP-A studied (0.039μg/mL) and became significant from 0.156μg/mL ($p=0.007$ ANOVA with LSD post hoc). Maximal inhibition of A-PS uptake occurred at ≥1.25 μg/mL with approximately 85-90% of A-PS uptake being inhibited at these concentrations.

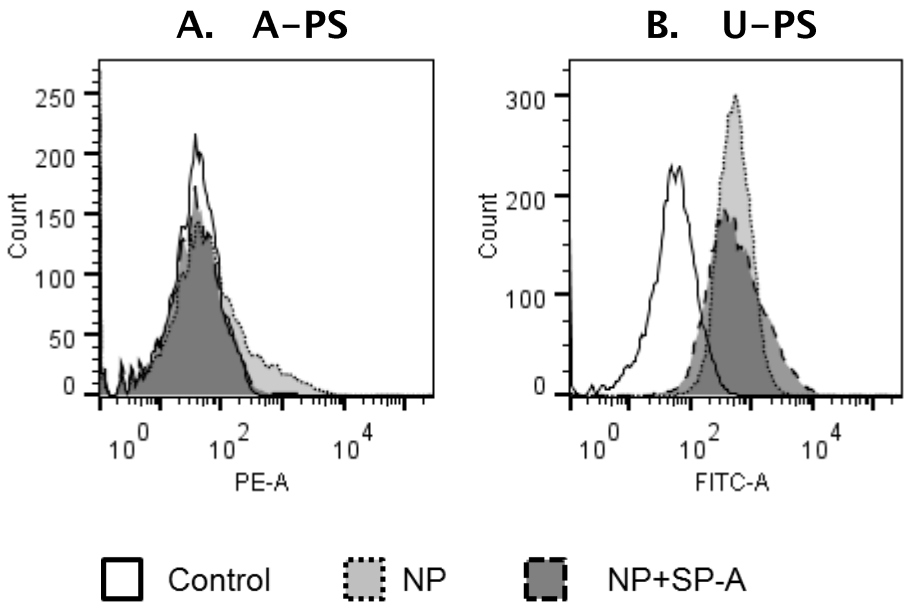

Figure 3.15: Effect of nhSP-A on 100nm A-PS and U-PS uptake in RAW264.7 cells. Flow cytometry histograms of **A.** A-PS and **B.** U-PS uptake following pre-incubation with 20μg/mL SP-A (dark grey shaded area with dashed line). Nanoparticle alone shown with dotted line (light grey shaded area). Nanoparticle free control shown as solid line (unshaded). Histograms represent data from at least three experiments conducted in duplicate.

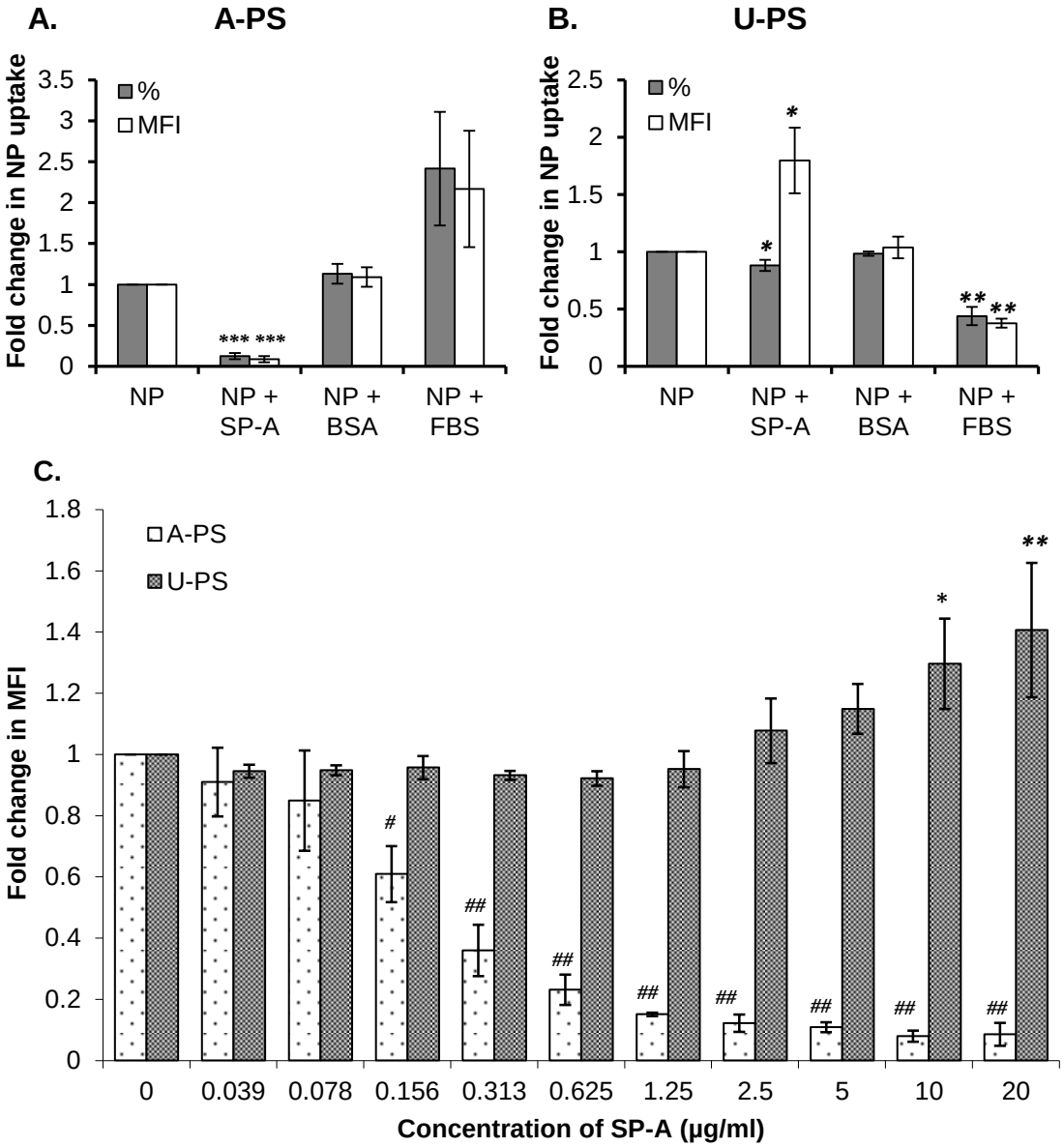

Figure 3.16. Effect of nhSP-A on A-PS and U-PS uptake in RAW264.7 cells.
Uptake of **A.** A-PS and **B.** U-PS in RAW264.7 cells following NP and protein pre-incubation measured by percent of NP containing cells (%) and mean fluorescent intensity (MFI). Data represents mean of four independent experiments conducted in duplicate (±SEM). *p<0.05 vs. NP control ** p<0.01 vs. NP control *** p<0.001 vs. NP control; Statistics determined using independent t test. **C.** Dose dependent effects of nhSP-A on A-PS and U-PS uptake in RAW264.7 cells. Data represents mean of four independent experiments conducted in duplicate (±SEM). * p<0.05 vs. U-PS only control; **p=0.004 vs. U-PS only control; # p=0.007 vs. A-PS only control; ## p<0.001 vs. A-PS only control. Statistics determined using ANOVA with LSD post hoc.

3.3.4.3 Effect of SP-A on NP uptake in AM from WT and SP-A$^{-/-}$ mice

In order to compare particle uptake in alveolar macrophages from wild type and SP-A deficient (SP-A$^{-/-}$) mice each treatment was normalised to the MFI of wild type mice for the respective particles. A-PS uptake was increased by 30% in the alveolar macrophages (AM) of SP-A deficient compared to wild type mice (see Figure 3.17). This difference was statistically significant with a p value of 0.017 (t test). The pre-incubation of A-PS with exogenous SP-A reduced NP uptake by 74% in the AM of wild type mice and 85% in the AM of SP-A deficient mice; these differences were highly statistically significant with p values of ≤0.001 (t test).

There was no difference in the uptake of unmodified polystyrene NP between wild type and SP-A deficient mice (p=0.997; t test). Although SP-A pre-incubation with these NP enhanced uptake by 17% in AM of wild type and 13% in AM of SP-A deficient mice, these differences were not statistically significant with respective p values of p=0.106 and 0.429.

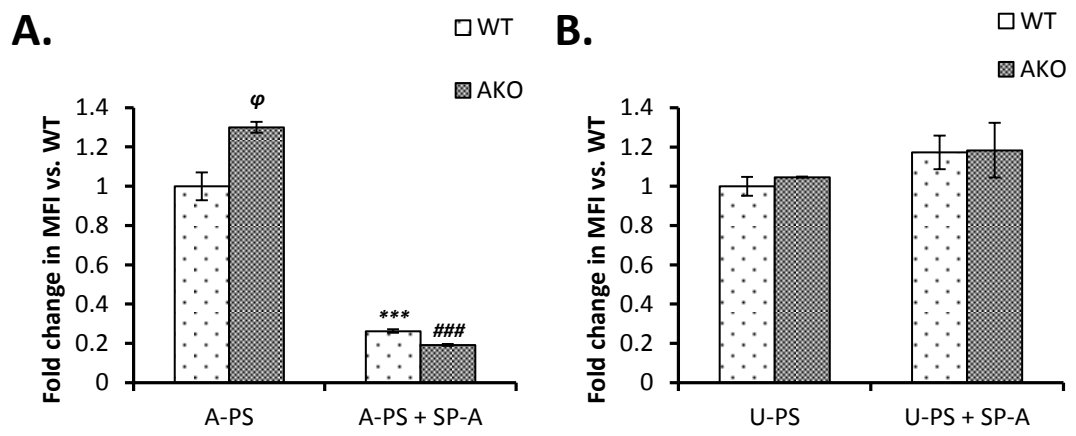

Figure 3.17. NP uptake in the alveolar macrophages of wild type (WT) and SP-A deficient mice (AKO): A. Amine and B. Unmodified 100nm polystyrene uptake in the alveolar macrophages of wild type and SP-A deficient mice. Statistics were determined using independent t test; ϕ p=0.017 vs. WT NP treatment; *** p≤0.001 vs. WT NP treatment; ### p≤0.001 vs. AKO NP treatment. Data normalised to the wild type nanoparticle only control. Extracellular fluorescence quenched with trypan blue.

3.3.4.4 Effect of SP-D on NP uptake in AM of WT and SP-D$^{-/-}$ mice

The effect of exogenous SP-D on the uptake of 100nm A-PS particles was also analysed. The uptake of A-PS in the AM of SP-D deficient mice was reduced by 94.5% compared to those from wild type mice (see Figure 3.18). This decrease was highly statistically significant with an associated p value of 0.008 (t test). In fact, less than 1% of cells contained NP in SP-D deficient macrophages. Following pre-incubation with nhSP-D there was a 5.7 fold increase in the percent of cells containing nanoparticles (%NP+) over the nanoparticle control in AM from SP-D deficient mice. This increase was statistically significant with an associated p value of 0.022 (t test). There was also an increase in the MFI following pre-incubation of A-PS with nhSP-D however, this increase did not reach statistical significance (p=0.080; t test data not shown). Pre-incubation of A-PS with rfhSP-D resulted in a 3.4% increase in NP+ cells in SP-D$^{-/-}$ AM representative of a 5.4 fold increase over the A-PS control; however, this increase did not reach statistical significance (p=0.112; t

test). Pre-incubation of A-PS with FBS resulted in a 2% increase in NP containing cells or 3.6 fold increase compared to the control. This increase was statistically significant with an associated p value of 0.046 (t test). BSA had no significant effect on A-PS uptake in AM from SP-D deficient mice (p=0.808).

In the AM from WT mice the pre-incubation of A-PS with nhSP-D or rfhSP-D resulted in 27.7% and 27.3% respective reductions in A-PS uptake compared to the NP control. However, these reductions were not statistically significant with associated p values of 0.286 and 0.279 respectively. BSA also resulted in a non-significant 20.3% reduction in A-PS uptake in WT AM (p=0.408). The pre-incubation of FBS with A-PS resulted in a 62.2% increase in A-PS uptake; however this increase was not statistically significant with an associated p value of 0.366 (t test).

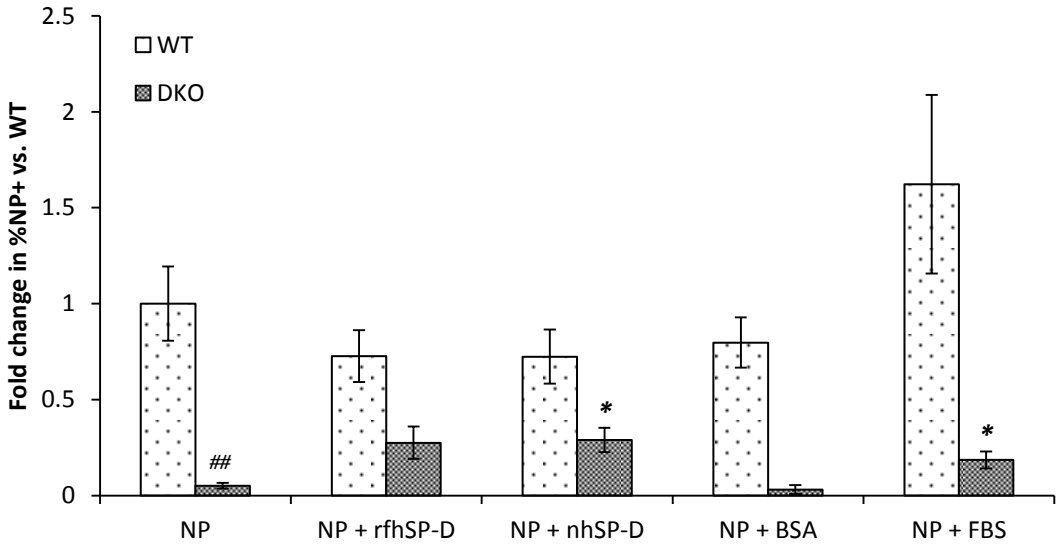

Figure 3.18. Effect of SP-D on the *in vitro* uptake of 100nm A-PS particles in alveolar macrophages from wild type (WT) and SP-D deficient (DKO) mice.
A-PS (3.8cm2/mL) were pre-incubated with 10μg/mL of rfhSP-D, nhSP-D, BSA or 20% FBS. Data represents mean nanoparticle uptake from the alveolar macrophages of at least three mice. Data normalised to nanoparticle only control of WT AM. Statistics determined using t test; *p<0.05 vs. DKO NP control; ## p=0.008 vs. WT NP control. Reproduced with permission from [291] with the addition of NP + rfhSP-D data (Licence number: 3235320787551).

3.3.5. Toxicity of particles in RAW264.7 cells

3.3.5.1 MTT assay;

In order to ensure that NP did not interfere with the MTT assay preliminary experiments were conducted. A NP spiked MTT sample and spiked acidified isopropanol sample were compared against unspiked controls in order to determine whether the A-PS or U-PS NP interfered with the assay or the optical density readings. The results showed that the MTT assay was suitable for the determination of toxicity of these particles (data not shown).

Incubation of RAW264.7 cells with A-PS or U-PS for 1 hour had no significant effect on cell viability at concentrations up to 15 cm^2/mL (see Figure 3.19A; p=0.847 and p=0.816 respectively ANOVA). Moreover, 100nm U-PS incubation for 24 hours also did not effect cell viability (p=0.788; ANOVA). Following 24 hour incubation 100nm A-PS resulted in a dose dependent reduction in cell viability. This dose dependent reduction became significant at 3.75cm^2/mL (see Figure 3.19).

3.3.5.2 Clonogenic assay

In order to corroborate the viability data the clonogenic survival of RAW264.7 cells was also assessed following 24 hour treatment with 100nm A-PS and U-PS particles. The results presented in Figure 3.20A show that A-PS particles resulted in a dose dependent reduction in clonogenic survival. This reduction became significant at a concentration 0.23 cm^2/mL with an associated p value of 0.020 (LSD post hoc). At higher concentrations the reduction in clonogenic survival was highly statistically significant with associated p values of less than 0.001 (LSD post hoc). Treatment of RAW264.7 cells with U-PS particles up to 15 cm^2/mL for 24 hours had no significant effect on clonogenic survival (see Figure 3.20B: p=0.530; ANOVA). A clonogenic assay of RAW264.7

cells with 3.75cm²/mL A-PS for 1 hour showed no significant change in clonogenic survival (data not shown).

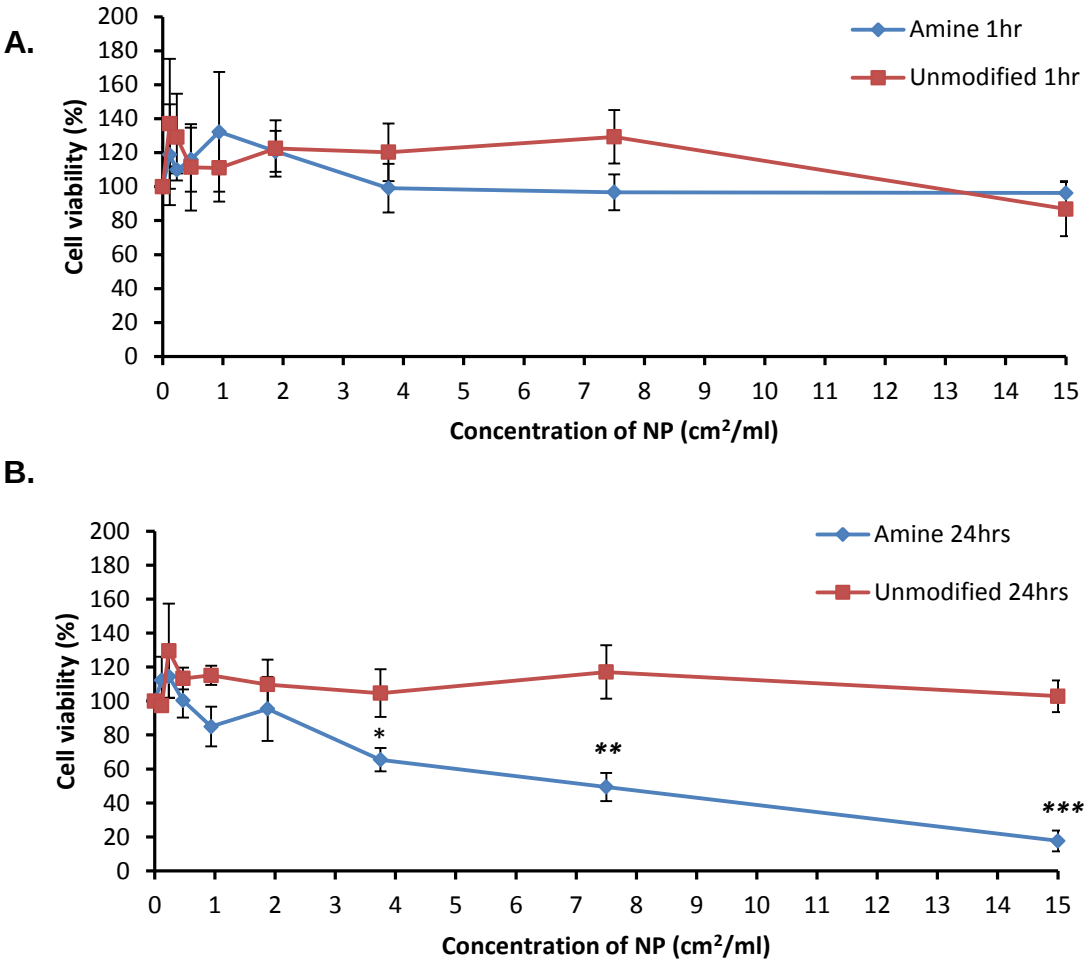

Figure 3.19. Cell viability of RAW264.7 cells following A. 1hr and B. 24hrs incubation with A-PS and U-PS. Data represents mean of three independent experiments conducted in triplicate. Statistics determined using ANOVA with LSD post hoc compared to nanoparticle free control; *p=0.040, **p=0.005, *** p<0.001

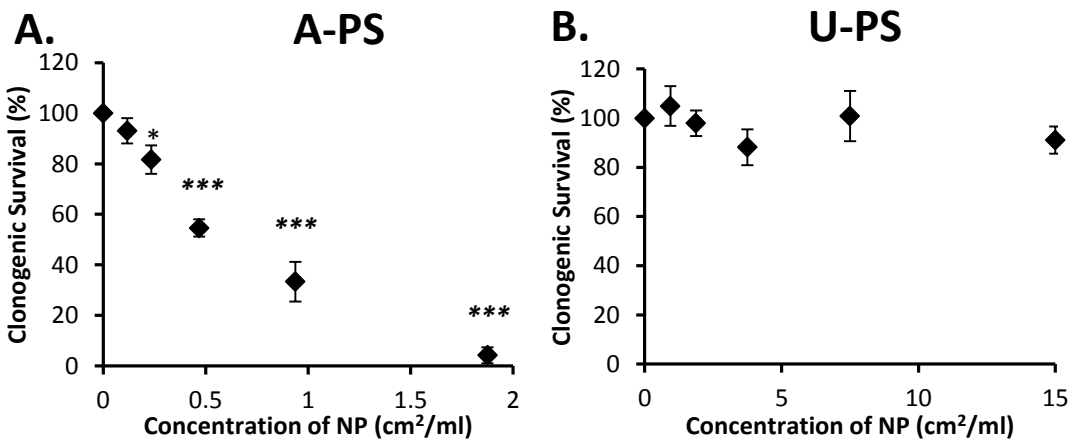

Figure 3.20. Clonogenic survival of RAW264.7 cells following 24hr incubation with A. 100nm A-PS and B.100nm U-PS; Data represents mean of at least three independent experiments ± SEM. Statistics determined using ANOVA with LSD post hoc test comparing against nanoparticle free control; *p=0.020; ***p<0.001

3.4. Discussion

When nanoparticles enter a biological fluid they quickly absorb biological macromolecules such as lipids and proteins onto their surface. This absorption lends a biological identity to exogenous particles and leads to altered nanoparticle uptake and distribution [298-300]. The protein corona has been reported to be multi-layered with a "hard" corona consisting of proteins strongly bound to the nanoparticle core and an outer "soft" corona of loosely associated proteins [250, 251]. Proteins within the soft corona are rapidly replaced with proteins from the surrounding biological medium; whereas proteins of the hard corona have much longer residence times and are frequently described as being irreversibly bound to the nanoparticle [248, 249]. Inhalation is one of the principle routes of nanoparticle exposure [7] and therefore the interaction of nanoparticles with components of pulmonary surfactant, which lines the surface of the alveolus, is of particular importance. This study concentrates on the interaction of nanoparticles with surfactant proteins A and D, which are integral to the innate immune defence of the lung.

Surfactant proteins A and D bind in a calcium dependent manner to various micro-organisms through their carbohydrate recognition domain as discussed in Chapter 1 [107, 196]. These collectins have also been reported to bind to surface impurities on carbon nanotubes in the presence of calcium but not the calcium chelator EDTA [263]. It was therefore hypothesised that SP-A and SP-D would bind to functionalised particles in a calcium dependent manner. In fact, SP-D and rfhSP-D showed enhanced binding to the studied particles in EDTA rather than calcium. This may be explained by the fact that the CRD of SP-D is less polar in the presence compared to the absence of calcium [301]. This suggests that the interaction is electrostatic rather than calcium dependent. Moreover, SP-D showed enhanced association with the negatively charged 100nm U-PS and C-PS over the positively charged A-PS particles. Unmodified or plain polystyrene particles are usually described nominally as being 'neutral' compared to the negatively charged carboxylate or positively charged amine modified particles. In fact, the current study shows that U-PS and C-PS possess similar negative zeta potentials; this has also been shown in other studies [251, 302]. The negative charge of unmodified polystyrene particles is due to the presence of sulphate ester on the nanoparticle surface which is an impurity derived from the polymerization process [251, 303]. The absorption of nhSP-A to A-PS, C-PS and U-PS was also investigated in the presence of calcium or EDTA. For the nhSP-A experiments, there was much more background protein detected (i.e. self-precipitated protein in tubes without nanoparticles) than either rfhSP-D or nhSP-D. This may be due to the high propensity of SP-A to self-aggregate in calcium containing buffers [304]. Indeed, more SP-A precipitated in the calcium compared to the EDTA control. Each of the particles studied showed slightly enhanced association to nhSP-A in the presence of calcium rather in EDTA. However, this may be due to the enhanced precipitation of unbound SP-A in the presence of calcium.

Interestingly, the negatively charged particles showed strong SP-A association in the presence of calcium and EDTA which demonstrates that the protein can associate with these particles in a calcium independent fashion. The amount of nhSP-A absorbed to A-PS particles was only slightly increased compared to the controls. However, DLS size and zeta potential measurements indicate the formation of a protein corona around A-PS particles. This was observed as an increase in A-PS particle size and a reduction in the particle zeta potential [305]. The inability to detect the corona following repeated ultracentrifugation and wash steps coupled with the DLS data suggests that SP-A forms a soft corona around the A-PS particles [251].

The electrostatic potential of the interaction between particles and rfhSP-D was further investigated by incubating 100nm and 3μm particles with rfhSP-D in pH adjusted buffers. When the pH of the buffer is below the pKa of the functional group then the group exists mainly in its protonated form. The pKa of an A-PS group is between 8 and 11; this means that at physiological pH (i.e. 7.2) and below the A-PS group will exist primarily in its charged $-NH_3^+$ form [306]. Increasing the acidity of the reaction buffer will increase the proportion of protonated A-PS groups (see Figure 3.21). The pH controlled experiment shows that the A-PS 3μm particles did not associate with the rfhSP-D at pH 9 or 10. Decreasing the pH of the buffer resulted in large increases in the affinity of rfhSP-D to the A-PS particles. At first glance these results supports the hypothesis that this interaction is electrostatic as at pH 9-10 the A-PS groups will primarily be in the deprotonated ($-NH_2$) uncharged state. However, the charge of the protein at these different pH values must also be considered. The isoelectric point (pI) is the pH at which a protein has no net charge. The theoretical pI of rfhSP-D was calculated using Expassy ProtProg to be 5.12; this means that at pHs less than 5 the rfhSP-D will possess a net positive charge. The

amine modified particles will also be positively charged at pH below 5 and therefore the protein and particle surfaces should repel each other.

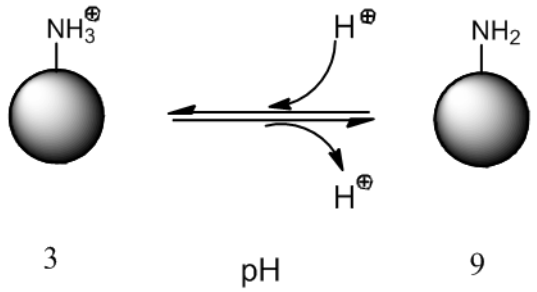

Figure 3.21. Protonation and deprotonation of A-PS functionalised particles; charge of the functional group is dependent on the pH of the buffer.

There are marked differences in the pH adsorption profiles for the 3µm and 100nm particles. The 3µm A-PS particles showed high levels of rfhSP-D binding at pH3-5. On the other hand the 100nm A-PS particles showed only minimal binding at pH1-4 which as discussed above is consistent with electrostatic forces inhibiting the nanoparticle and protein interaction. The 100nm A-PS used in this study possessed a positive surface charge at physiological pH consistent with the nanoparticle containing amine surface functionaliations. However, some amine modified polystyrene particles have been reported to have negative zeta potentials at physiological pH [302, 307]. This may be due to the number/density of functional groups on the nanoparticle surface or an inefficient functionalization process; the surface charge of the 3µm particles could therefore be negatively charged. However, this would have to be confirmed by determining the particle zeta potential. These differences may also reflect differences in the isoelectric points of the particles.

Even at pH6 to 10 where rfhSP-D adsorption was maximal for 100nm A-PS particles the amount of protein associating with the particles was much less than for the other particle types. The pH adsorption profiles of the U-PS 3µm / U-PS 100nm particles were also very different. The 3µm U-PS particles showed

minimal rfhSP-D association within the pH range studied; whereas rfhSP-D was highly associated with the U-PS and C-PS 100nm particles, especially at acidic pH. The pKa of surface bound carboxylic acid has been reported to be between 4.4-5.5 [308, 309]. Therefore at pH below these values the carboxyl groups on the C-PS particles will therefore tend to be in its protonated uncharged state (COOH). These results indicate that electrostatic interactions can influence the association of rfhSP-D to particles but that these interactions are not solely responsible for the interactions. The hydrophobicity of the particle surface is a key determinant of nanoparticle interaction with proteins [250, 267]. The differences in rfhSP-D absorption between the 100nm and 3μm particles may also be due to differences in particle hydrophobicity. Particle size influences the hydrophobicity of a particle surface, the bulk material may have hydrophilic properties whereas at the nanoscale the material can adopt hydrophobic surface characteristics [310].

An immunofluorescent co-localisation assay was performed to determine whether rfhSP-D could be detected on the particle surface of 200nm A-PS *in vitro*. The immunofluorescent co-localisation assay for rfhSP-D and 200nm A-PS particles indicate that the protein does not localise with the epithelial A549 cells in the absence of these particles. This may indicate that these particles could increase the bioavailability of this recombinant protein by bringing it into proximity of the cells. There appeared to be a distinct pattern to the association of 200nm A-PS particles with the A549 cells. The particles were located in discrete groups rather than spread evenly throughout the cell. This pattern has been shown in other reports investigating particle-cell interactions; previous studies have shown that adhered particles move centripetally (i.e. towards nucleus) on the membrane of fibroblasts due to the action of actin filaments in cell migration [311]. This movement may account for the formation of these discrete particle groups seen in these micrographs.

The trimerisation of rfhSP-D occurs in the neck region through non-covalent and van der Waal interactions between tyrosine residues on each monomer [44]. The collagenous region of rfhSP-D contains eight Gly-Xaa-Yaa triplets, compared to 59 in native human SP-D, and the fragment collagenous domain is unable to form the collagen triple helix [36, 48]. The rfhSP-D exists primarily in trimeric form as the amino terminus is not able to oligomerise with other trimers. During SDS PAGE under both reducing and non-reducing conditions the non-covalent interactions between rfhSP-D monomers are disrupted and should therefore appear solely in monomeric form on either gel type. The results from these experiments however, show a small proportion of the rfhSP-D in dimer form in reducing and trimer form in non-reducing conditions. This indicates that a small proportion of the rfhSP-D is incorrectly folded and that covalent interactions may have formed between monomers which are resistant to SDS induced denaturation [312]. This occurred despite the fact that size exclusion chromatography was conducted on the protein; this indicates either that these bonds did not effect the lectin activity or size/molecular mass of the protein or that they were formed after protein purification. The interaction of 200nm particles with rfhSP-D caused the appearance of bands corresponding to dimers, trimers and higher order oligomers on non-reduced SDS PAGE gels. The functionalization of 200nm particles had profound effects on particle association of rfhSP-D. 200nm particles with amine functionalised surfaces showed the least amount of monomeric rfhSP-D in reduced and non-reduced gels. However, the higher order oligomers were more apparent under reducing conditions after interaction with A-PS rather than with U-PS or C-PS particles. The size of the monomeric band of rfhSP-D was much larger for the treatments of U-PS and C-PS 200nm particles than the A-PS particles. At the $50cm^2/mL$ concentration this band represented at least 5μg of rfhSP-D with these particles which is around

half the total amount of rfhSP-D that was incubated with the particles. In order to investigate this interaction further, different techniques to detect and quantify the adsorption of proteins to particles could be used; circular dichroism will enable the quantification of free protein in solution and measure changes to the protein secondary structure [313]. Isothermal titration calorimetry could be used to determine enthalpy characteristics of the interaction and transmission electron microscopy to visualise the protein/particle complexes [250, 251]. Crystallographic images demonstrate that the rfhSP-D protein is less than 8nm in width and height. In the TEM images the rfhSP-D protein is extends 50-60nm around U-PS particles. This suggests that rfhSP-D is forming a multi-layered corona around the particle.

SP-A enhanced the size distribution of both A-PS and U-PS particles however, the degree of this change was markedly different. SP-A resulted in a 13.5fold increase in U-PS but only a 2.2 fold increase in in the size of A-PS particles. Moreover, with the A-PS particles the increase in size distribution was rapid, mostly occurring within the first 2 minutes of incubation with SP-A. On the other hand, the incubation of SP-A with U-PS resulted in a large increase in particle size which was sustained up to and including the 1 hour time point. Interestingly, the C-PS particles also show enhanced aggregation in the presence of calcium and a similar absorption profile to the U-PS particles. SP-A self-aggregates in calcium containing buffers, this aggregation is dependent on a number of factors such as ionic strength, pH and temperature [304]. SP-A in TBS with calcium showed large aggregates by DLS; this may interfere with determining the degree of particle aggregation as the protein self-agglomeration will also influence the size distribution of the suspension. Therefore, other methods were employed to determine the effect of SP-A on particle aggregation. Monitoring the percent transmittance at 350nm has previously been used to measure the surfactant protein mediated aggregation

of influenza virus. In these experiments a reduction in the relative transmission was associated with increased virus aggregation [297]. This technique was therefore investigated as a method to determine SP-A mediated nanoparticle aggregation. The results showed that C-PS and U-PS particles aggregated in a time dependent fashion following the addition of SP-A. This aggregation was enhanced in the presence of calcium compared to EDTA. Importantly, SP-A had little effect on the percent transmittance in the absence of particles in either calcium or EDTA containing buffers. In the case of A-PS particles, SP-A had little effect on the aggregation of A-PS particles by spectrophotometry. These results corroborate the DLS data that calcium enhances the aggregation of C-PS and U-PS particles but has a limited effect on A-PS particles.

Due to experimental limitations DLS measurements had to be taken at room temperature. At room temperature the A-PS, and U-PS were stable in TBS and calcium buffer over the studied time period. It was therefore, important to study the effect of SP-A on aggregation at physiological temperatures. Fluorescent microscopy was used for this purpose. U-PS and C-PS particles were stable at physiological temperatures and SP-A mediated aggregation was greatly enhanced with the addition of calcium. On the other hand, A-PS particles showed a high propensity to self-aggregate at physiological temperature in physiological buffers; A-PS particles remained relatively monodispersed at room temperature in TBS and calcium or at 37°C in milliQ water. Interestingly the addition of SP-A but not BSA inhibited the self-agglomeration of A-PS particles in physiological conditions. Foetal bovine serum has previously been shown to inhibit the self-agglomeration of cationic CeO_2 nanoparticles through the formation of smaller heteroaggregates [314]. However, this may also be due to other factors such as steric hindrance [315].

Lehr and colleagues have published a few papers investigating the effect of SP-A on nanoparticle aggregation and cellular uptake [265-267]. These

papers have focused on the interaction between SP-A with magnetite nanoparticles with different polymer coatings as well as metal oxide nanoparticles. Magnetite particles coated with cationic polymers tended to aggregate in the presence of BSA or SP-A this is in contrast to the current study which showed that SP-A did not aggregated anionic U-PS particles to a much greater extent than A-PS particles. This is likely due to the different surface chemistries of the particles. They also showed that more SP-A associated to cationic polymer coated particles than their anionic counterparts which is again in contrast to the current study which showed the reverse absorption profile. However, in these published studies, the total protein corona was determined whereas in the current study, the SP-A content in the hard corona was investigated. Interestingly, SP-A enhanced the association of cationic magnetite particles to macrophages compared to the BSA and particle control. However, SP-A only enhanced the macrophage uptake of particles coated with anionic phosphidylcholine (PI) and this enhancement was not due to aggregation as these particles remained colloidally stable following incubation with SP-A [266]. This could be due to an increase in receptor mediated phagocytosis of SP-A opsonised anionic particles. The lack of aggregation of PI coated particles following SP-A incubation could be due to low calcium concentrations in the buffers. The current study demonstrates that SP-A greatly enhances the aggregation of U-PS and C-PS particles in calcium containing buffers. This aggregation was associated with enhanced uptake of U-PS particles by RAW264.7 cells following incubation with SP-A. Although SP-A also enhanced the uptake of U-PS particles by alveolar macrophages from wild type and SP-A deficient mice these increases were not statistically significant. Further experiments will have to be conducted to improve the power of this study. The increased uptake of 100nm U-PS particles following incubation with SP-A is in agreement with previously published data which showed that SP-A enhanced

the uptake 1μm latex particles and titanium dioxide nanoparticles by rat AM. However, this paper did not examine the effect of these proteins on particle aggregation [264].

In RAW264.7 cells SP-A resulted in a dose dependent reduction in A-PS uptake and dose dependent increase in U-PS. BSA had no effect on A-PS or U-PS uptake by RAW cells. FBS reduced U-PS uptake and tended to increase A-PS uptake however, the latter did not reach statistical significance. The lack of statistical significance may be due to large variance in the degree of FBS mediated opsonisation as FBS enhanced A-PS uptake in each of the experiments. This demonstrates that the surface of the particle is important in determining the composition of the corona and the resulting effect on particle uptake. The effects of SP-A on the uptake of A-PS and U-PS are likely due to the aggregation states of each of the particles. However, since A-PS particles were taken up more readily by SP-$A^{-/-}$ over WT AM other mechanisms may also be involved.

A recent paper has shown that SP-A can enhance the uptake of hydrophobic PI coated nanoparticles to a greater extent than SP-D. However, with starch coated hydrophilic nanoparticles the reverse was true. Interestingly, the effect of surfactant proteins on particle uptake was negated following pre-incubation with surfactant lipids [267]. This suggests that the effect of SP-A and SP-D on particle uptake and distribution *in vivo* may be limited. This is supported by another recent paper which showed that pre-coating gold nanoparticles with SP-D had only a small and non significant effect on their bio-distribution in mice [268]. It must be noted however, that this study used wild type (i.e. SP-$D^{+/+}$) mice and that in the current study exogenous SP-D only enhanced A-PS uptake in the AM of SP-$D^{-/-}$ mice. In future studies it will therefore be interesting to study the bio-distribution of particles in both wild type and SP-$D^{-/-}$ mice.

Cationic particles such as A-PS interact with anionic patches on the lipid membrane of cells and are readily internalised following this interaction [240]. The interaction of SP-D or SP-A with these particles altered their cellular uptake. The AM from SP-D$^{-/-}$ mice took up very few particles (less than 1% NP+) compared to the WT. This represented a 94.5% relative reduction over the WT uptake. The pre-incubation of A-PS with SP-D and rfhSP-D resulted in a partial restoration of the A-PS uptake in these SP-D deficient cells. The increased A-PS uptake in the phagocytically compromised SP-D$^{-/-}$ cells following incubation with SP-D likely represents an increase in receptor mediated uptake. This was a specific opsonic effect as BSA had no effect on A-PS uptake in these cells. However, in WT AM (i.e. phagocytically competent) the absorption of protein (rfhSP-D, SP-D and BSA) but not FBS tended to reduce particle uptake. The increase in receptor mediated uptake in these cells did not compensate for the reduced interaction of the cationic particles with the cell membrane. The difference between the uptake kinetics between FBS and the other proteins may be due to the much higher protein concentration in FBS compared.

The toxicity of 100nm A-PS and U-PS particles were assessed in RAW264.7 cells by the MTT and clonogenic assays to ensure that these particles were not cytotoxic to these cells. The tetrazolium salt MTT is converted into an insoluble formazan product in the mitochondria of metabolically active cells. The formazan product is unable to cross the lipid membrane of viable cells and therefore accumulates within the cell until it is dissolved in an alcohol based solvent [316]. The MTT and other colorimetric based cytotoxicity assays have previously been shown to be susceptible to interference by certain nanoparticles [317-319]. It was therefore important to ensure that the particles of interest did not interfere with the assay. To this end, control samples were run with nanoparticle spikes in the MTT solution and acidified isopropanol solution. The A-PS and U-PS had no effect on the resulting optical density readings of control

cells. This is consistent with previously published data for these particle types [243]. U-PS particles did not significantly effect cell viability at either the 1 or 24 hour time points. This was confirmed with the clonogenic assay, which showed that U-PS treatment of RAW264.7 cells for 24 hours had no effect on the clonogenic survival. A-PS particles did not effect cell viability following the short 1 hour incubation used in the uptake experiments. However, 24 hour incubation with A-PS significantly reduced both the viability and clonogenic survival. This is consistent with previous studies which have shown that cationic particles are more cytotoxic than their anionic counterparts. The reported mechanisms of cationic particle toxicity range from increased reactive oxygen species generation, creating holes in the cell membrane and inducing lysosomal rupture [241, 243, 245, 320-323]. In future work it would be interesting to investigate the effect of surfactant protein absorption on the toxicity of these particles.

This study used nanoparticles in which the hydrophobic fluorescent dye was internalised within the particle in order to study the effect of surfactant proteins on nanoparticle uptake by macrophages. Trypan blue was used to quench the extracellular fluorescence of these fluorescent nanoparticles and therefore, the uptake of particles is measured rather than the particle association. It is also an important point to note that A-PS particles were not toxic at the indicated time point in RAW264.7 cells. Moreover, the viability of AM, as determined by a trypan blue exclusion assay, exposed to A-PS particles remained >90%. This is especially important due to the use of trypan blue to quench extracellular fluorescence in these experiments. If the particles had resulted in cell toxicity or increased membrane permeability, the trypan blue could enter the cells and thus quench the fluorescence of both internalised and extracellular particles.

This chapter focuses primarily on the effect of SP-A and SP-D absorption to nanoparticles and the effect of this interaction on particle aggregation and uptake by phagocytic cells. The association of surfactant proteins to nanoparticles and enhanced particle clearance following this association could lead to SP-A and/or SP-D deficiencies in the alveolus. This could occur either through sequestration of the surfactant proteins or through altered SP-A and SP-D clearance. SP-A and SP-D deficiencies have been shown to be associated with increased risk and severity of pulmonary infections [85-87]. The effect of the particle interaction with SP-A and SP-D on protein function will be discussed further in Chapter 5.

Chapter 4: Development of *in vitro* models of influenza infection

4.1. Introduction

In order to investigate the effects of nanoparticles on IAV infection, the IAV *in vitro* infection models first had to be developed and refined. It has been well established that Surfactant Proteins A and D neutralise IAV in both *in vitro* and *in vivo* models. However, the ability of these proteins to attenuate IAV infection are dependent on a number of factors including the glycosylation status of the viral envelope proteins. In this chapter, the amplification of IAV by two methods were employed and the purification of viral stocks were conducted. Infection models were developed and refined to increase the through put and reliability of the results obtained. Next, the functionality of Surfactant Proteins were determined against the purified IAV stocks in epithelial cell lines. Finally, a differentiation protocol was evaluated to differentiate the THP-1 monocyte cell line into macrophage-like cells in order to test the effect of surfactant proteins and NP on IAV infection in macrophages.

4.2. Methods

4.2.1. Cell culture

TT1 cells were kindly provided by Professor Terry Tetley and were grown in DCCM1 media (Cellseco, Porton Down, UK) containing 10% heat inactivated new born calf serum, 100units/mL penicillin and 100µg/mL streptomycin, 2mM L-glutamine (Invitrogen, UK) and 0.5mg/mL G418 (Sigma, UK) as described previously [324]. A549 and MDCK cells were grown in RPMI1640 (Invitrogen, UK) containing 10% foetal bovine serum (FBS; Sigma, UK) and 100units/mL

penicillin and 100µg/mL streptomycin. THP-1 cells were kindly provided by Liku Tezera and were grown in RPMI1640 medium containing 10% heat inactivated FBS (PAA, UK) and 1% Penicillin and streptomycin. A549, TT1 and MDCK cells were routinely sub-cultured every 2-3 days using trypsin. THP-1 cells grow in suspension and were sub-cultured by diluting cell suspensions in growth medium every 2-3 days to maintain cell density at around $5x10^5$-$1.5x10^6$ cells/mL.

4.2.2. Influenza A virus

Two strains of H3N2 influenza A virus were used in this study; X-79 and X-79Δ167. The parental X-79 strain is a laboratory derived high yielding re-assorted virus of H3N2 A/Philippines/82 and H1N1 A/Puerto Rico/34. The X-79 virus contains envelope proteins (HA, NA, M2) derived from the A/Phil/82 strain and viral capsid proteins from the A/PR/34 strain [192]. The X-79Δ167 strain contains a point mutation at position 167 causing an amino acid change from threonine to isoleucine; this mutation results in loss of a glycosylation site at the collectin binding site at codon 165 [195].

4.2.2.1 Virus amplification

4.2.2.1.1. Virus propagation in MDCK cells

MDCK cells were grown to confluence in tissue culture flasks (175cm²) in RPMI containing 10% FBS. These cells were then washed once in serum free (SF) RPMI1640 media and then incubated with virus in SF RPMI media. These cells were then incubated for 1 hour at 37°C and then washed twice in fresh SF media. The cells were then incubated for 4 days at 37°C 5% CO_2 in SF RPMI media containing 1µg/mL trypsin (Invitrogen). After 4 days these flasks were frozen at -80°C to lyse the cells. After defrosting the solution was clarified by centrifuging at 1000g for 30 minutes and the supernatant was either aliquoted

and frozen at -80°C until needed or further purified as described below. Mock infected lysate was prepared as above but without the addition of virus.

4.2.2.1.2. Virus propagation in allantoic fluid

Ten day old eggs were disinfected using TCP (Omega Pharma, UK) and small holes were made approximately 1cm above and 1cm below the air sac. The eggs were then inoculated with 100µL of 100HA IAV using a 25 gauge needle and the holes sealed with wax. The eggs were incubated at 37°C for 48 hours in a rotary incubator. Following incubation the eggs were disinfected again with TCP and the top of the eggs around the air sac line removed using scissors. The sac was opened and the allantoic fluid removed using a pipette and centrifuged at 2000g for 10 minutes. Viral titres were determined using the haemagglutination assay and screened for bacterial contamination on agar plates incubated at 37°C for 48 hours. Allantoic fluid containing bacterial contamination was discarded.

4.2.2.2 Fluorescent focus assay for IAV

MDCK cells were plated in 48 well plates ($1.25x10^5$ cells/ well) in complete RPMI and incubated at 37°C 5% CO_2 for 4-6 hours. The cells were washed and then incubated in SF medium containing serial dilutions of IAV for 1 hour. The virus solution was then removed; the cells washed three times and then incubated for 16 hours in SF medium 37°C 5% CO2 in a humidified atmosphere. The cells were then fixed for 1 hour in 1% formaldehyde and then washed three times in PBS. The cell membranes were permeabilised using PBS containing 0.3% triton X-100 (TrPBS) before incubation for 1 hour at RT with a mouse anti-influenza A virus antibody (1µg/mL) in TrPBS and then for a further hour with an anti-mouse IgG secondary antibody (667ng/mL in TrPBS) coupled to Alexa596 fluorophore. DAPI was used as a DNA counter stain. Infected cells were visualised using a fluorescent microscope with rhodamine

and UV filters. The viral titre obtained from this assay is described as fluorescent foci units (FFU)/mL.

4.2.2.3 Flow cytometry for detecting IAV infection

To compare flow cytometry with the FFA MDCK cells were plated and infected with IAV as described in section 4.2.2.2. Following incubation for 16 hours the cells were washed with calcium/magnesium free PBS and trypsinised for 5 minutes. The trypsin was deactivated by adding a 10 fold excess of complete medium and then centrifuging for 5 minutes at 400g. The cell pellet was resuspended in 1% formaldehyde in PBS and incubated for 1 hour at room temperature. The cells were resuspended in 1mL PBS then centrifuged at 400g for 5 minutes. The pellet was then resuspended in 1mL TrPBS to permeabilise the cell membranes, the cells were then centrifuged at 400g for 5 minutes. The cells were resuspended in TrPBS containing 1.5µg/mL of mouse anti-influenza A nucleoprotein (Abcam, UK) and incubated for 1 hour at room temperature. The cells were washed (2 x 1mL) in TrPBS by centrifuging the sample at 400g for 5 minutes. The cells were resuspended in TrPBS containing 1 µg/mL of goat anti-mouse IgG secondary antibody coupled to allophycocyanin (APC) fluorophore and incubated for 1 hour at room temperature. The cells were then washed in TrPBS (2 x 1mL) then resuspended in 100µL of PBS. The percent of cells infected with IAV was determined using a FACSAria, 10,000 cells were analysed per sample and each sample was conducted in duplicate. Virus inoculation buffer was SF RPMI unless otherwise stated in text. TT1 and A549 cells were plated in 48 well plates at a density of 1.25 x 10^5 cells / well in relevant growth media (see 4.2.1) for 6-8 hours then serum starved for 24 hours in SF RPMI. The cells were then infected as described above.

4.2.2.3.1. Flow cytometry for detecting surfactant protein IAV inhibition

Cells were plated as described in section 4.2.2.3. Surfactant proteins were incubated for 1 hour with virus in virus inoculation buffer (SF RPMI unless otherwise indicated) at 37°C. The cells were then washed twice in serum free RPMI and the virus-protein inoculum was added to the cells and incubated for a further hour at 37°C. The cells were then washed and fresh SF RPMI added to the cells and then incubated for 16 hours at 37°C. The cells were then trypsinised, fixed and stained as described in section 4.2.2.3.

4.2.2.4 Virus Purification

Following clarification of cell lysate as described in the IAV amplification section the virus was purified as described previously [325]. The supernatant was centrifuged at 135,000g for 1 hour at 4°C and then re-suspended at in phosphate buffered saline (PBS) with calcium or magnesium at 1% of its original volume. The virus was then centrifuged over a discontinuous 30-60% sucrose gradient at 104,000g for 90minutes at 4°C. The virus containing sucrose fractions were located using the fluorescent focus assay and SDS PAGE followed by Simplyblue (Invitrogen, UK) staining and these fractions were pooled. The buffer was exchanged to remove the sucrose using Amicon filters (MWCO 3000). The virus was aliquoted and frozen at -80°C until needed.

4.2.2.5 Haemagglutination assay

Human red blood cells were isolated from human type O negative blood by centrifuging at 500 g for 10 minutes. The pellets were resuspended in a 10 fold excess of phosphate buffered saline (PBS) and centrifuged for a further 10 minutes at 500 g. This was repeated twice further for a total of three washes. A stock solution of 10% RBC was prepared in PBS which was further diluted to a concentration of 0.75% RBC immediately before use. The use of human blood

cells was approved by the Southampton and South West Hampshire Research (reference; 2634/03/W). Commercial sheep RBC (Sigma, UK) were also prepared at a final concentration of 0.5%. Serial dilutions of virus were prepared in PBS or TBS (as indicated in text) and mixed with equal volumes (50µL;50µL) of RBCs in round bottom 96 well plates (Corning, UK). The plate was left undisturbed for 1 hour at room temperature and then photographed using a Canon EOS400D camera.

4.2.2.5.1. Haemagglutination Inhibition Assay

The haemagglutination inhibition assay was conducted as has been previously described [326]. Briefly, serial dilutions of collectins were prepared in TBS containing 5mM calcium or 5mM EDTA and mixed in equal quantities (25µL;25µL) with 4HAU/well of virus diluted in the same buffer. Human red blood cells were prepared as described in section 4.2.2.5 except the final stock was prepared at 0.75% in TBS with Calcium or EDTA. Aliquots of RBCs (50µL) were then incubated with the virus and collectin suspensions for 1 hour at room temperature in round bottom 96 well plates.

4.2.3. THP-1 cell differentiation

THP-1 cells were suspended at a concentration of $5x10^5$ cells/mL in growth medium containing 0, 10 or 100nM phorbol 12-myristate 13-acetate (PMA). Cells were plated in 6 well plates and incubated for 72 hours at 37°C 5% CO2 in a humidified atmosphere. PMA was dissolved in dimethyl sulfoxide (DMSO) which was used as a vehicle control and kept at less than 0.1% in all experiments. Following differentiation cells were washed three times in PBS without calcium or magnesium and incubated in the final wash for 30 minutes at 37°C. The cells were trypsinised for 5 minutes at 37°C and then the trypsin was deactivated in complete growth medium. The cells were centrifuged and

counted using trypan blue and the counts used to assess cell proliferation. Expression of cluster of differentiation (CD) markers and the ability of the cells to phagocytose bacteria were then analysed as described below.

4.2.3.1 CD expression

Trypsinised differentiated THP-1 cells in 0.1mL aliquots at a concentration of 1 x 10^6 cells/mL in PBS containing 10% FBS where incubated on ice for 30 minutes to block non-specific staining. The cells were then incubated with antibodies directed against CD14-FITC (IgG_1) or CD11b-PE (IgG_1 κ) or relevant isotype controls (BD Biosciences, Oxford, UK) for 1 hour on ice. The cells were then washed in PBS with 1% bovine serum albumin (BSA) (2x 1mL) by centrifuging at 300g for 5 minutes. The samples were resuspended in PBS with 1%BSA and 10,000 cells per sample were analysed using a BD FACS Aria.

4.2.3.2 Bacteria uptake

Trypsinised differentiated THP-1 cells were washed three times in SF RPMI by centrifuging the cells at 400g for 10 minutes. The cells were then counted and resuspended at a concentration of 1 x 10^6 cells/mL; 50µL aliquots containing 50,000 cells were added to each well of a 96 well round bottom plate. *Escherichia coli (E. coli)* pHrodo bioparticles (Invitrogen, UK) were then added to the samples at a concentration of 8 bioparticles per cell. The plate was then incubated for 1 hour at 37°C then 10,000 cells per sample were analysed using a BD FACS aria flow cytometer. The level of bacteria uptake was assessed by analysing the percent of PE positive cells. The size and granularity of control cells were evaluated using the mean forward scatter and side scatter measurements respectively.

4.2.3.3 IAV infection

THP-1 cells were plated at a concentration of $1.25x10^5$ cells per well in a 48 well plate and incubated with 10nM PMA for 72 hours in at 37°C 5% CO2 in a humidified atmosphere. Following 72 hour differentiation the cells were washed twice in SF RPMI then serum starved for 24 hours in SF RPMI at 37°C. The differentiated cells were treated with 300µL of a IAV at various concentrations as described for other adherent cell types (see section 4.2.2.3). Undifferentiated cells were incubated in a 6 well plate at the same density as the differentiated cells. Following 72 hours incubation in vehicle control the cells were washed twice by centrifugation at 300g in SF RPMI then resuspended in SF RPMI and incubated for a further 24 hours. The cells were then centrifuged and resuspended at $4.26x10^5$ cells per mL and 300µL aliquots were added to sterile FACS tubes (BD, UK). The cells were infected with the same concentrations of IAV as the differentiated cells for 1 hour, then washed three times in SF RPMI and incubated for a further 16 hours at 37°C. The cells were then fixed, stained and analysed as described in section 4.2.2.3.

4.2.4. Statistics

The relative percent infection was determined by normalising the percent infection in treatment wells to the percent infection in IAV only control wells. The results were considered normally distributed and the significance was determined between concentrations using analysis of variance (ANOVA) with a Bonferroni or least significant difference post hoc test. Differences in the CD expression, bacteria uptake, proliferation, size and granularity of differentiated versus undifferentiated THP-1 cells were determined using the independent t test. P values were determined using IBM SPSS v21 and were considered statistically significant were $p \leq 0.05$. IC50 values were determined using GraphPad Prism v6.

4.3. Results

4.3.1. Haemagglutination assay

The haemagglutination assay (HAA) is a rapid test to determine the number of influenza virons in a sample however, the assay is unable to differentiate between infectious and non-infectious viral particles. The HAA is conducted by incubating serial dilutions of virus with a fixed concentration of red blood cells (RBC). Haemaglutinin binds to N-acetylneuraminic acid containing proteins on the surface of red blood cells [327]. This binding results in the formation of an influenza-RBC matrix and prevents the settling of the RBCs. Therefore, in samples with insufficient virus to result in haemagglutination the RBCs can be observed as a discreet dot at the bottom of the well (see Figure 4.1A). Whereas, in the presence of IAV the RBCs do not settle out and a hazy red appearance to the well is observed (see Figure 4.1B).

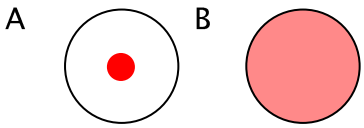

Figure 4.1: Haemagglutination of RBC's; A. No haemagglutination; **B.** haemagglutination of red blood cells

It has previously been reported that both avian and mammalian red blood cells may be used in the HAA and therefore initial experiments were conducted with commercial RBC isolated from sheep [328]. However, the results from these experiments were highly variable and generally produced very low haemagglutination titres therefore, human RBC were isolated and the results compared to the sheep RBC. Figure 4.2 shows a direct comparison between the haemagglutination activity of sheep and human RBCs. These results show that sheep RBC could not detect IAV even at low dilution factors in this sample, whereas human RBCs were much more sensitive with

haemagglutination starting at a dilution of 128. It was therefore decided to use human RBCs for future experiments.

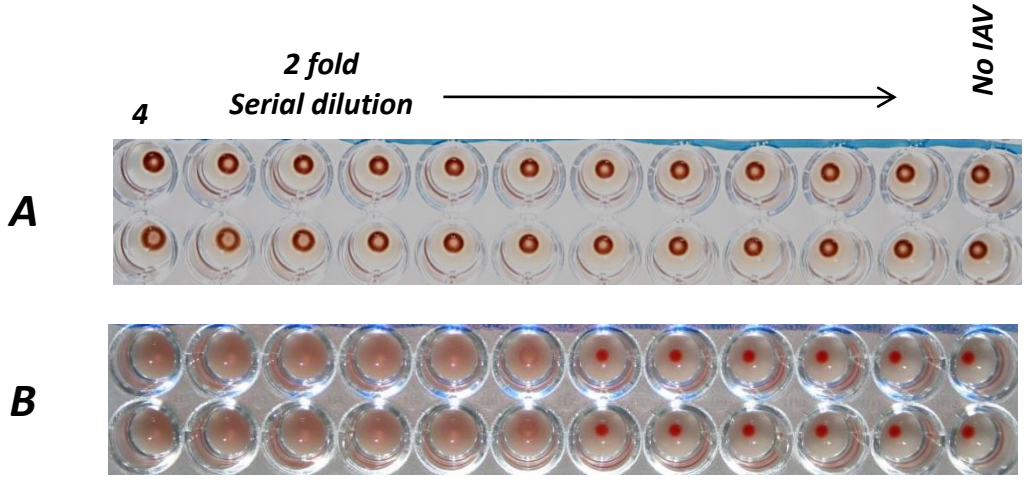

Figure 4.2: Comparing Red blood cells from A. Sheep and B. Humans in the Haemagglutination assay for X-79 IAV. Number above the first well indicates initial dilution factor.

4.3.2. Amplification of IAV in allantoic fluid and MDCK cells

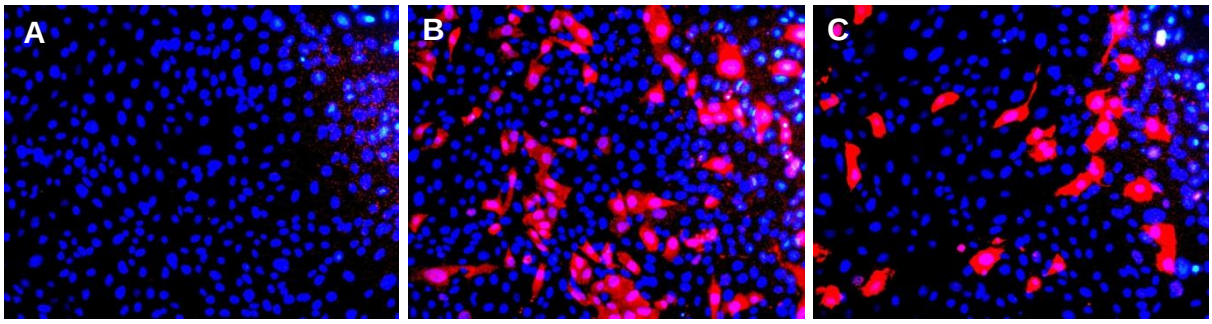

Figure 4.3: Fluorescent focus assay for influenza A virus in MDCK cells; **A.** Control (no virus); **B**. X-79 (1 in 2 dilution) and **C.** X-79Δ167 (1 in 2 dilution); Images represent merged images from UV and rhodamine filters taken at x200 magnification. Red cells indicate IAV infection (Alexa596); blue represents DNA counter stain (dapi)

Two strains of IAV, X-79 and X-79Δ167 were amplified in MDCK cells. The viral titres were determined in MDCK cells using the fluorescent focus assay (FFA) (see Figure 4.3); this was achieved by calculating the average number of infected cells in multiple fields of vision and extrapolating this data to determine the number of infected cells per mL of virus. The viral titres of the

X-79 and X-79Δ167 strains were determined to be $1.7x10^6$ fluorescent foci units (FFU)/mL and $1.4x10^6$ FFU/mL respectively.

The amplification of these strains of IAV in allantoic fluid was also conducted and the resulting titres determined using the haemagglutination assay. However, the viral yields were not sufficiently improved compared to the MDCK amplification method to justify the use of eggs (data not shown). Therefore, it was decided to use IAV from MDCK amplification in all resulting experiments.

4.3.3. Virus purification

Influenza virus (X-79) was purified on a sucrose gradient to remove contaminating host cell lysate components and proteins. Virus containing fractions were identified using the FFA and SDS PAGE. The FFA showed that fractions 6 to 39 had high levels of infectious particles present; this was evident by more than 70% infection of MDCK cells infected with a 1 in 10 dilution of each fraction (data not shown). Fractions 1 to 5 had very low (<10%) infection rates present and as such these fractions were not included in the SDS PAGE analysis. Figure 4.4 shows the reduced SDS PAGE gels of the fractions from this purification. The gels show that in fractions 6 to 25 bands at the approximate molecular weights of IAV nucleoprotein (NP), HA1 and M1/HA2 are present. These fractions were therefore pooled and the sucrose removed using Amicon filters. Following purification of the virus the X-79 stock was determined to be $4.45x10^7$ FFU/mL as determined by FFA.

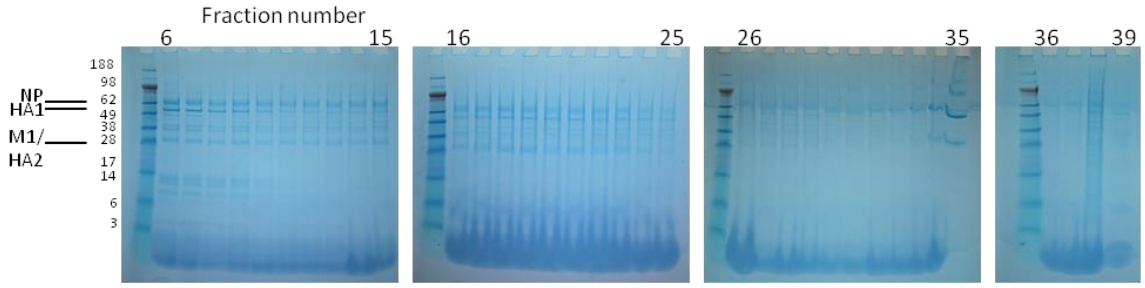

Figure 4.4: Purification of X-79 IAV. Reduced SDS PAGE of fractions of sucrose gradient containing X-79 IAV showing representative molecular weights of major IAV proteins nucleoprotein (NP), haemaglutinin (HA) and matrix protein 1 (M1).

4.3.4. Optimising Flow Cytometry to replace FFRA

The fluorescent focus assay (FFA) is a useful experiment to determine the number of infectious viral particles in a stock virus solution. The adapted form of this assay, the fluorescent focus reduction assay (FFRA) utilises the same methods but allows the evaluation of the effect of exogenous factors (e.g. surfactant proteins) on IAV infection *in vitro*. There are a number of disadvantages to this assay, including the fact that analysing large numbers of samples is extremely time consuming and there is a risk of observer bias on both choosing the fields of vision and also identifying IAV positive cells. As the FFRA uses normalised infection levels for each treatment (i.e. each treatment is normalised to the IAV control) it was decided to develop a flow cytometry based assay to replace the FFRA.

Antibody concentrations and FACS buffer were optimised for flow cytometry then the FFA and flow cytometry were directly compared in MDCK cells. The results, presented in Figure 4.5 shows that flow cytometry tended to result in slightly higher levels of infection detected. However, the degree of variation between experiments was reduced in some samples with flow cytometry compared to the FFA. Importantly, both techniques showed a good dose response relationship between the concentration of virus and the number

of IAV infected cells. It was therefore decided to adopt flow cytometry as the method of detection to replace the FFRA.

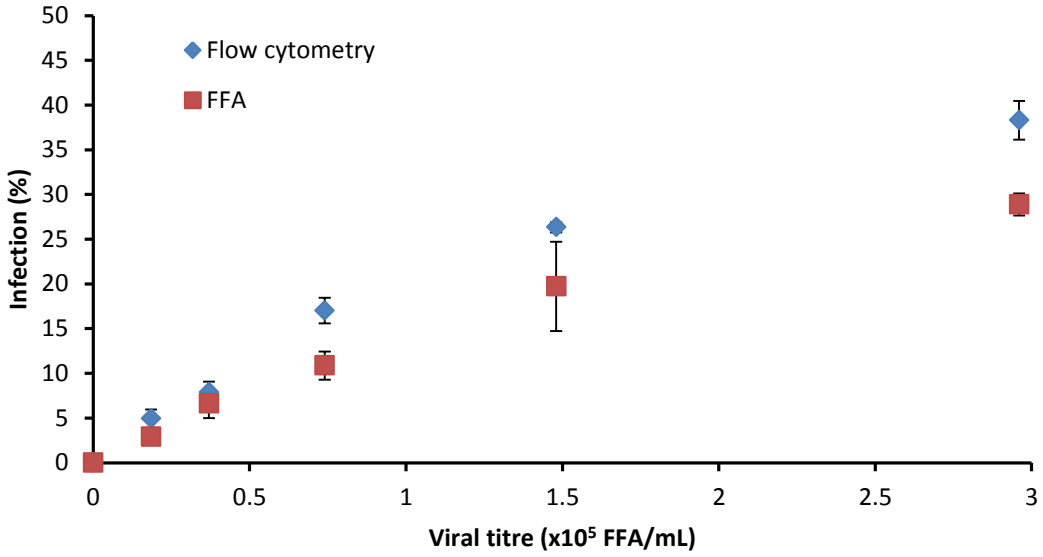

Figure 4.5: Comparison of fluorescent focus assay (FFA) and flow cytometry for determining percentage IAV infection in MDCK cells. Data represents absolute infection levels in mean of three independent experiments conducted in duplicate (± SEM).

Following purification of X-79 virus, stocks of virus were stored in 300µL aliquots at -80°C until needed. In order to determine whether these stocks could be freeze-thawed and still provide similar levels of infection, dose response curves before and after a freeze thaw cycle were conducted. The results shown in Figure 4.6 shows that freeze thawing virus typically resulted in approximately 5% reduction in IAV infection in MDCK cells. Due to these results it was determined that virus freeze thawed once could be used without radically affecting infection levels but that subsequent freeze thaws should be avoided.

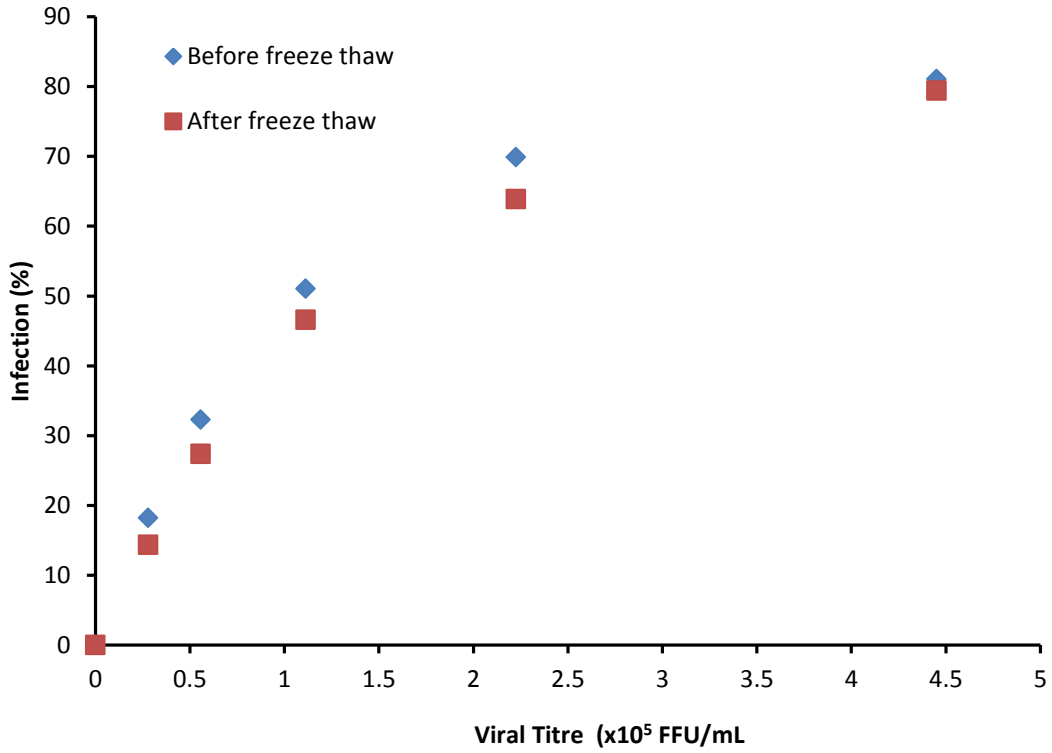

Figure 4.6: Comparison of purified X-79 IAV infection in MDCK cells before and after freeze thaw. Data represents mean of one experiment conducted in duplicate.

nhSP-A and two oligomeric forms of nhSP-D were tested for their ability to neutralise X-79 in the MDCK cell line. These experiments were conducted to ensure that the collectins were able to neutralise this strain of virus. Although, previous studies have shown SP-D can neutralise X-79 viruses, IAV can mutate following repeated amplification cycles and lose their susceptibility to SP-D mediated neutralisation. The ability of these collectins to neutralise IAV was evaluated against a concentration of virus ($4.45x10^4$ FFU/mL) shown to produce a submaximal infection rate in this model (see Figure 4.6). The results presented in Figure 4.7 show that both the 800kDa and 1.7mDa SP-D inhibited IAV infection in a dose dependent manner. The reduction of X-79 infection by 1.7mDa SP-D was significant from 0.01µg/mL whereas the 800kDa mediated inhibition was significant from 0.078 µg/mL ($p<0.01$ and $p<0.05$ respectively). The higher order 1.7mDa oligomer was a more effective IAV inhibitor with an

IC50 of 0.019 μg/mL compared to 0.199 μg/mL for the 800kDa SP-D in MDCK cells. nhSP-A also resulted in a dose dependent reduction in IAV infection in this system with an associated IC50 of 0.803 μg/mL.

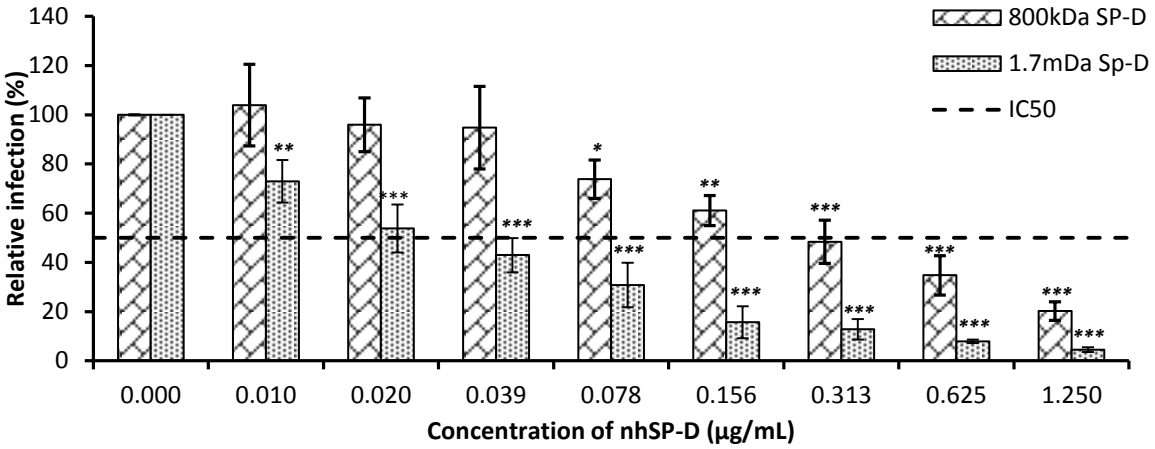

Figure 4.7: nhSP-D and X-79 IAV infection in MDCK cells; Comparison of purified X-79 IAV ($4.45x10^4$ FFU/mL) infection in MDCK cells following pre-incubation with two forms of nhSP-D. The percent of APC positive cells in each sample were normalised to the sample where no collectin was present. Dashed line represents IC50. Data represents mean of at least three independent experiments conducted in duplicate (±SEM). Experiments conducted by Zofi McKenzie and Jacqueline Pugh. Statistics determined using ANOVA with LSD post hoc test where *p<0.05,**p<0.01,***p<0.001 vs. IAV control with no SP-D.

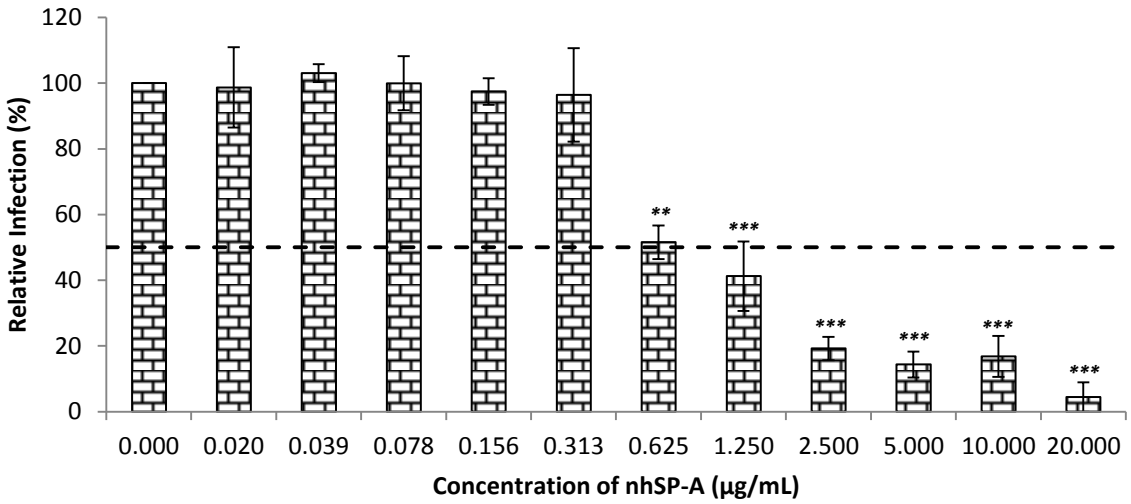

Figure 4.8: nhSP-A and X-79 IAV infection in MDCK cells; Comparison of purified X-79 IAV ($4.45x10^4$ FFU/mL) infection in MDCK cells following pre-incubation for 1 hour with nhSP-A. Dashed line represents IC50. The percent of APC positive cells in each sample were normalised to the sample where no collectin was present. Data represents mean of at least three independent experiments conducted in duplicate (± SEM). Experiments conducted by Zofi McKenzie and Jacqueline Pugh. Statistics determined using ANOVA with LSD post hoc test where ** p=0.001, ***p<0.001 vs. IAV control with no SP-A.

4.3.5. Haemagglutination Inhibition Assays

In order to corroborate these results the ability of these collectins to inhibit the haemagglutination of X-79 was also investigated. Hartshorn *et. al.* (1998) described a protocol in which the inhibitory capacity of collectins against IAV haemagglutination could be determined using a modified HAA termed the haemagglutination inhibition assay (HIA). The highest dilution factor of IAV stock which results in haemagglutination of the RBCs is given the value of 1 haemagglutination unit (HAU). In the HIA protocol 4 HAU of IAV is incubated with increasing concentrations of proteins to determine the lowest concentration which results in complete inhibition of IAV haemagglutination with RBCs. This concentration is termed the haemagglutination inhibitory concentration (HIC).

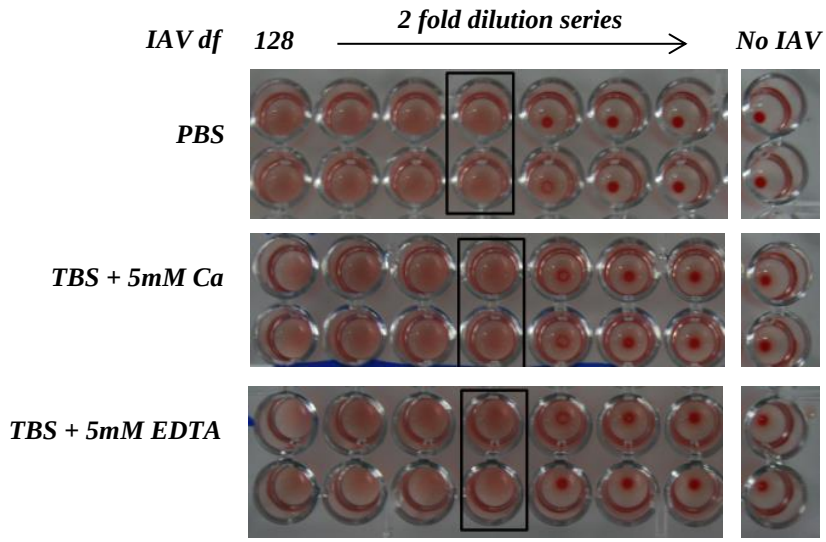

Figure 4.9: Effect of buffer on haemagglutination of purified X-79 with human RBCs; Abbreviations df; dilution factor.

Firstly, it was determined whether the HAU was consistent between PBS and TBS buffers with 5mM calcium or 5mM EDTA. This was conducted as PBS becomes saturated in the presence of 2mM calcium, the minimum calcium concentration required for the lectin activity of collectins. The results, presented in Figure 4.9, shows that changing the buffer from PBS to either TBS with 5mM calcium or TBS with 5mM EDTA had no effect on the HAU. One haemagglutination unit was determined to be equivalent to a 1 in 1024 dilution of the IAV and therefore 4HAU was equivalent to 1 in 256 dilution of the purified stock or $1.74x10^5$ FFU/mL.

The results, shown in Figure 4.10 and summarised in Table 4.1, demonstrate that SP-A is unable to inhibit haemagglutination of X-79 in TBS with calcium at the concentrations studied (HIC; >20μg/mL). Interestingly, in TBS with EDTA haemagglutination was inhibited with 20 μg/mL nhSP-A. The 1.7mDa and 800kDa oligomers of nhSP-D inhibited X-79 haemagglutination in a calcium dependent manner with HICs of 0.625 μg/mL and 5 μg/mL respectively. The 1.7mDa SP-D oligomer could also inhibit X-79 in the presence

of EDTA however, the HIU was much higher in EDTA than in calcium with a HIC concentration of 5μg/mL. The effect of rfhSP-D and BSA on X-79 haemagglutination were also studied however, they failed to inhibit haemagglutination at any of the concentrations studied (HIC; >10μg/mL).

As was observed with the flow cytometry studies of collectin inhibition of X-79 infection in MDCK cells, the 1.7mDa SP-D is around 10 times more effective at neutralising X-79 than the 800kDa oligomer.

Protein	HIC in 5mM Ca.	HIC in 5mM EDTA
nhSP-A	>20μg/mL	20μg/mL
nhSP-D; 800kDa	5 μg/mL	>20μg/mL
nhSP-D; 1.7mDa	0.625 μg/mL	5 μg/mL
rfhSP-D	>20μg/mL	>20μg/mL
BSA	>10μg/mL	>10μg/mL

Table 4.1: Collectin inhibition of X-79 haemagglutination. Haemagglutination inhibition concentrations (HIC) of pulmonary collectins against 4HAU of purified X-79 IAV with human RBCs. 4HAU of this viral stock was equivalent to a viral titre of $1.74x10^5$ FFU/mL. Where no haemagglutination inhibition was observed the HIC is reported as >x μg/mL where x is the highest concentration tested.

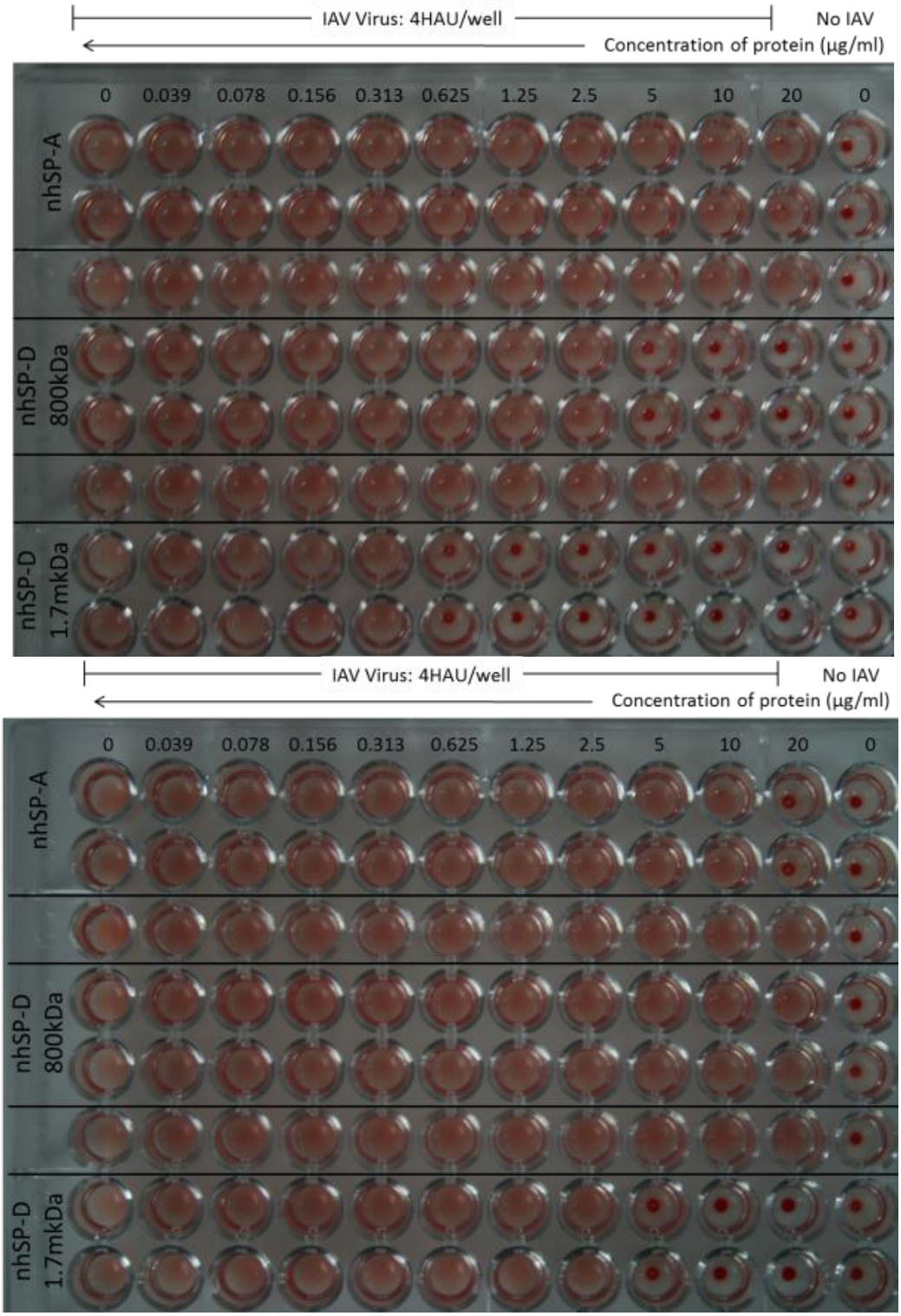

Figure 4.10: Collectin inhibition of X-79 haemagglutination. nhSP-A and nhSP-D inhibition of haemagglutination of human RBCs by purified X-79 IAV. Experiments were conducted in TBS with A. 5mM $CaCl_2$ or B. 5mM EDTA. Results representative of at least two similar experiments.

A preliminary experiment using the X-79Δ167 strain in the HAA with the 1.7mDa SP-D showed that the HIC against this strain was 0.125 μg/mL in the presence of calcium. This indicates that the X-79Δ167 strain is more sensitive to inhibition by SP-D than the parental X-79 strain. This is in contrast to the previously published results and may indicate that the virus has mutated and become glycosylated. This was supported by preliminary *in vivo* experiments in which no morbidity or mortality was observed in mice infected with X-79Δ167 (data not shown).

4.3.6. Development of IAV reduction assay

MDCK cells are a canine kidney cell line which is often used for the amplification and subsequent quantification of IAV *in vitro*. However, they are not a representative cell type for the alveolar epithelium. It was therefore decided to optimise IAV infection in two cell lines derived from the alveolar epithelium A549 and TT1 cells. A549 cells were originally derived from a type II pneumocyte lung carcinoma [293] A549 cells are one of the most commonly used cell lines in *in vitro* nanotoxicology studies. TT1 cells were immortalised from primary alveolar type II pneumocytes. However, following immortalisation they were discovered to have the phenotype of type I cells and are therefore regarded as type I cell like [324].

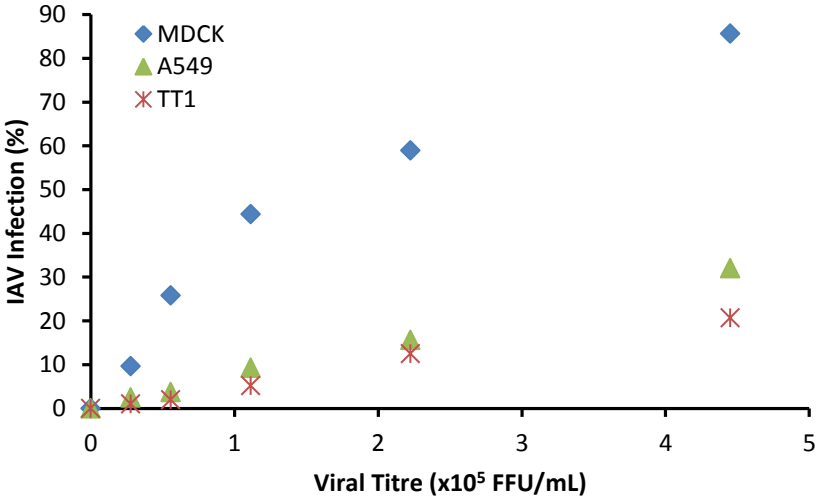

Figure 4.11: Influenza infection by purified X-79 IAV in MDCK, A549 and TT1 cells (SF RPMI). Data represents mean of duplicate results. A549 cell $R^2 = 0.9976$ and TT1 cell $R^2 = 0.9869$. MDCK cell $R^2 = 0.9121$

Firstly, influenza infection in A549, TT1 and MDCK cells were compared. The results, shown in Figure 4.11, show that MDCK cells were much more readily infected with IAV compared to both A549 and TT1 epithelial cell lines. A549 and TT1 cells tended to infect to a similar extent at the concentrations studied. IAV infection in A549 and TT1 cell lines showed a linear relationship with viral titre at the concentrations studied. This was showed with coefficient of determination (R^2) values of 0.9976 and 0.9869 for A549 and TT1 cells respectively. On the other hand in MDCK cells IAV infection started to become saturated over 50% cell infection and therefore had a R^2 value 0.9121.

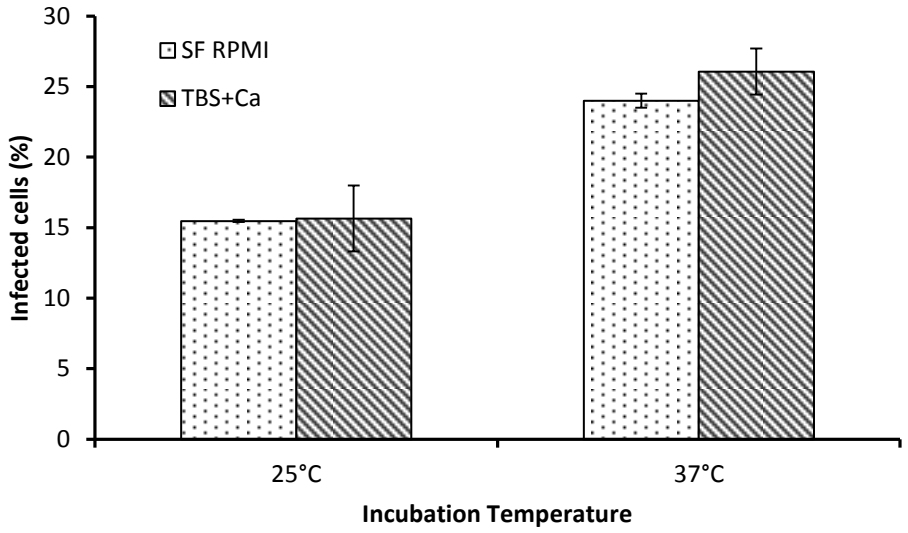

Figure 4.12: Comparison of inoculation buffers and temperature on IAV infection in MDCK cells. Data represents mean of duplicate results ± stdev.

RPMI is a phosphate containing cell culture media which contains 11.11mM of glucose but only 0.424mM of calcium. Glucose is a ligand for SP-D and has previously been shown to inhibit the binding of this collectin to various microorganisms. Also, a calcium concentration of 2mM is required for the lectin activity of the collectins and supplementing RPMI with added calcium results in calcium precipitation (data not shown). Hartshorn *et al.* use PBS containing 2mM calcium as an inoculation buffer to study collectin inhibition of IAV infection *in vitro* however, PBS becomes saturated at this calcium concentration and therefore it was decided that this was inappropriate to use with nanoparticles, influenza and surfactant proteins. Tris buffered saline containing 5mM calcium was therefore investigated as a suitable alternative. This buffer was used previously as a nanoparticle buffer in many of the characterisation experiments in Chapter 4. In these characterisation experiments it was shown that amine nanoparticles were relatively stable in TBS and calcium at room temperature, although they tended to self agglomerate at 37°C. Therefore, the effect of changing the inoculation buffer and temperature was examined on IAV

infection. MDCK cells were therefore infected with IAV at two different temperatures (25°C and 37°C) in either TBS with 5mM calcium or SF RPMI. The results, presented in Figure 4.12, shows that changing the inoculation buffer from SF RPMI to TBS and calcium did not effect IAV infection at either concentration. However, altering the temperature during influenza infection did alter cell IAV infection. Lowering the temperature from physiological (37°C) to room temperature (25°C) resulted in a relative reduction of approximately 40% in infection. It was therefore decided that experiments should continue to be conducted at physiological temperatures.

Before a change in inoculation buffer could be carried out, the effect of these buffers on cell viability was determined. Growth curves of A549 and TT1 cells were conducted; cells were plated for 24 hours then serum starved for a further 24 hours in serum free RPMI. The cells were then treated for 1 hour in RPMI or TBS and calcium and then further incubated in SF RPMI for 16 hours. Cell viability was then assessed using the MTT assay following this period. Figure 4.13 shows that changing the inoculation buffer from SF RPMI to TBS and calcium did not affect cell viability in either TT1 or A549 cells. It was therefore decided that for subsequent influenza experiments the inoculation buffer would be TBS with calcium.

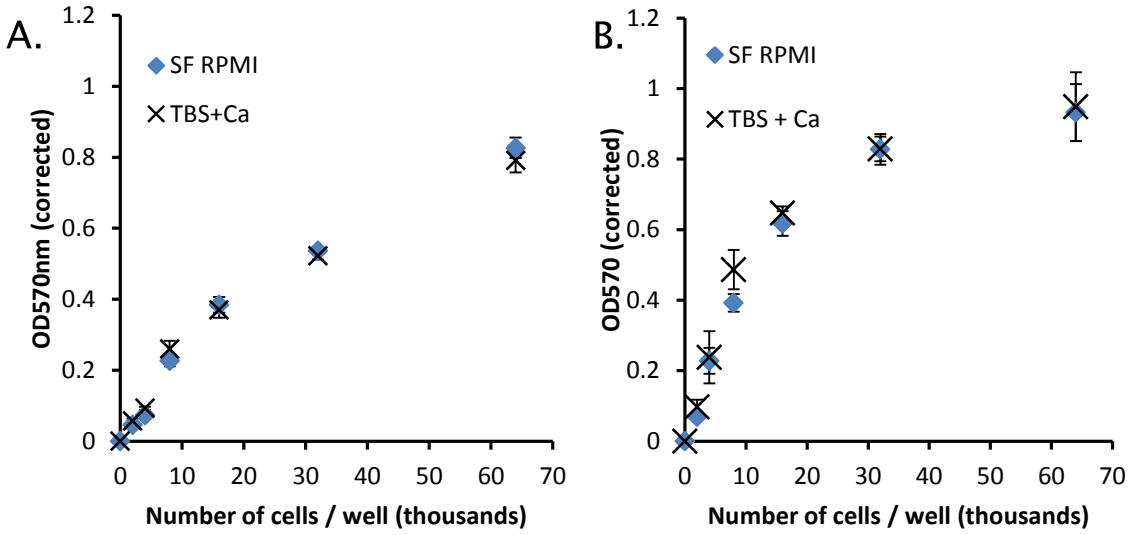

Figure 4.13: Cell viability in serum free RPMI (SF RPMI) and TBS with 5mM calcium. Growth curves of **A.** A549 cells and **B.** TT1 cells following 1 hour exposure to either TBS and calcium or SF RPMI. Data represent mean ± SEM of triplicate measurements.

Next, the effect of nhSP-A and nhSP-D on IAV infection were determined. A concentration of 2.23x105 FFU/mL of X-79 was chosen as it was shown to provide a submaximal infection level in both A549 and TT1 cells (see Figure 4.11). Due to the high levels of nhSP-A in the 800kDa preparation of SP-D (see Chapter 3) it was decided not to use this oligomer for the nanoparticle experiments. Therefore, only the 1.7mDa SP-D was optimised for the use in the A549 and TT1 alveolar epithelial cell lines. Figure 4.14 shows the effect of nhSP-A (Figure 4.14A) and 1.7mDa nhSP-D (Figure 4.14B) on X-79 infection in these alveolar epithelial cell lines. The results show that both nhSP-A and nhSP-D result in dose dependent decreases in IAV infection in A549 and TT1 cells. IC50 values for these treatments were also calculated and are summarised in Table 4.2. The results show that surfactant proteins were slightly more effective, at sub-maximal collectin concentrations, at neutralising X-79 infection in the A549 compared with the TT1 cell line.

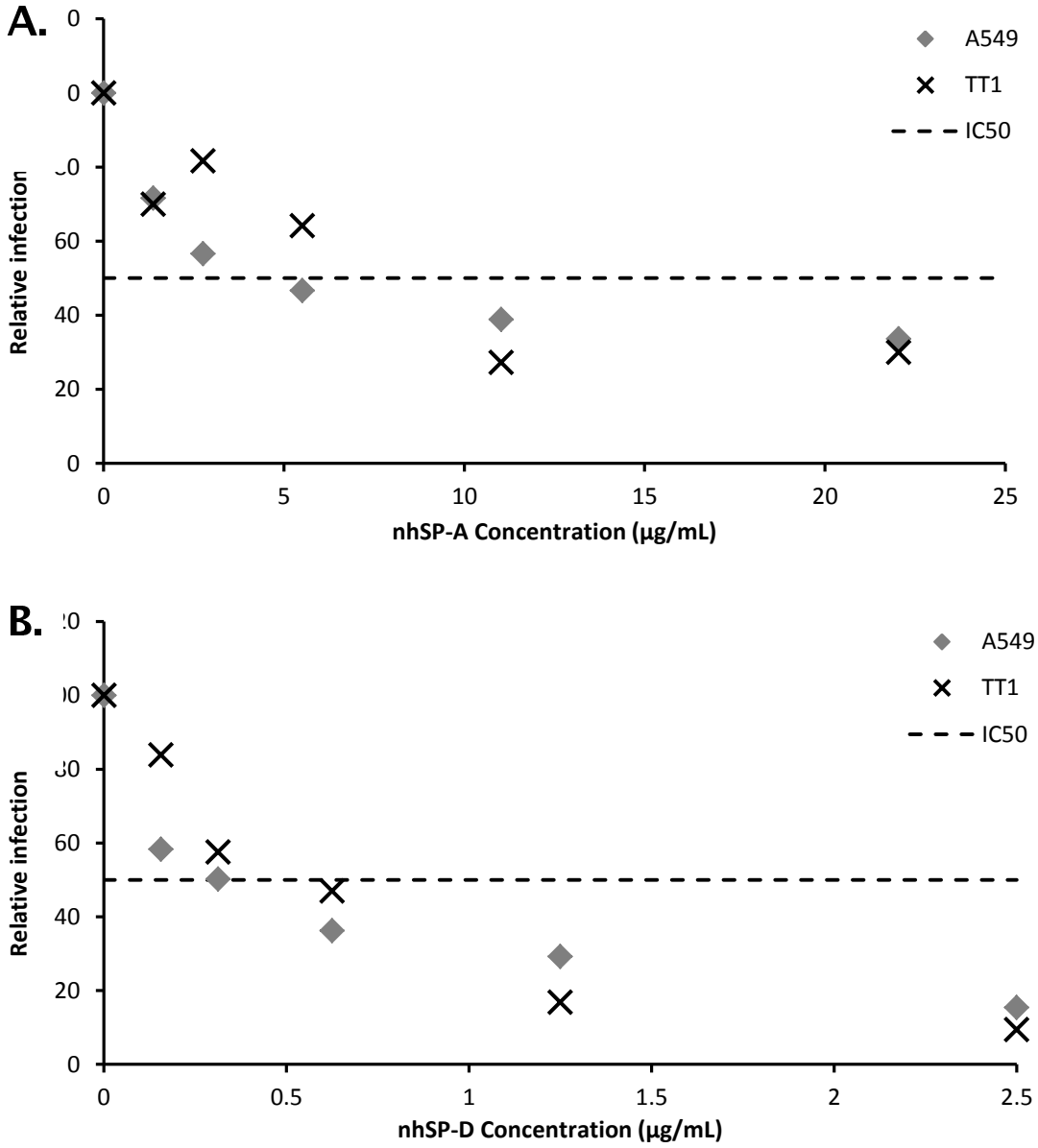

Figure 4.14: Pulmonary collectins and X-79 IAV infection in alveolar epithelial cell lines. Effect of **A**. nhSP-A and **B.** nhSP-D (1.7mDa) on X-79 infection (2.2x105 FFU/mL) in A549 and TT1 cells in TBS containing 5mM calcium. Data represents mean of at least two experiments conducted in duplicate. Dashed line represents IC50.

IC50	**A549**	**TT1**
nhSP-A	5.22	7.27
nhSP-D (1.7mDa)	0.33	0.47

Table 4.2: IC50 (μg/mL) for collectins against X-79 infection in A549 and TT1 cells.

Preliminary experiments using the FFA showed that rfhSP-D had a strong inhibitory effect on X-79 IAV infection in MDCK cells. However, subsequent experiments in MDCK cells using flow cytometry showed that rfhSP-D increased X-79 infection in this cell line (data not shown). In order to determine whether rfhSP-D could reduce X-79 infection in either A549 or TT1 cells concentration gradients of rfhSP-D in these cells were conducted. The results show that rfhSP-D tended to result in a dose dependent reduction of X-79 infection in A549 cells up to 5 μg/mL. At higher concentrations the effect of rfhSP-D on IAV infection seemed to be negated. In TT1 cells, rfhSP-D tended to increase X-79 IAV infection (see Figure 4.15A). Further experiments were conducted to determine the significance of these differences (see Chapter 6). BSA had little effect on IAV infection in either TT1 or A549 cell lines (see Figure 4.15B).

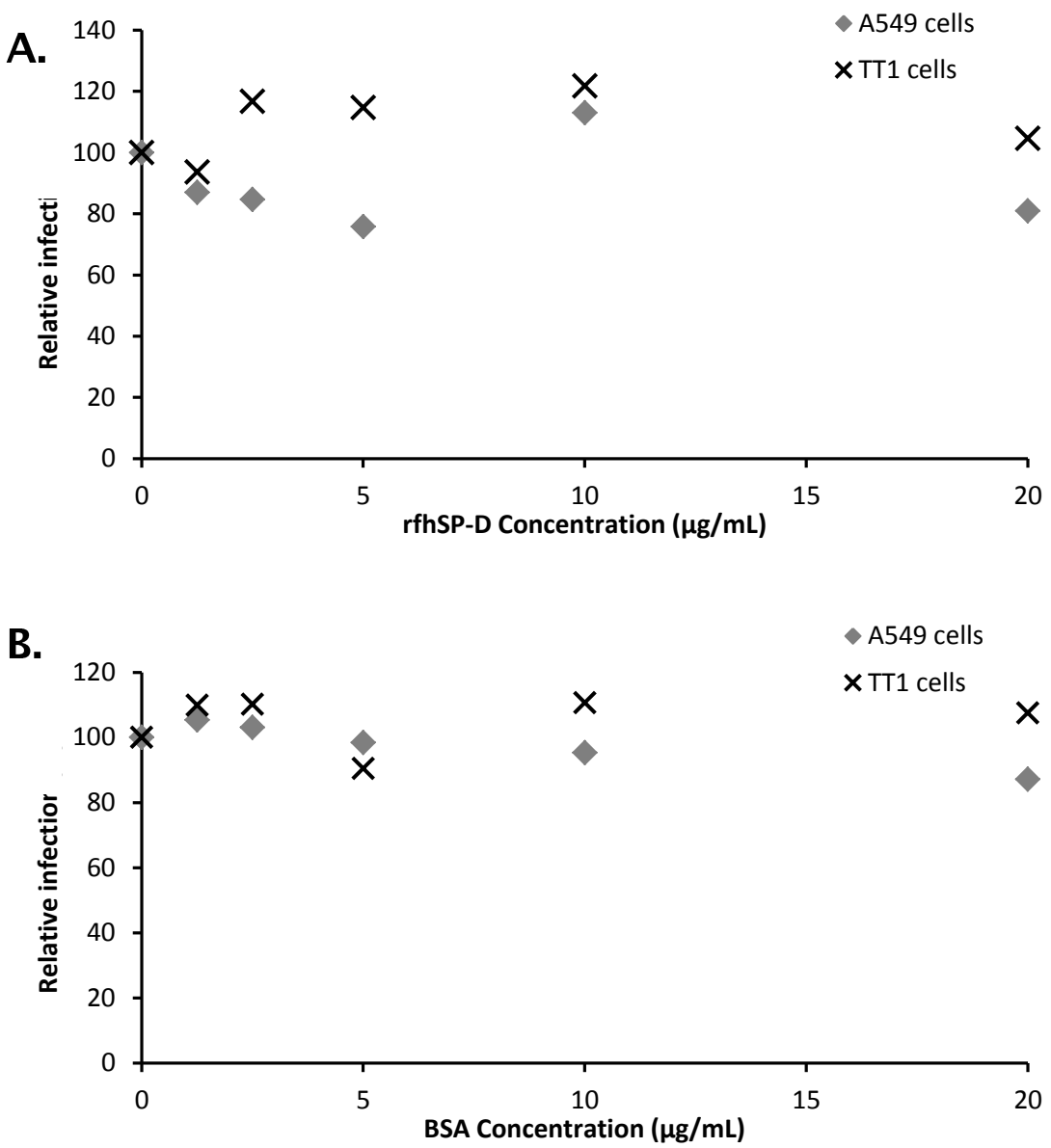

Figure 4.15: The effect of A. rfhSP-D and B. BSA on X-79 IAV infection in A549 and TT1 cells. Data represents mean of two experiments conducted in duplicate.

4.3.7. Optimisation of THP-1 cells

Macrophages are the principle immune cell resident in the alveolus and are crucial to maintaining a healthy lung environment. Influenza is able to infect macrophages and this infection has been reported to result in terminal replication of the virus, although this is dependent on the virus subtype and source of macrophage [329, 330]. It is therefore, important to understand how the interaction of nanoparticles with surfactant proteins will impact infection in

these cells. In order to do this THP-1 cells, a human monocytic cell line was obtained and a differentiation protocol developed to differentiate these cells into macrophage like cells.

THP-1 cells are a human monocytic suspension cell line derived from the peripheral blood of a male infant with acute monocytic leukemia (ATCC). These cells can be differentiated into a macrophage like phenotype using a number of agents. Many studies have used phorbol 12-myristate 13-acetate (PMA) to differentiate THP-1 cells into macrophages; however, the differentiation dose and time scale differs between these studies. Additionally, the resulting phenotype of the cells appears to be different between some of these studies. Therefore, in order to determine the optimum PMA concentration to differentiate these cells into macrophages and characterise their phenotype following differentiation a number of experiments were conducted. The morphological characteristics were assessed using microscopy to assess the acquisition of morphology and adherent characteristics and flow cytometry to measure the relative size (forward scatter; FSC) and granularity (side scatter; SSC) of the cells. The expression of typical monocyte-macrophage differentiation markers and the phagocytic capacity of the cells were assessed by flow cytometry. Cell counts following differentiation were used to determine the extent of cell proliferation.

THP-1 cells acquired an adherent characteristic within 24 hours of differentiation with either 10nM or 100nM PMA (see Figure 4.16A). This characteristic was maintained throughout the 72hour period. THP-1 cells treated with the vehicle control remained in suspension, although some settled on the bottom of the well they did not adhere. Following adhesion of 10nM PMA differentiated cells the cells gradually spread out generating filopodia-like projections. DMSO was used as a vehicle control (VC) in these experiments and

was kept <0.1% in all experiments. Following PMA differentiation, there was a loss in cell proliferation as shown in Figure 4.16E.

4.3.7.1 Size and granularity

There were large increases in the SSC in both 10nM and 100nM versus VC treatments. These 81% and 89% increases were highly statistically significant with respective p values of 0.001 and 0.002 (independent t test). There was a 13% increase in the FSC following 10nM PMA compared to vehicle control treatments. However, this increase did not reach statistical significance (independent t test; p=0.075). This indicates that PMA differentiation significantly increases the granularity of the cells but does not significantly alter their size.

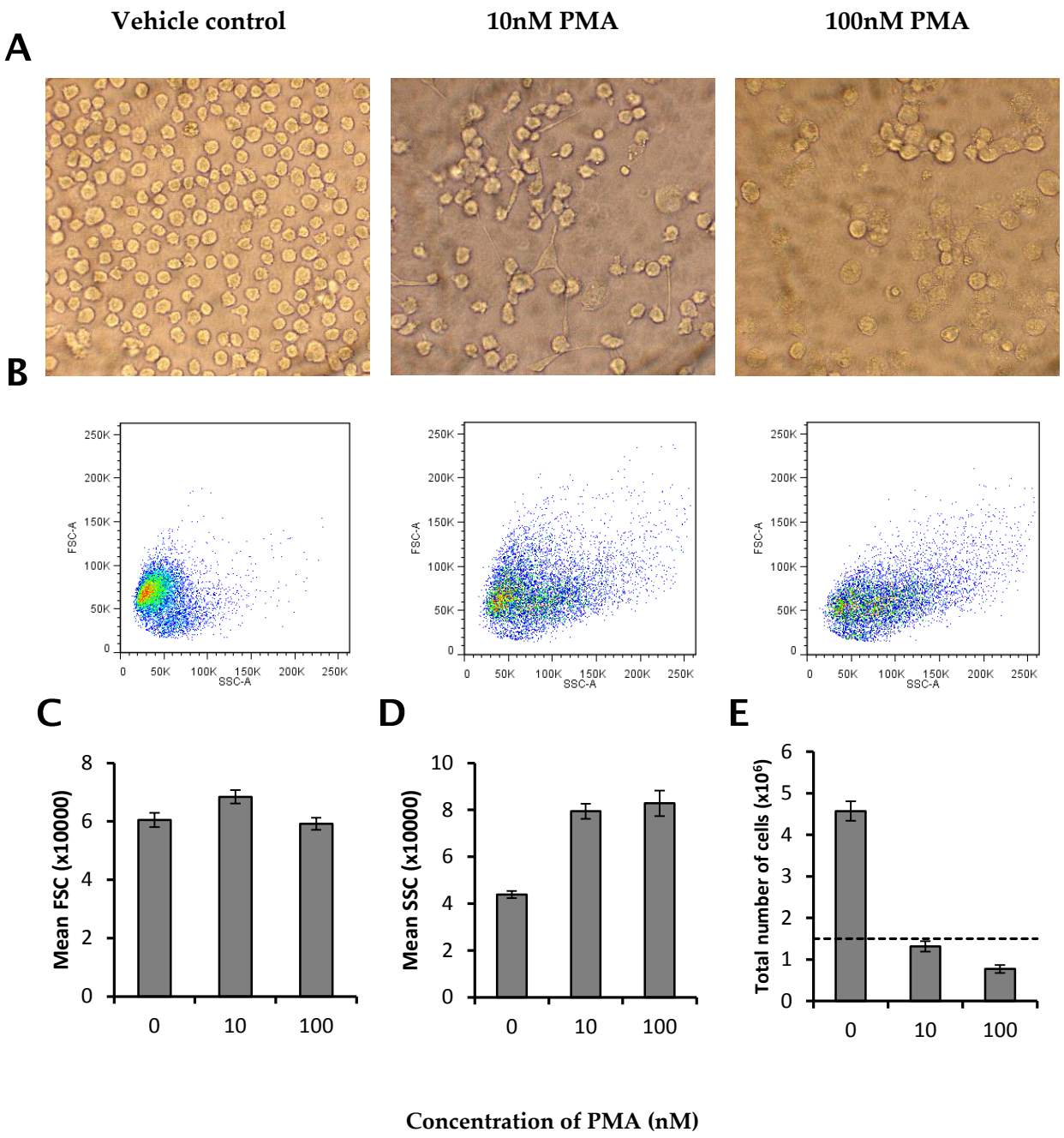

Figure 4.16: Morphology of PMA differentiated THP-1 cells; Morphological characteristics of THP-1 cells following differentiation with PMA. **A**. Microphotographs following 48 hour differentiation and **B.** Forward scatter (FSC) / side scatter (SSC) plots of THP-1 cells following treatment with vehicle control, 10nM and 100nM PM for 72 hours **C.** Mean Forward scatter and **D**. mean side scatter of THP-1 cells differentiated for 72hours with PMA. **E.** Total number of cells recovered following 72hours differentiation. Dashed line represents number of cells plated. Data represents mean of three experiments conducted in duplicate (n=3±SEM).

4.3.7.2 CD expression

The cell surface markers CD11b and CD14 are up-regulated during monocyte-macrophage differentiation [329]. Following 72 hours of 10nM PMA differentiation 92% of cells were CD11b+ compared to 23% following VC treatment (data not shown). The expression of CD11b as measured by the mean fluorescent intensity was increased by 17.4 fold in the 10nM PMA compared to the VC treatments. This was statistically significant with an associated p value of 0.004 (independent t test). There was no significant difference between the percent of CD14+ cells between VC and 10nM PMA treatments (p=0.424) with approximately 90% of the THP-1 cells CD14+ for both treatments. However, the level of CD14 expression in 10nM PMA treated THP-1 cells was 2.4fold higher than the VC as measured by the MFI (see Figure 4.17). This increase was highly statistically significant with an associated p value of 0.007 (independent t test). The number of cells expressing CD14 in 100nM PMA treated THP-1 cells reduced by 15% and the level of expression also reduced to 20% below the VC treated cells. However, only the difference in percent CD14+ was statistically significant with p values of 0.007 and 0.136 for the percent CD14+ and MFI respectively.

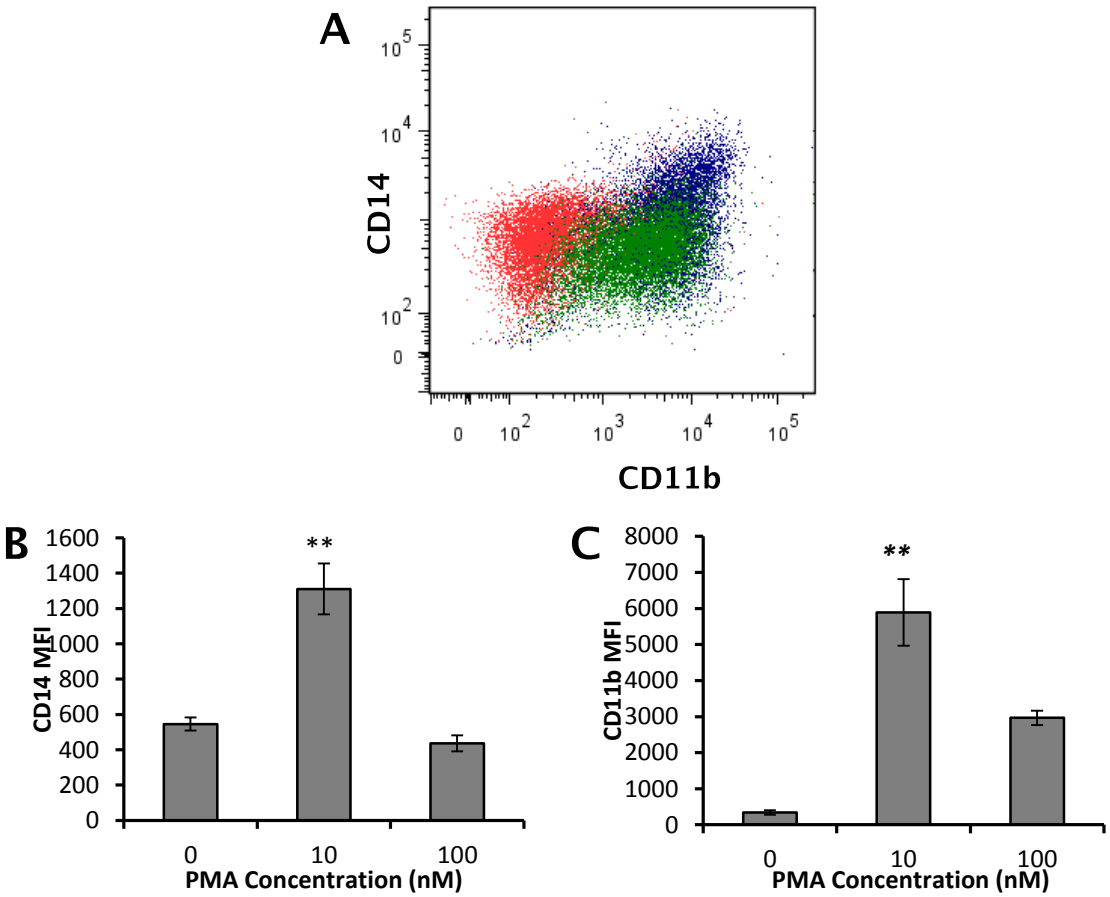

Figure 4.17: CD11b and CD14 expression in PMA differentiated THP-1 cells.
A. CD14 and CD11b expression in THP-1 cells treated with vehicle control (red), 10nM PMA (blue) and 100nM PMA (green). Mean fluorescent intensity (MFI) of **B.** CD14 and **C.** CD11b of PMA differentiated THP-1 cells. Results represent mean of three independent experiments conducted in duplicate (± SEM). **p<0.01 versus vehicle control.

4.3.7.3 Phagocytic capacity following differentiation

The phagocytic capacity of the cells following PMA differentiation was assessed using pHrodo labelled *E. coli* bioparticles and compared to VC treated cells. Differentiation of THP-1 cells with 10nM PMA resulted in a 3.1 fold increase in the number of phagocytising cells compared with the vehicle control. This increase was highly statistically significant with a p value of 0.003 (independent t test). Although 100nM PMA resulted in a 2 fold increase in the phagocytic activity of the cells, this increase did not reach statistical significance (p=0.062). The results clearly demonstrate that 10nM PMA for 72hours is optimal for the differentiation of THP-1 cells into macrophage like cells.

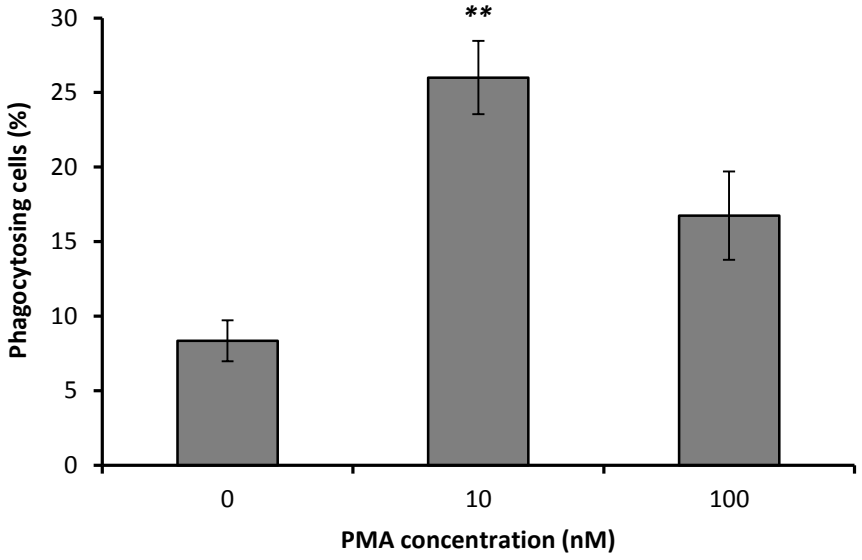

Figure 4.18: Phagocytic capacity of THP-1 cells following 72hour PMA differentiation. Uptake of *E. coli* bioparticles in THP-1 cells following PMA differentiation. Results representative of three independent experiments conducted in duplicate (n=3 ±SEM). **p=0.003 vs. VC (0nM PMA); independent t test

4.3.7.4 Influenza infection and THP-1 cells

In order to examine the effect of nanoparticles and surfactant proteins on IAV infection in differentiated THP-1 cells the amount of IAV required to produce a sub-maximal level of infection was established. Figure 4.19 shows that THP-1 cells differentiated with 10nM PMA for 72 hours were infected in a dose dependent manner up to $4.45x10^5$ FFU/mL. Non-differentiated cells infected much more readily than their differentiated counterparts. It was therefore decided to use a concentration of $2.23x10^5$ FFU/mL in future experiments to infect 10nM PMA differentiated cells as this concentration produces a sub maximal infection level in these cells and also reflects the concentration of virus optimised for the A549 and TT1 cell lines. Due to these results it was decided to use the same concentration of virus and surfactant proteins for the nanoparticle experiments.

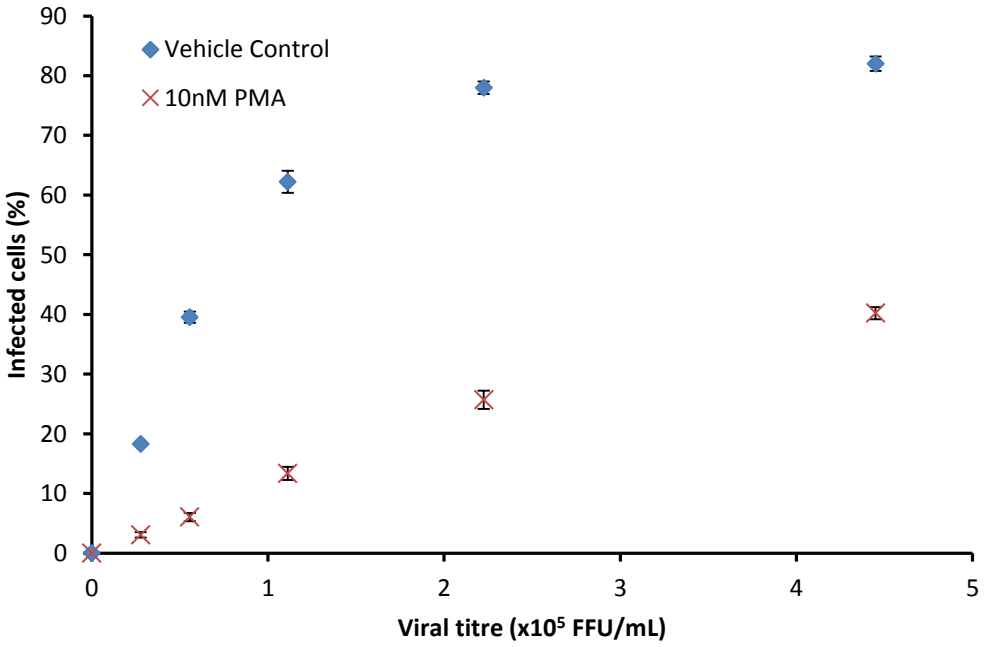

Figure 4.19: IAV infection in THP-1 monocytic and macrophage like cells. IAV infection in differentiated (10nM PMA) and non-differentiated (vehicle control) THP-1 cells following inoculation in TBS and calcium. Data represents 1 experiment conducted in triplicate (n=3±SEM).

4.4. Discussion

The H3N2 Influenza A virus (IAV) subtype was first detected in humans during the Hong Kong pandemic of 1968 and is still regarded to be one of the most virulent human IAV subtypes [331]. Over the last 4 decades this virus has evolved within the human population through the increasing addition of glycans to the viral HA. This process has led to reduced susceptibility to antibody mediated neutralisation but enhanced susceptibility to SP-D inhibition [190]. The ability of SP-D to neutralise IAV is dependent on the glycosylation of the HA proteins on the viral membrane. SP-A is less effective at neutralising IAV than SP-D; however, SP-A binding to IAV is independent of HA glycosylation and acts through the inhibition of IAV attachment to cells by competing for sialic acid binding sites [332, 333]. This is due to the partially sialylated residue at position 187 in the CRD of SP-A [73, 74, 334]. The glycosylation site at codon 165 of SP-D has previously been shown to be

important in determining the sensitivity of IAV strains containing the H3 subtype to β inhibitors. Glycosylation is the biological process in which carbohydrates are linked to biological molecules and glycosylation sites require an amino acid sequence of Asn-X-Ser or Asn-X-Thr where X is any amino acid [335]. The X-79Δ167 strain contains a threonine to isoleucine amino acid change at codon 167 and as a consequence the asparagine at position 165 cannot be glycosylated. This chapter focuses on the propagation and purification of the β sensitive H3N2 X-79 strain and its variant the β resistant X-79Δ167 strain of IAV in order to study the effects of nanoparticles on collectin mediated IAV inhibition. X-79 has previously been shown to replicate ineffectively in wild type and SP-A$^{-/-}$ mice; whereas it replicates effectively in SP-D$^{-/-}$ and SP-A/SP-D$^{-/-}$ double knockout mice with maximal infection occurring 4 days post infection (dpi) [336]. This indicates the relative importance of SP-A and SP-D in the defence against X-79 infection in mice; mice with functional SP-D are able to neutralise X-79 infections whereas SP-A is unable to effectively neutralise these infections. X-79Δ167 virus is able to efficiently replicate in wild type mice with similar levels of IAV infection seen in wild type, SP-A$^{-/-}$ and SP-D$^{-/-}$ 4dpi [336]. Preliminary *in vitro* experiments with HAA and infection assays indicated that the X-79Δ167 strain was sensitive to SP-D mediated neutralisation. In fact in the HAA the X-79Δ167 strain was more sensitive than the parental X-79 strain. Furthermore, wild type C57BL/6 mice infected with varying concentrations of X-79Δ167 showed no signs of morbidity and mortality. This is in contrast to previously published data which showed that this strain is highly virulent in wild type mice [336]. Although this could be due to low viral titres, coupled with the preliminary *in vitro* experiments showing SP-D sensitivity strongly suggests that the virus has mutated. This could be verified by sequencing. Therefore, further experiments were not conducted with this viral strain; in

order to perform further experiments with X-79Δ167 a new viral stock will have to be sourced.

The purification of the X-79 virus strain was conducted using a sucrose gradient as previously described [325]. Studying the effect of nanoparticles on surfactant protein mediated IAV inhibition will involve dynamic interactions between particle, protein and virus at the nano-bio interface; the addition of host cell proteins and contaminants could interfere or alter these interactions. The purification of the virus was therefore an important step prior to the commencement of these nanoparticle studies.

The fluorescent focus assay (FFA) is an assay which has been used since the 1960's to identify and quantify infectious virus in *in vitro* cell models [337]. The FFA has a number of disadvantages including having the possibility of observer bias, being time consuming and having a low throughput. Therefore, an alternative assay was required in order to accurately and reproducibly quantify infection *in vitro*. Flow cytometry is a highly sensitive method for the quantification of cellular fluorescence and has previously been used to monitor IAV infection in *in vitro* cell models [338]. Flow cytometry was therefore compared to the FFA in the quantification of IAV in MDCK cells. Both techniques showed a linear relationship between viral titre and infection levels; however the percent of infected cells was higher using flow cytometry than the FFA. This may be due to the increased detection sensitivity of flow cytometry compared with fluorescent microscopy. Flow cytometry also quantifies a much greater number of cells from a more representative sample selection. In a typical FFA experiment IAV infection is evaluated in approximately 500 cells per treatment whereas in flow cytometry, ten thousand cells are counted per sample. Overall, the results show that flow cytometry provides a reliable and sensitive technique to quantify IAV infection of cell cultures. Flow cytometry is also a high throughput technique which eliminates the issue of observer bias.

Another advantage of flow cytometry is that it will allow the simultaneous quantification of IAV infection and uptake of fluorescent nanoparticles in future experiments. Flow cytometry was therefore adopted as the detection method for evaluating the effects of collectins on IAV infection. A secondary antibody with the allophycocyanin (APC) fluorophore conjugate was chosen for flow cytometry experiments as this fluorophore has minimal overlap with any of the fluorescent nanoparticles to be used in later co-exposure experiments.

IAV has previously been shown to be able to mutate during propagation *in vitro* [339]. Alterations to the envelope proteins of IAV can alter virus susceptibility to antibody or collectin mediated neutralisation [195, 340]. It was therefore important to ensure that the virus was still susceptible to SP-A and SP-D mediated neutralisation. The IC50 values of nhSP-A and two oligomeric preparations (800kDa and 1.7mDa) of nhSP-D against purified X-79 IAV in MDCK cells were determined. These results revealed that X-79 IAV maintained its β inhibitor sensitivity. This was also confirmed using the haemagluttination inhibition assay.

Glutaradehyde fixed sheep red blood cells have previously been successfully used for determining viral titres of Newcastle disease and influenza viruses with the HAA [328]. They were therefore investigated for use in this assay. During the course of a number of experiments they produced highly variable and unreliable viral titres, and therefore the use of human RBCs were investigated. Determining viral titre was much more reliable and reproducible using human RBCs. Moreover, changing the buffer to TBS with either calcium or EDTA had no effect on viral titre. Therefore, human RBCs were chosen to determine the effect of nhSP-A and nhSP-D on X-79 IAV haemagglutination in the presence of calcium or EDTA. nhSP-A has been previously reported to inhibit haemagglutination of RBC by the Mem7lH-BeIN strain of IAV; the ability of nhSP-A to inhibit this haemagglutination of this IAV strain was more

than ten times less than nhSP-D. Moreover, the addition of maltose and EDTA had no effect of nhSP-A mediated haemagglutination inhibition (HAI) but completely abrogated nhSP-D mediated HAI [326]. These results were confirmed in another study with various IAV strains. This study noted the differences in the ability of nhSP-A to inhibit haemagglutination of different IAV strains; the removal of a high mannose oligosaccharide residue close to the SA binding site on the HA resulted in an increase in the inhibitory capacity of nhSP-A against virus HA [196]. This is consistent with the mechanism of SP-A neutralisation of IAV as SP-A binding is calcium independent and relies on the partially sialyated asparagine 187 residue on nhSP-A. In the current study, nhSP-A inhibited the haemagglutination of X-79 at concentrations of 20μg/mL in EDTA but not in calcium. This is consistent with the haemagglutination of IAV by SP-A being calcium independent as described in the literature.

Hartshorn et al. (2007) reported that human SP-D trimers showed reduced activity against various IAV strains compared to their multimeric counterparts. This was observed by enhanced binding, and greater inhibitory capacity against virus haemagglutination and *in vitro* infection of multimeric SP-D [196]. These results have been confirmed with those of the current study which showed around a ten times decrease in the haemagglutination inhibition concentration and eight times decrease in IC50 of IAV infection in MDCK cells in 1.7mDa compared to 800kDa SP-D. As mentioned in Chapter 2 the 800kDa SP-D oligomer contained large amounts of nhSP-A. As nhSP-A did not inhibit X-79 haemagglutination at concentrations up to and including 20μg/mL in the presence of calcium it is reasonable to assume that the HAI observed in the 800kDa preparation is due to the presence of SP-D in the preparation. Moreover, the recombinant fragment of SP-D (rfhSP-D) which is unable to produce supratrimeric oligomers showed no inhibitory effect on the haemagglutination of X-79 IAV.

A549 cells were originally derived from a lung adenocarcinoma and is one of the most commonly used cells in nanotoxicity studies as a model for alveolar epithelial cells [293]. It was originally proposed that A549 cells were a good model for ATII cells; however, as they do not express surfactant or possess alkaline phosphatase activity which are characteristics of the ATII phenotype the suitability of these cells as ATII models has been widely debated in the literature [293, 324, 341-344]. TT1 were originally derived from primary ATII cells however, following transformation they developed an ATI like phenotype and are therefore regarded as a ATI like cell line [324]. A549 and TT1 were infected with a concentration gradient of IAV to determine the optimum IAV concentration to use for reduction experiments. The results show that these cells infect to a similar degree to each other however, MDCK cells infected much more readily than the alveolar epithelial cells. This is likely due to the virus undergoing positive selection during propagation in the MDCK cells.

Due to the similar levels of infectivity in the A549 and TT1 cell lines a concentration of $2.2x10^5$ FFU/mL was chosen for both cell types for the reduction experiments. This concentration produced a sub-maximal yet detectable level of infection in both cell lines. The use of a sub-maximal level of infection is important in order to effectively detect any modulation in infection levels by the exogenous factors to be tested (i.e. nanoparticles and proteins).

The inoculation buffer for the infection experiments was changed from serum free RPMI to TBS containing 5mM calcium. This change had no effect on either the infection levels in MDCK cells or the viability of A549 or TT1 cells. This change was conducted to ensure sufficient calcium for the lectin function of the surfactant proteins. Moreover, the amine nanoparticles also showed enhanced stability in the TBS buffer at room temperature compared to RPMI (see Chapter 4).

As MDCK cells infect much more readily than either A549 or TT1 cells 5 times more virus was required to yield similar infection rates. The range of protein concentrations required to produce submaximal reductions in IAV infection was therefore altered accordingly. This strategy was successful in identifying the IC50 values for SP-A and SP-D against X-79 infection. SP-A and SP-D resulted in dose dependent reductions in IAV infection in the A549 and TT1 cell lines. At sub-maximal concentrations SP-D was more effective at neutralising IAV infection in A549 versus TT1 cells. According to the IC50 values SP-D was 15.5 times more effective at neutralising IAV X-79 than SP-A in A549 cells and 15.9 times more effective in TT1 cells. Whereas in MDCK cells SP-D was 21 times more effective at neutralising X-79 infection than SP-A.

In order to determine the effects of nanoparticles and surfactant proteins on influenza infection in macrophages a macrophage cell line had to be optimised for use with influenza. As the other cells optimised for these experiments were derived from humans, human macrophage cells were wanted to maintain species specificity within these experiments. As the macrophage like cells used in previous chapters, RAW264.7 cells are murine derived a human alternative was found. THP-1 cells are a human leukemic monocytic cell line which grow in suspension and can be differentiated into macrophage like cells using agents such as PMA or VD3 (1,25-dihydroxyvitamin D3) [345]. PMA was chosen as a differentiation agent as it is one of the most commonly used in the literature and has been shown to result in enhanced markers of macrophage differentiation as compared to other agents such as VD3 [346]. A number of differentiation protocols have been described in the literature and different resulting phenotypes have also been described. In one study PMA differentiated cells phagocytosed less latex beads than human monocytes; in this study a non-significant increase in CD14 expression was also reported [347]. In another study PMA differentiation resulted in enhanced phagocytic activity

and increased CD11b and CD14 expression compared with untreated cells [346]. Several markers of macrophage differentiation were therefore characterised following PMA differentiation to ensure optimal differentiation of these monocytic cells to macrophage like cells. It has been reported that before PMA induces the differentiation of THP-1 cells, PMA must inhibit cell growth through inducing G1 arrest in the cell cycle [348]. The proliferation of cells following PMA differentiation was therefore, examined in this study using cell counts. The results confirm that PMA inhibits cell proliferation at a concentration of 10nM. A higher concentration of 100nM resulted in a 50% reduction in cell numbers compared to the number of cells plated which may indicate toxicity of this treatment. Consistent with previous studies, PMA differentiated cells became adherent within 24 hours of treatment and developed macrophage-like morphology with 10nM PMA treatment [349, 350]. The granularity of the cells significantly increased following PMA differentiation which is consistent with previous studies [347, 350]. However, the cell size did not significantly increase. This may be due to loss of the filipodia like projections and cell rounding following cell trypsinisation.

CD14 is a 55kDa glycoprotein found on the surface of monocytes, macrophages and on a lesser extent on neutrophils. CD14 plays an important role in recognising bacterial challenge as it binds bacterial LPS and through a complex with TLR4 activates NF-κB intracellular signalling. A number of studies have shown that differentiation of THP-1 cells into macrophage like cells results in up-regulation of this differentiation marker [346, 347, 351]. The current study supports these findings in showing an increase in the CD14 expression on THP-1 cells treated with 10nM PMA. CD11b is a cell adhesion molecule commonly used as a marker of macrophage differentiation. In this study 10nM PMA resulted in increased CD11b expression, consistent with macrophage differentiation [346].

One of the most important functions of macrophages is their ability to phagocytose microbial challenges. The phagocytic capacity of monocytes is typically increased following monocyte-macrophage differentiation. However, as mentioned previously different effects of PMA differentiation on THP-1 phagocytic ability have been reported previously. It was therefore, important to characterise the effect of PMA differentiation on the ability of THP-1 cells to phagocytose a bacterial challenge. In this study, *E. coli* bioparticles labelled with a pH sensitive dye was used to assess the phagocytic capacity of THP-1 cells following PMA differentiation. The pH sensitivity of the dye means that only bioparticles within the acidic environment of the lysosome will fluoresce. The results show that 10nM PMA resulted in a 3 fold enhancement in the uptake of these bacterial particles. Due to the culmination of these results, 10nM PMA treatment for 72 hours was chosen as the treatment to differentiate THP-1 cells into macrophage like cells.

Previous studies have shown that macrophages and monocytes are susceptible to IAV infection [329]. The ability of influenza to productively replicate in macrophages is widely disputed in the literature. Some studies have shown that although IAV can infect and produce viral proteins within macrophages the replicative cycle is abortive and progeny virions are not produced [352, 353]. Whereas other studies have reported that IAV infection of macrophages can result in productive virus replication [354, 355]. On the other hand strains of IAV which have been shown to reproduce ineffectively in alveolar macrophages could productively replicate in peripheral blood derived monocytes (PBDM) [354]. In this study a concentration gradient of virus were conducted in differentiated (10nM PMA) and non-differentiated THP-1 cells. The results showed that non-differentiated cells infected more readily than their differentiated counter parts which may be due to differences in the cell surface receptors. The differentiated THP-1 cells infected to a similar degree than the

A549 and TT1 cells and therefore, a concentration of 2.23 x10^5FFU/mL will be used for the reduction assays for all three cell lines. The same concentration of proteins for these cell lines will also be used for these experiments to ensure that the results can be directly compared between the cell lines.

Chapter 5: Nanoparticles modulate Surfactant Protein A and D neutralisation of Influenza A infection *in vitro*.

5.1. Introduction

Numerous epidemiological and toxicological studies have shown that enhanced exposure to airborne particulates can enhance susceptibility, severity and/or resolution of pulmonary infections [215, 216, 221, 222]. These effects are especially evident in individuals with existing pulmonary conditions such as chronic obstructive pulmonary disease or other at risk groups such as the elderly and young children [216, 217]. Surfactant Proteins A and D have been reported to associate with nanoparticles and this interaction has been shown to alter the cellular uptake of these nanoparticles (Chapter 3 and [266, 267, 291]). It was therefore hypothesised that the interaction between nanoparticles and SP-A and SP-D could lead to a deficiency in these innate immune molecules and enhanced susceptibility to infection. In order to test this hypothesis an *in vitro* infection model, optimised in Chapter 4, was used to determine the effect of 100nm U-PS and A-PS particles on the SP-A and SP-D mediated neutralisation of influenza virus. This was conducted in three cell lines, TT1, A549 and differentiated THP-1 cells to reflect the major cell types found in the alveolar epithelium, namely the alveolar type I and type II cells and the alveolar macrophages.

5.2. Methods

5.2.1. Cell culture

A549, TT1 and THP-1 cells were routinely sub-cultured as described previously in Chapter 4. TT1 and THP-1 cells were kindly provided by Professor Terry Tetley and Liku Tezera respectively.

5.2.2. IAV infection

5.2.2.1 Plating cells

A549 and TT1 cells (0.3mL) were seeded at a density of $4.16x10^5$/mL in 48 well plates (Corning, UK). The cells were incubated for 24 hours in relevant growth medium then serum starved for 24 hours in serum free RPMI. THP-1 cells (0.3mL) were seeded at a density of $4.16x10^5$/mL in 48 well plates in growth medium containing 10nM PMA and incubated at 37°C 5% CO_2 in a humidified atmosphere for 72 hours as described in Chapter 4. The cells were then serum starved for 24 hours in SF RPMI.

5.2.2.2 Preparing IAV/NP/protein inoculum

Fluorescent orange A-PS (100nm; Sigma, UK) or green U-PS (100nm; Polysciences, UK) particles were prepared at three times the final concentration in TBS with 5mM calcium. SP-A, SP-D (1.7mDa), rfhSP-D and BSA were also prepared in TBS with 5mM calcium at three times the final concentration. Equal volumes of NP suspension and protein suspensions were added to 48 well plate, the plate was gently agitated and incubated at 37°C for 1 hour. IAV was prepared at three times the final concentration ($2.23x10^5$ FFU/mL) in TBS with calcium and then added to the NP and protein suspension. The inoculum was then incubated for a further hour at 37°C.

5.2.2.3 Infecting cells

The medium was removed from the serum starved cells and replaced with the inoculum from section 5.2.2.2. The cells were then incubated for 1 hour at 37°C 5% CO2 in a humidified atmosphere. The cells were washed three times in SF RPMI and the cells were then incubated in fresh SF RPMI (0.5mL) for 18 hours at 37°C 5% CO2 in a humidified atmosphere. Following this period, the cells were trypsinsed, fixed, stained and analysed by flow cytometry as described in Chapter 4.

5.2.3. Clonogenic assay

TT1 cells (3mL) were seeded in growth medium at a density of $2x10^2$ cells /mL in 6 well plates and incubated for 24 hours at 37°C 5% CO_2 in a humidified atmosphere. The medium was then removed and replaced with 100nm A-PS or U-PS particles in TBS with calcium at the indicated concentrations which had been pre-incubated for 2 hours at 37°C. The cells were then incubated for 1 hour with the particles and then the medium was replaced with fresh growth medium and incubated for 7 days undisturbed. The cells were then stained using crystal violet staining solution and the colonies counted as described in Chapter 3.

5.2.4. MTT assay

A549 and TT1 cells were seeded at a density of $8x10^3$ cells per well in the appropriate growth medium in Nuncalon 96 well plates (Fisher, UK). This density of cells was shown in Chapter 4 to result in a sub-maximal production of formazan. The cells were then incubated for 24 hours at 37°C 5% CO_2 in a humidified atmosphere then serum starved for a further 24 hours in SF RPMI. The cells were then exposed to A-PS or U-PS particles in TBS with 5mM calcium

which had been pre-incubated for 1 hour at 37°C and then for a further hour with IAV ($2.23x10^5$ FFU/mL) as described in section 5.2.2.2.

5.2.5. Statistics

Relative infection rates, relative mean fluorescence intensity (MFI) and the percent of nanoparticle positive (%NP+) cells are reported as mean values. Differences between two treatments were determined using the Mann-Whitney U test. p values of ≤0.05 were considered statistically significant. p values were determined using the Mann-Whitney U test unless otherwise stated. Infection rates and nanoparticle uptake were normalised for each experiment prior to analysis. The ability of the particles to modify surfactant protein neutralisation was calculated using the following formula;

Equation 3: Relative change in IAV neutralisation (%) = ((B – A) / A) x 100

Where B is the percent of uninfected cells in the NP, protein and IAV treatment and A is the percent of uninfected cells in the appropriate IAV and protein control.

5.3. Results

In this study concentrations of 5μg/mL nhSP-A and 0.4μg/mL nhSP-D were chosen which have previously been shown in Chapter 4 to induce a submaximal inhibition of IAV infection. Thus any nanoparticle induced modulation in the ability of these proteins to neutralise infection may be detected. Nanoparticles were initially pre-incubated with proteins for one hour then influenza was added to the inoculum and incubated for a further hour. This procedure was chosen in order to test the hypothesis that NP would sequester surfactant proteins and thereby attenuate their ability to neutralise infection. Incubations were conducted in Tris buffered saline containing 5 mM

calcium, sufficient for the lectin functionality of the collectins. This buffer was shown not to alter cell viability or influenza infection rates compared to serum free RPMI media (see Chapter 4). The effect of nanoparticles on rfhSP-D mediated neutralisation was examined in order to determine whether nanoparticles could enhance the therapeutic potential of this protein. Bovine serum albumin (BSA) was used to determine the effect of a non-specific protein on influenza infection and nanoparticle uptake in these experiments.

5.3.1. Effect of Surfactant Proteins on IAV infection

Three cell lines were used to study the effect of nanoparticles on SP-A and SP-D mediated neutralisation of influenza A virus (IAV). These cells were the alveolar type I (ATI) like epithelial TT1 cells, the ATII like A549 cell line and a macrophage like (THP-1) cell line. These cells represent the predominant cell types found in the alveolus [16]. All THP-1 cells used in these experiments were differentiated for 72 hours with PMA. This treatment was shown in Chapter 4 to induce a macrophage like phenotype including enhanced CD11b and CD14 expression, increased phagocytic ability, loss of proliferative potential and development of filopodia like projections.

nhSP-A and nhSP-D significantly reduced X-79 IAV infection in each of the cell lines studied. These reductions are summarised in Figure 5.1A and B and Table 5.1. The pre-incubation of nhSP-A with IAV resulted in 16.5%, 31.6% and 36% reductions in IAV infection in THP-1, TT1 and A549 cells respectively. Each of these differences was highly statistically significant with p values of ≤0.001. nhSP-D resulted in highly significant 34.6%, 36.5% and 58.8% reductions in IAV infection in THP-1, TT1 and A549 cells ($p<0.001$). The pre-incubation of rfhSP-D attenuated IAV infection by 11.8% and 6.5% in A549 cells and TT1 cells respectively. These reductions were highly statistically significant with respective p values of <0.001 and 0.007 (see Figure 5.1C). IAV infection was also

reduced in THP-1 cells following pre-incubation with rfhSP-D. However, this 5.2% reduction was not statistically significant (p=0.132). BSA had no significant effect on IAV infection in THP-1, A549 or TT1 cells at the dose studied (see Figure 5.1D and Table 5.1).

The efficacy of surfactant proteins on IAV neutralisation was also compared between these cell lines. Figure 5.1 shows that the attenuation of IAV infection by SP-A and SP-D was greatest in the A549 cell line followed by TT1 then THP-1 cells (A549>TT1>THP-1). In the case of SP-A only the difference between A549 and THP-1 was statistically significant with an associated p value of 0.01. In the case of SP-D, the difference between A549 and THP-1 as well as A549 and TT1 were statistically significant (p=0.003 and p=0.005 respectively). Interestingly, the attenuation of IAV by rfhSP-D in these cell lines was also of the order A549>TT1>THP-1. However, there was no statistical significance between these variations.

	A549		**TT1**		**THP-1**	
	Mean	**p value [#]**	**Mean**	**p value[#]**	**Mean**	**p value[#]**
SP-A	62.1	**<0.001**	70.3	**<0.001**	79.5	**0.001**
SP-D	41.1	**<0.001**	60.6	**<0.001**	65.8	**<0.001**
rfhSP-D	88.9	**<0.001**	93.6	**0.007**	92.6	0.132
BSA	101.2	0.616	97.7	0.073	111.2	0.132

Table 5.1: Relative infection rates in A549, TT1 and THP-1 cells following pre-incubation with proteins

[#] Mann-Whitney U test compared to IAV only control. Significant values in bold.

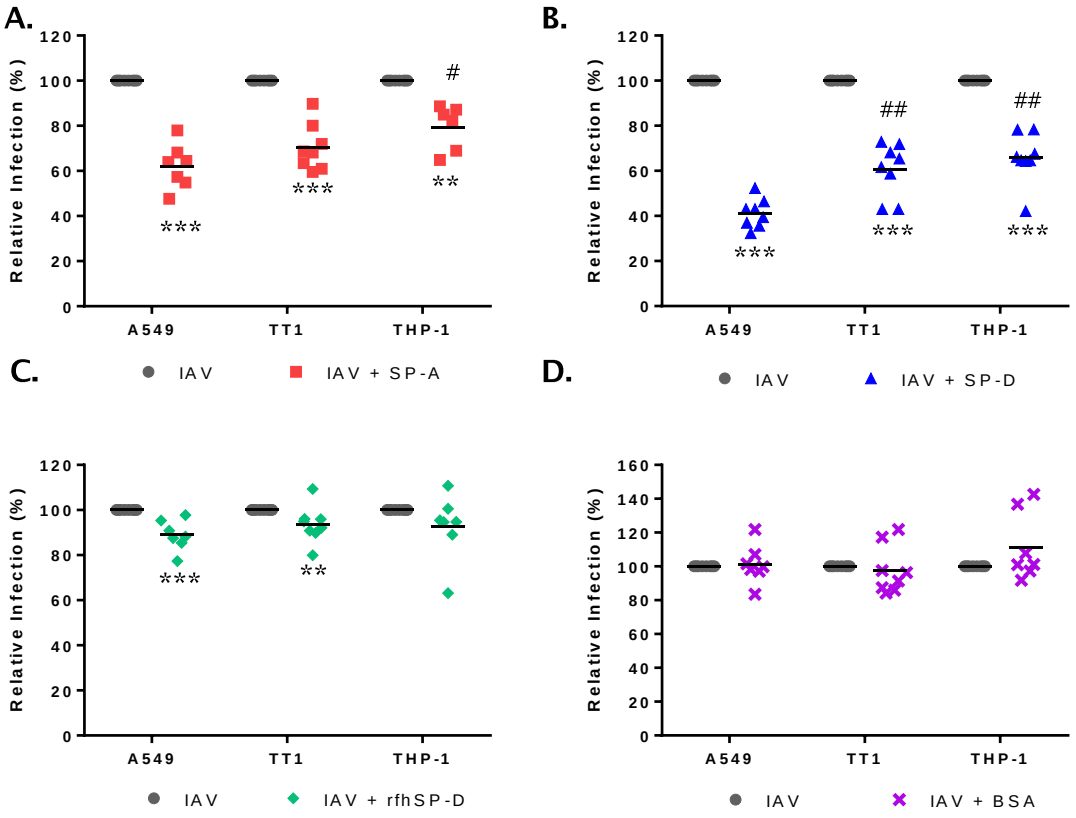

Figure 5.1: Comparing the efficacies of surfactant proteins on influenza infection between A549, TT1 cells and differentiated THP-1. Effect of **A.** nhSP-A (5µg/mL); **B.** nhSP-D (0.4 µg/mL); **C.** rfhSP-D (5 µg/mL) and **D.** BSA (5 µg/mL) Data represents mean (black horizontal line) of at least six independent experiments conducted in duplicate. Statistics determined using Mann-Whitney U test; *** $p<0.001$ vs. IAV control; **$p<0.01$ vs. IAV control; # $p<0.05$ vs. A549 protein control; ## $p<0.01$ vs. A549 protein control.

5.3.2. Nanoparticles, surfactant proteins and IAV infection

5.3.2.1 Effect of U-PS on IAV infection

The effect of 100nm cationic A-PS and anionic U-PS nanoparticles on influenza infection in these cell lines was examined in the A549, TT1 and THP-1 cell lines. The pre-incubation of 100nm U-PS with IAV had no significant effect on IAV infection in A549 cells at any of the NP concentrations studied; 0.0016, 0.04, 1 or 5 cm^2/mL (see Table 5.2). In TT1 cells, the pre-incubation of 100nm U-PS particles with IAV tended to result in reduced infection. The pre-incubation of 0.04 cm^2/mL U-PS with IAV resulted in a 7.3% reduction in infection in TT1

cells compared to IAV alone. This was statistically significant with an associated p value of 0.037. Pre-incubation of 0.0016, 1 and 5 cm^2/mL U-PS with IAV resulted in 1.6%, 7.8% and 5% non-significant reductions in IAV infection in TT1 cells (p=0.487 for each). In THP-1 cells, the pre-incubation of U-PS particles with IAV tended to increase infection in these cells. However, these increases were not statistically significant (see Table 5.2). For ease of comparison the effect of the nanoparticles on influenza infection are graphically represented against each individual protein tested. As the incubation of 0.04 cm^2/mL U-PS with IAV resulted in a significant reduction in the IAV infection in TT1 cells, the effect of proteins on this treatment will be directly compared to the nanoparticle and IAV treatment.

Treatment	NP concentration (cm²/mL)					
A549 cells		**0**	**0.0016**	**0.04**	**1**	**5**
U-PS	Mean	100.0	100.4	97.0	98.7	100.2
	p value	-	0.219 [b]	0.219 [b]	0.219 [b]	1.000 [b]
U-PS + SP-A	Mean	65.5	73.5	74.1	63.4	48.8
	p value	**0.019** [a]	**0.050** [b]	**0.050** [b]	0.275 [b]	**0.050** [b]
U-PS + SP-D	Mean	44.7	48.6	44.2	45.3	13.9
	p value	**0.014** [a]	0.386 [b]	0.773 [b]	1.000 [b]	**0.021** [b]
U-PS + rfhSP-D	Mean	86.9	90.4	91.9	91.9	85.5
	p value	**0.019** [a]	0.827 [b]	0.513 [b]	0.275 [b]	0.827 [b]
U-PS + BSA	Mean	101.8	108.6	100.3	99.1	98.8
	p value	0.435 [a]	0.275 [b]	0.827 [b]	0.827 [b]	0.513 [b]
TT1 cells						
U-PS	Mean	100.0	98.4	92.7	92.2	95.0
	p value	-	0.487 [b]	**0.037** [b]	0.487 [b]	0.487 [b]
U-PS + SP-A	Mean	73.6	67.7	63.8	74.4	60.6
	p value	**0.037** [a]	0.513 [b]	0.513 [b]	0.827 [b]	0.127 [b]
U-PS + SP-D	Mean	60.1	69.1	78.8	59.7	16.3
	p value	**0.037** [a]	0.513 [b]	**0.050** [b]	0.827 [b]	**0.050** [b]
U-PS + rfhSP-D	Mean	92.7	98.7	93.7	92.1	95.2
	p value	**0.037** [a]	0.513 [b]	0.658 [b]	0.827 [b]	0.513 [b]
U-PS + BSA	Mean	99.7	92.5	94.0	88.1	101.7
	p value	0.487 [a]	0.513 [b]	0.827 [b]	0.513 [b]	0.827 [b]
THP-1 cells						
U-PS	Mean	100.0	112.4	105.6	106.3	102.0
	p value	-	0.219 [b]	0.219 [b]	0.219 [b]	1.000 [b]
U-PS + SP-A	Mean	90.0	97.0	101.5	91.5	98.1
	p value	**0.014** [a]	0.564 [b]	0.149 [b]	0.386 [b]	0.564 [b]
U-PS + SP-D	Mean	68.4	70.7	75.6	67.1	46.4
	p value	**0.014** [a]	0.386 [b]	0.386 [b]	0.773 [b]	**0.021** [b]
U-PS + rfhSP-D	Mean	89.6	89.3	95.9	101.7	90.3
	p value	0.435 [a]	0.827 [b]	0.827 [b]	0.513 [b]	0.827 [b]
U-PS + BSA	Mean	111.7	109.2	86.2	103.9	90.6
	p value	0.435 [a]	0.827 [b]	0.275 [b]	0.827 [b]	0.275 [b]

Table 5.2: Relative Infection following influenza pre-incubation with U-PS and proteins. [a] p values determined using Mann-Whitney U test versus protein free control; [b] p values determined using Mann-Whitney U test versus nanoparticle free protein containing control.

5.3.2.1.1. Effect of U-PS on SP-A mediated IAV neutralisation

In A549 cells, a biphasic modulation of SP-A mediated IAV neutralisation was observed following the pre-incubation with 100nm U-PS. The pre-incubation of low concentrations of 100nm U-PS particles with nhSP-A resulted in an increase in infection rates in A549 cells compared to when IAV was incubated with SP-A alone (see Figure 5.2A). There were significant 8.0% and 8.6% increases in relative infection rates in A549 cells following pre-incubation of SP-A with 0.0016 cm^2/mL and 0.04 cm^2/mL U-PS. These differences were statistically significant with associated p values of 0.050 (see Table 5.2). These differences represent 23.2% and 24.9% relative decreases in the ability of nhSP-A to neutralise IAV infection. The pre-incubation of 5 cm^2/mL U-PS with nhSP-A resulted in a 16.7% reduction in IAV infection compared to the IAV and SP-A control. This difference was statistically significant with a p value of 0.050. This represents a 48.4% increase in the ability of nhSP-A to neutralise IAV infection (see Table 5.2).

In TT1 cells, pre-incubation of 100nm U-PS with nhSP-A had no significant effect on IAV infection rates (see Table 5.2). The pre-incubation of 5 cm^2/mL of U-PS with nhSP-A resulted in a 13% reduction in IAV infection in TT1 cells compared to the protein control, which represents a 49.2% increase in the ability of nhSP-A to neutralise IAV infection; however this modification did not reach statistical significance (p=0.127; see Figure 5.2B). The addition of SP-A to the 0.04cm^2/mL U-PS and IAV treatment resulted in a 28.9% reduction in IAV infection. This was statistically significant with an associated p value of 0.050.

In differentiated THP-1 cells, U-PS tended to result in increases in the IAV infection compared to nhSP-A in the absence of particles. However, these differences were not statistically significant (see Table 5.2 and Figure 5.2C).

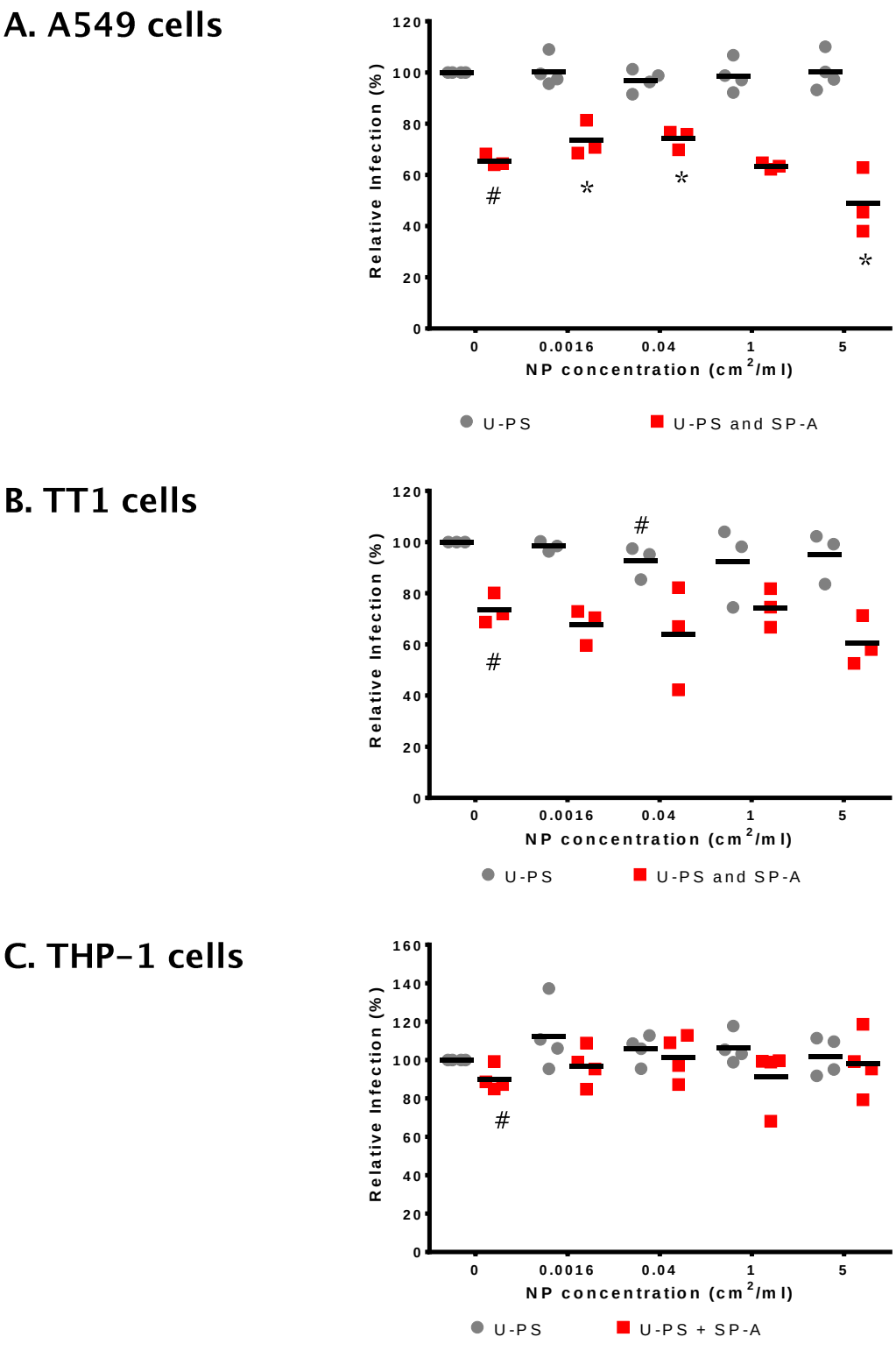

Figure 5.2: Effect of 100nm U-PS on nhSP-A mediated neutralisation in A. A549; B. TT1 and C. THP-1 cells; Horizontal line represents mean of at least three independent experiments conducted in duplicate. Statistics determined using Mann-Whitney U test where *p≤0.050 compared to relative infection in particle free protein control; #p≤0.050 versus IAV alone.

5.3.2.1.2. Effect of U-PS on SP-D mediated IAV neutralisation

In A549 cells, pre-incubation of nhSP-D with 0.0016 cm^2/mL U-PS resulted in a 3.9% increase in IAV infection compared to the IAV and SP-D control. However, this increase was not statistically significant with an associated p value of 0.386. Concentrations of 0.04 and 1 cm^2/mL of U-PS had no significant effect on the nhSP-D mediated inhibition of IAV infection with less than a 2% difference in the mean values between these concentrations and the control (p=0.773 and p=1.000 respectively). Pre-incubation of 5 cm^2/mL U-PS with nhSP-D resulted in a 30.8% reduction in infection compared to SP-D and IAV alone. This difference was statistically significant with an associated p value of 0.021 (refer to Figure 5.3A). This represents a 55.7% relative increase in the inhibition of IAV infection compared to nhSP-D. (see Table 5.1)

In TT1 cells, a biphasic modulation of SP-D mediated IAV neutralisation was observed. The pre-incubation of 0.04 cm^2/mL U-PS with nhSP-D resulted in a significant 18.7% increase in IAV infection compared to the nhSP-D and IAV control (p=0.050). This represents a 46.9% decrease in the ability of SP-D to neutralise IAV infection in this cell line (see Equation 3). However, the level of infection in this triple treatment was still significantly reduced by 13.9% compared to the IAV and NP treatment (p=0.050). Pre-incubation of 0.0016 cm^2/mL with nhSP-D resulted in a 9% increase in the mean infection levels compared to SP-D alone; however, this increase was not statistically significant with an associated p value of 0.513. Pre-incubation of 1 cm^2/mL had no significant effect on nhSP-D mediated IAV reduction in TT1 cells (p=0.827). The highest concentration of U-PS studied, 5 cm^2/mL, resulted in a significant 43.8% reduction in relative infection rates compared to the absence of U-PS (p=0.050; refer to Figure 5.3B and Table 5.2)). This represents a 109.8% relative increase in the inhibition of infection rates compared to nhSP-D).

In differentiated THP-1 cells, pre-incubation of 0.04 cm^2/mL U-PS with nhSP-D enhanced the mean infection rate by 7.2% compared to the NP and SP-D treatment. However, this difference was not statistically significant with a p value of 0.386. Pre-incubation of 0.0016 or 1 cm^2/mL U-PS with nhSP-D had no significant effect on IAV infection rates compared the nhSP-D control (p=0.386 and p=0.773 respectively). Pre-incubation of 5 cm^2/mL of U-PS with nhSP-D resulted in a 22% reduction in IAV infection compared to the nhSP-D and IAV control. This was statistically significant with an associated p value of 0.021 (refer to Figure 5.3C and Table 5.2). This represents a 69.6% relative increase in the inhibition of infection compared to that of nhSP-D alone.).

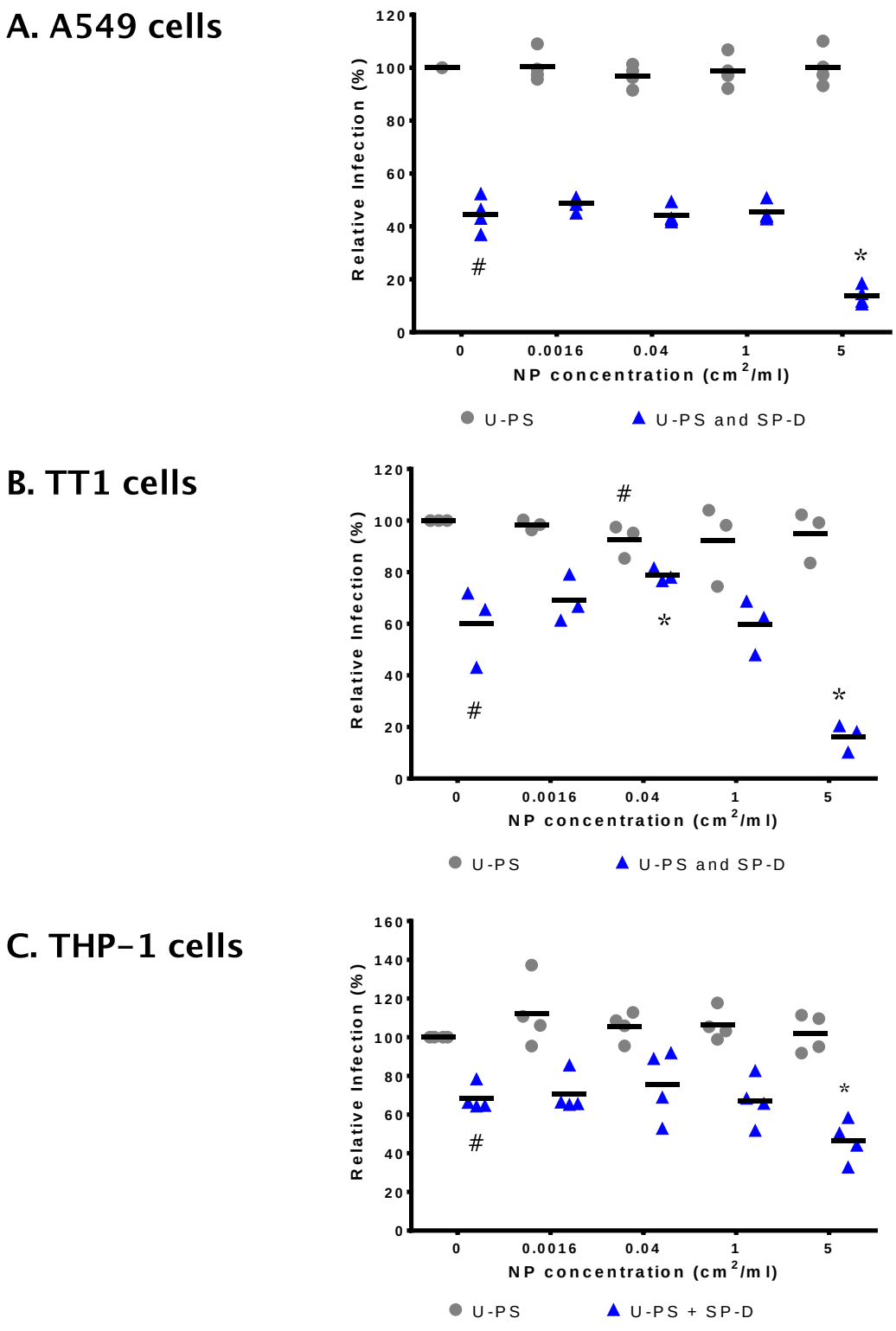

Figure 5.3: Effect of U-PS on nhSP-D mediated IAV neutralisation in A. A549; B. TT1 cells; and C. THP-1 cells. Horizontal line represents mean of at least three independent experiments conducted in duplicate. Statistics determined using Mann-Whitney U test where *p≤0.050 versus relative infection in particle free protein control; #p≤0.050 versus IAV alone.

5.3.2.1.3. Effect of U-PS on rfhSP-D mediated IAV neutralisation

In A549 cells, the pre-incubation of 100nm U-PS with rfhSP-D at concentrations up to and including 1 cm^2/mL tended to cause an increase in IAV infection. The pre-incubation of 5 cm^2/mL U-PS with rfhSP-D reduced IAV infection by 1.3% compared to rfhSP-D alone. However, these differences were not statistically significant (see Table 5.2 and Figure 5.4A).

In TT1 cells, the pre-incubation of 0.0016 cm^2/mL and 5 cm^2/mL with rfhSP-D resulted in 6% and 2.5% respective increases in IAV infection compared to the rfhSP-D control. However, these increases were not statistically significant with p values of 0.513 for each comparison. The pre-incubation of 0.04 cm^2/mL and 1 cm^2/mL with rfhSP-D had no effect on IAV infection in TT1 cells compared to the rfhSP-D control (see Table 5.2 and Figure 5.4B). There was also no significant difference in the IAV infection following the addition of rfhSP-D to the 0.04cm^2/mL U-PS and IAV treatment (p=0.827).

In differentiated THP-1 cells 0.04 and 1 cm^2/mL U-PS pre-incubation with rfhSP-D resulted in 6.3% and 12.1% increases in IAV infection. However, these differences were not statistically significant with associated p values of 0.827 and 0.513 respectively (see Table 5.2 and Figure 5.4C).

5.3.2.1.4. Effect of U-PS and BSA on IAV infection

In A549 cells there were less than 3% non-significant differences in the mean infection rates following pre-incubation of 0.04, 1, and 5 cm^2/mL with BSA compared to the BSA control (see Figure 5.5A and Table 5.2). Pre-incubation of 0.0016 cm^2/mL 100nm U-PS with BSA resulted in a 6.8% increase in IAV infection in A549 cells compared to the BSA control. This increase was not statistically significant with an associated p value of 0.275.

In TT1 cells, 0.0016, 0.04 and 1 cm^2/mL U-PS pre-incubation with BSA resulted in 7.2, 5.7 and 11.7% respective non-significant reductions in IAV infection compared to the BSA and IAV control. The addition of BSA to the 0.04cm^2/mL U-PS and IAV treatment resulted in a non-significant 1.3% increase in IAV infection ($p=0.513$) Pre-incubation of 5 cm^2/mL U-PS enhanced IAV infection in TT1 cells by 2% compared to the protein control. However, this increase was not statistically significant (see Figure 5.5B and Table 5.2).

In differentiated THP-1 cells, pre-incubation of U-PS with BSA tended to result in reduced IAV infection compared to the BSA and IAV controls. However, these reductions were not statistically significant (see Figure 5.5C and Table 5.2).

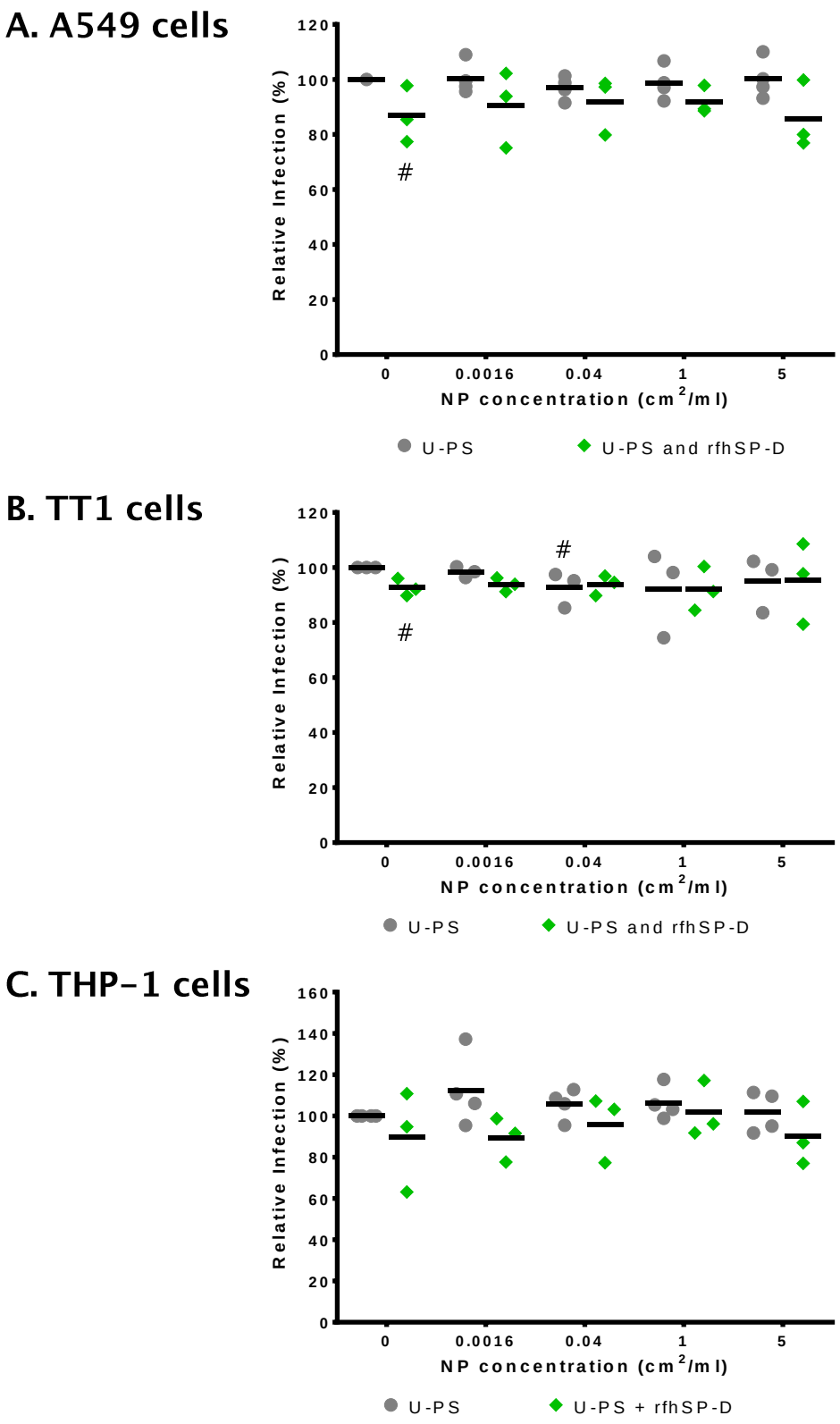

Figure 5.4: Effect of U-PS on rfhSP-D mediated IAV neutralisation in A. A549; B. TT1 cells; and C. THP-1 cells. Horizontal line represents mean of at least three independent experiments conducted in duplicate. Statistics determined using Mann-Whitney U test where *p≤0.050 compared to relative infection in particle free protein control; #p≤0.050 versus IAV alone.

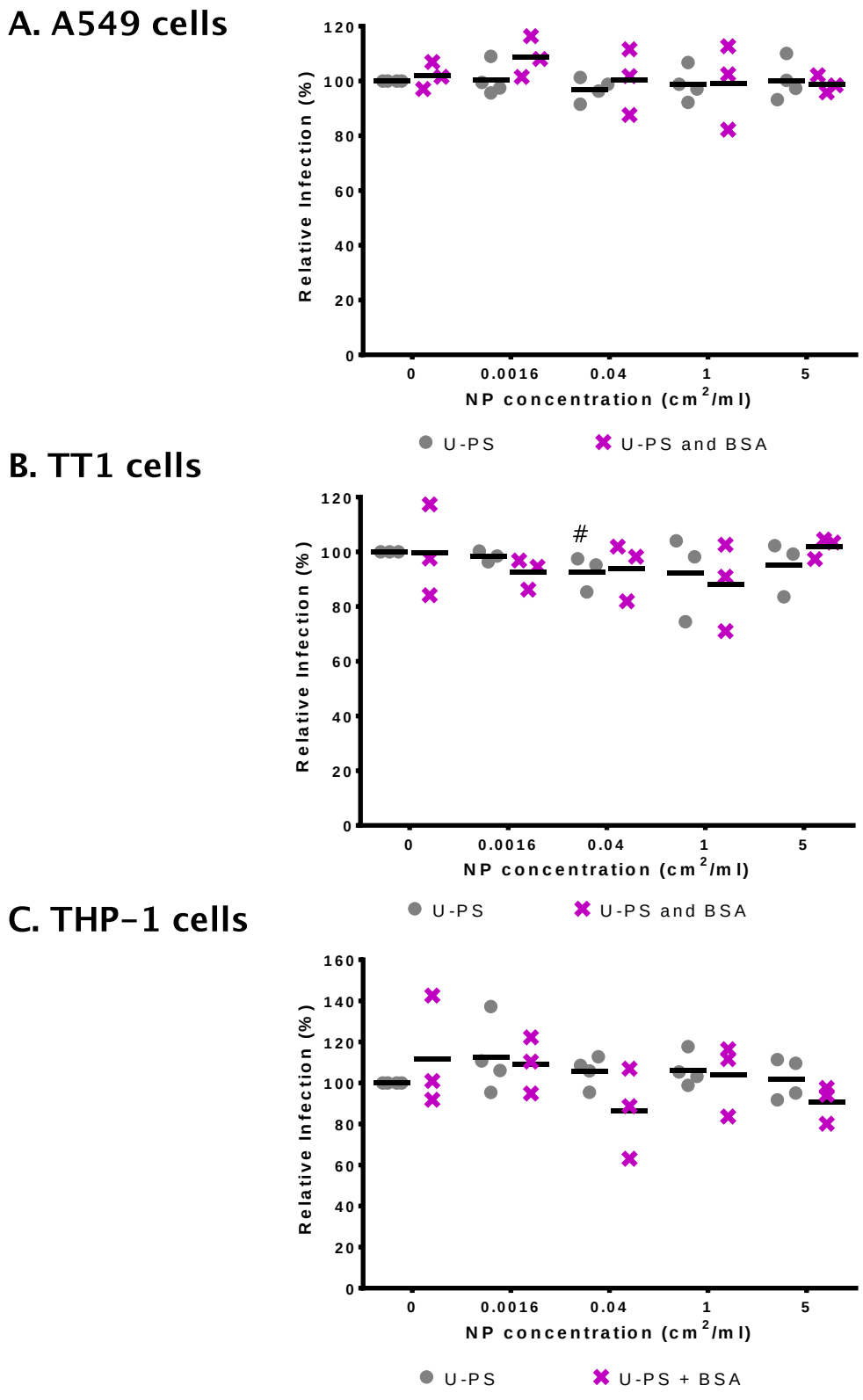

Figure 5.5: Effect of U-PS and BSA on IAV infection in A. A549; B. TT1 cells; and C. THP-1 cells. Horizontal line represents mean of at least three independent experiments conducted in duplicate. Statistics determined using Mann-Whitney U test where *p≤0.050 compared to relative infection in particle free protein control; #p≤0.050 versus IAV alone.

5.3.2.2 Effect of A-PS on IAV infection

In A549 cells 100nm A-PS resulted in a dose dependent decrease in IAV infection, with 0.0016, 0.04, and 1cm^2/mL resulting in 2%, 4%, and 7.4% respective reductions in IAV infection. However, these differences were not statistically significant with p values of 1.000, 0.219 and 0.219 respectively. A-PS particles at 5cm^2/mL resulted in a significant 33.2% reduction in IAV infection in A549 cells (p=0.014). In TT1 cells 5 cm^2/mL of 100nm A-PS resulted in a 19.8% reduction in IAV infection. This was highly statistically significant with an associated p value of 0.005. Lower A-PS concentrations (0.0016, 0.04 and 1cm^2/mL) had ≤2.5% modulatory effect on the mean IAV infection in TT1 cells. However, these differences were not statistically significant (see Table 5.3). In THP-1 cells A-PS particles had no significant effect on IAV infection at the studied concentrations (see Table 5.3). As the 5cm^2/mL and IAV treatment resulted in significant reductions in the IAV infection in A549 and TT1 cells, the infection rates following the addition of protein to these treatments will be directly compared to the relevant NP and IAV co-treatment.

Treatment		NP concentration (cm²/mL)				
A549 cells		**0**	**0.0016**	**0.04**	**1**	**5**
A-PS	Mean	100.0	98.0	96.0	92.6	66.8
	p value	-	1.000 [b]	0.219 [b]	0.219 [b]	**0.014** [b]
A-PS + SP-A	Mean	53.3	52.5	53.6	60.6	46.8
	p value	**0.019** [a]	0.513 [b]	0.827 [b]	0.513 [b]	0.513 [b]
A-PS + SP-D	Mean	37.6	45.7	42.5	42.5	33.3
	p value	**0.019** [a]	**0.043** [b]	0.248 [b]	0.248 [b]	0.248 [b]
A-PS + rfhSP-D	Mean	90.5	88.6	88.2	93.9	73.9
	p value	**0.014** [a]	0.564 [b]	1.000 [b]	1.000 [b]	**0.021** [b]
A-PS + BSA	Mean	101.1	110.1	102.9	101.5	82.0
	p value	0.219 [a]	0.513 [b]	0.827 [b]	0.827 [b]	0.275 [b]
TT1 cells						
A-PS	Mean	100.0	102.5	101.2	102.5	80.2
	p value	-	0.577 [b]	0.095 [b]	0.577 [b]	**0.005** [b]
A-PS + SP-A	Mean	63.0	69.0	74.0	69.7	57.3
	p value	**0.007** [a]	0.248 [b]	**0.021** [b]	0.386 [b]	0.386 [b]
A-PS + SP-D	Mean	60.9	54.0	55.2	55.5	46.6
	p value	**0.016** [a]	0.251 [b]	0.602 [b]	0.465 [b]	0.076 [b]
A-PS + rfhSP-D	Mean	90.4	96.9	89.5	84.3	81.3
	p value	**0.007** [a]	0.248 [b]	0.773 [b]	0.386 [b]	0.386 [b]
A-PS + BSA	Mean	96.6	105.2	101.7	97.9	89.0
	p value	0.180 [a]	0.117 [b]	0.465 [b]	0.917 [b]	0.602 [b]
THP-1 cells						
A-PS	Mean	100.0	101.4	99.9	101.9	96.2
	p value	-	0.219 [b]	1.000 [b]	1.000 [b]	0.219 [b]
A-PS + SP-A	Mean	72.0	80.2	72.1	68.5	74.4
	p value	**0.019** [a]	0.127 [b]	0.827 [b]	0.827 [b]	0.827 [b]
A-PS + SP-D	Mean	63.1	69.4	60.5	64.3	64.1
	p value	**0.014** [a]	0.386 [b]	0.885 [b]	1.000 [b]	0.885 [b]
A-PS + rfhSP-D	Mean	93.1	100.4	92.4	90.2	89.7
	p value	**0.019** [a]	0.127 [b]	0.513 [b]	0.275 [b]	0.513 [b]
A-PS + BSA	Mean	102.0	108.2	103.5	84.2	100.6
	p value	0.435 [a]	0.513 [b]	0.827 [b]	0.513 [b]	0.513 [b]

Table 5.3: Relative Infection following influenza pre-incubation with A-PS and proteins. [a] p values determined using Mann-Whitney U test versus protein free control; [b] p values determined using Mann-Whitney U test versus nanoparticle free protein containing control. Significant values in bold.

5.3.2.2.1. Effect of A-PS on SP-A mediated IAV neutralisation

Pre-incubation of 0.0016 or 0.04 cm^2/mL of 100nm A-PS with nhSP-A had less than a 1% non-significant modulatory effect on the mean relative infection levels in A549 cells compared with the nhSP-A control (see Table 5.3 and Figure 5.6A). In A549 cells, the pre-incubation of 1 or 5 cm^2/mL A-PS with nhSP-A resulted in a 7.3% increase and 6.5% reduction respectively in IAV infection compared to the IAV and SP-A control. However, these differences were not statistically significant with associated p values of 0.513. The addition of SP-A to the 5 cm^2/mL A-PS and IAV treatment resulted in a 20% reduction in the IAV; however, this reduction did not reach statistical significance with an associated p value of 0.077.

In TT1 cells, pre-incubation of 0.0016 and 1 cm^2/mL A-PS with nhSP-A resulted in 6.0% and 6.7% respective increases in IAV infection. However, these differences were not statistically significant with p values of 0.248 and 0.386 respectively. Pre-incubation of 0.04 cm^2/mL with nhSP-A resulted in an 11.0% increase in IAV infection in TT1 cells compared to the SP-A control. This increase was statistically significant with an associated p value of 0.021 (see Table 5.3 and Figure 5.6B). This represents a 29.7% reduction in the ability of nhSP-A to neutralise IAV infection. Incubation of 5 cm^2/mL A-PS with nhSP-A resulted in a 5.7% non-significant decrease in IAV infection compared to the nhSP-A control (p=0.386). The addition of SP-A to the 5 cm^2/mL A-PS and IAV treatment resulted in a 22.9% reduction in IAV infection. This reduction was statistically significant with an associated p value of 0.014.

In differentiated THP-1 cells pre-incubation of A-PS at concentrations of 0.0016 or 5 cm^2/mL with nhSP-A resulted in 8.2% and 2.4% respective increases in IAV infection compared to the SP-A control. Pre-incubation of 1 cm^2/mL A-PS with nhSP-A resulted in a 3.5% reduction in IAV infection compared to the

SP-A and IAV control. However, these differences were not statistically significant (see Table 5.3 and Figure 5.6C).

5.3.2.2.2. Effect of A-PS on SP-D mediated IAV neutralisation

In A549 cells, pre-incubation of 0.0016 cm^2/mL A-PS with nhSP-D resulted in a 8.1% increase in IAV infection compared to the nhSP-D control. This difference was statistically significant with an associated p value of 0.043 (see Figure 5.7A and Table 5.3). This represents a 13.0% reduction in the capability of nhSP-D to neutralise IAV infection. Pre-incubation of 0.04 and 1 cm^2/mL of A-PS resulted in 4.9% increases in IAV infection in A549 cells over the nhSP-D control. However, these differences were not statistically significant with p values of 0.248. Pre-incubation of 5 cm^2/mL A-PS with nhSP-D resulted in a 4.3% reduction in IAV infection in A549 cells compared with compared with nhSP-D alone. This difference was not statistically significant with an associated p value of 0.248. The addition of SP-D to the 5 cm^2/mL A-PS and IAV treatment resulted in a significant 33.5% reduction in IAV infection (p=0.021).

In TT1 cells, pre-incubation of A-PS with nhSP-D tended to result in reduced IAV infection compared to the IAV and SP-D control. However, these reductions were not statistically significant (see Figure 5.7B and Table 5.3). The addition of SP-D to the 5 cm^2/mL A-PS and IAV treatment resulted in a 33.6% reduction in IAV infection. This difference was highly statistically significant with an associated p value of 0.009.

In differentiated THP-1 cells, pre-incubation of 0.0016cm^2/mL A-PS with nhSP-D resulted in a non-significant 6.3% relative increase in the mean infection levels compared to the nhSP-D control (p=0.386). Pre-incubation of 0.04, 1 and 5 cm^2/mL A-PS resulted in a less than a 3% modulatory effect in IAV infection compared to the IAV and nhSP-D control. These differences were not statistically significant (see Figure 5.7C and Table 5.3C).

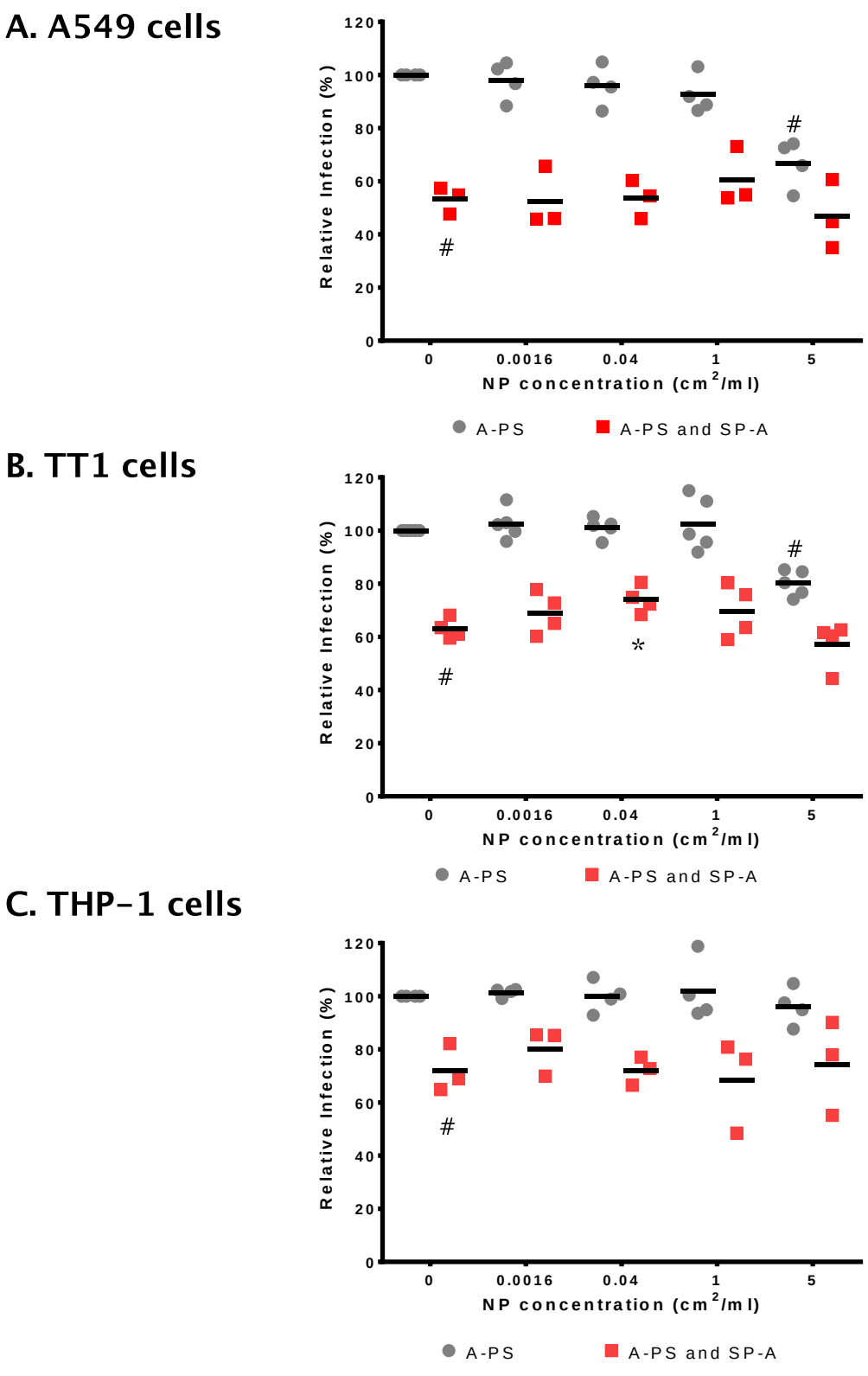

Figure 5.6: Effect of A-PS on nhSP-A mediated IAV neutralisation in A. A549; B. TT1 cells; and C. THP-1 cells. Horizontal line represents mean of at least three independent experiments conducted in duplicate. Statistics determined using Mann-Whitney U test where *p≤0.050 compared to relative infection in particle free protein control; #p≤0.050 versus IAV alone.

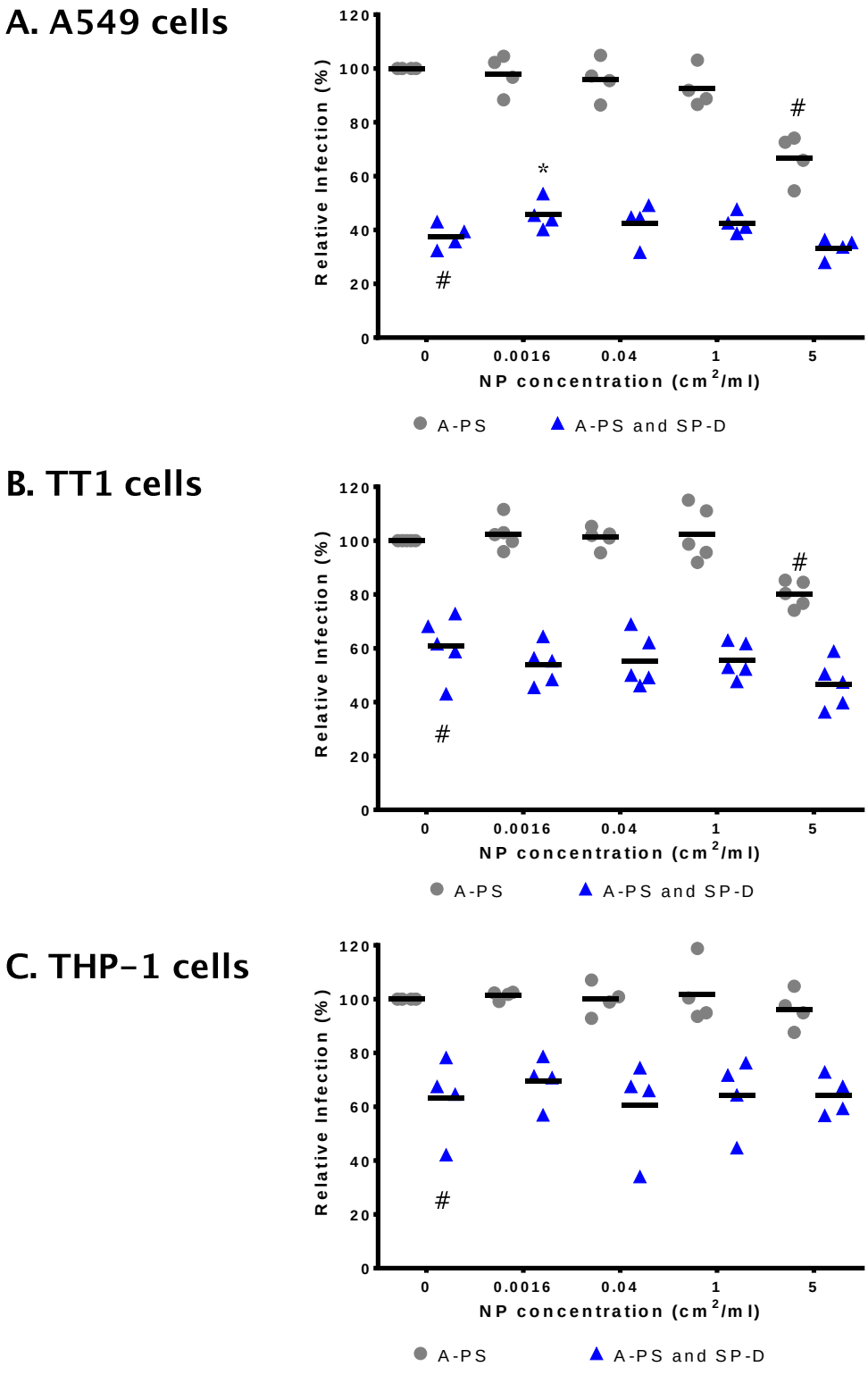

Figure 5.7: Effect of A-PS on nhSP-D mediated IAV neutralisation in A. A549; B. TT1 cells; and C. THP-1 cells. Horizontal line represents mean of at least three independent experiments conducted in duplicate. Statistics determined using Mann-Whitney U test where *p≤0.050 versus nanoparticle free protein control; #p≤0.050 versus IAV alone.

5.3.2.2.3. Effect of A-PS on rfhSP-D mediated IAV neutralisation

In A549 cells, pre-incubation of 0.0016 or 0.04 cm^2/mL A-PS with rfhSP-D resulted in 1.9% and 2.3% reductions in infection compared to rfhSP-D in the absence of particles. These differences were not statistically significant with associated p values of 0.564 and 1.000 respectively (see Figure 5.8A and Table 5.3). Pre-incubation of 1 cm^2/mL A-PS with rfhSP-D resulted in a 3.4% non-significant increase in IAV infection compared with rfhSP-D (p=1.000). Pre-incubation of 5 cm^2/mL of A-PS resulted in a 16.6% reduction in IAV infection; this was statistically significant with an associated p value of 0.021. This represented a non-significant increase of 7.1% in infection compared to influenza infection in cells with 5 cm^2/mL A-PS without the addition of protein (p=0.564).

In TT1 cells, 0.0016 cm^2/mL A-PS with rfhSP-D resulted in a 6.5% increase in influenza infection compared to rfhSP-D. A-PS at concentrations of 0.04, 1 and 5 cm^2/mL when incubated with rfhSP-D resulted in 0.9%, 6.1% and 9.1% reductions in IAV infection compared to rfhSP-D alone. These differences were not statistically significant (see Figure 5.7B and Table 5.3B). IAV infection in TT1 cells when treated with 5 cm^2/mL A-PS, IAV and rfhSP-D was 1.1% higher than those infected with this concentration of particles without protein. This difference was not statistically significant with an associated p value of 1.000.

In differentiated THP-1 cells, 0.0016 cm^2/mL with rfhSP-D resulted in a 7.3% increase in IAV infection compared to rfhSP-D in the absence of particles. However, this did not reach statistical significance with an associated p value of 0.127. Concentrations of 0.04, 1 and 5 cm^2/mL incubated with rfhSP-D resulted in 0.7%, 2.9% and 3.4% respective decreases IAV infection compared to rfhSP-D. These differences were not statistically significant with associated p values of

0.513, 0.275 and 0.513 respectively. Incubation of 5 cm^2/mL A-PS with rfhSP-D resulted in a 6.5% reduction in infection compared to this particle concentration without rfhSP-D. This difference was not statistically significant with an associated p value of 0.289 (see Figure 5.7C and Table 5.3).

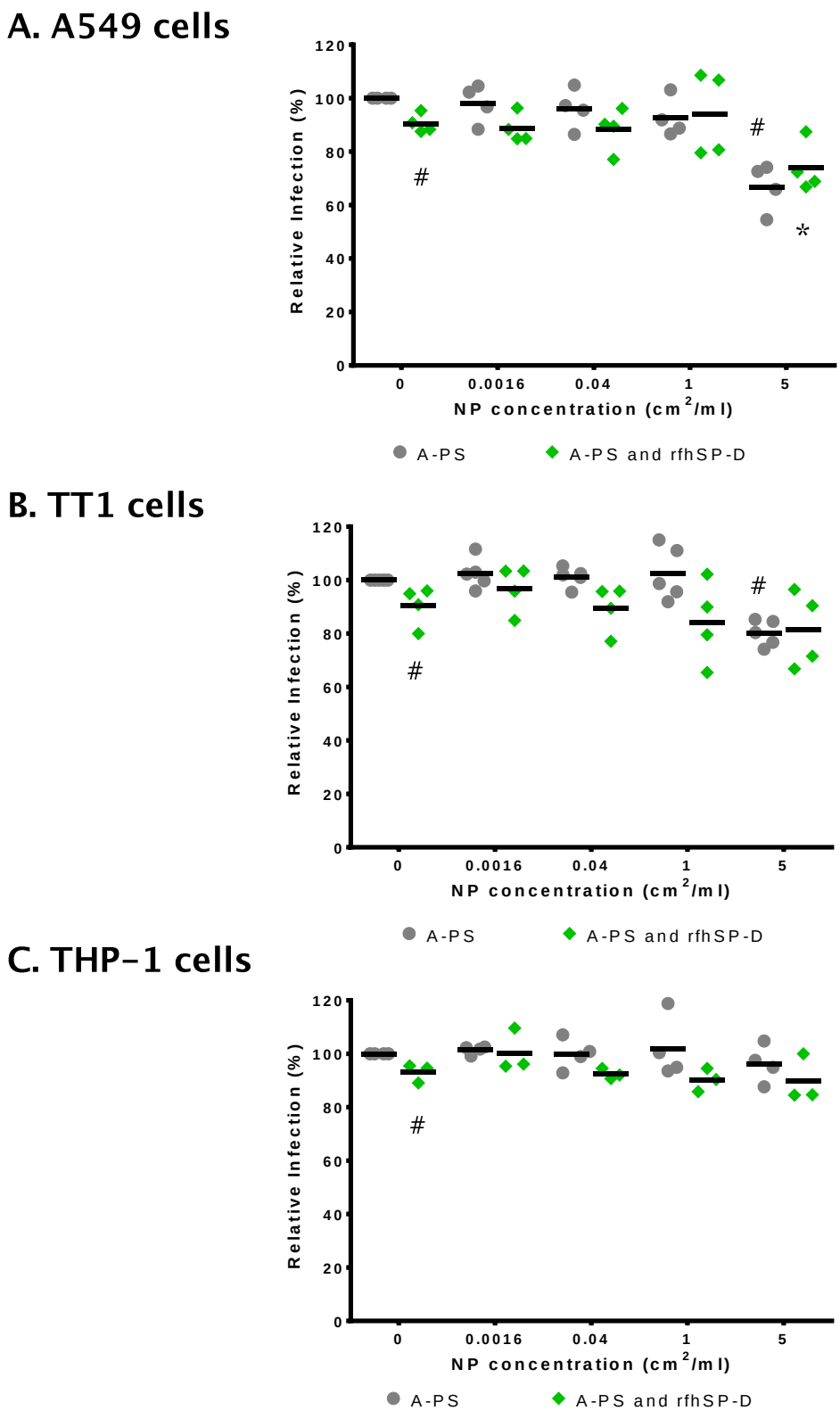

Figure 5.8: Effect of A-PS on rfhSP-D mediated IAV neutralisation in A. A549; B. TT1 cells; and C. THP-1 cells. Horizontal line represents mean of at least three independent experiments conducted in duplicate. Statistics determined using Mann-Whitney U test where *p≤0.050 versus nanoparticle free protein control; #p≤0.050 versus IAV alone.

5.3.2.2.4. Effect of A-PS and BSA on IAV infection

In A549 cells, pre-incubation of 0.0016, 0.04 and 1 cm^2/mL with BSA resulted in 9%, 1.9% and 0.4% increases in infection compared to the BSA control. 5 cm^2/mL A-PS resulted in a 19.1% reduction in IAV infection compared with the BSA control. These differences were not statistically significant (see Figure 5.9A and Table 5.3). There was a 15.2% increase in influenza infection in the 5 cm^2/mL with BSA treatment compared to the particle and IAV treatment in the absence of BSA. This difference was not statistically significant with an associated p value of 0.289.

In TT1 cells, pre-incubation of 0.0016, 0.04 and 1 cm^2/mL resulted in 8.6%, 5.1% and 1.3% respective non-significant increases in influenza infection compared with the BSA control (see Table 5.3). Incubation of 5 cm^2/mL A-PS with BSA resulted in a 7.6% reduction in influenza infection compared to the BSA control. These differences were not statistically significant (see Figure 5.9B). Incubation of 5 cm^2/mL A-PS with BSA resulted in an 8.8% increase in IAV infection in TT1 cells compared to this particle and IAV treatment in the absence of BSA. This difference was statistically significant with an associated p value of 0.047.

In differentiated THP-1 cells, 0.0016 and 0.04 cm^2/mL A-PS with BSA resulted in 6.2% and 1.5% respective increases in influenza infection compared to the BSA control. Concentrations of 1 and 5 cm^2/mL resulted in 17.8% and 1.4% respective decreases in influenza infection compared to the control. These differences were not statistically significant (see Figure 5.9C and Table 5.3). Incubation of 5 cm^2/mL with BSA resulted in a 4.4% increase in influenza infection compared to this NP concentration in the absence of protein. This difference was not statistically significant with an associated p value of 0.480.

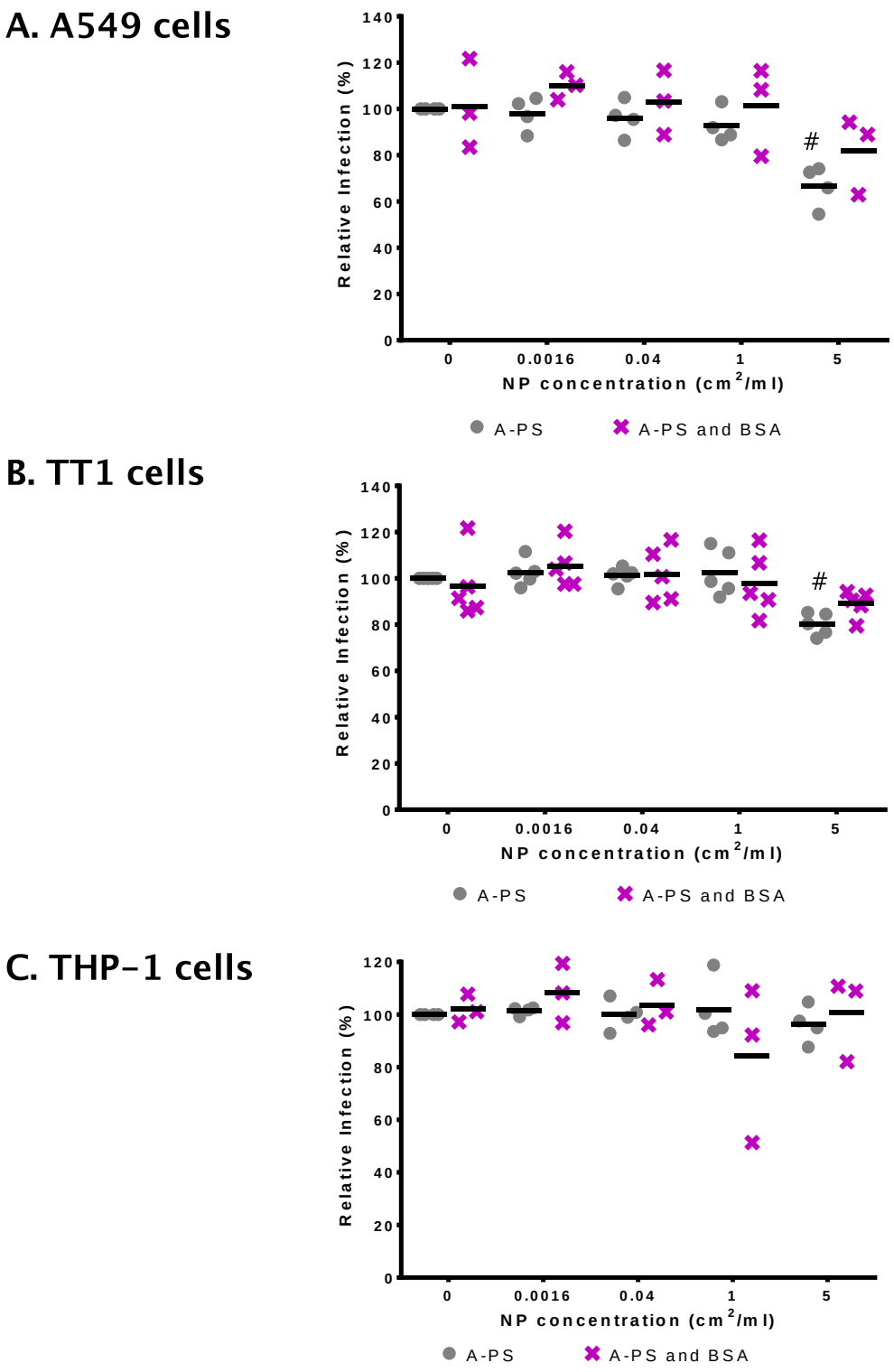

Figure 5.9: Effect of A-PS and BSA on IAV infection in A. A549; B. TT1 cells; and C. THP-1 cells. Horizontal line represents mean of at least three independent experiments conducted in duplicate. Statistics determined using Mann-Whitney U test where *p≤0.050 compared to relative infection in particle free protein control; #p≤0.050 versus IAV alone.

5.3.3. Nanoparticle uptake

Nanoparticle uptake was also examined in these experiments. Nanoparticle uptake was measured as the mean fluorescence intensity (MFI) and the percent of NP positive cells (%NP+) which reflect the number of nanoparticles within each cell and the number of nanoparticle containing cells respectively. The uptake of A-PS and U-PS particles was compared between the A549, TT1 and THP-1 cell lines. Due to the different dye intensities for the A-PS and U-PS particles the uptake of each particle were not compared between particles.

The MFI of THP-1 and TT1 cells were 55.7% and 51.7% higher respectively following treatment with 1 cm^2/mL U-PS compared to A549 cells. However, with respective p values of 0.289 and 0.050 only the latter was statistically significant (see Figure 5.10A). A similar trend was also observed for 5 cm^2/mL U-PS whereby the MFI of THP-1 and TT1 cells were 47.9% and 38.6% higher compared to A549 cells and only the latter being statistically significant ($p=0.289$ and $p=0.050$ respectively). There were no significant differences in the MFI between TT1 and THP-1 cells at either 1 or 5 cm^2/mL ($p=0.724$ for each comparison). The number of cells containing U-PS nanoparticles was significantly higher in the epithelial A549 and TT1 cells compared to the macrophage like THP-1 cells at both the concentrations tested (see Figure 5.10B). The number of NP+ cells was 1.9 fold higher in A549 cells and 2.1 fold higher in TT1 cells compared to the THP-1 cells following treatment with 1 cm^2/mL U-PS. These differences were statistically significant with associated p values of 0.034 for each comparison. The number of NP+ cells was also increased in A549 and TT1 cells compared to THP-1 cells following treatment with 5 cm^2/mL U-PS. These 1.3fold and 1.2fold respective increases were statistically significant with associated p values of 0.034 for each.

A-PS uptake was greatest in THP-1 cells than the epithelial A549 or TT1 cell lines. This was evident using both the number of particles per cell and the number of cells containing nanoparticles but was more pronounced for the former measurement. The number of A-PS particles per cell in THP-1 cells treated with 5 cm^2/mL A-PS was 4.9fold higher than in A549 cells and 4.1fold higher than in TT1 cells. These increases were statistically significant with associated p values of 0.021 and 0.014 respectively. The MFI of THP-1 cells treated with 1 cm^2/mL was 6.3fold higher than in A549 cells and 3.1fold higher than TT1 cells. These increases were statistically significant with associated p values of 0.034 and 0.014 respectively (see Figure 5.11A). The number of THP-1 cells containing A-PS particles was also significantly increased by 2.4 fold and 1.6 fold compared to A549 cells at both 1 and 5 cm^2/mL respectively. These increases were statistically significant with associated p values of 0.034 and 0.043 respectively. The number of THP-1 cells containing nanoparticles was also increased by 1.2 fold and 1.5 fold compared to in TT1 cells for the 1 and 5 cm^2/mL A-PS concentrations respectively. However, with associated p values of 0.086 and 0.014 respectively, only the higher concentration achieved statistical significance (see Figure 5.11B). There were no significant differences in the number of A-PS particles taken up per cell or number of cells containing nanoparticles between A549 and TT1 cells at either 1 cm^2/mL ($p=0.101$ and $p=0.053$ respectively) or 5 cm^2/mL ($p=0.482$ and $p=0.624$) nanoparticle concentrations.

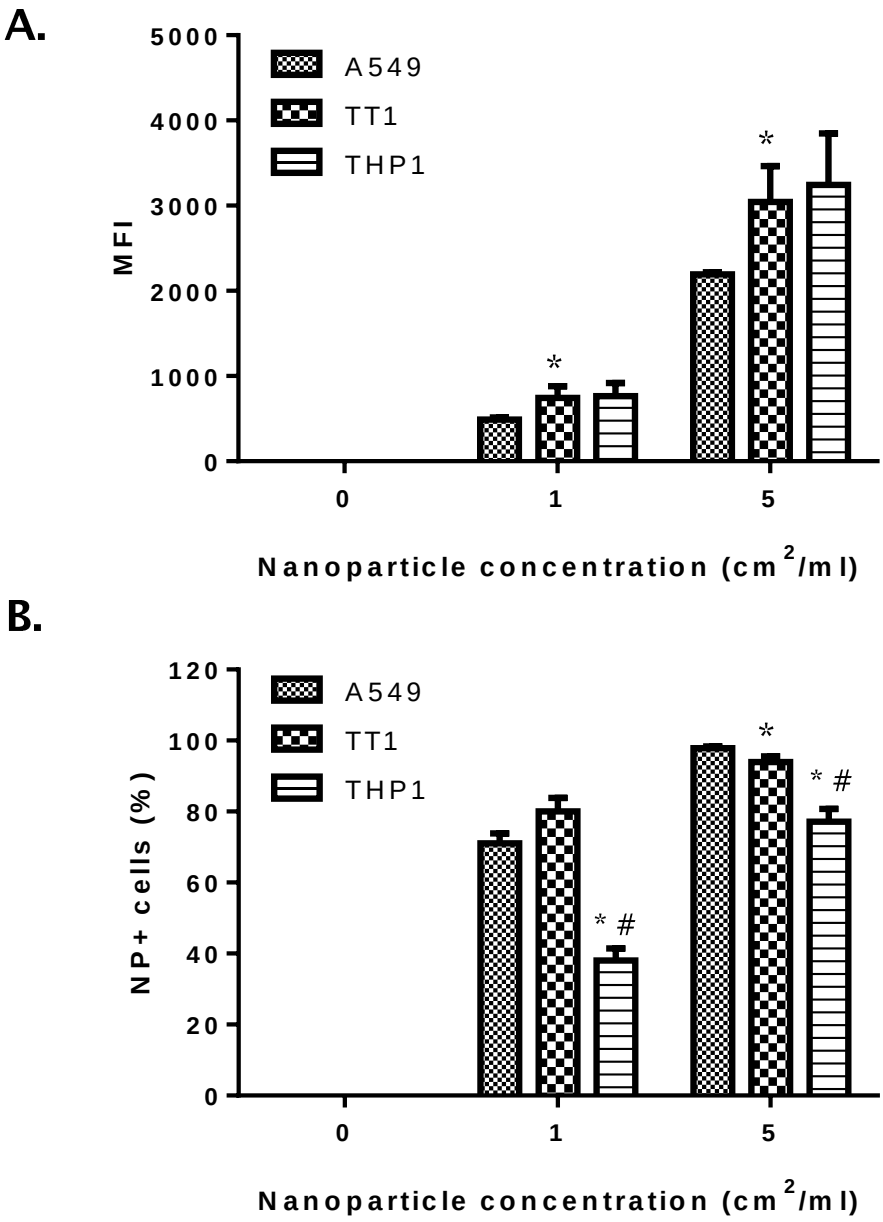

Figure 5.10: U-PS uptake in A549, TT1 and THP-1 cell lines. **A**. Mean fluorescent intensity (MFI) and **B**. Percent NP+ cells in A549, TT1 and THP-1 cells. Data represents mean +SEM of at least three independent experiments. Statistics determined using Mann-Whitney U test where *p≤0.05 compared to A549 cells; # p≤0.05 compared to TT1 cells.

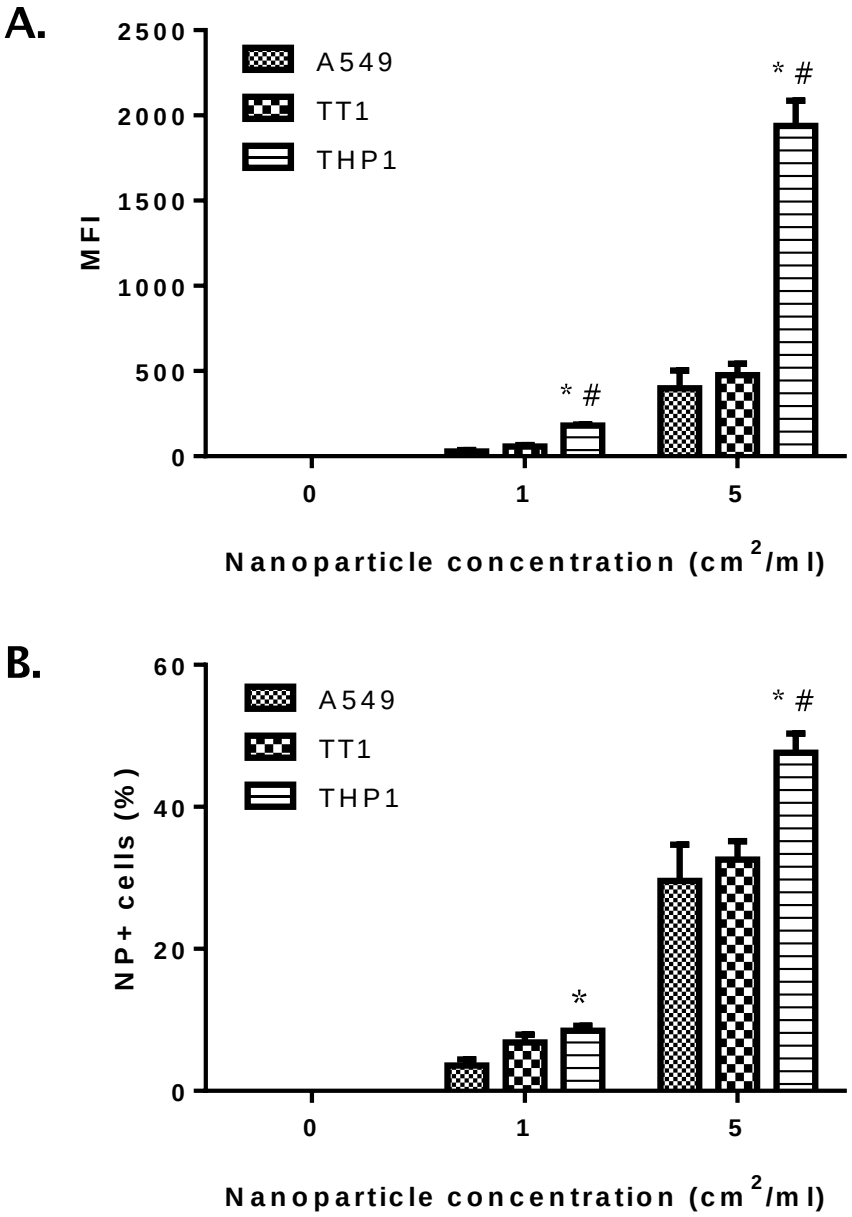

Figure 5.11: A-PS uptake in A549, TT1 and THP-1 cells. A. Mean fluorescent intensity (MFI) and **B.** Percent NP+ cells in A549, TT1 and THP-1 cells. Data represents mean +SEM of at least three independent experiments. Statistics determined using Mann-Whitney U test where *p≤0.05 compared to A549 cells; # p≤0.05 compared to TT1 cells.

5.3.3.1 Effect of IAV on U-PS uptake

In order to examine the effect of influenza and proteins on nanoparticle uptake the %NP+ and MFI measurements were normalised to the particle control for each concentration. The studied concentrations of A-PS and U-PS less than 1 cm^2/mL could not be detected using flow cytometry. Therefore, only the effect of IAV and proteins on NP uptake at 1 and 5 cm^2/mL are reported here. The effect of proteins and IAV on U-PS uptake in A549, TT1 and THP-1 cells are summarised in Tables 5.4 – 5.7.

In A549 cells, pre-incubation of 1 cm^2/mL of U-PS with IAV resulted in 15.0% increases in the both %NP+ cells and the MFI. These increases were statistically significant with associated p values of 0.037. IAV had no significant effect on the number of NP+ cells when incubated with 5 cm^2/mL U-PS (<0.5% change; p=0.487) but significantly enhanced the MFI at this NP concentration by 33.7% (p=0.037).

In TT1 cells, pre-incubation of IAV with 1 cm^2/mL U-PS resulted in 0.7% and 7.0% reductions in the %NP+ cells and MFI. However, these reductions were not statistically significant (p=0.487). The pre-incubation of 5 cm^2/mL U-PS with IAV resulted in a 1.0% non-significant increase in the %NP+ cells (p=0.487). This treatment did result in a significant 10.0% increase in the MFI in TT1 cells (p=0.037).

In THP-1 cells, the pre-incubation of U-PS (5 cm^2/mL) with IAV resulted in a 3.5% reduction in the MFI and a 1% reduction in percent of NP+ cells. These differences were not statistically significant with associated p values of 0.219 and 1.000 respectively. The pre-incubation of 1 cm^2/mL U-PS with IAV had less than a 1% modulatory effect on both %NP+ and MFI (p=1.000 and p=0.219 respectively).

5.3.3.1.1. Effect of SP-A and IAV on the uptake of U-PS

In A549 cells, nhSP-A resulted in 97% and 98% reductions in the MFI and %NP+ cells respectively at 1 cm^2/mL U-PS. These reductions were statistically significant with associated p values of 0.037. Following the addition of IAV the MFI and percent NP+ cells increased by 30.7% and 18.3% respectively compared to the U-PS and SP-A treatment. These increases were statistically significant with associated p values of 0.05. However, the relative values of these NP measurements were 81.3% and 94.7% lower than the NP and IAV treatment. These differences were statistically significant with associated p values of 0.05. nhSP-A also reduced 5 cm^2/mL U-PS uptake by 76.7% and 85.7% for the %NP+ cells and MFI respectively in A549 cells. These differences were statistically significant with associated p values of 0.037. Following the addition of IAV, these were increased by 17% and 21.7% respectively compared to the NP and SP-A treatment. However, these increases did not reach statistical significance with associated p values of 0.275 and 0.127 respectively. This treatment did result in 59.7% and 97.7% reductions in %NP+ cells and MFI compared to the NP and IAV treatment. These differences were statistically significant with associated p values of 0.050 (see Table 5.4 and Figure 5.12A).

In TT1 cells, pre-incubation of 1 cm^2/mL U-PS with nhSP-A resulted in 56.7% and 32.3% reductions in the %NP+ cells and MFI. These reductions were statistically significant with associated p values of 0.037 (see Figure 5.12B and Table 5.4). Following the addition of IAV to this treatment the %NP+ cells and MFI increased by 14.7% and 37.3% respectively. These differences were statistically significant with associated p values of 0.05. The %NP+ cells was significantly reduced by 41.3% in the U-PS, SP-A and IAV treatment compared to the U-PS and IAV treatment (p=0.05). The MFI was increased by 12% of this triple treatment compared to the NP and IAV however, this did not reach statistical significance (p=0.127). At 5 cm^2/mL U-PS the pre-incubation with

nhSP-A resulted in a 30.3% reduction in the %NP+ cells. This reduction was statistically significant with an associated p value of 0.037. Following the addition of IAV the %NP+ cells increased by 5.6% although this was not statistically significant (p=0.275). The %NP+ cells in this treatment was significantly reduced by 25.7% compared to the NP and IAV treatment (p=0.05). Pre-incubation of 5 cm^2/mL U-PS with nhSP-A resulted in a 21.0% increase in the MFI of TT1 cells. However, this increase was not statistically significant with an associated p value of 0.487. Following the addition of IAV the MFI increased by 17.0% however, this increase was not statistically significant (p=0.513). The addition of SP-A to U-PS and IAV resulted in a 28.0% significant increase in the MFI. This increase was statistically significant with an associated p value of 0.050.

Pre-incubation of 5 μg/mL nhSP-A with 100nm U-PS (5 cm^2/mL) resulted in a significant 84.3% increase in MFI (p=0.014) in THP-1 cells. When IAV was added to this treatment MFI increased 2.9 fold compared to the control or 109% compared to U-PS and SP-A (p=0.034). This represents a synergistic enhancement in UPS association with IAV and SP-A (see Figure 5.12C). This synergistic enhancement was also evident at 1 cm^2/mL of U-PS in THP-1 cells where nhSP-A resulted in a non-significant 6.7% increase in NP uptake (MFI) but the addition of IAV to this treatment increased this to 88.7% (p=0.021). Interestingly, nhSP-A resulted in 27.3% and 25.7% reductions in NP+ THP-1 cells when pre-incubated with 1 and 5 cm^2/mL U-PS respectively. These reductions were statistically significant with associated p values of p=0.014. Following the addition of IAV NP+ cells increased by 42.0% and 14.0% with 1 and 5 cm^2/mL U-PS respectively compared to the NP+SP-A samples. These increases were statistically significant with associated p values of 0.021 (see Table 5.4).

Cell type	NP (cm²/mL)			U-PS [b]	U-PS + SP-A [c]	U-PS + IAV [d]	U-PS+IAV +SP-A
A549	1	MFI	Mean	1.000	0.030	1.150	0.337
			p value	**0.015** [a]	**0.037** [b]	**0.037** [b]	**0.050** [c] **0.050** [d]
		NP+	Mean	1.000	0.020	1.150	0.203
			p value	**0.015** [a]	**0.037** [b]	**0.037** [b]	**0.050** [c] **0.050** [d]
	5	MFI	Mean	1.000	0.143	1.337	0.360
			p value	**0.018** [a]	**0.037** [b]	**0.037** [b]	0.127 [c] **0.050** [d]
		NP+	Mean	1.000	0.233	1.000	0.403
			p value	**0.031** [a]	**0.037** [b]	0.487 [b]	0.275 [c] **0.050** [d]
TT1	1	MFI	Mean	1.000	0.677	0.930	1.050
			p value	**0.031** [a]	**0.037** [b]	0.487 [b]	**0.050** [c] 0.127 [d]
		NP+	Mean	1.000	0.433	0.993	0.580
			p value	**0.022** [a]	**0.037** [b]	0.487 [b]	**0.050** [c] **0.050** [d]
	5	MFI	Mean	1.000	1.210	1.100	1.380
			p value	0.125 [a]	n/a	n/a	n/a
		NP+	Mean	1.000	0.697	1.010	0.753
			p value	**0.031** [a]	**0.037** [b]	0.487 [b]	0.275 [c] **0.050** [d]
THP-1	1	MFI	Mean	1.000	1.067	0.995	1.887
			p value	**0.020** [a]	0.435 [b]	0.219 [b]	**0.034** [c] **0.021** [d]
		NP+	Mean	1.000	0.727	1.000	1.147
			p value	**0.044** [a]	**0.019** [b]	1.000 [b]	**0.034** [c] 0.248 [d]
	5	MFI	Mean	1.000	1.843	0.965	2.927
			p value	**0.011** [a]	**0.019** [b]	0.219 [b]	**0.050** [c] **0.034** [d]
		NP+	Mean	1.000	0.743	0.990	0.883
			p value	**0.008** [a]	**0.019** [b]	1.000 [b]	**0.034** [c] **0.021** [d]

Table 5.4: Fold change in U-PS uptake following co-treatment with SP-A and IAV. [a] Kruskal-Wallis between group differences; [b] Mann-Whitney U test versus U-PS treatment; [c] Mann-Whitney U test versus U-PS + protein treatment; [d] Mann-Whitney U test versus U-PS + IAV treatment. Significant differences in bold. n/a; Mann-Whitney U test not conducted where Kruskal-Wallis p>0.050.

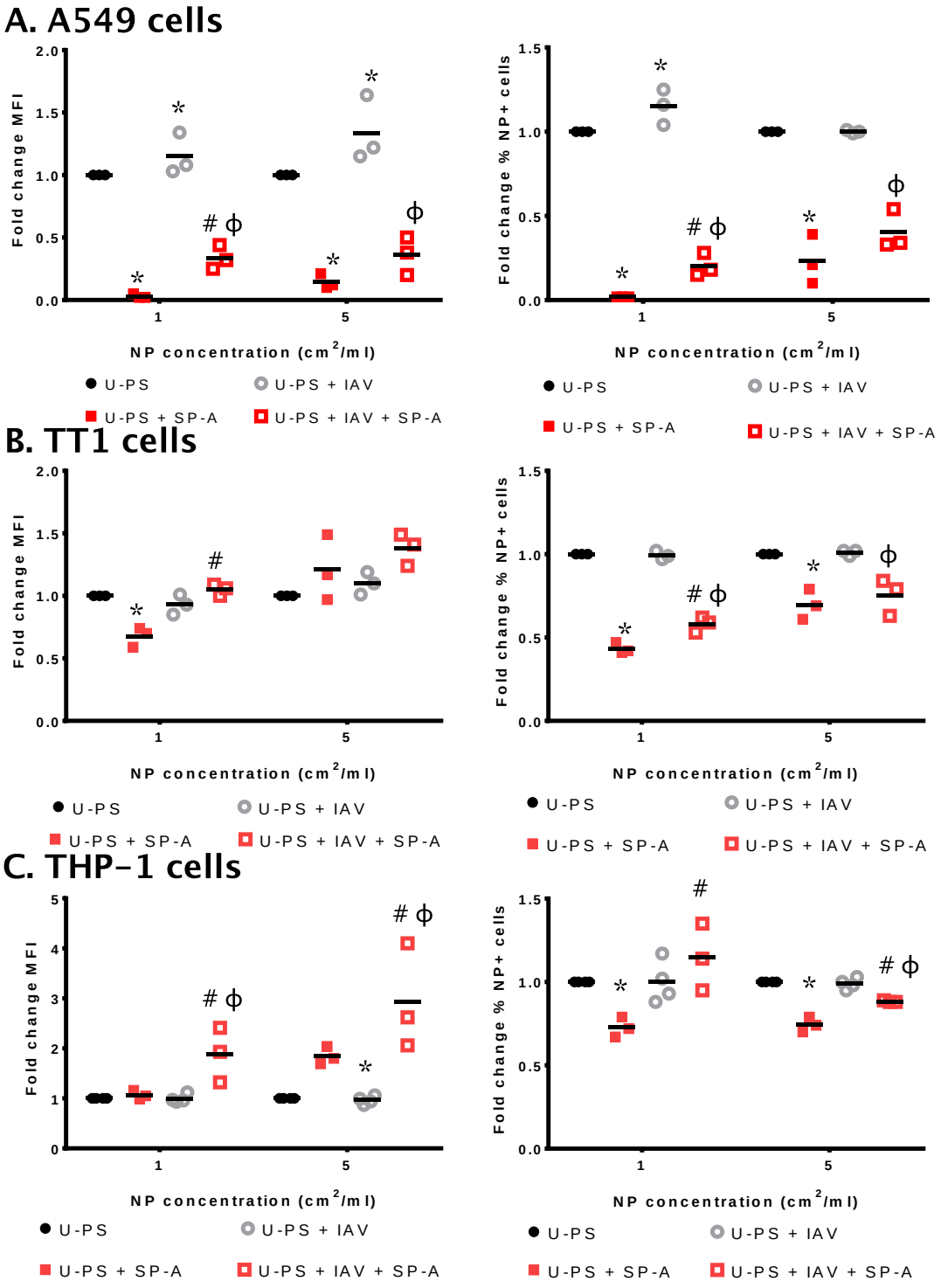

Figure 5.12: Effect of nhSP-A and IAV on U-PS NP association. Relative cell association of unmodified polystyrene NP in A. A549 cells, B. TT1 cells and C. THP-1 cells following pre-incubation with 5µg/mL nhSP-A and IAV. *Left panel* shows relative mean fluorescence intensity (MFI) and *right panel* shows relative number of NP positive (%NP+) cells. Data represents mean (black horizontal line) of at least three independent experiments. Statistics determined by Kruskal-Wallis and Mann Whitney U test. * p≤0.05 versus U-PS; # p≤0.05 versus U-PS and SP-A; ϕ p≤0.05 versus U-PS and IAV.

5.3.3.1.2. Effect of nhSP-D and IAV on U-PS uptake

In A549 cells, the pre-incubation of nhSP-D with 5 cm^2/mL U-PS resulted in a 10.0% reduction in the MFI. This reduction was statistically significant with an associated p value of 0.037. The addition of IAV to this treatment had no significant effect compared to the U-PS and SP-D control (p=0.827; see Table 5.5 and Figure 5.13A). However, the MFI of the 5 cm^2/mL U-PS, IAV and SP-D treatment was significantly reduced by 44.7% compared to the U-PS and IAV control (p=0.050). The MFI of A549 cells treated with 1 cm^2/mL did not significantly change following the addition of IAV and/or nhSP-D (p=0.125; Kruskal-Wallis). Moreover, the %NP+ cells did not significantly differ following the addition of IAV and/or nhSP-D to the 1 or 5 cm^2/mL U-PS treatments (p=0.313 and p=0.143 respectively; Kruskal-Wallis).

In TT1 cells, the pre-incubation of 1 cm^2/mL or 5 cm^2/mL U-PS with nhSP-D and/or IAV had no significant effect on either the %NP+ or MFI (see Table 5.5 and Figure 5.13B).

The pre-incubation of nhSP-D with 1 cm^2/mL U-PS resulted in a 15.5% reduction in the %NP+ THP-1 cells. This was statistically significant with an associated p value of 0.014 (see Table 5.5 and Figure 5.13C). The addition of IAV to this treatment resulted in a 4% increase in the relative number of NP+ cells however this increase was not statistically significant (p=0.773). At 5 cm^2/mL the pre-incubation of U-PS with nhSP-D also tended to result in a decrease in the %NP+ THP-1 cells with a small concomitant increase following the addition of IAV. However, these differences did not achieve statistical significance (p=0.190; Kruskal-Wallis). The MFI of THP-1 cells was also reduced following the pre-incubation of 1 or 5 cm^2/mL U-PS with nhSP-D however these did not achieve statistical significance (p=0.379 and p=0.070 respectively; Kruskal-Wallis).

Cell type	NP (cm²/mL)			U-PS [b]	U-PS + SP-D [c]	U-PS + IAV [d]	U-PS+IAV +SP-D
A549	1	MFI	Mean	1.000	0.953	1.150	1.057
			p value	0.125 [a]	n/a	n/a	n/a
		NP+	Mean	1.000	1.040	1.150	1.060
			p value	0.313 [a]	n/a	n/a	n/a
	5	MFI	Mean	1.000	0.900	1.337	0.890
			p value	**0.023** [a]	**0.037** [b]	**0.037** [b]	0.827 [c] **0.050** [d]
		NP+	Mean	1.000	0.987	1.000	0.993
			p value	0.143 [a]	n/a	n/a	n/a
TT1	1	MFI	Mean	1.000	0.977	0.930	0.917
			p value	0.333 [a]	n/a	n/a	n/a
		NP+	Mean	1.000	0.997	0.993	0.973
			p value	0.836 [a]	n/a	n/a	n/a
	5	MFI	Mean	1.000	0.983	1.100	0.887
			p value	0.089 [a]	n/a	n/a	n/a
		NP+	Mean	1.000	1.003	1.010	0.980
			p value	0.125 [a]	n/a	n/a	n/a
THP-1	1	MFI	Mean	1.000	0.868	0.995	0.858
			p value	0.319 [a]	n/a	n/a	n/a
		NP+	Mean	1.000	0.845	1.000	0.885
			p value	**0.039** [a]	**0.014** [b]	1.000 [b]	0.773 [c] 0.149 [d]
	5	MFI	Mean	1.000	0.803	0.965	0.895
			p value	0.070 [a]	n/a	n/a	n/a
		NP+	Mean	1.000	0.935	0.990	0.995
			p value	0.190 [a]	n/a	n/a	n/a

Table 5.5: Fold change in U-PS uptake following co-treatment with SP-D and IAV. [a] Kruskal-Wallis between group differences; [b] Mann-Whitney U test versus U-PS treatment; [c] Mann-Whitney U test versus U-PS + protein treatment; [d] Mann-Whitney U test versus U-PS + IAV treatment. Significant differences in bold. n/a; Mann-Whitney U test not conducted where Kruskal-Wallis p>0.050.

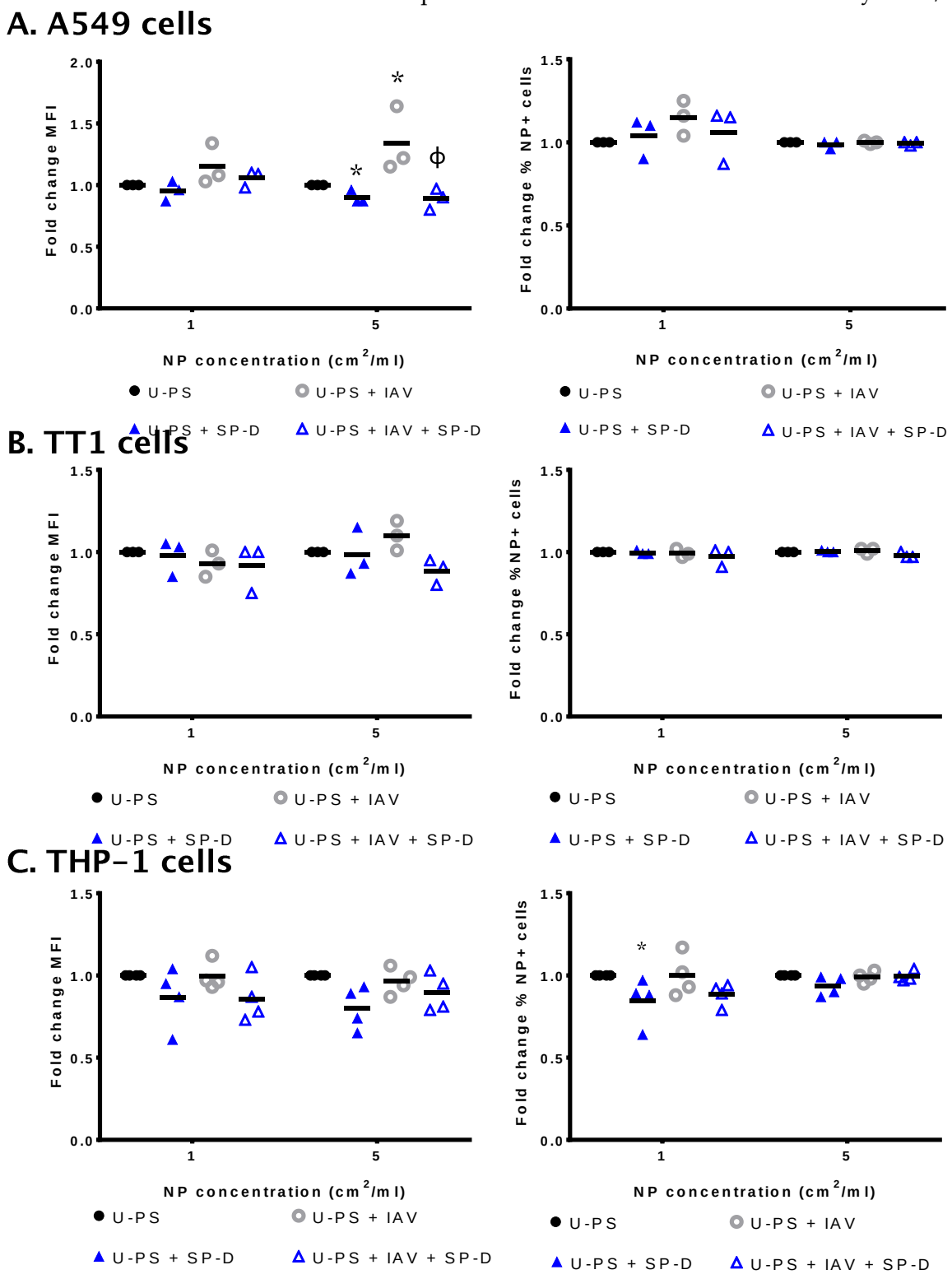

Figure 5.13: Effect of nhSP-D and IAV on U-PS NP association. Relative cell association of unmodified polystyrene NP in A. A549 cells, B. TT1 cells and C. THP-1 cells following pre-incubation with 0.4µg/mL nhSP-D and IAV. *Left panel* shows relative mean fluorescence intensity (MFI) and right panel shows relative number of NP positive (%NP+) cells. Data represents mean (black horizontal line) of at least three independent experiments. Statistics determined by Kruskal-Wallis and Mann Whitney U test. * p≤0.05 versus U-PS; # p≤0.05 versus U-PS and SP-D; ϕ p≤0.05 versus U-PS and IAV.

5.3.3.1.3. Effect of rfhSP-D and IAV on U-PS uptake

In A549 cells, pre-incubation of 1 cm^2/mL with rfhSP-D resulted in 48.3% and 59.7% reductions in the %NP+ cells and MFI. These reductions were statistically significant with associated p values of 0.037. Following the addition of IAV these measures increased by 13.0% and 8.4% respectively however, these increases were not statistically significant (p=0.827 and p=0.513 respectively). The %NP+ and the MFI in A549 cells treated with 1 cm^2/mL U-PS, IAV and rfhSP-D were significantly reduced by 50.3% and 66.3% compared to those treated with U-PS and IAV (p=0.050; Table 5.6 and Figure 5.14A). A similar trend in the MFI of A549 cells treated with 5 cm^2/mL U-PS with rfhSP-D and/or IAV was observed however, these differences did not achieve statistical significance (p=0.063; Kruskal-Wallis). There was also no significant difference in the %NP+ A549 cells following the addition of rfhSP-D with or without IAV to 5 cm^2/mL U-PS (p=0.711).

In TT1 cells, pre-incubation of 1 cm^2/mL or 5 cm^2/mL U-PS with rfhSP-D with or without IAV had no significant effect on nanoparticle uptake by either %NP+ cells or MFI measure (see Table 5.6 and Figure 5.14B).

Pre-incubation of 1 or 5 cm^2/mL U-PS with 5 μg/mL rfhSP-D resulted in 34.7% and 17.0% reductions in MFI in THP-1 cells. These reductions were statistically significant with associated p values of 0.037. The addition of IAV to the 5 cm^2/mL and rfhSP-D treatment resulted in a 9.7% further reduction to the MFI. However, this difference was not statistically significant with an associated p value of 0.127 (see Table 5.6 and Figure 5.14C). Following the addition of IAV to the 1 cm^2/mL and rfhSP-D treatment the MFI increased 7.0% compared to the NP and rfhSP-D treatment (p=0.513). The addition of rfhSP-D to the U-PS and IAV treatment in THP-1 cells at either 1 cm^2/mL or 5 cm^2/mL resulted in significant 27.2% and 23.2% respective reductions in the MFI compared to the U-PS and IAV treatments (p=0.050). The addition of rfhSP-D

and/or IAV to U-PS had no significant effect on the %NP+ THP-1 cells at either 1 cm^2/mL or 5 cm^2/mL (p=0.055 and p=0.401 respectively; Kruskal-Wallis).

5.3.3.1.4. Effect of BSA and IAV on U-PS uptake

Pre-incubation of 5 cm^2/mL U-PS with BSA resulted in a 2.3% increase in the MFI of A549 cells. This increase was statistically significant with an associated p value of 0.037. The addition of IAV to this treatment resulted in a significant 14.0% increase in MFI over the NP and protein control (p=0.050). This represented a 17.4% reduction compared to the UPS and IAV control however, this was not statistically significant (p=0.275; see Table 5.7 and Figure 5.15A). The pre-incubation of U-PS with BSA with or without IAV had no significant effect on the %NP+ A549 cells at either 1 cm^2/mL or 5 cm^2/mL (p=0.091 and p=0.540 respectively).

In TT1 cells, the pre-incubation of 1 cm^2/mL or 5 cm^2/mL U-PS with BSA with or without IAV had no significant effect on nanoparticle uptake (see Figure 5.15B and Table 5.7).

The pre-incubation of U-PS with BSA with or without IAV had no significant effect on the uptake of U-PS particles by THP-1 cells at either 1 cm^2/mL or 5 cm^2/mL concentrations (see Table 5.7). Although non-significant, BSA did tend to increase the uptake of 5 cm^2/mL U-PS by THP-1 cells (see Figure 5.15C).

Cell type	NP (cm^2/mL)			U-PS [b]	U-PS + rfhSP-D [c]	U-PS + IAV [d]	U-PS+IAV +rfhSP-D
A549	1	MFI	Mean	1.000	0.403	1.150	0.487
			p value	**0.022** [a]	**0.037** [b]	**0.037** [b]	0.513 [c] **0.050** [d]
		NP+	Mean	1.000	0.517	1.150	0.647
			p value	**0.023** [a]	**0.037** [b]	**0.037** [b]	0.827 [c] **0.050** [d]
	5	MFI	Mean	1.000	0.687	1.337	0.867
			p value	0.063 [a]	n/a	n/a	n/a
		NP+	Mean	1.000	0.983	1.000	0.993
			p value	0.711 [a]	n/a	n/a	n/a
TT1	1	MFI	Mean	1.000	0.863	0.930	0.940
			p value	0.264 [a]	n/a	n/a	n/a
		NP+	Mean	1.000	0.890	0.993	0.930
			p value	0.823 [a]	n/a	n/a	n/a
	5	MFI	Mean	1.000	0.977	1.100	1.183
			p value	0.072 [a]	n/a	n/a	n/a
		NP+	Mean	1.000	0.997	1.010	1.017
			p value	0.355 [a]	n/a	n/a	n/a
THP-1	1	MFI	Mean	1.000	0.653	0.995	0.723
			p value	**0.022** [a]	**0.037** [b]	0.219 [b]	0.513 [c] **0.050** [d]
		NP+	Mean	1.000	0.693	1.000	0.820
			p value	0.055 [a]	n/a	n/a	n/a
	5	MFI	Mean	1.000	0.830	0.965	0.733
			p value	**0.022** [a]	**0.037** [b]	0.219 [b]	0.127 [c] **0.050** [d]
		NP+	Mean	1.000	1.003	0.990	0.960
			p value	0.401 [a]	n/a	n/a	n/a

Table 5.6: Fold change in U-PS uptake following co-treatment with rfhSP-D and IAV. [a] Kruskal-Wallis between group differences; [b] Mann-Whitney U test versus U-PS treatment; [c] Mann-Whitney U test versus U-PS + protein treatment; [d] Mann-Whitney U test versus U-PS + IAV treatment. Significant differences in bold. n/a; Mann-Whitney U test not conducted where Kruskal-Wallis p>0.050.

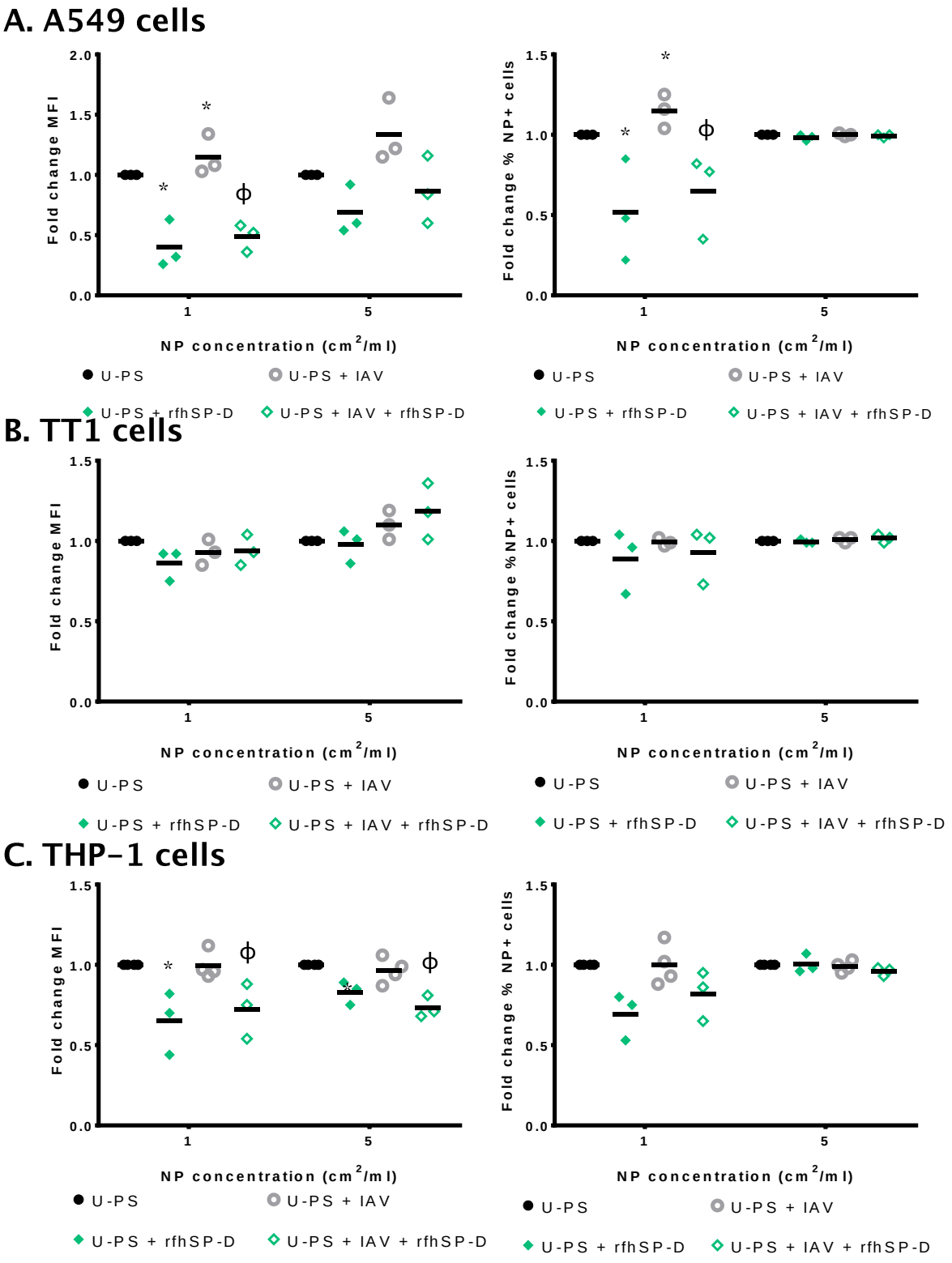

Figure 5.14: Effect of rfhSP-D and IAV on U-PS NP association. Relative cell association of unmodified polystyrene NP in A. A549 cells, B. TT1 cells and C. THP-1 cells following pre-incubation with 5µg/mL rfhSP-D and IAV. *Left panel* shows relative mean fluorescence intensity (MFI) and right panel shows relative number of NP positive (%NP+) cells. Data represents mean (black horizontal line) of at least three independent experiments. Statistics determined by Kruskal-Wallis and Mann Whitney U test. * p≤0.05 versus U-PS; # p≤0.05 versus U-PS and rfhSP-D; ϕ p≤0.05 versus U-PS and IAV.

Cell type	NP (cm^2/mL)			U-PS [b]	U-PS + BSA [c]	U-PS + IAV [d]	U-PS+IAV + BSA
A549	1	MFI	Mean	1.000	1.073	1.150	1.027
			p value	0.453 [a]	n/a	n/a	n/a
		NP+	Mean	1.000	1.133	1.150	1.130
			p value	0.091 [a]	n/a	n/a	n/a
	5	MFI	Mean	1.000	1.023	1.337	1.163
			p value	**0.020** [a]	**0.037** [b]	**0.037** [b]	**0.050** [c] 0.275 [d]
		NP+	Mean	1.000	1.000	1.000	0.997
			p value	0.540 [a]	n/a	n/a	n/a
TT1	1	MFI	Mean	1.000	0.973	0.930	0.800
			p value	0.401 [a]	n/a	n/a	n/a
		NP+	Mean	1.000	1.010	0.993	0.940
			p value	0.760 [a]	n/a	n/a	n/a
	5	MFI	Mean	1.000	0.940	1.100	1.007
			p value	0.401 [a]	n/a	n/a	n/a
		NP+	Mean	1.000	1.003	1.01	1.003
			p value	0.931 [a]	n/a	n/a	n/a
THP-1	1	MFI	Mean	1.000	0.960	0.995	0.980
			p value	0.551 [a]	n/a	n/a	n/a
		NP+	Mean	1.000	0.943	1.000	1.020
			p value	0.785 [a]	n/a	n/a	n/a
	5	MFI	Mean	1.000	1.157	0.965	1.113
			p value	0.163 [a]	n/a	n/a	n/a
		NP+	Mean	1.000	1.037	0.990	1.050
			p value	0.333 [a]	n/a	n/a	n/a

Table 5.7: Fold change in U-PS uptake following co-treatment with BSA and IAV. [a] Kruskal-Wallis between group differences; [b] Mann-Whitney U test versus U-PS treatment; [c] Mann-Whitney U test versus U-PS + protein treatment; [d] Mann-Whitney U test versus U-PS + IAV treatment. Significant differences in bold. n/a; Mann-Whitney U test not conducted where Kruskal-Wallis p>0.050.

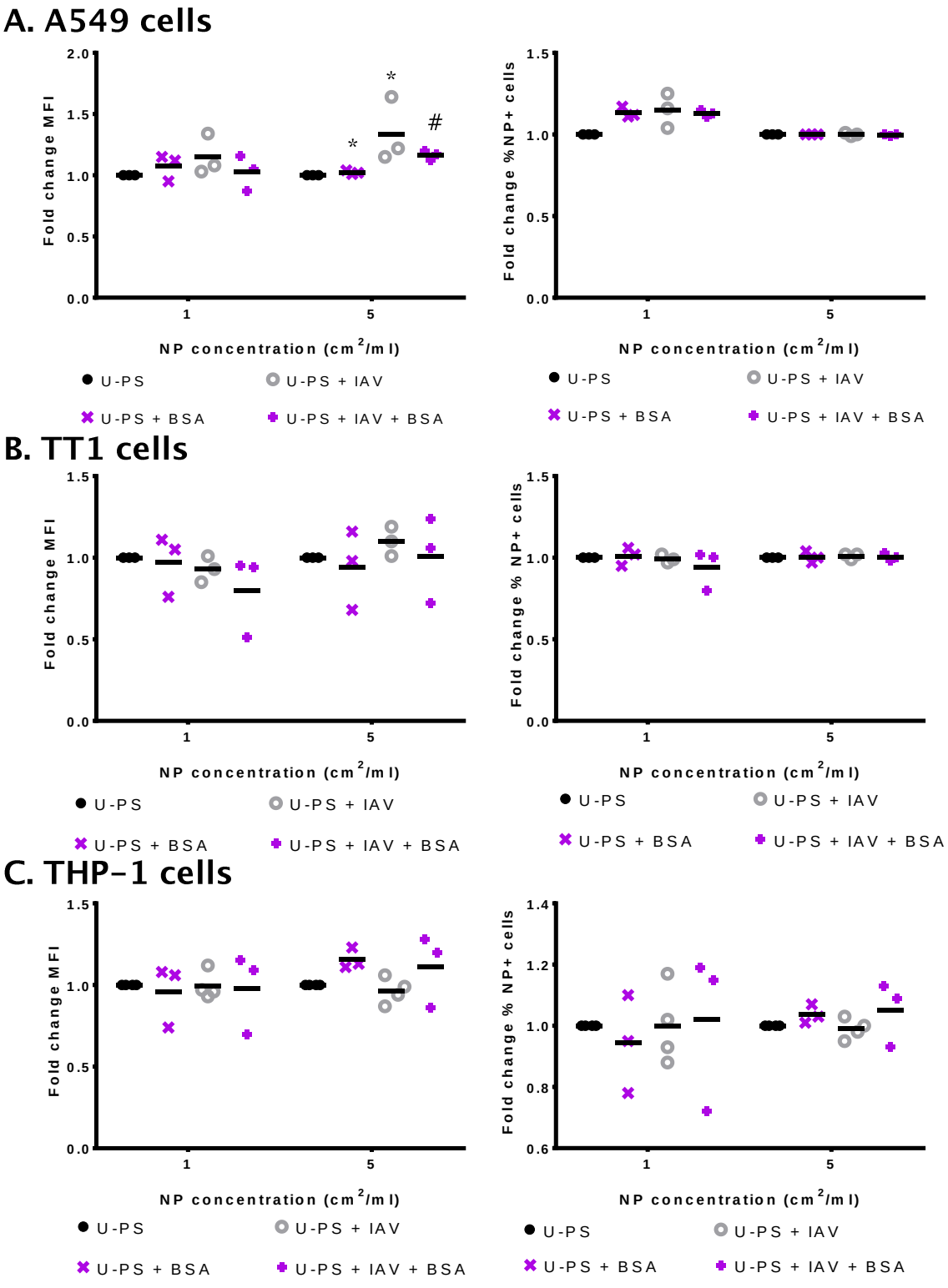

Figure 5.15: Effect of BSA and IAV on U-PS NP association. Relative cell association of unmodified polystyrene NP in A. A549 cells, B. TT1 cells and C. THP-1 cells following pre-incubation with 5μg/mL BSA and IAV. *Left panel* shows relative mean fluorescence intensity (MFI) and right panel shows relative number of NP positive (%NP+) cells. Data represents mean (black horizontal line) of at least three independent experiments. Statistics determined by Kruskal-Wallis and Mann Whitney U test. * p≤0.05 versus U-PS; # p≤0.05 versus U-PS and BSA; ϕ p≤0.05 versus U-PS and IAV.

5.3.3.2 Effect of IAV on A-PS uptake

The effect of proteins and IAV on A-PS uptake are summarised in Tables 5.8-5.11. IAV resulted in increased 100nm A-PS uptake in A549 cells. This was evident at both 1 and 5 cm^2/mL concentrations using both %NP+ cells and MFI measurements. At 1 cm^2/mL %NP+ cells and MFI were enhanced by 93.3% and 81.4% respectively. These were statistically significant with associated p values of 0.014. At 5 cm^2/mL A-PS these were enhanced by 24.6% and 32.9% with associated p values of 0.014.

In TT1 cells, the pre-incubation of 1 cm^2/mL A-PS with IAV resulted in 14.6% and 10.0% increases in the MFI and %NP+ cells. However, these increases did not reach statistical significance with associated p values of 0.095. Pre-incubation of 5 cm^2/mL A-PS with IAV resulted in 12.6% and 12.2% relative increases in the MFI and %NP+ cells. These increases were highly statistically significant with associated p values of 0.005.

In THP-1 cells, the pre-incubation of 1 or 5 cm^2/mL A-PS with IAV resulted in 14.2% and 3.6% increases in the MFI in these cells. However, these increases were not statistically significant with associated p values of 1.000 and 0.219 respectively. The pre-incubation of 1 or 5 cm^2/mL A-PS with IAV resulted in 14.5% and 7.3% respective increases in the %NP+ cells. However, only the higher concentration achieved statistical significance as they had respective p values of 0.219 and 0.014.

5.3.3.2.1. Effect of SP-A and IAV on A-PS uptake

In A549 cells, the pre-incubation of 1 cm^2/mL A-PS with SP-A resulted in a 30.2% relative increase in the number of NP+ cells; however, this increase was not statistically significant with an associated p value of 0.435 (see Table 5.8 and Figure 5.16A). The addition of IAV to this treatment resulted in a 40.1%

decrease in the NP+ cells; however, this was also not statistically significant (p=0.480). The %NP+ cells in this triple treatment in A549 cells was significantly reduced by 103.2% compared to the A-PS and IAV treatment (p=0.021). The pre-incubation of 5 cm^2/mL with SP-A with or without IAV had no significant effect on the %NP+ cells (p=0.095; Kruskal-Wallis). Moreover, the MFI of 1 cm^2/mL or 5 cm^2/mL A-PS with SP-A with or without IAV was also not significantly different in A549 cells (p=0.165 and p=0.085 respectively; Kruskal-Wallis). In TT1 cells the pre-incubation of 5 cm^2/mL A-PS with nhSP-A resulted in 81.0% and 54.8% respective increases in the MFI and %NP+ cells. These increases were statistically significant with associated p values of 0.005 (see Table 5.8 and Figure 5.16B). Following the addition of IAV NP uptake was reduced by 24.2% and 20.8% respectively, although these reductions were not statistically significant (p=0.602 and p=0.347 respectively). The addition of SP-A to the A-PS and IAV treatment resulted in 44.2% and 21.8% increases in the MFI and %NP+ cells. These increases were statistically significant with associated p values of 0.009. In TT1 cells, the pre-incubation of 1 cm^2/mL A-PS with SP-A with and without IAV had no significant effect on the MFI or %NP+ cells (p=0.332 and p=0.283 respectively; Kruskal-Wallis).

Pre-incubation of 5 cm^2/mL A-PS with 5 μg/mL nhSP-A resulted in a 5.4% reduction in the MFI in THP-1 cells. However, this difference was not statistically significant with an associated p value 0.219. The addition of IAV to this treatment resulted in a significant 17.3% increase in the MFI of THP-1 cells over the NP and protein control (p=0.021; see Table 5.8 and Figure 5.16C). This represented a 8.3% increase in MFI over the A-PS and IAV control; however, this increase did not achieve statistical significance (p=0.149). The pre-incubation of 5 cm^2/mL A-PS with nhSP-A resulted in a 4.3% increase in the %NP+ cells; however, this increase was not statistically significant with an associated p value of 0.219. Following the addition of IAV the %NP+ cells

increased by 13.5% compared to the A-PS and SP-A control; this increase was statistically significant with an associated p value of 0.021. Moreover, the %NP+ cells was also significantly enhanced by 10.3% in this triple treatment compared to the NP and IAV control (p=0.021). The pre-incubation of 1 cm^2/mL with SP-A with or without IAV had no significant effect on the MFI or %NP+ THP-1 cells (p=0.778 and p=0.190 respectively; Kruskal-Wallis).

Cell type	NP (cm^2/mL)			A-PS [b]	A-PS + SP-A [c]	A-PS + IAV [d]	A-PS+IAV + SP-A
A549	1	MFI	Mean	1.000	1.399	1.814	0.851
			p value	0.165 [a]	n/a	n/a	n/a
		NP+	Mean	1.000	1.302	1.933	0.901
			p value	**0.035** [a]	0.435 [b]	**0.014** [b]	0.480 [c] **0.021** [d]
	5	MFI	Mean	1.000	1.039	1.329	1.230
			p value	0.084 [a]	n/a	n/a	n/a
		NP+	Mean	1.000	1.195	1.246	1.222
			p value	0.095 [a]	n/a	n/a	n/a
TT1	1	MFI	Mean	1.000	0.952	1.146	1.022
			p value	0.332 [a]	n/a	n/a	n/a
		NP+	Mean	1.000	1.268	1.100	1.283
			p value	0.283 [a]	n/a	n/a	n/a
	5	MFI	Mean	1.000	1.81	1.126	1.568
			p value	**0.001** [a]	**0.005** [b]	**0.005** [b]	0.602 [c] **0.009** [d]
		NP+	Mean	1.000	1.548	1.122	1.340
			p value	**0.001** [a]	**0.005** [b]	**0.005** [b]	0.347 [c] **0.009** [d]
THP-1	1	MFI	Mean	1.000	0.739	1.142	1.131
			p value	0.778 [a]	n/a	n/a	n/a
		NP+	Mean	1.000	0.705	1.145	1.147
			p value	0.190 [a]	n/a	n/a	n/a
	5	MFI	Mean	1.000	0.946	1.036	1.119
			p value	**0.023** [a]	0.219 [b]	0.219 [b]	**0.021** [c] 0.149 [d]
		NP+	Mean	1.000	1.043	1.073	1.178
			p value	**0.009** [a]	0.219 [b]	**0.014** [b]	**0.021** [c] **0.021** [d]

Table 5.8: Fold change in A-PS uptake following co-treatment with SP-A and IAV. [a] Kruskal-Wallis between group differences; [b] Mann-Whitney U test versus A-PS treatment; [c] Mann-Whitney U test versus A-PS + protein treatment; [d] Mann-Whitney U test versus A-PS + IAV treatment. Significant differences in bold. n/a; Mann-Whitney U test not conducted where Kruskal-Wallis p>0.050.

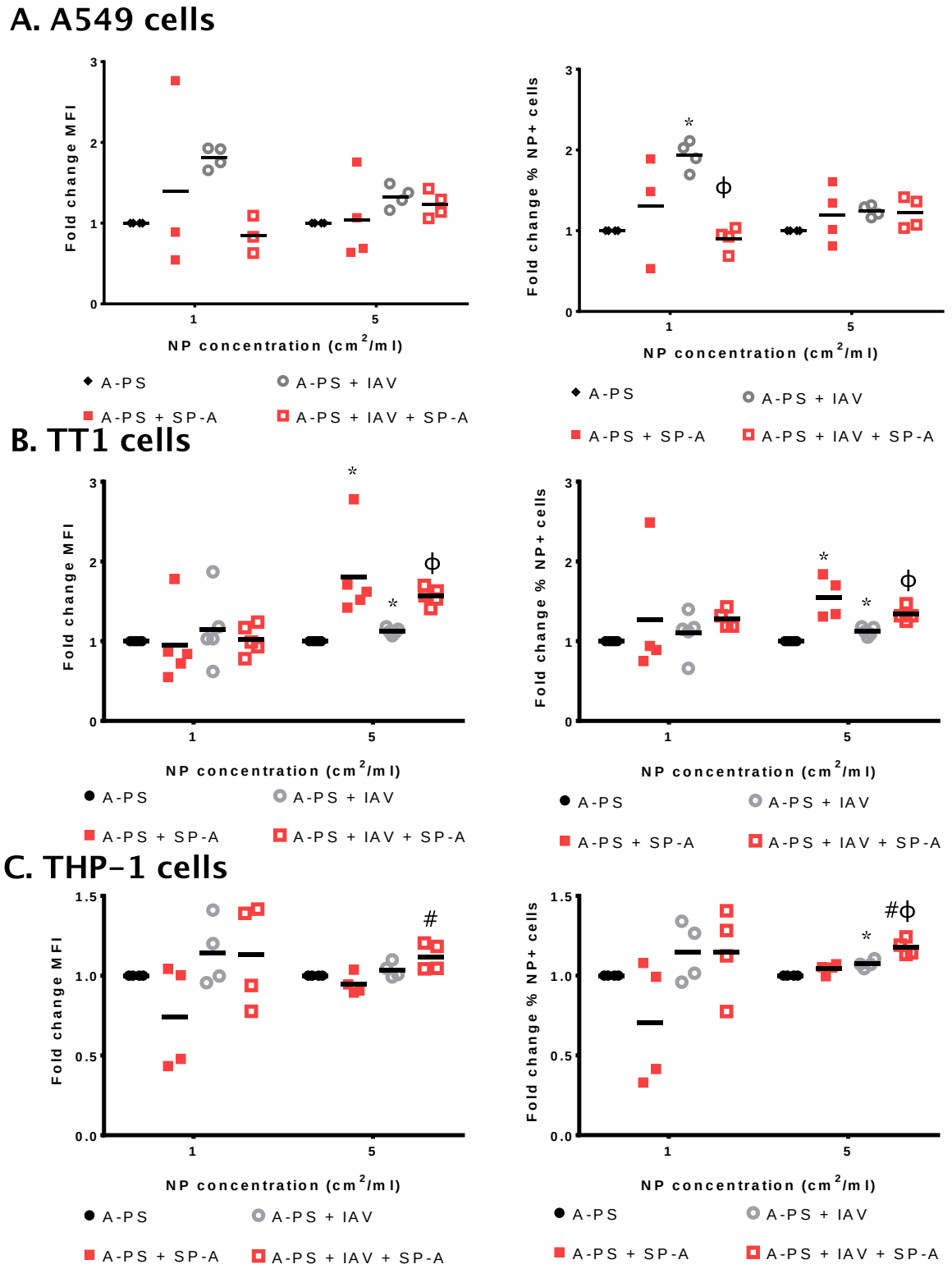

Figure 5.16: Effect of nhSP-A and IAV on A-PS NP association. Relative cell association of amine polystyrene NP in A. A549 cells, B. TT1 cells and C. THP-1 cells following pre-incubation with 5μg/mL nhSP-A and IAV. *Left panel* shows relative mean fluorescence intensity (MFI) and right panel shows relative number of NP positive (%NP+) cells. Data represents mean (black horizontal line) of at least three independent experiments. Statistics determined by Kruskal-Wallis and Mann Whitney U test. * p≤0.05 versus A-PS; # p≤0.05 versus A-PS and SP-A; ϕ p≤0.05 versus A-PS and IAV.

Cell type	NP (cm^2/mL)			A-PS [b]	A-PS + SP-D [c]	A-PS + IAV [d]	A-PS+IAV + SP-D
A549	1	MFI	Mean	1.000	0.992	1.814	2.286
			p value	0.092 [a]	n/a	n/a	n/a
		NP+	Mean	1.000	1.401	1.932	2.331
			p value	0.059 [a]	n/a	n/a	n/a
	5	MFI	Mean	1.000	1.059	1.329	1.389
			p value	**0.014** [a]	0.219 [b]	**0.014** [b]	**0.043** [c] 0.773 [d]
		NP+	Mean	1.000	1.136	1.246	1.361
			p value	0.172 [a]	n/a	n/a	n/a
TT1	1	MFI	Mean	1.000	1.122	1.146	1.256
			p value	0.132 [a]	n/a	n/a	n/a
		NP+	Mean	1.000	1.038	1.100	1.218
			p value	0.262 [a]	n/a	n/a	n/a
	5	MFI	Mean	1.000	0.980	1.126	1.180
			p value	**0.001** [a]	0.577 [b]	**0.005** [b]	**0.009** [c] **0.047** [d]
		NP+	Mean	1.000	1.088	1.122	1.216
			p value	**0.002** [a]	**0.005** [b]	**0.005** [b]	**0.028** [c] **0.047** [d]
THP-1	1	MFI	Mean	1.000	0.487	1.142	1.161
			p value	**0.017** [a]	**0.014** [b]	1.000 [b]	**0.021** [c] 0.773 [d]
		NP+	Mean	1.000	0.471	1.145	1.182
			p value	**0.021** [a]	**0.014** [b]	0.219 [b]	**0.021** [c] 0.773 [d]
	5	MFI	Mean	1.000	0.995	1.036	1.023
			p value	0.799 [a]	n/a	n/a	n/a
		NP+	Mean	1.000	1.051	1.073	1.083
			p value	0.490 [a]	n/a	n/a	n/a

Table 5.9: Fold change in A-PS uptake following co-treatment with SP-D and IAV. [a] Kruskal-Wallis between group differences; [b] Mann-Whitney U test versus A-PS treatment; [c] Mann-Whitney U test versus A-PS + protein treatment; [d] Mann-Whitney U test versus A-PS + IAV treatment. Significant differences in bold. n/a; Mann-Whitney U test not conducted where Kruskal-Wallis p>0.050.

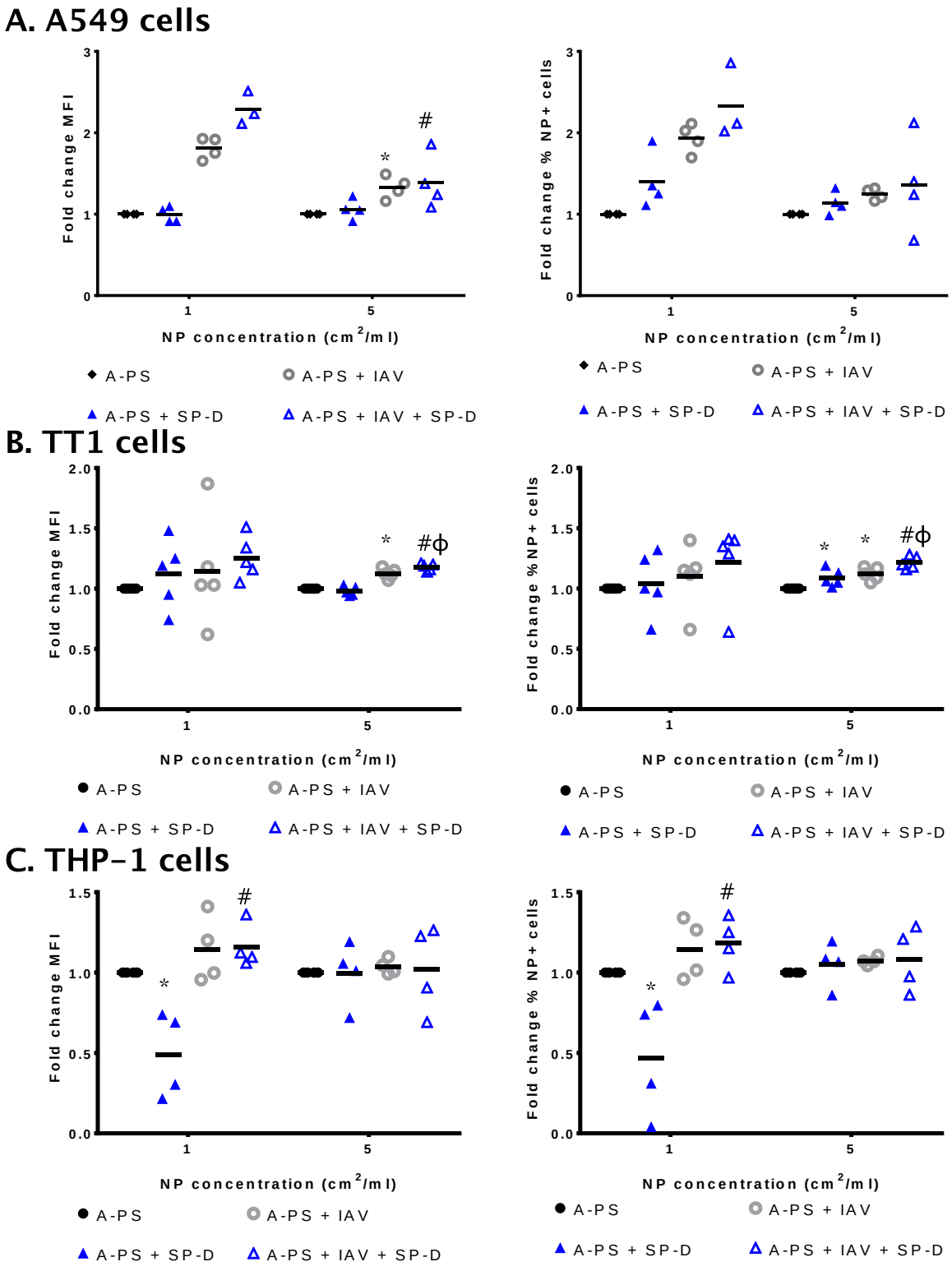

Figure 5.17: Effect of nhSP-D and IAV on A-PS NP association. Relative cell association of amine polystyrene NP in A. A549 cells, B. TT1 cells and C. THP-1 cells following pre-incubation with 0.4µg/mL nhSP-D and IAV. *Left panel* shows relative mean fluorescence intensity (MFI) and right panel shows relative number of NP positive (%NP+) cells. Data represents mean (black horizontal line) of at least three independent experiments. Statistics determined by Kruskal-Wallis and Mann Whitney U test. * p≤0.05 versus A-PS; # p≤0.05 versus A-PS and SP-D; ϕ p≤0.05 versus A-PS and IAV.

5.3.3.2.2. Effect of SP-D and IAV on A-PS uptake

The pre-incubation of 5 cm^2/mL A-PS with nhSP-D resulted in a 5.9% increase in the MFI in A549 cells. However, this was not statistically significant with an associated p value of 0.219 (see Table 5.9 and Figure 5.17A). Following the addition of IAV to this treatment the MFI significantly increased by 33.0% compared to the A-PS and SP-D treatment (p=0.043). However, the MFI was not significantly different in this triple treatment compared to the A-PS and IAV co-treatment (p=0.773). The pre-incubation of 1 cm^2/mL A-PS with IAV with or without IAV had no significant effect on the MFI in A549 cells (p=0.092; Kruskal-Wallis). The pre-incubation of 1 or 5 cm^2/mL A-PS with nhSP-D tended to increase %NP+ A549 cells and this was further enhanced with the addition of IAV; however, there was no significant difference between these treatments (p=0.059 and p=0.172 respectively; Kruskal-Wallis).

In TT1 cells, the pre-incubation of 1 cm^2/mL A-PS with nhSP-D tended to increase the MFI and NP+ cells which was further enhanced with the addition of IAV. However, there were no significant differences between these treatments (p=0.132 and p=0.262 respectively; Kruskal-Wallis; see Table 5.9 and Figure 5.17B). The pre-incubation of 5 cm^2/mL A-PS with nhSP-D resulted in a 2% reduction in MFI compared to the NP control; however this reduction was not statistically significant with an associated p value of 0.577. The addition of IAV to this treatment resulted in a 20% increase in the MFI over the A-PS and SP-D control. This increase was highly statistically significant with an associated p value of 0.009. Moreover, the MFI of this triple treatment was also significantly enhanced by 5.4% over the A-PS and IAV control (p=0.047). The pre-incubation of 5 cm^2/mL with nhSP-D also resulted in a 8.8% increase in the number of NP+ cells. This increase was statistically significant with an associated p value of 0.009. The addition of IAV resulted in a 12.8% significant increase in the number of NP+ cells compared to the A-PS and IAV control

(p=0.028). Moreover, the NP+ cells was also significantly enhanced by 9.4% over the A-PS and IAV control (p=0.047).

Pre-incubation of 1 cm^2/mL A-PS with 0.4 μg/mL nhSP-D in THP-1 cells resulted in 51.3% and 52.9% reductions in the MFI and number of NP+ cells respectively. These reductions were statistically significant with associated p values of 0.014 (see Table 5.9 and Figure 5.17C). The addition of IAV to this treatment enhanced these measurements of NP uptake by 67.4% and 71.1% respectively in comparison to the A-PS and SP-D treatments. These increases were statistically significant with associated p values of 0.021. However, the difference between the A-PS, IAV and SP-D treatment to A-PS and IAV were not significant for either measurement (p=0.773). The pre-incubation of 5 cm^2/mL A-PS in THP-1 cells with nhSP-D with or without IAV had no significant effect on nanoparticle uptake by either MFI or NP+ measures (p=0.799 and p=0.490 respectively; Kruskal-Wallis).

5.3.3.2.3. Effect of rfhSP-D and IAV on A-PS uptake

In A549 cells, the pre-incubation of 1 cm^2/mL A-PS with rfhSP-D resulted in 31.8% and 24.5% in the MFI and number of NP+ cells respectively. These increases were statistically significant with associated p values of 0.047 and 0.014 respectively (see Figure 5.18A and Table 5.10). The addition of IAV to this treatment resulted in 70.3% and 68.1% significant increases in the MFI and NP+ cells over the A-PS and rfhSP-D control (p=0.021 for both measures). These represented significant 42.9% and 49.6% reductions over the A-PS and IAV control (p=0.021 and p=0.043 respectively). The pre-incubation of 5 cm^2/mL A-PS with rfhSP-D in A549 cells resulted in 5% reduction in the MFI and 8% increase in the %NP+ cells; however, these differences were not statistically significant with associated p values of 0.219 and 1.000 respectively. The

addition of IAV to this treatment had no significant effect on either MFI or NP+ cells (p=0.083 for both measures).

In TT1 cells, the pre-incubation of 5 cm^2/mL A-PS with rfhSP-D resulted in 26.8% increases in the number of NP+ cells. This increase was highly statistically significant with an associated p value of 0.005 (see Table 5.10 and Figure 5.18B). The addition of IAV to the A-PS and rfhSP-D had no significant effect on the NP+ cells compared to the A-PS and rfhSP-D control (p=0.754). Moreover, the number of NP+ cells was also not significantly different in this triple treatment compared to the A-PS and IAV control (p=0.754). The pre-incubation of 5 cm^2/mL A-PS with rfhSP-D with or without IAV had no significant effect on NP+ cells (p=0.240; Kruskal-Wallis). The pre-incubation of 1 cm^2/mL A-PS with rfhSP-D in TT1 cells with or without IAV had no significant effect on NP uptake as measured by MFI or NP+ cells (p=0.344 and p=0.159; Kruskal-Wallis).

Pre-incubation of 1 cm^2/mL or 5 cm^2/mL A-PS with rfhSP-D with or without IAV had no significant effect on the uptake of A-PS in THP-1 cells (see Table 5.10 and Figure 5.18C).

Cell type	NP (cm^2/mL)			A-PS [b]	A-PS + rfhSP-D [c]	A-PS + IAV [d]	A-PS+IAV + rfhSP-D
A549	1	MFI	Mean	1.000	0.682	1.814	1.385
			p value	**0.003** [a]	**0.047** [b]	**0.028** [b]	**0.021** [c] **0.021** [d]
		NP+	Mean	1.000	0.755	1.932	1.436
			p value	**0.003** [a]	**0.014** [b]	**0.014** [b]	**0.021** [c] **0.043** [d]
	5	MFI	Mean	1.000	0.950	1.329	1.231
			p value	**0.034** [a]	0.219 [b]	**0.014** [b]	0.083 [c] 0.564 [d]
		NP+	Mean	1.000	1.080	1.246	1.283
			p value	**0.049** [a]	1.000 [b]	**0.014** [b]	0.083 [c] 0.773 [d]
TT1	1	MFI	Mean	1.000	1.062	1.146	1.190
			p value	0.344 [a]	n/a	n/a	n/a
		NP+	Mean	1.000	1.300	1.100	1.492
			p value	0.159 [a]	n/a	n/a	n/a
	5	MFI	Mean	1.000	0.968	1.126	1.058
			p value	0.240 [a]	n/a	n/a	n/a
		NP+	Mean	1.000	1.268	1.122	1.290
			p value	**0.012** [a]	**0.005** [b]	**0.005** [b]	0.754 [c] 0.754 [d]
THP-1	1	MFI	Mean	1.000	1.021	1.142	1.135
			p value	0.637 [a]	n/a	n/a	n/a
		NP+	Mean	1.000	0.984	1.145	1.184
			p value	0.399 [a]	n/a	n/a	n/a
	5	MFI	Mean	1.000	0.859	1.036	0.861
			p value	0.193 [a]	n/a	n/a	n/a
		NP+	Mean	1.000	1.020	1.073	1.011
			p value	0.424 [a]	n/a	n/a	n/a

Table 5.10: Fold change in A-PS uptake following co-treatment with rfhSP-D and IAV. [a] Kruskal-Wallis between group differences; [b] Mann-Whitney U test versus A-PS treatment; [c] Mann-Whitney U test versus A-PS + protein treatment; [d] Mann-Whitney U test versus A-PS + IAV treatment. Significant differences in bold. n/a; Mann-Whitney U test not conducted where Kruskal-Wallis p>0.050

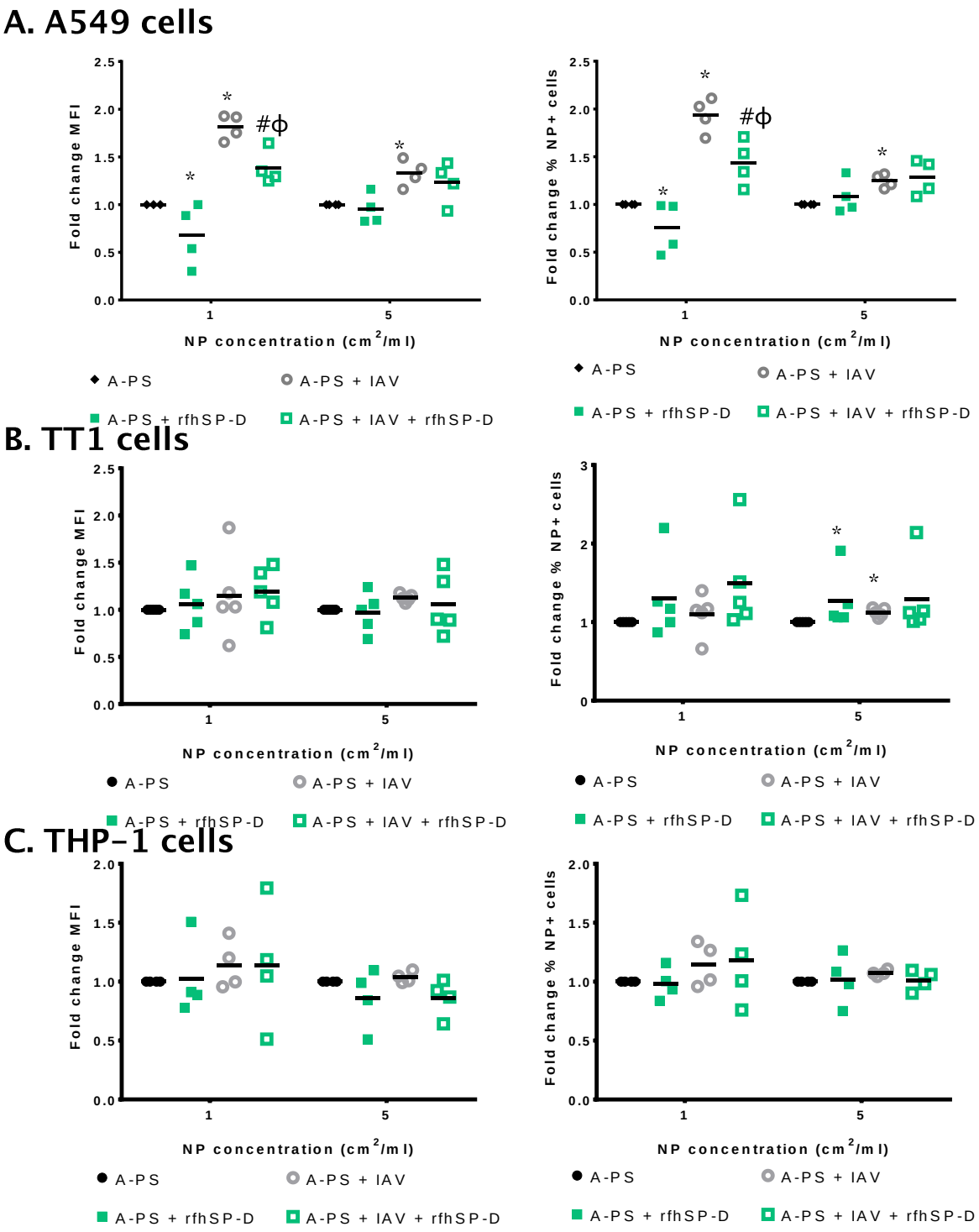

Figure 5.18: Effect of rfhSP-D and IAV on A-PS NP association. Relative cell association of amine polystyrene NP in A. A549 cells, B. TT1 cells and C. THP-1 cells following pre-incubation with 5μg/mL rfhSP-D and IAV. *Left panel* shows relative mean fluorescence intensity (MFI) and right panel shows relative number of NP positive (%NP+) cells. Data represents mean (black horizontal line) of at least three independent experiments. Statistics determined by Kruskal-Wallis and Mann Whitney U test. * p≤0.05 versus A-PS; # p≤0.05 versus A-PS and rfhSP-D; ϕ p≤0.05 versus A-PS and IAV.

5.3.3.2.4. Effect of BSA and IAV on A-PS uptake

In A549 cells, the pre-incubation of 1 or 5 cm^2/mL with BSA had no significant effect on NP association by either MFI or %NP+ measures (p=1.000 for each comparison). Following the addition of IAV the MFI increased 74.7% and 44.7% respectively for the 1 and 5 cm^2/mL concentrations. However, these increases failed to reach statistical significance with associated p values of 0.248 and 0.083 respectively (see Table 5.11 and Figure 5.19A). The %NP+ cells increased 75.4% and 25.5% following the addition of IAV to the 1 and 5 cm^2/mL A-PS and BSA treatment. However, these increases were not statistically significant with associated p values of 0.149. There was also no significant difference in nanoparticle uptake in the triple co-treatments at either nanoparticle concentration compared to the relevant A-PS and IAV controls.

In TT1 cells, the pre-incubation of 5 cm^2/mL A-PS with BSA resulted in a 5.8% reduction the MFI. However this reduction was not statistically significant (p=0.095; see Figure 5.19B and Table 5.11). The addition of IAV to this treatment resulted in a non-significant 3.2% increase in the MFI (p=0.602). The level of nanoparticle uptake by MFI was still significantly reduced by 15.2% in this triple treatment compared to the A-PS and IAV control (p=0.016). The pre-incubation of 1 cm^2/mL or 5 cm^2/mL A-PS in TT1 cells with BSA with or without IAV had no significant effect on the number of cells containing nanoparticles (p=0.316 and 0.090 respectively; Kruskal-Wallis). Moreover, BSA with or without IAV also had no significant effect on the MFI of 1 cm^2/mL A-PS in TT1 cells (p=0.687; Kruskal-Wallis).

Pre-incubation of 5 cm^2/mL A-PS with 5 μg/mL BSA μg/mL resulted in a 16.1% significant reduction in MFI of THP-1 cells (p=0.014). The addition of IAV to this treatment enhanced the MFI by 10.6%, however, this was not statistically significant (p=0.386; see Figure 5.19C and Table 5.11). The pre-incubation of 5

cm^2/mL A-PS in THP-1 cells with BSA with or without IAV had no significant effect on the number of NP+ cells (p=0.067; Kruskal-Wallis). In THP-1 cells, the pre-incubation of 1 cm^2/mL A-PS with BSA with or without IAV also had no significant effect on either the MFI or number of NP+ cells (p=0.783 and p=0.190 respectively; Kruskal-Wallis).

Cell type	NP (cm^2/mL)			A-PS [b]	A-PS + BSA [c]	A-PS + IAV [d]	A-PS+IAV + BSA
A549	1	MFI	Mean	1.000	0.893	1.814	1.640
			p value	**0.049** [a]	1.000 [b]	**0.028** [b]	0.248 [c] 0.248 [d]
		NP+	Mean	1.000	0.964	1.932	1.718
			p value	0.053 [a]	n/a	n/a	n/a
	5	MFI	Mean	1.000	0.989	1.329	1.436
			p value	**0.017** [a]	1.000 [b]	**0.014** [b]	0.083 [c] 0.386 [d]
		NP+	Mean	1.000	1.032	1.246	1.287
			p value	**0.040** [a]	1.000 [b]	**0.014** [b]	0.149 [c] 1.000 [d]
TT1	1	MFI	Mean	1.000	1.015	1.146	1.050
			p value	0.687 [a]	n/a	n/a	n/a
		NP+	Mean	1.000	0.908	1.100	0.910
			p value	0.316 [a]	n/a	n/a	n/a
	5	MFI	Mean	1.000	0.942	1.126	0.974
			p value	**0.023** [a]	0.095 [b]	**0.005** [b]	0.602 [c] **0.016** [d]
		NP+	Mean	1.000	1.034	1.122	1.030
			p value	0.090 [a]	n/a	n/a	n/a
THP-1	1	MFI	Mean	1.000	1.040	1.142	1.170
			p value	0.783 [a]	n/a	n/a	n/a
		NP+	Mean	1.000	0.909	1.145	1.103
			p value	0.190 [a]	n/a	n/a	n/a
	5	MFI	Mean	1.000	0.839	1.036	0.945
			p value	**0.048** [a]	**0.014** [b]	0.219 [b]	0.386 [c] 0.248 [d]
		NP+	Mean	1.000	0.975	1.073	1.058
			p value	0.067 [a]	n/a	n/a	n/a

Table 5.11: Fold change in A-PS uptake following co-treatment with BSA and IAV. [a] Kruskal-Wallis between group differences; [b] Mann-Whitney U test versus A-PS treatment; [c] Mann-Whitney U test versus A-PS + protein treatment; [d] Mann-Whitney U test versus A-PS + IAV treatment. Significant differences in bold. n/a; Mann-Whitney U test not conducted where Kruskal-Wallis p>0.050.

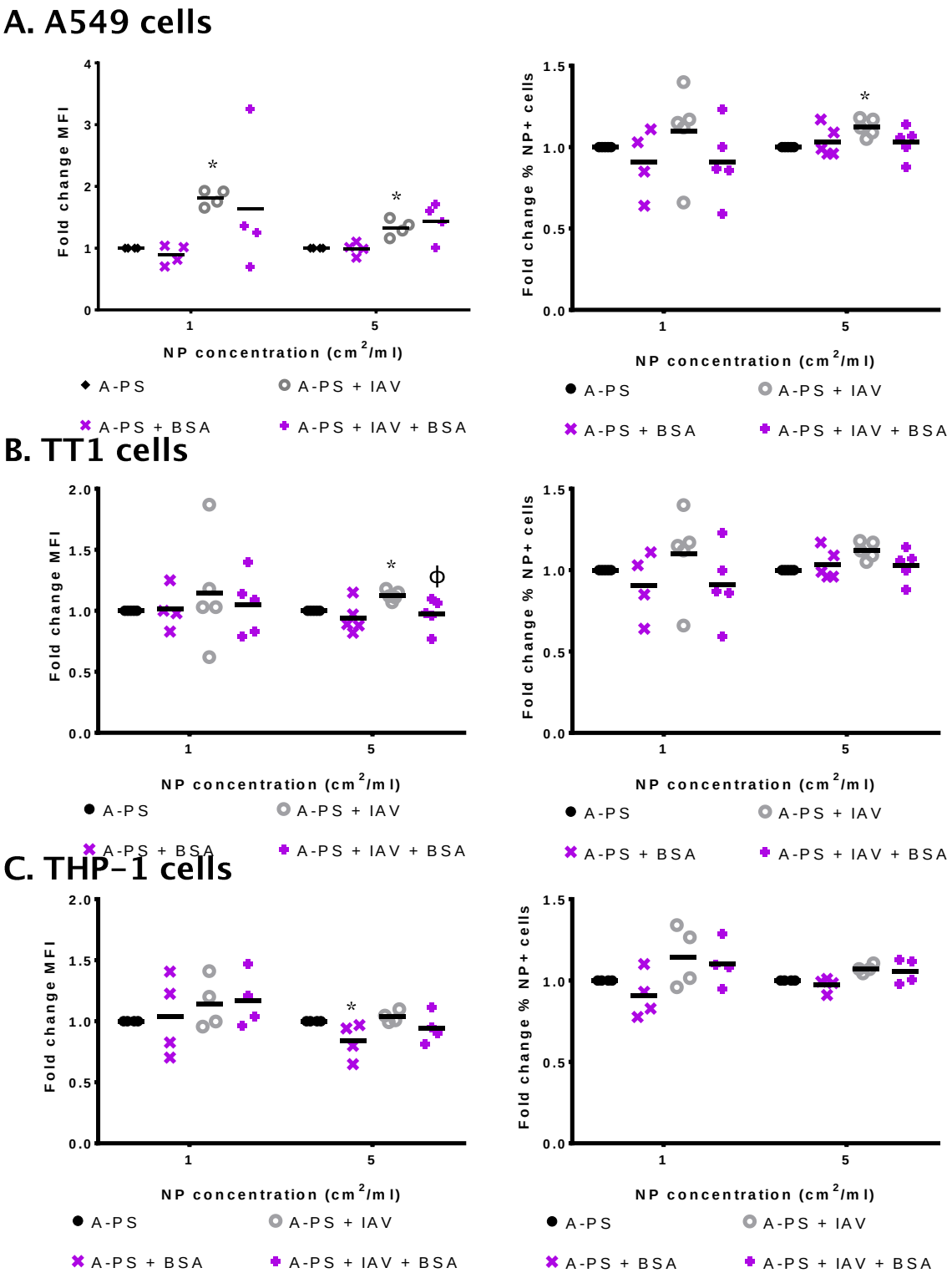

Figure 5.19: Effect of BSA and IAV on A-PS NP association. Relative cell association of amine polystyrene NP in A. A549 cells, B. TT1 cells and C. THP-1 cells following pre-incubation with 5μg/mL BSA and IAV. *Left panel* shows relative mean fluorescence intensity (MFI) and right panel shows relative number of NP positive (%NP+) cells. Data represents mean (black horizontal line) of at least three independent experiments. Statistics determined by Kruskal-Wallis and Mann Whitney U test. * p≤0.05 versus A-PS; # p≤0.05 versus A-PS and BSA; ϕ p≤0.05 versus A-PS and IAV.

5.3.4. Toxicity of NP and IAV

In order to assess the toxicity of the particle and influenza treatments MTT assays were conducted. Protocols were established to reflect the exposure conditions of the infection assays; particles were pre-incubated for an hour then IAV added to the particles and incubated for a further hour. The inoculum was added to serum starved cells for 1 hour then washed off and the cells incubated for a further 16 hours in serum free medium. The number of cells plated per well was optimised to produce a sub-maximal optical density reading for each cell type.

A-PS and U-PS particles had no significant effect on the viability of A549 cells up to 5 cm^2/mL in the absence of IAV (p=0.871 and p=0.398 respectively; Kruskal-Wallis). IAV treatment in A549 cells resulted in an 11.5% reduction in cell viability. This was statistically significant with an associated p value of 0.037. Pre-incubation of IAV with A-PS or U-PS tended to reduce IAV mediated toxicity in A549 cells. However, this was only statistically significant with the 0.04 cm^2/mL A-PS with IAV treatment that had an associated p value of 0.050.

A-PS and U-PS particles had no significant effect on the viability of THP-1 cells (p=0.191 and 0.411 respectively; Kruskal-Wallis). IAV resulted in a 17.3% reduction in THP-1 cell viability. This was statistically significant with an associated p value of 0.037. The pre-incubation of IAV with A-PS or U-PS had no significant effect on the IAV induced reduction in cell viability (p=0.399 and p=0.586 respectively; Kruskal-Wallis).

A-PS and U-PS had no significant effect on the viability of TT1 cells for the studied time period (p=0.209 and p=0.339 respectively; Kruskal-Wallis see Figure 5.20B and Figure 5.21B). TT1 cells treated with IAV resulted in a significant 26.6% reduction in cell viability (p=0.037); however, the addition of A-PS or U-PS to IAV had no significant modulatory effect on this reduction

(p=0.375 and p=0.748 respectively; Kruskal-Wallis). UPS had no significant effect on TT1 clonogenic survival following 1 hour treatment (p=0.748; Kruskal-Wallis see Figure 5.22). A-PS resulted in a dose dependent reduction in clonogenic survival which became significant at 0.04 cm^2/mL with an associated p value of 0.037.

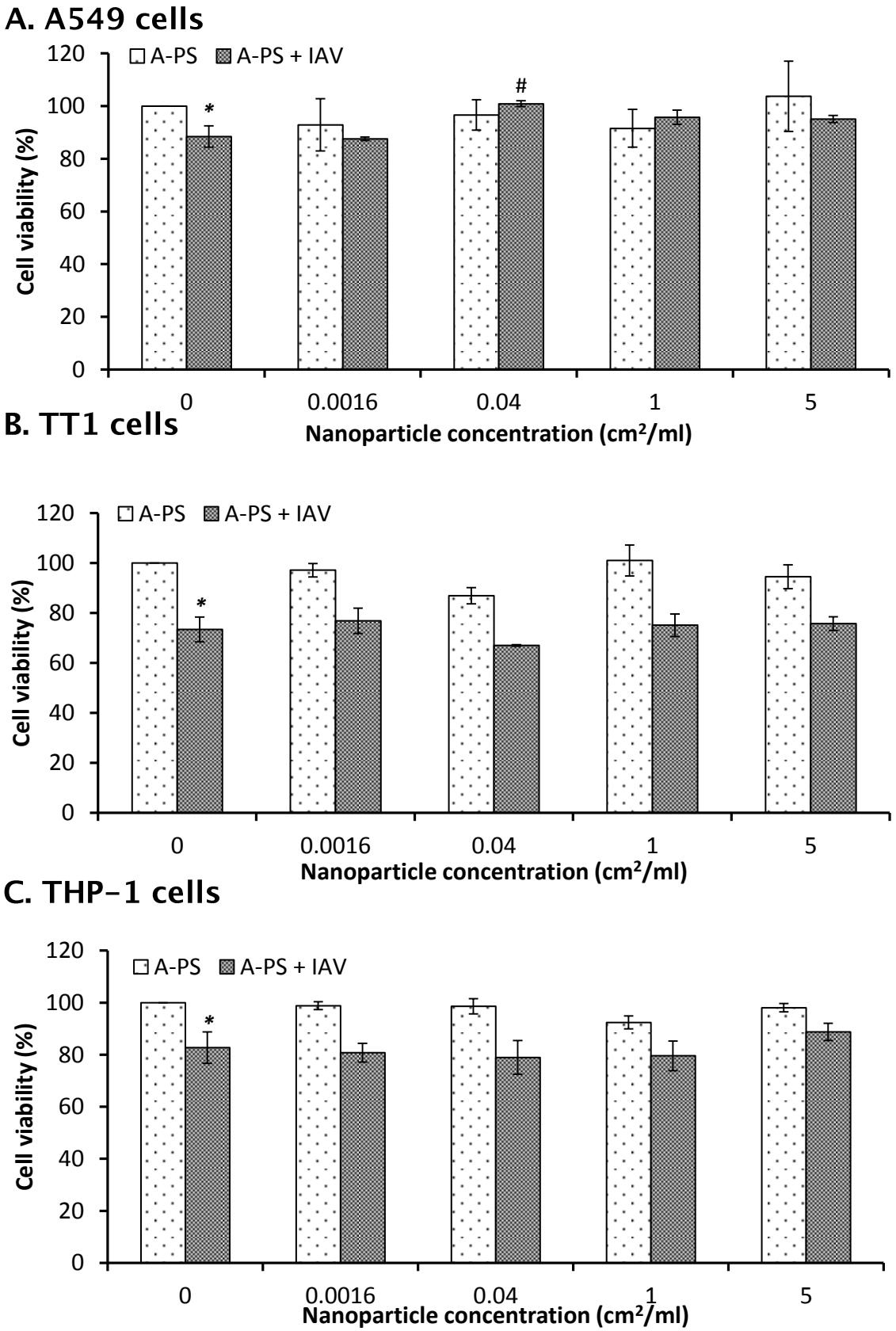

Figure 5.20: Cell viability following exposure to A-PS particles and influenza A virus in A. A549 B. TT1 and C. THP-1 cells. Data represents mean (±SEM) of three independent experiments. Statistics determined using Kruskal-Wallis and Mann Whitney U test where *p≤0.050 vs. control; # p≤0.050 vs. IAV control.

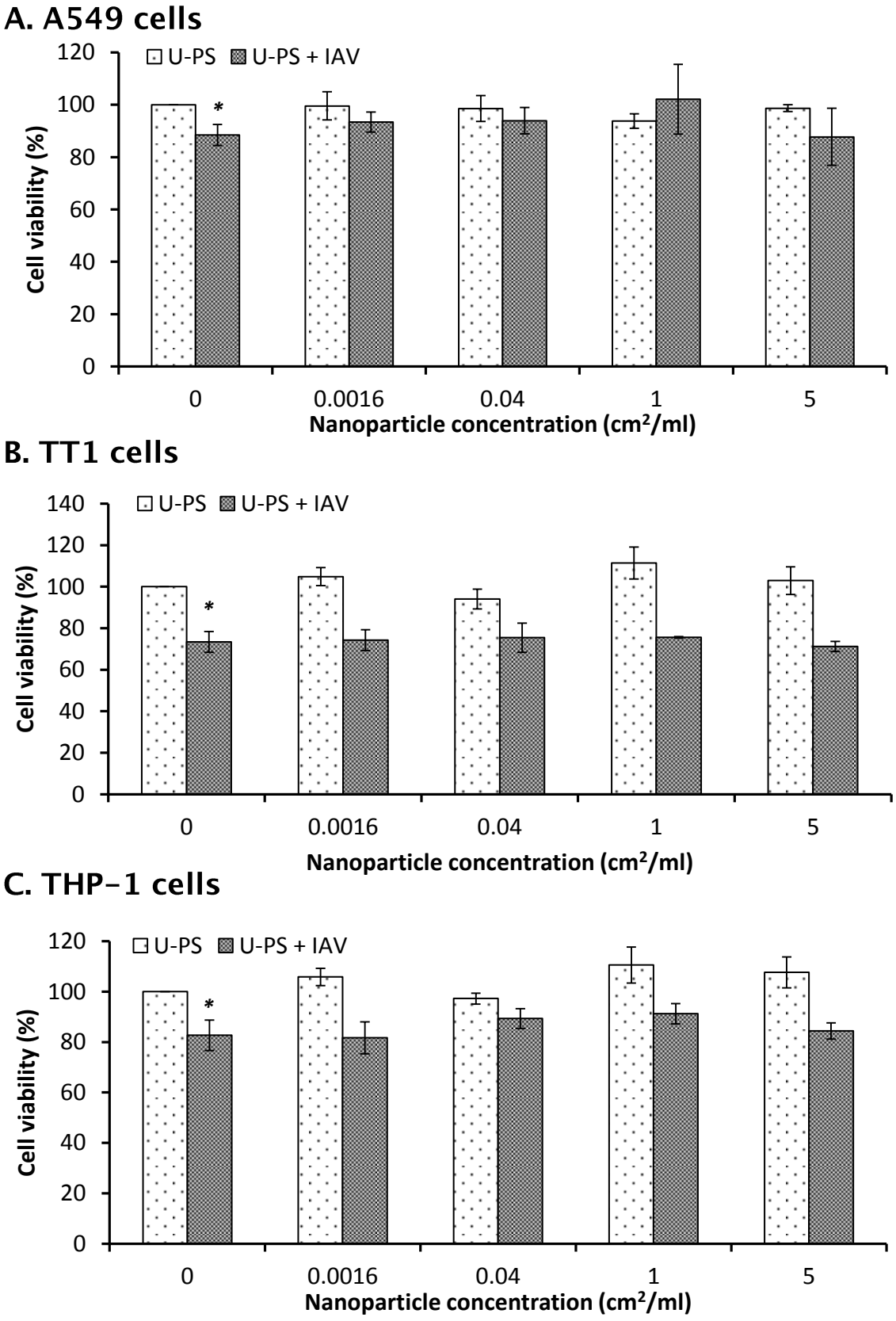

Figure 5.21: Cell viability following exposure to U-PS particles and influenza A virus in A. A549 B. TT1 and C. THP-1 cells. Data represents mean (±SEM) of three independent experiments. Statistics determined using Kruskal-Wallis and Mann Whitney U test where *p≤0.050 vs. control; # p≤0.050 vs. IAV control.

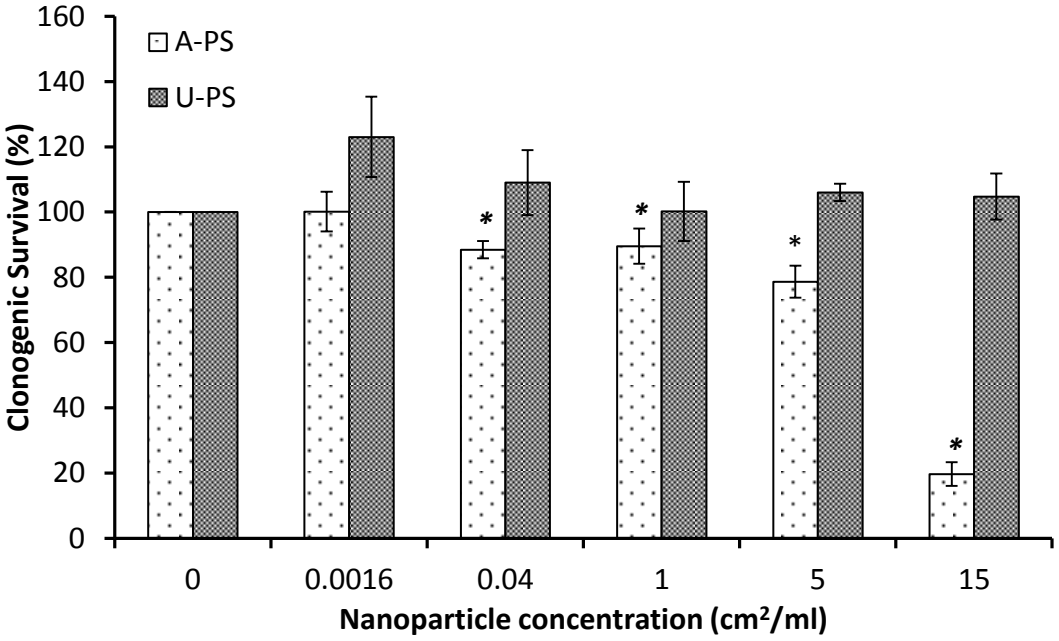

Figure 5.22: Clonogenic survival of TT1 cells following 1 hour treatment with 100nm A-PS or U-PS. Data represents mean (±SEM) of three independent experiments.

5.4. Discussion

Exposure to airborne particulate matter has been shown in numerous epidemiological and toxicological studies to be associated with increased incidence and altered resolution of respiratory infections [215-217, 221, 222]**.** However, the mechanisms behind this susceptibility remain poorly understood. We have previously shown that polystyrene nanoparticles can interact with SP-A and SP-D and that this interaction can alter nanoparticle cellular uptake (see Chapter 3 and [291]). It was therefore hypothesised that nanoparticles would inhibit the ability of these collectins to neutralise viral challenges through sequestering the protein to the nanoparticle surface. Here we show for the first time that nanoparticles can modulate the ability of the innate immune molecules SP-A and SP-D to neutralise *in vitro* viral infection. This modulation was dependent on the protein, nanoparticle, nanoparticle concentration and cell type under investigation. This could be an important step in establishing the

mechanisms behind the increased susceptibility to infection following particle exposure.

The current study evaluated the effect of a range of concentrations of 100nm A-PS and U-PS particles on the surfactant protein mediated neutralisation of influenza infection in three cell lines. The cell lines were chosen to reflect those found within the alveolus, namely TT1, A549 and THP-1 cells as models for ATI, ATII and AM respectively. A549 cells were derived from a lung adenocarcinoma and originally considered to be a model for ATII cells [293, 343, 344]. However, other investigators have shown that as they do not possess many of the typical ATII phenotypic characteristics such as surfactant production or alkaline phosphatase activity that they are not a good ATII model [324, 341, 342]. Despite these findings, A549 cells are one of the main cell types used to investigate the toxicity of nanoparticles on alveolar epithelial cells and have therefore been included in this study [295, 296, 356-358].

Unmodified polystyrene nanoparticles resulted in a biphasic modulation of influenza infection when incubated with SP-A in A549 cells or SP-D in TT1 cells. Interestingly, low concentrations of amine-modified polystyrene also inhibited the neutralisation of IAV infection by SP-A in TT1 cells and with SP-D in A549 cells (i.e. the reciprocal to the effect with U-PS). This indicates that low *in vitro* nanoparticle concentrations can lead to deficiencies in surfactant proteins A and D which in turn can enhance the susceptibility to infection.

U-PS pre-incubation with SP-A resulted in biphasic modulation of SP-A mediated IAV neutralisation in A549 cells. At low concentrations (0.0016 and 0.04 cm^2/mL) U-PS resulted in significant increases in IAV infection in A549 cells compared to the IAV and SP-A treatment. These represented 23.2% and 24.9% respective reductions in the ability of nhSP-A to neutralise IAV infection

in this system. Whereas, at the high concentration of 5cm^2/mL a 48.4% increase in the neutralisation capability of SP-A was observed. At the same time, nhSP-A almost completely abolished U-PS uptake in A549 cells, as measured by either the number of NP positive cells or the MFI. This may be due to the high degree of SP-A mediated aggregation of U-PS particles seen in Chapter 3. This is supported by the concomitant enhancement of U-PS uptake by SP-A in the macrophage like THP-1 cells. The addition of IAV to the SP-A and U-PS treatment partially restored particle uptake in A549 cells. Moreover, IAV alone enhanced the uptake of U-PS particles by A549 cells and this effect was cell specific as it was not observed in either TT1 or THP-1 cells. The increase in U-PS uptake by IAV in A549 cells may be due to incidental uptake of U-PS particles during receptor mediated endocytosis of influenza virons. However, U-PS particles alone had no effect on IAV infection in the A549 cells at the concentrations studied. The addition of SP-A to IAV and U-PS treatments, enhanced the internalisation of U-PS over both the NP/SP-A and NP/IAV controls in each of the cell lines. This SP-A and IAV mediated increase was most pronounced in THP-1 cells whereby a synergistic enhancement of U-PS uptake was observed following SP-A and IAV treatment. SP-A has previously been reported to be an opsonin for IAV in rat alveolar macrophages [197]. It has also been shown that SP-A can enhance the aggregation of IAV virions [196]. The synergistic enhancement of U-PS uptake following SP-A and IAV pre-treatment could therefore be due to increased activation of SP-A and IAV exposed macrophages and/or, through the formation of SP-A/IAV/U-PS heteroaggregates. However, the difference between the A-PS and U-PS particles in this regard may suggest particle aggregation rather than activation. Heteroaggregation could also explain the reduction in IAV infection in A549 cells at the higher concentration of particles in combination with SP-A. The opsonisation of IAV by SP-A into the THP-1 macrophage like cells could also

account for the reduced neutralising ability of SP-A in the THP-1 compared to the other cell lines. On the one hand, SP-A can reduce IAV infection by aggregating IAV virions and acting as a sialic acid reservoir thereby inhibiting the binding of IAV haemaglutinin to sialic acid cell receptors [196]. On the other hand, SP-A can enhance the phagocytic clearance and cellular uptake by macrophages [197]. The increase in U-PS uptake by SP-A in THP-1 cells was in agreement with the earlier work in RAW264.7 cells shown in Chapter 3.

U-PS particles resulted in a biphasic modulation of SP-D activity against IAV in TT1 cells; the low 0.04 cm^2/mL concentration resulted in a 46.9% reduction in SP-D function whereas at 5cm^2/mL a 109.8% increase was observed. Moreover, the enhanced neutralising of IAV at the higher concentration was observed in all the cell lines following pre-incubation of U-PS, IAV and nhSP-D. This could suggest that heteroaggregation of IAV and U-PS mediated by SP-D. The reduced activity of surfactant protein function following interaction with low *in vitro* concentrations of nanoparticles shows that exposure to nano-sized materials can result in surfactant protein deficiencies. The implications of this could extend far beyond virus neutralisation by these collectins. As discussed in Chapter 1, the functions of SP-A and SP-D are multifaceted and the perturbation of their function has been linked to the pathogenesis of a number of diseases (e.g. COPD and idiopathic pulmonary fibrosis). Further work is necessary to determine the effect of nanoparticles on the other functions of SP-A and SP-D.

The U-PS enhancement of SP-D mediated neutralisation at 5cm^2/mL was most pronounced in TT1 and A549 cells. At this concentration the pre-incubation of U-PS, SP-D and IAV resulted in a reduction in the number of U-PS particles per cell in both of these cell lines compared to the respective IAV and NP treatment. However, this only achieved statistical significance in the A549 cells. Interestingly, at the 1cm^2/mL NP concentration there was little effect

on the number of nanoparticles per cell between the IAV/NP and IAV/NP/SP-D treatments. This could support the hypothesis that high concentrations of nanoparticles are facilitating the aggregation of IAV virions by SP-D. The level of U-PS uptake was also not significantly different in the U-PS/IAV/SP-D treatment in A549 and TT1 cells compared to the U-PS and SP-D control. The proportion of cells containing nanoparticles however, was not significantly altered following the addition of SP-D to the U-PS and IAV treatment.

In a previous study, acute high doses of carbon black resulted in a protective effect in mice against *Streptococcus pneumonia* [223]. The dose used in that study however, was 1000μg/ mouse given in 2 equal installations three days apart represents a dose far in excess of environmentally relevant concentrations. The current study shows that concentration is a critical factor in determining the effect of nanoparticles in infection models and that acute doses are not representative of chronic or low dose effects.

rfhSP-D resulted in a modest reduction in A549 and TT1 cells but a non-significant reduction in THP-1 cells. The concentration of rfhSP-D used in this study was 12.5 times more than that of the native protein. However, the level of IAV neutralisation was still much less with the fragment compared to the native protein. This is consistent with previous reports and the work in Chapter 4 which shows that the oligomerisation of SP-D is an important mediator of IAV neutralisation [297, 333, 359].

In chapter 3 it was shown that the interaction between nanoparticles and rfhSP-D resulted in the appearance of high molecular weight bands following SDS PAGE. It was therefore hypothesised that NP interaction with rfhSP-D could induce the formation of supratrimeric structures at the nano-bio interface and that this could potentially enhance the therapeutic potential of this protein. Furthermore, the ability of nanoparticles to enhance the nhSP-D mediated

neutralisation of IAV also indicated that a nanoparticle-SP-D conjugate may have therapeutic uses. However, the incubation of rfhSP-D with either A-PS or U-PS had no significant effect on the infection rate in the cell lines studied. This indicates that the oligomeric structure is important in this effect and may support the role of aggregation in this process as U-PS particles aggregated in the presence of nhSP-D but not rfhSP-D (Chapter 3 and [291]). In order to further study the effect of oligomerisation on nanoparticle modulation of SP-D neutralisation of IAV, recombinant full length Met11 and Thr11 SP-D preparations could be used to study supratrimeric and trimeric SP-D respectively [64]. In the future the effect of rfhSP-D interaction with nanoparticles with other viruses such as RSV should also be investigated.

Interestingly, rfhSP-D but not BSA also resulted in a reduction in U-PS uptake in A549 cells. This suggests that surfactant proteins can reduce the uptake of unmodified polystyrene particles in A549 cells in a mechanism independent of particle aggregation. The incubation of U-PS with nhSP-D resulted in a much smaller reduction in NP uptake compared to either nhSP-A or rfhSP-D. This may be due to the much lower concentration used of nhSP-D (0.4 μg/mL) compared to SP-A/rfhSP-D used in the experiments (5 μg/mL). In order to establish the relative effects of these proteins on nanoparticle uptake in these cells these experiments could be repeated using the same protein concentrations.

In these experiments the intracellular trafficking of the protein, nanoparticle and influenza virus will be important. Lamellar bodies are specialised organelles found in ATII cells which are involved in the packaging, storage and secretion of pulmonary surfactant [135, 136]. A549 cells appear to contain lamellar body like structures, typical of ATII cells, following prolonged culture at confluence [343, 360]. Extracellular SP-A is internalised by ATII cells by clathrin dependent endocytosis and is transported to lamellar bodies. The

contents of these lamellar bodies are then exocytosed into the surrounding medium [344, 361, 362]. Nanoparticles have been shown to localise to lamellar bodies in A549 cells and this localisation has been proposed as a possible route of exocytosis [363]. It is therefore possible that SP-A is enhancing the localisation of U-PS to the lamellar body like structures and thereby facilitating their exocytosis. In comparison, TT1 cells have been shown to contain much fewer lamellar body like structures than A549 cells which is consistent with their representation as ATI and ATII models respectively [364]. A strong association of SP-A was observed with U-PS particles in the absorption experiments. rfhSP-D and SP-A possess similar theroretical isoelectric points of 5.12 and 4.89 respectively. In the pH absorption experiments, a strong association was observed between rfhSP-D and the negatively charged 100nm particles but a weak association with the positively charged A-PS particles at acidic pH. At the lysosomal acidic pH therefore, the association between SP-A and U-PS could be maintained, therefore facilitating the transfer of SP-A/U-PS complexes to the lamellar bodies and the exocytosis from the A549 cells. However, the SP-A corona around the A-PS particles, which was only weakly associated with SP-A in the first place would be degraded at lysosomal pH and therefore the A-PS particles would not co-localise with SP-A in the lamellar bodies. It would be interesting to confirm this hypothesis using co-localisation assays for SP-A, nanoparticles and lamellar bodies. The role of exocytosis in A549 and the other cell types in these experiments should also be investigated.

BSA was used in this study to examine the effect of a non-specific protein corona on IAV infection rates and nanoparticle uptake. This was done to determine whether any effects observed with surfactant proteins were due to surfactant protein specific effects or due to the presence of protein. BSA had no significant effect on IAV infection in any of the cells studied. The incubation of U-PS particles with BSA had no significant effect on IAV infection at any of the

concentrations or cell lines tested. BSA tended to result in a slight increase in the uptake of U-PS particles in A549 cells however, this was only significant for the MFI at the highest concentration. On the other hand BSA tended to reduce U-PS uptake in TT1 cells.

In chapter 3, it was shown that A-PS particle uptake in the murine macrophage RAW264.7 cells was reduced following pre-incubation with nhSP-A. However, in the current experiments, nhSP-A had little effect on the uptake of A-PS in the human macrophage like THP-1 cells. This difference may be due to a number of factors. Firstly, a different nanoparticle batch was used for these experiments. Although the particles had similar stabilities in the buffer used (i.e. stable at room temperature and self-agglomerating at physiological temperatures) and zeta potential to the particles used in Chapter 3. Different buffers were used in the experiments; in chapter 3 particles were pre-incubated with SP-A in TBS with calcium then diluted in SF RPMI, however in this chapter the cells were incubated with A-PS and SP-A in TBS with calcium. The current experiments also exposed the cells for an hour to the particles then the cells were washed and incubated in particle free buffer for 16 hours. However, in the previous experiments, uptake was quantified immediately following incubation for 1 hour.

Biphasic modulations in surfactant protein function was also observed with A-PS particles in A549 with SP-D and in TT1 with SP-A. In A549 cells, the pre-incubation of 0.0016 cm^2/mL A-PS with SP-D resulted in a significant 13% reduction in the ability of SP-D to neutralise IAV infection. Whereas in TT1 cells, the pre-incubation of 0.04cm^2/mL with nhSP-A resulted in a significant 29.7% reduction in the ability of SP-A to neutralise IAV infection. Unlike the U-PS particles, the high concentrations of A-PS particles did not enhance SP mediated IAV neutralisation in the cell lines studied. This may be due to the differences in the surface chemistries, protein binding affinities and the SP

mediated aggregation as discussed in chapter 3. This could also be due to the self agglomeration of A-PS particles at physiological temperatures. It may prove that at higher concentrations of A-PS particles than those studied here may also enhance the neutralisation capabilities of these surfactant proteins. However, due to the reduction in IAV infection at the highest concentration of A-PS studied in this investigation, it would not be advisable to use higher concentrations.

Amine particles have been proposed to act as a proton sponge within the lysosome, resulting in enhanced proton pump activity, lysosomal swelling and rupture [246]. The acidification of the endosome is an important step in virus entry as it initiates the conformational change in the haemaglutinin and the fusion of viral and endosomal membranes [177, 184]. This could explain the reduction of IAV infection at the highest A-PS concentration studied; as the amine particles could be perturbing the acidification of the endosome and inhibiting IAV release and replication within the cell. However, other mechanisms may also be involved. For instance, the envelope of the IAV virion is derived from the host cellular membrane. Amine particles have been shown to bind anionic patches on cell membranes and this interaction has been shown to cause membrane disruptions [242, 243]. It is therefore possible that A-PS particles could be binding to the lipid virion envelope and either disrupting the integrity of the virion or sterically hindering its attachment to the cell membrane. As the A-PS particles self-aggomerate at physiological temperatures, the IAV could become entrapped within these aggregates thereby inhibiting virus attachment entry into the cell. This may be the reason that the effect of high concentrations of A-PS on IAV infection is less pronounced with the THP-1 cells, as phagocytes preferentially internalise larger particles [365]. Interestingly, in preliminary experiments high concentrations of U-PS particles (50 cm^2/mL) were shown to inhibit IAV infection in A549 cells. Gold

nanoparticles have also been previously shown to inhibit HIV-1 infection through binding the surface viral glycoprotein (gp120) and inhibiting its attachment with CD4 cells [366]. The binding of these polystyrene nanoparticles to haemaglutinin should therefore be investigated.

It was shown that BSA tended to enhance IAV infection in each of the cell lines when combined with 5cm^2/mL A-PS compared to the particle treatment alone. However, this only achieved statistical significance in TT1 cells. This indicates that a non-specific coating, reduced the ability of A-PS particles to reduce infection.

The biphasic modulation of surfactant protein mediated IAV neutralisation by A-PS and U-PS could suggest a protein sequestration mechanism at low particle concentrations and a particle aggregation mechanism at higher concentrations. Namely as the amount of particle in the *in vitro* system increases, the amount of 'available protein' in solution will decrease as the particles sequester the surfactant protein. As the concentration of nanoparticle increases further, the effect of protein sequestration on influenza infection is minimised and then reversed by the aggregation of nanoparticle and influenza complexes. The differences in the ability of the particles to modulate surfactant protein neutralisation in different cell lines could be linked to the ability of the cells to internalise the heteroaggregates. The effect of nanoparticle concentration on surfactant protein mediated nanoparticle aggregation with and without IAV needs to be evaluated further. This could be achieved using a combination of DLS, differential centrifugation sedimentation (DCS) and electron/fluorescent microscopy.

The issues presented in this discussion highlight a number of mechanistic pathways which could be involved in the effects observed during these experiments. It is likely that a combination of some or all of these factors

influence the resulting nanoparticle modulation of SP neutralisation of IAV infection and/or particle uptake.

These experiments use a simple exposure system in TBS with calcium to minimise any differences in sugar inhibition between cell culture media and also to ensure sufficient calcium for the lectin activity of SP.

ATI and ATII cells infect to a similar extent with human IAV strains however, the kinetics of progeny virion release differs between these cell types [354, 367]. This is consistent with observations in the current study of similar IAV infection rates in the TT1 and A549 cell lines. ATI cells are more sensitive to oxidant induced cell death following influenza infection than ATII cells [367]. Interestingly, TT1 cells showed a greater reduction in cell viability following IAV treatment compared with A549 cells however, this was not statistically significant. Macrophages show different susceptibilities to IAV depending on the strain and differentiation status [329]. The ability of IAV strains to productively replicate in macrophages has been associated with enhanced IAV pathogenesis [330]. Virulent IAV strains, such as the avian IAV H5N1 and human H3N2, show enhanced pro-inflammatory and enhanced apoptosis in human blood derived macrophages [368]. A macrophage cell line showed enhanced oxidant induced apoptosis in IAV infected cells occurred between 8-12 hours following infection [369]. In the current experiments the viability of THP-1 macrophages was analysed 16 hours post infection and therefore, the within the time frame of IAV induced apoptosis in macrophages. Indeed, IAV resulted in a significant 17% reduction in cell viability in the THP-1 cells. Low concentrations of A-PS particles antagonised the reduction in cell viability by IAV in A549 cells. This was not evident in the other cell lines. Interestingly, A-PS particles had the greatest effect on IAV infection in this cell line. A-PS particles resulted in a dose dependent reduction in IAV infection in A549 cells and culminated in a significant 33.2% reduction in infection at 5cm^2/mL. In TT1

cells the same treatment resulted in a significant 19.8% reduction in IAV and in THP-1 cells a non-significant 3.4% reduction was observed.

Influenza entry is classically considered to be dependent on clathrin mediated endocytosis however, non-clathrin mediated endocytosis of influenza virus such as macropinocytosis, caveolae mediated and non-clathrin, non caveolae mediated endocytosis has also been described [178, 370, 371]. Nanoparticles have been reported to share these many of these endocytic pathways; the route of nanoparticle entry is not only dependent on the nanoparticle properties such as size, surface chemistry and the presence and content of the protein corona but also the cell type under investigation [240, 372-376]. In this study nanoparticle uptake was quantified by flow cytometry in the two alveolar epithelial cell lines TT1 and A549 and macrophage like THP-1 cells. The current study has reported the nanoparticle uptake as the relative number of particles per cell (MFI) and the relative number of cells containing nanoparticles. In these experiments excess particles were washed off following 1 hour treatment and the cells incubated for a further 16 hours in serum free RPMI. Therefore, the quantification of nanoparticles should largely reflect nanoparticle uptake rather than association [324]. The three cell lines showed differential particle distributions with more U-PS positive A549 and TT1 cells than the THP-1 cells. However, A549 cells tended to contain less particles per cell than the other two cell lines. The distribution of U-PS in THP-1 cells may be due to the "positive selection" of macrophages containing particles preferentially internalising particles. This has been reported previously for 500nm and 1μm particles in macrophages [377]. There was also a much greater increase in the MFI compared to the NP+ cells between the 1 and 5 cm^2/mL concentrations for the U-PS particles in each of the cell lines. This is because the proportion of nanoparticle containing cells approaching maximal levels and indicates that the nanoparticles are accumulating within the cell. A-PS uptake

was greatest in the THP-1 cells compared to the other cell lines. This increase was evident in terms of both number of nanoparticle positive cells and relative number of particles in the cell. Macrophages are professional phagocytes and as such are capable of phagocytosing infectious and non-infectious particles. Macrophages have been shown to phagocytise particles between 300nm to more than 20μm [378-380]. However, the optimal size range for phagocytosis has been reported is 2-3μm [381]. Macrophages have been shown to favour the uptake of large particles whereas non-phagocytic cells favour smaller particles [365]. The self-agglomeration of the A-PS particles could therefore enhance the phagocytosis of these amine particles by THP-1 cells and reduce cellular uptake by the epithelial cells. Immortalised ATI like cells have previously been shown to internalise a greater number of negatively charged particles (C-PS; 50nm and 1μm) than primary human ATII cells. Although the effect was much more pronounced in the published compared to the current study [324].

Here I propose that the differences in the ability of nanoparticles to modulate the surfactant protein under investigation may be due to the different capabilities of the cell lines to internalise NP/protein/IAV complexes. As mentioned previously, macrophages tend to favour the uptake of larger particles through phagocytosis and epithelial cells tend to take up smaller particles through endocytosis. Caveolin-1 is a structural protein in caveolae and is involved in caveolae mediated endocytosis [382]. One of the biomarkers for the trans-differentiation of ATII cells into ATI cells is the expression of caveolin-1 in ATI but not their progenitor [383]. A549 cells have been shown to be able to internalise particles through caveolae mediated endocytosis [372, 376, 384, 385]. However, A549 cells have been shown to previously been shown to express little caveolin-1 in comparison to the TT1 cell line [341]. This is consistent with their respective alveolar epithelial cell phonotype. Particles less than 200nm are internalised almost exclusively by clathrin mediated endocytosis; whereas

larger particles 200 to 500nm in size are internalised by caveolae mediated endocytosis [386]. It is therefore, hypothesised that the TT1 cells which have higher caveolin-1 expression compared to A549 cells will have a greater capacity to internalise nanoparticles following surfactant protein mediated aggregation.

In addition of endocytosis, exocytic mechanisms may also influence nanoparticle accumulation within the cells. Cationic particles have been shown to be internalised by clathrin dependent and exoytosed by caveolae dependent mechanisms in an airway epithelial cell line [240]. In order to establish the role of exocytosis and endocytic mechanisms in the uptake of particles with and without IAV transport, inhibitors could be used to block each of these pathways before particle treatment. The current study utilised an antibody which detected cellular infection with influenza. It would be interesting to also determine whether similar effects are observed with influenza uptake into each of these cell lines. It is conceivable that the nanoparticle and protein treatments could alter the ability of the virus to escape the endosomal compartment or replicate within the host cell. It would be especially interesting to determine IAV uptake and co-localisation in the THP-1 cells where U-PS and SP-A where a synergistic enhancement of U-PS uptake was observed with the triple treatment.

Cytokine and chemokine expression in influenza infection plays a key role in pathogenesis of the infection. Influenza has been shown to activate the NLRP inflammasome [387]. The dysregulation of NLRP3 activation has been associated with IAV disease severity [388]. Interestingly, NLRP3 activation by A-PS, titanium dioxide and silica particles has also been reported [245, 389]. Some nanoparticles may therefore be able to exacerbate IAV cytokine expression and increase the severity of the infection. Supernatants from these experiments have been retained and could be analysed at a later date to examine inflammatory response to these treatments.

It has previously been shown that SP-A and SP-D can modulate the uptake of nanoparticles by macrophages and that this effect is dependent on the hydrophobicity of the nanoparticle surface. However, following pre-incubation with surfactant lipids, the effect of SP-A and SP-D on nanoparticle uptake is negated [267]. In future studies, it would therefore be interesting to study the effect of surfactant lipids on the nanoparticle mediated reduction in surfactant protein function.

Individuals with existing respiratory conditions such as COPD show reduced levels of pulmonary SP-A and SP-D levels due to their translocation to the systemic circulation. These individuals show enhanced susceptibility to infections especially following enhanced particulate matter exposure. The sequestration of SP-A and SP-D by particles within the alveolus could therefore, play an important role in the pathogenesis of this susceptibility. The results from the current study show that nanoparticles can sequester surfactant proteins and that this sequestration can lead to a reduction in surfactant protein function. However, there were a number of factors, which affected the ability of the nanoparticle to alter protein function. A key determining factor was the concentration of the nanoparticles used in the study. Reductions in the surfactant protein function were only observed at the lower two concentrations used in this study. At higher concentrations, either no effect was observed or nanoparticles resulted in enhanced surfactant protein activity. Many toxicity studies use high acute doses to determine the toxicokinetics of exogenous substances; this practice seems to be particularly prevalent in nanotoxicology. However, this study shows fundamental differences between high (acute) and low (chronic) concentrations. The highest concentration used in the current study was 5cm^2/mL which is equivalent to approximately 8.8 μg/mL. Even this dose is modest compared to other *in vitro* nanotoxicology studies, which typically range between 10 and 300μg/mL [243, 390-393]. The low

concentrations used this study therefore, represent several times less than those used in conventional nanotoxicology studies. The low doses used in this study (0.0028 and 0.07μg/mL for 0.0016cm^2/mL and 0.04cm^2/mL respectively) are more likely to represent chronic exposure whereby the surfactant system is gradually depleted rather than acute concentrations where the surfactant is rapidly overwhelmed.

These results demonstrate the difficulties in using acute high concentrations *in vitro* and extrapolating the results towards environmentally relevant concentrations associated with chronic exposure. This model is the first step in developing a chronic *in vitro* exposure system. In future, the model will be developed further to determine the effect of chronic long term pre-exposure to nanoparticles on influenza infection and surfactant protein mediated neutralisation. This study highlights the urgent need for further investment and research into SP-A and SP-D sequestration by nanoparticles and the resulting effects of this sequestration on protein function.

Chapter 6: Development of *in vitro* bacterial opsonisation and stimulation assays

6.1. Introduction

The pulmonary collectins are involved in the clearance and resolution of bacterial infections. This process involves modulating the inflammatory response to bacterial components such as lipopolysaccharide [34, 101-103]. In this chapter the ability of rfhSP-D to modulate the inflammatory response, namely the production of tumour necrosis factor-alpha (TNFα), by macrophages following LPS stimulation was investigated. This chapter also investigates the effect of two different oligomeric forms of SP-D on the aggregation and uptake of *E. coli* in the murine RAW264.7 macrophage like cell line. This experimental protocol was optimised in order to develop an assay to investigate the effect of nanoparticles on collectin mediated opsonisation of bacteria.

6.2. Methods

6.2.1. Bacterial opsonisation

E. coli (K-12 strain) pHrodo bio-particles were purchased from Invitrogen (UK). *E. coli* bioparticles (4 x10^5/well) were seeded into 96 well round bottom plates in 10µl aliquots in TBS containing 5mM calcium. Equal volumes of protein or FBS were added to each well at 5 times the final concentration in TBS with calcium. SP-D used in these experiments was purified by Paul Townsend. The bacteria and protein suspensions were then incubated for 1 hour at 37°C. RAW264.7 cells were washed three times in serum free RPMI, scraped and 30µl per well was added at a density of 1.67x10^6 cells/mL. The cells were incubated in

suspension with the bacteria and protein for 1 hour at 37°C in a humidified atmosphere. The cells were then placed on ice and 10,000 cells per sample were analysed using a BD FACS Aria.

6.2.2. Bacterial aggregation

Fluorescein labelled *E. coli* (K-12 strain) bioparticles (Molecular Probes, Invitrogen, UK) were incubated with collectins in TBS with calcium as described in section 6.2.1. Following incubation for 1 hour at 37°C the bacteria and protein suspensions were placed on microscope slides, covered with coverslips and imaged using a fluorescent microscope.

6.2.3. LPS stimulation

RAW264.7 cells were stimulated with LPS as described previously [394]. RAW 264.7 cells were seeded into 24 well plates ($2.5x10^5$ /well) in complete RPMI and incubated for 42 hours at 37°C 5% CO^2. The medium was then removed and replaced with complete medium containing 0, 0.01, 0.1, 1, 10 or 100ng/mL smooth LPS from *Klebsella pneumonia* (L1770, Sigma, UK) with or without 10µg/mL rfhSP-D and incubated for 0.5, 1, 2, 4, 6 or 24 hours at 37°C 5%CO_2. Supernatants were then aliquoted and frozen at -20°C until needed. The concentration of TNFα in these supernatants was determined by enzyme linked immunosorbant analysis (ELISA) and the cells were fixed in 1% formaldehyde for 1 hour.

6.2.4. ELISA

A mouse TNFα ELISA was carried out as recommended by the manufacturer (R and D Systems, Abington, UK). Briefly, 96 well plates were coated with 100µL of capture antibody (0.8µg/mL in PBS) and incubated at room temperature overnight. The wells were washed three times in PBS

containing 0.05% Tween20 (wash buffer) and then incubated for 1 hour in 300μL of PBS containing 1% bovine serum albumin (reagent diluent). The wells were then washed again three times with wash buffer. A 7 point two fold serial dilution standard curve with a top concentration of 2000pg/mL was prepared in duplicate in RPMI containing 10% FBS. Samples and standards (100μL) were added to the wells and incubated for 2 hours at room temperature. The wells were washed three times with wash buffer and then incubated in 100μL of detection antibody (200ng/mL diluted in reagent diluent) at room temperature for two hours. The wells were washed three times with wash buffer and then incubated with a 100μL of Streptavidin-HRP (diluted 1 in 200 in reagent diluent) for 20 minutes at room temperature. The wells were washed three times with wash buffer and then incubated for 20 minutes in 100μL tetramethylbenzidine (TMB; Thermo Scientific, Northumberland, UK). The reaction was stopped using 50μL of 0.5M sulphuric acid and the absorbance was measured at 450nm.

6.2.5. Statistics

In the opsonisation experiments the difference between each concentration of protein was determined using the independent t test against *E. coli* alone. The significance of the differences between LPS treatments was determined using analysis of variance (ANOVA) followed by a post hoc test for the least significant difference (LSD). p values of ≤0.05 were considered statistically significant. All statistical tests were carried out using SPSS/PASW version 17 or 21.

6.3. Results

6.3.1. Opsonisation of bacteria by collectins

SP-D has previously been reported to enhance *E. coli* clearance by phagocytes [395]. In order to determine whether nanoparticles could effect SP-D mediated opsonisation concentration curves of 800kDa and 1.7mDa nhSP-D were performed to determine their effect on *E. coli* uptake in RAW264.7 macrophage-like cells. The results, presented in Figure 6.1, shows that low concentrations of 1.7mDa nhSP-D resulted in increased *E. coli* uptake by RAW264.7 cells. This culminated in increases of 13.4% and 26.2% in the number of *E. coli* containing cells at 0.004 and 0.016μg/mL 1.7mDa SP-D respectively. These increases were statistically significant with associated p values of 0.045 and 0.036 respectively (t test). Pre-incubation of *E. coli* with 0.008 μg/mL of 1.7mDa SP-D also resulted in a 10% increase in *E. coli* uptake. However, this increase did not reach statistical significance (p=0.091; t test). At higher concentrations (>0.25μg/mL) pre-incubation of *E. coli* with 1.7mDa nhSP-D resulted in a dose dependent decrease in *E. coli* uptake. This dose dependent reduction *in E. coli* uptake achieved statistical significance at 1 μg/mL 1.7mDa SP-D (p=0.004; t test). The 800kDa nhSP-D oligomer resulted in a 15.7% increase in *E. coli* uptake at 0.5μg/mL. This was statistically significant with an associated p value of 0.050 (t test). No other concentration of 800kDa nhSP-D resulted in a significant change in *E. coli* uptake.

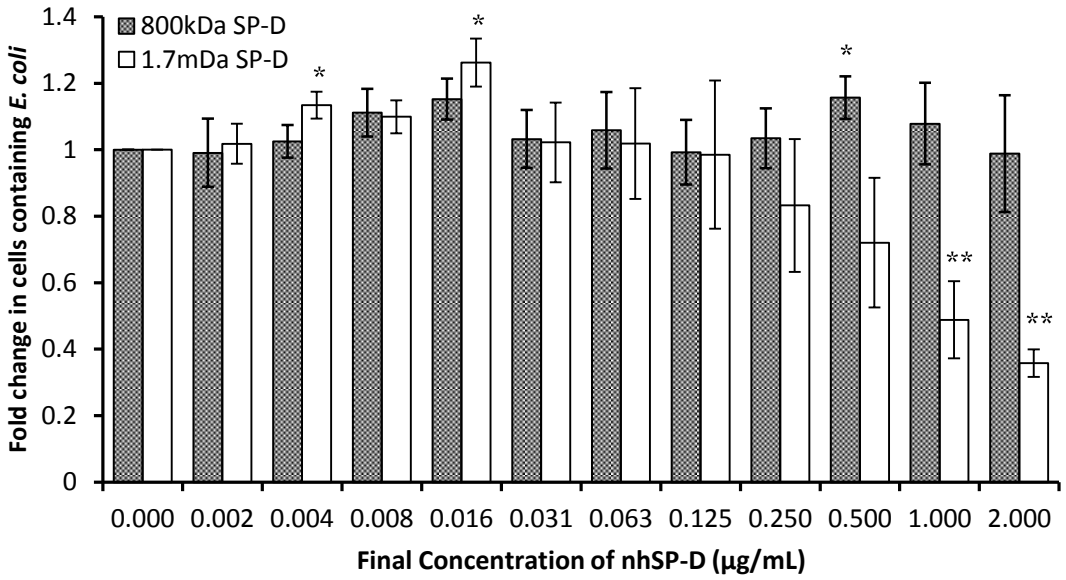

Figure 6.1: Effect of nhSP-D multimerisation on *E. coli* uptake in RAW264.7 cells. Data represents mean (±SEM) of four independent experiments conducted in duplicate. Statistics determined using t test where * p≤0.05 compared with *E. coli* control; **p<0.005 compared with *E. coli* control.

The effect of nhSP-A and rfhSP-D on *E. coli* uptake was also examined to determine whether these could be used in nanoparticle containing experiments. The results shown in Figure 6.2, show that the pre-incubation of *E. coli* with 10µg/mL nhSP-A resulted in a 13.9% reduction in *E. coli* uptake. However, this reduction did not reach statistical significance with an associated p value of 0.152 (t test). Pre-incubation of *E. coli* with 10 µg/mL rfhSP-D resulted in an 11% increase in bacteria uptake by RAW cells although this did not reach statistical significance (p=0.130; t test). Preliminary dose response curves were also conducted using nhSP-A and rfhSP-D and showed similar results to those presented here (data not shown). The effect of bovine serum albumin (BSA) and foetal bovine serum (FBS) on *E. coli* uptake were used as negative and positives controls respectively. BSA had no significant effect on *E. coli* uptake (p=0.594; t test) whereas 10% FBS resulted in a significant 2.3fold increase in bacteria uptake (p=0.010; t test). This confirms that the *E. coli* bioparticles are susceptible to opsonisation in this assay system.

Due to the biphasic effect of 1.7mDa SP-D and the lack of effect of the other collectins on *E. coli* uptake in RAW264.7 cells it was decided not to examine the effect of nanoparticles in this system.

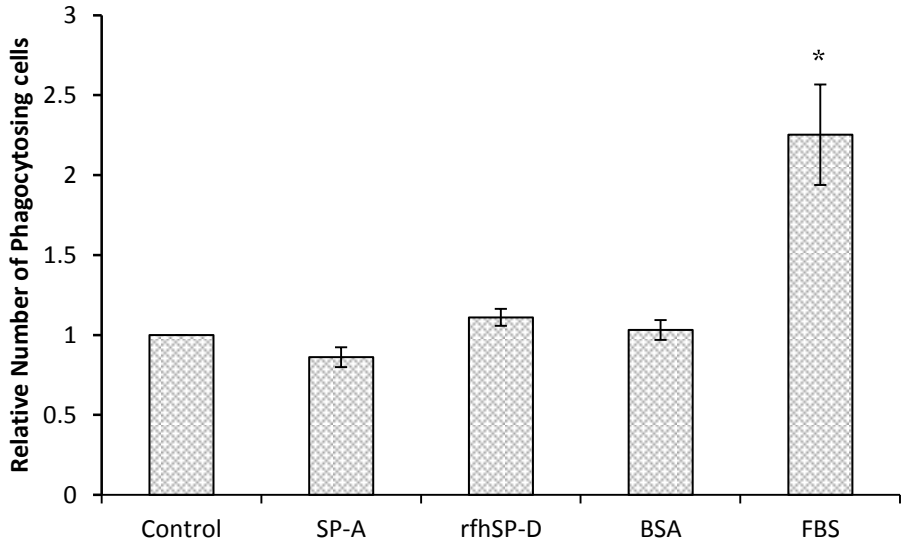

Figure 6.2: Effect of proteins on *E. coli* uptake in RAW264.7 cells; 10μg/mL SP-A, rfhSP-D or bovine serum albumin (BSA) or 10% foetal bovine serum (FBS) were pre-incubated with pHrodo labelled *E. coli* bioparticles for 1 hour prior to incubation with RAW264.7 cells. Results represent mean (±SEM) of at least three independent experiments. *$p<0.050$ verses *E coli* alone (control) using independent t test

6.3.2. Aggregation of bacteria by collectins

The 1.7mDa SP-D mediated reduction in *E. coli* uptake by the RAW264.7 cells was unexpected. SP-D has previously been reported to enhance *E. coli* uptake in part through inducing the agglomeration of this bacteria. Due to the initial increase in *E. coli* uptake at lower concentrations before the incremental reduction it was hypothesised that the 1.7mDa SP-D was aggregating the *E. coli* and that at higher concentrations the formation of 'super-aggregates' would inhibit bacterial clearance. In order to test this hypothesis, FITC labelled bacteria were pre-incubated with nhSP-D and bacterial aggregation was examined using fluorescent microscopy. The results summarised in Figure 6.3 show that low concentrations of 1.7mDa resulted in the formation of small bacterial aggregates. At higher concentrations (up to 2.5μg/mL) aggregates up

to 80μm in size were observed. The effect of 800kDa SP-D on *E. coli* aggregation was also examined (see Figure 6.3G). Even at 2.5μg/mL only small bacterial aggregates were observed. Due to the SP-A contamination of the 800kDa SP-D preparation (see Chapter 3) it was also examined whether nhSP-A could induce *E. coli* aggregation or whether it could inhibit the formation of 'super-aggregates' by 1.7mDa SP-D. Figure 6.3H shows that 2.5μg/mL nhSP-A tended not to induce *E. coli* aggregation. Moreover, nhSP-A did not affect the aggregation of *E. coli* induced by 1.7mDa SP-D (data not shown).

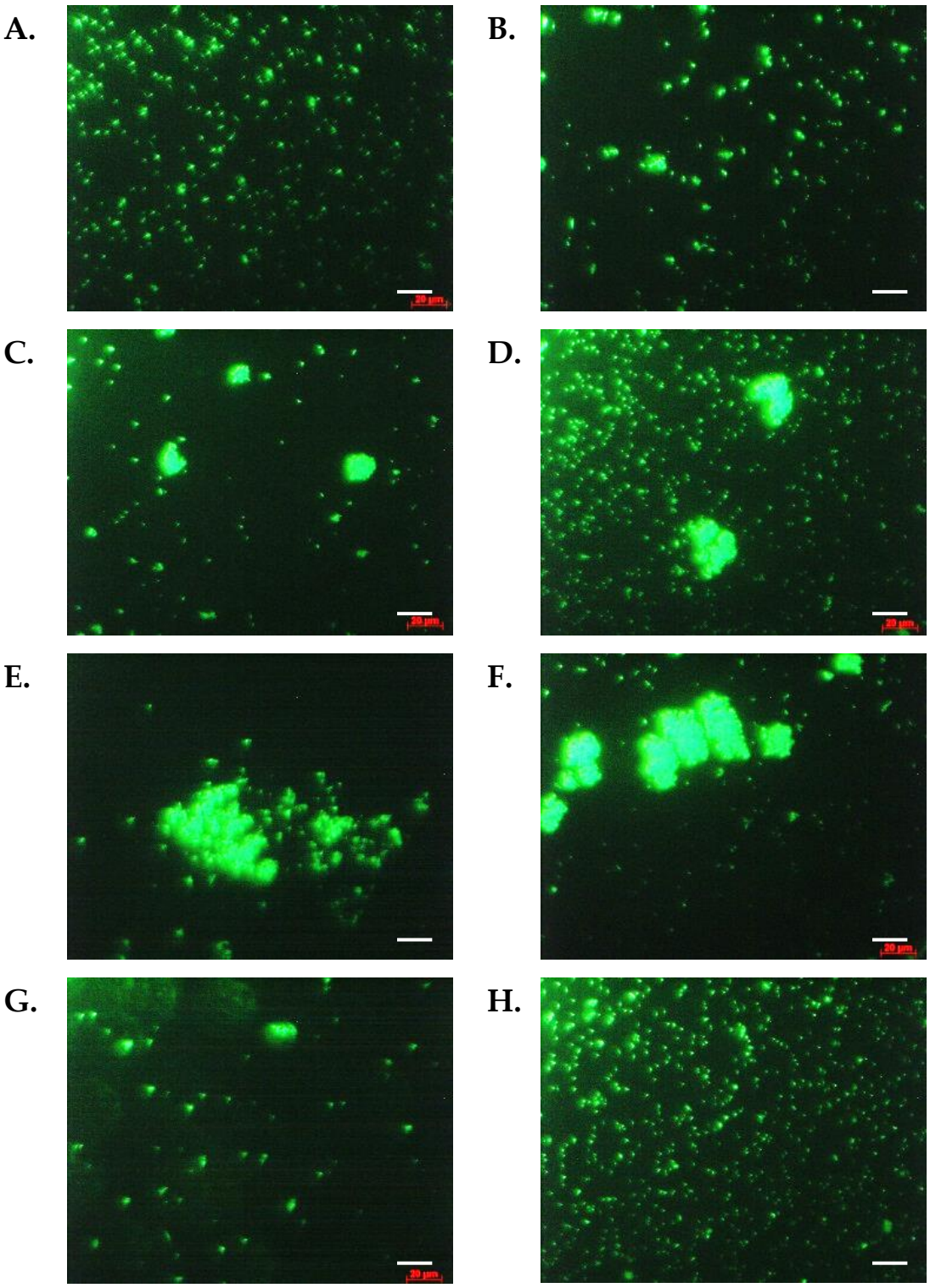

Figure 6.3: Effect of nhSP-D on *E. coli* aggregation. A. FITC labelled *E. coli* were incubated in TBS and 5mM calcium with B. 0.01 μg/mL 1.7mDa nhSP-D; C. 0.04 μg/mL 1.7mDa nhSP-D; D. 0.15 μg/mL 1.7mDa nhSP-D; E. 0.625 μg/mL 1.7mDa nhSP-D; F. 2.5 μg/mL 1.7mDa nhSP-D; G. 2.5 μg/mL 800kDa nhSP-D; H. 2.5 μg/mL nhSP-A. Represent micrographs from three similar independent experiments. Scale bar represents 20μm.

6.3.3. LPS stimulation

TNFα secretion is a well characterised response to LPS stimulation in macrophages [103]. The murine macrophage cell line RAW264.7 was first stimulated with smooth lipopolysaccharides (LPS) from *Klebsella pneumonia* to confirm that these cells were sensitive to LPS induced TNFα secretion. Smooth LPS was chosen as both SP-A and SP-D have previously been reported to inhibit sLPS induced TNFα in macrophages [103, 105, 396]. Preliminary experiments showed that LPS induced a dose dependent increase in TNFα secretion in RAW264.7 cells following incubation for 6hours (see Figure 6.4). Cells stimulated with 0.01 and 0.1ng/mL of LPS showed minor increases of 3 and 14% respectively in TNFα secretion compared to basal levels. These differences were not statistically significant with p values of 0.996 and 0.986 respectively (LSD). Stimulation of these macrophages with 1ng/mL LPS resulted in an 8 fold increase in TNFα production; however, this increase was not statistically significant (p=0.346; LSD). RAW264.7 cells stimulated with 10 and 100ng/mL LPS resulted in large 63 and 115 fold increases in TNFα production compared to un-stimulated cells. These increases were highly statistically significant with p values of <0.001 (LSD). Secondly, we wanted to determine whether rfhSP-D could modulate LPS induced TNFα secretion in these cells. The co-incubation of 10μg/mL of rfhSP-D with LPS tended to result in a reduction in the amount of TNFα secreted. Basal concentrations of TNFα were not modified by the addition of 10μg/mL rfhSP-D. rfhSP-D resulted in an 18% reduction in TNFα secretion induced by 1ng/mL LPS. However, this reduction was not statistically significant with a p value of 0.829. TNFα induced by 10 and 100ng/mL LPS were also reduced by rfhSP-D; these 16% and 12% reductions were not statistically significant with p values of 0.189 and 0.070 respectively.

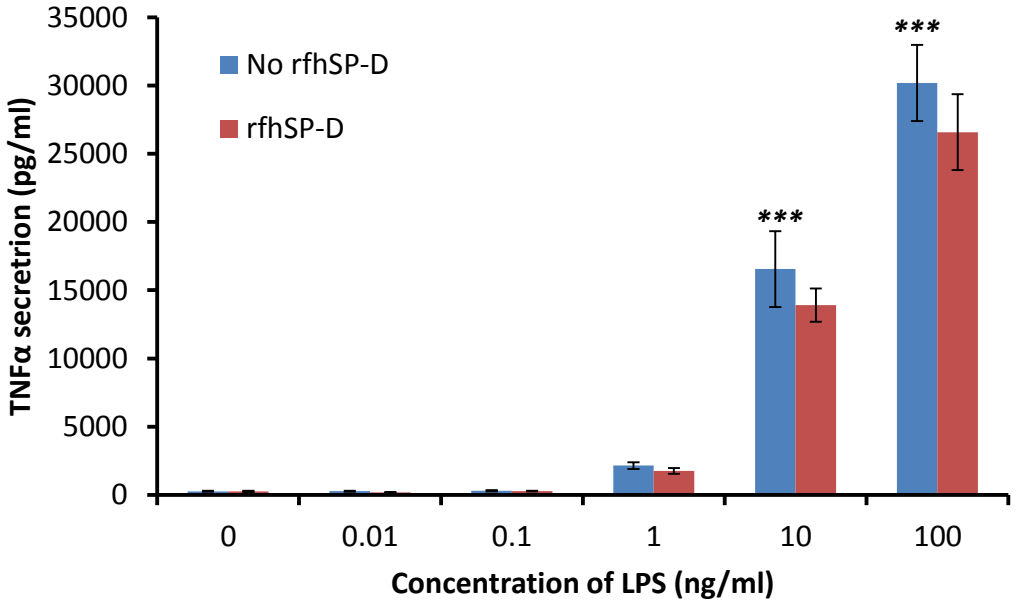

Figure 6.4: TNFα secretion by RAW264.7 cells stimulated for 6 hours with LPS from *Klebsiella pneumoniae* with or without the addition of 10µg/mL of rfhSP-D; results represent mean (±SEM; n=7); ***p<0.001 vs. un-stimulated (LSD).

In order to determine the time course of LPS induction of TNFα in macrophages RAW264.7 cells were incubated for 30minutes, 1, 2, 4, 6 and 24 hours with varying concentrations of LPS (Figure 6.5). The results show that TNFα could not be detected after incubation with up to 100ng/mL of LPS for 30 minutes. Following 1 hour of incubation LPS induction of TNFα was evident at the 3 highest LPS concentrations where 1, 10 and 100 ng/mL of LPS resulted in 1.2 fold, 7 fold and 26 fold respective increases in TNFα; however, with respective p values of 0.982, 0.571 and 0.027 only the highest concentration achieved statistical significance (LSD). Incubation of RAW264.7 cells with 1ng/mL LPS for 2, 4, 6 and 24 hours resulted in 5, 8, 7 and 4 fold respective increases in TNFα production over un-stimulated controls. However, these increases were not statistically significant with p values of 0.354, 0.467 0.515 and 0.664 respectively (LSD). Stimulation of RAW264.7 cells with 10ng/mL LPS for 2, 4, 6 and 24 hours resulted in 51, 46, 50 and 22 fold respective increases in TNFα production compared to un-stimulated cells. These increases were highly

statistically significant with associated p values of <0.001 for the 2, 4, and 6 hour and 0.006 for the 24 hour time point (LSD). RAW264.7 cells stimulated with 100ng/mL LPS for 2, 4, 6 and 24 hours secreted 63, 96, 92 and 63 fold more TNFα than their un-stimulated counterparts. These increases were highly statistically significant with p values of <0.001 (LSD).

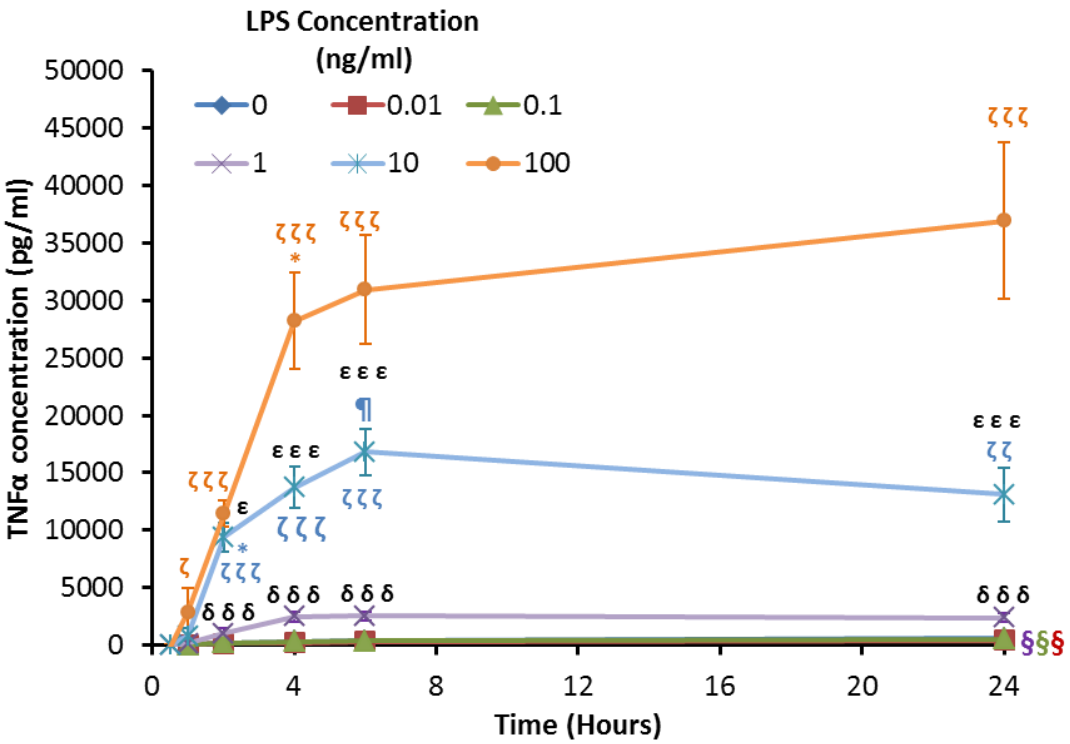

Figure 6.5: Timeline of TNFα secretion by RAW264.7 cells stimulated with varying concentrations of LPS from *Klebsiella pneumoniae*; results represent mean (±SEM; n=3 except 6 hour time point where n=7) ζ p<0.05 vs. un-stimulated levels at same time point; ζ ζ ζ p<0.001 vs. un-stimulated levels at same time point; ε p<0.05 10 vs. 100ng/mL LPS at same time point**;** ε ε ε p<0.001 10 vs. 100ng/mL LPS at same time point **δ δ δ** p<0.001; 1 vs. 10ng/mL LPS at same time point *p<0.05 vs. preceding time point; ¶ p=0.002; vs. 2 hour time point § p<0.05; 2 vs. 24 hour treatment. Significance determined by post hoc test for LSD. The colour of the symbol represents the concentration of LPS to which it applies; where the symbol is black it represents variance between adjacent concentrations.

Un-stimulated RAW264.7 cells secreted increasing amounts of TNFα over 24 hours (p=0.001; ANOVA) with a significant 75% increase between 6 and 24 hours (p=0.022; LSD). RAW264.7 cells stimulated with 0.01 and 0.1ng/mL LPS also showed significant increases in TNFα production over time (p=0.001 and p<0.001 respectively; ANOVA). However, no increases in TNFα production was seen between un-stimulated and 0.01 or 0.1ng/mL LPS treated cells at any time point (p=0.919 and p=0.955 respectively; ANOVA). RAW264.7 cells treated with 10ng/mL LPS showed a statistically significant 12 fold increase in TNFα secretion between 1 and 2 hours (p=0.002; LSD). TNFα secretion continued to increase steadily up to 6 hours with incremental increases of 46 and 22% between 2-4 and 4-6 hours respectively. These increases were not statistically significant with respective p values of 0.071 and 0.186 (LSD). The 79% increase in TNFα secreted by cells stimulated with 10ng/mL LPS between 2 and 6 hours was statistically significant with a p value of 0.002. There was a 3.9 fold increase between 1 and 2 hours in TNFα production by cells treated with 100ng/mL LPS. However, this increase was not statistically significant (p=0.148; LSD). The 2.4 fold increase in TNFα production between 2 and 4 hours in the 100ng/mL LPS treatment was statistically significant (p=0.011; LSD). The level of TNFα secretion continued to rise incrementally between 4, 6 and 24 hours with respective 9 and 19% increases between these time points; however, these increases were not statistically significant. There was a 30% increase in TNFα production by cells stimulated with 100ng/mL of LPS between 4 and 24 hours; however, this increase was not statistically significant (p=0.141; LSD).

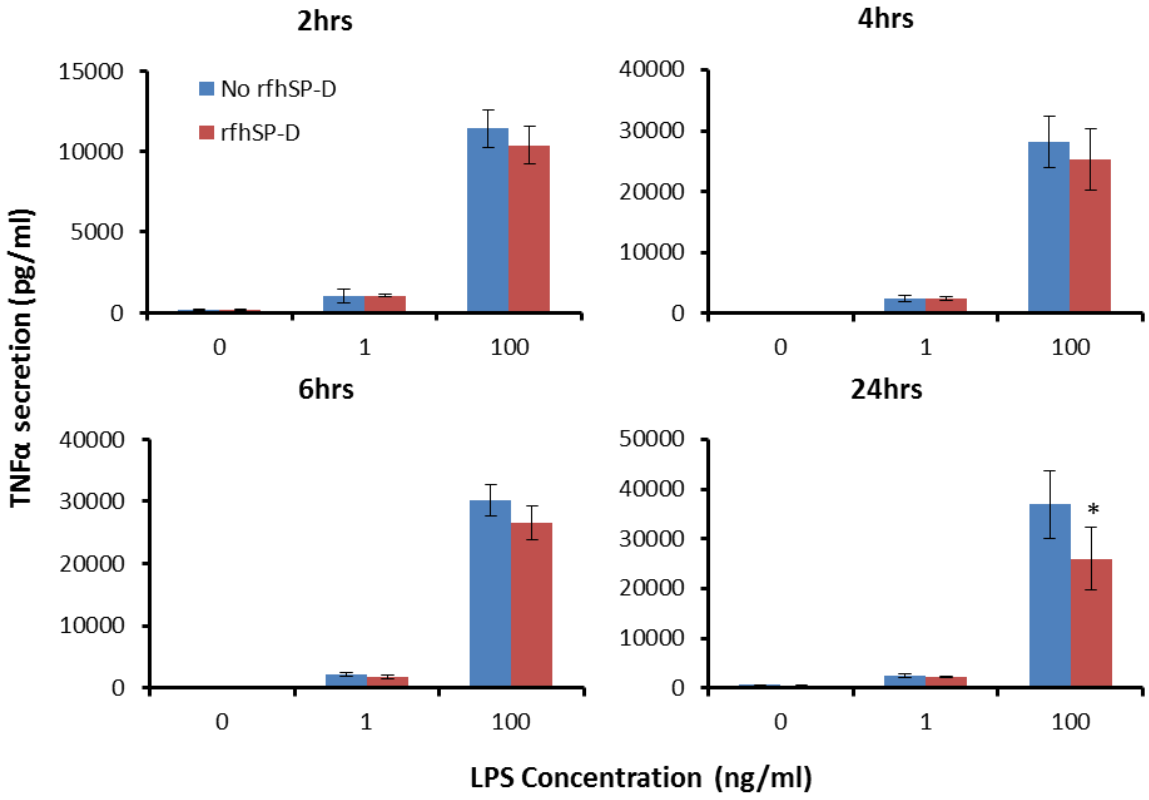

Figure 6.6: TNFα secretion by RAW267.4 cells following co-incubation of 10 µg/mL rfhSP-D with LPS from *Klebsella pneunomoniae* at different time points; data represents mean ±SEM (n=3; except for 6 hours where n=7) * p=0.014 vs. 100ng/mL without rfhSP-D (LSD). Note different scales on the y axis.

The effect of rfhSP-D on LPS stimulation over this time course was also studied (see Figure 6.6). rfhSP-D tended to cause a reduction in the amount of TNFα secreted by RAW264.7 cells at various time points. Co-treatment with rfhSP-D with 100ng/mL LPS reduced TNFα secretion by 9 and 10.5% after incubation for 2 and 4 hours respectively. However, these reductions were not statistically significant with p values of p=0248 and p=0.318 (LSD). rfhSP-D did not modify the TNFα secretion induced by 100ng/mL LPS at either 2 or 4 hours. There was a 12% reduction following 24 hours co-incubation of rfhSP-D with 1ng/mL LPS but this was not statistically significant (p=0.971). Maximal inhibition of TNFα secretion by rfhSP-D occurred following co-incubation with 100ng/mL of LPS for 24 hours; this treatment resulted in a significant 29.5% reduction in TNFα production (p= 0.014).

6.4. Discussion

Increased particulate burden in rats has been shown to lead to worse outcomes in pulmonary bacterial infections [397]. It has also been shown that macrophage exposure to particles reduces the phagocytic capacity of alveolar macrophages [398-400]. SP-D has been reported to neutralise gram negative bacteria through binding to lipopolysaccharide on the outer membrane of the bacterial cell. This binding has reported to be result in the agglutination and/or opsonisation of gram negative bacteria such as *E. coli* and *H. influenzae* [401, 402]. It was therefore hypothesised that nanoparticles could alter the ability of SP-A and SP-D to opsonise bacteria. In order to test this hypothesis a reliable assay needed to be developed. In the course of this development it was observed that the higher order 1.7mDa SP-D oligomer resulted in a biphasic modulation of *E. coli* uptake with low concentrations enhancing uptake and higher concentrations reducing uptake. This is consistent with a previously published paper which showed that multimeric SP-D enhanced phagocytosis of *E. coli* at lower concentrations but not at higher concentrations [395]. However, this paper did not report a reduction in *E. coli* clearance by higher concentrations of SP-D even at concentrations twice the effective dose of the current study. The incubation of 1.7mDa SP-D resulted in a dose dependent increase in the size of bacteria aggregates, at 2.5μg/mL this resulted in aggregates reaching sizes of up to 80μm in size. These results suggest that whilst low concentrations can enhance the phagocytosis of these bacteria, higher concentrations may enhance the uptake by other non-phagocytic mechanisms (i.e. mucociliary escalator). The lack of opsonisation of *E. coli* by SP-A may be due to insufficient SP-A concentrations; Hartshorn and colleagues (1998) showed that concentrations of more than 16 μg/mL nhSP-A was required to produce marked aggregation of *E. coli*.

It has previously been shown that a recombinant fragment of SP-D containing 2 Gly-X-Y triplets is approximately 6 times less effective at inducing *E. coli* aggregation than native protein [403]. However, in the current study concentrations up to 10 μg/mL had no significant effect on the uptake of *E. coli.* This highlights the importance of the oligomeric state of SP-D in *E. coli* aggregation and uptake as this is more than 600 times the concentration of 1.7mDa SP-D shown to enhance *E. coli* uptake in RAW264.7 cells.

As the opsonic effect of 1.7mDa was fairly narrow and higher concentrations of protein resulted in significant reductions in bacterial uptake it was not an appropriate system to examine nanoparticle modulation of SP opsonisation. In the future, different bacterial bioparticles such as the gram positive bacteria *S. aureus* could be developed for this use. Furthermore, the effect of nanoparticles on the AP-A and SP-D mediated neutralisation of live bacterial infections could be investigated *in vitro* or *in vivo*.

The *E. coli* that was used in this study was tagged with a pH dependent fluorescent dye. This means that only bacteria inside phago-lysosomes can be detected. The level of background fluorescence by these bio-particles was assessed by exposing fixed cells to these bio-particles (data not shown). This confirmed that the mean percent of bacteria positive RAW264.7 cells represents only active uptake.

TNFα is a pyrogenic cytokine which is one of the first cytokines to be produced by macrophage-like cells following LPS stimulation [404]. SP-A and SP-D have been shown to modulate the cellular response to LPS, causing a reduction in TNFα production by sLPS stimulated macrophages. SP-A has previously been shown to be more effective at inhibiting the interaction of CD14 with sLPS than SP-D [101, 104]. A neck, CRD SP-D fragment has previously been shown to bind to LPS from *K. pneumonia*, and *E. coli* to a similar degree to

native SP-D [405]. In order to assess the ability of rfhSP-D to modulate TNFα secretion by sLPS stimulated macrophages, an *in vitro* assay was developed using the murine macrophage RAW264.7 cell line. The stimulation of RAW264.7 cells with sLPS from *K. pneumonia* was concentration dependent and reached maximal levels following 4-6 hours incubation. This is consistent with previous reports which have shown that LPS stimulation of PBMCs or PMA differentiated U937 macrophages resulted in maximal levels at 4 and 6-12 hours respectively [404, 406, 407]. The ability of rfhSP-D to reduce the production of this pyrogenic cytokine was increased with incubation time at the highest concentration of LPS. This shows that the protein is functionally active. Interestingly, rfhSP-D did not appear to reduce TNFα production by RAW264.7 cells following stimulation with 1ng/mL LPS. This may be due the presence of FBS in the system which can suppress the production of TNFα in macrophage like cells following LPS stimulation [408]. This could be due to the presence of collectins in FBS such as MBL, conglutinin, CL-43 and CL-46 [409]. In future studies, the effect of rfhSP-D on LPS stimulation of macrophages will be investigated in the absence of serum. Following this optimisation, this assay could be used to assess the effect of nanoparticles on the biological activity of this protein.

The inability of rfhSP-D to induce a TNFα response in these cells supports the Limulus Amoebocyte Lysate assay which showed minimal endotoxin contamination of the rfhSP-D preparation (0.105ng/µg). Low endotoxin levels in these preparations are critical as excess endotoxin may modify lectin activity, induce inflammatory response in cells and/ or alter cellular response to experimental stressors [410]. Lei *et al*. 2011 showed that 0.1 and 1ng/mL sLPS from *E. coli* induced the production of ~2000 and 12000pg/mL of TNFα respectively in RAW264.7 cells over 6 hours. The results from the current study showed that the threshold for TNFα induction was between 0.1

and 1ng/mL of sLPS from *Klebsella pneumonia*. This study showed 2000pg/mL TNFα production by RAW264.7 cells following 1ng/mL LPS over the same time period as the Lei (2011) study; the difference between these values is likely to be due to differences in LPS subtypes. The results indicate that rfhSP-D may reduce the inflammatory response to bacterial ligands and aid in the resolution of bacterial induced inflammation.

Chapter 7: Development of Coherent Anti-Stokes Ramen Scattering as a detection method for unlabelled lipids and nanoparticles.

7.1. Introduction

Coherent anti-stokes raman scattering (CARS) was first developed in the 1960's as a method for spectroscopic analysis of crystalline structures [411]. Pioneering work by Duncan *et al.* in 1982 developed a microscope based on CARS principles [412]. However, it wasn't until developments by Xie and colleagues in 1999 who showed that CARS could be used to resolve sub-cellular components within cells that the possible advantages of CARS especially for biomedical applications became apparent [413]. CARS utilises three electromagnetic fields termed the "pump", "stoke" and "probe" fields; the probe field is usually at the same frequency and emitted by the same laser as the pump providing a two photon resonance beam. The role of the pump and stokes beams in generating the anti-stokes signal is summarised in Figure 7.1. When the energy difference between the pump and stokes frequencies, termed the beating frequency, is in resonance (i.e. equal to) the energy difference between the ground and vibrational state then a strong anti-stokes signal is produced. The photons of the anti-stokes signal are collected for imaging [412, 413].

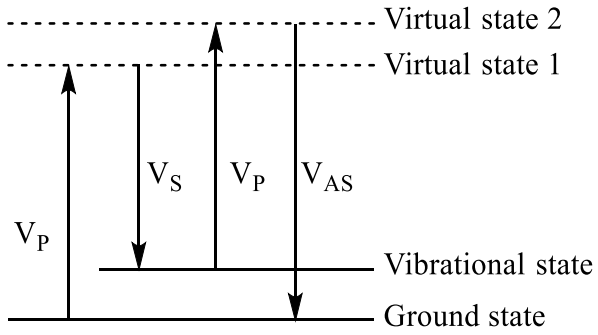

Figure 7.1: Energy level diagram for CARS. The pump beam (V_P) illuminates the sample and forces the photon from its native ground state into a virtual state. Simultaneous illumination with the longer wavelength stokes beam (V_S) is achieved through a shorter path length and forces the photon to the vibrational state. The probe field shifts the photon into a second virtual state from where it relaxes back to the ground state emitting an anti-stokes signal (V_{AS}). Adapted from [413].

The intensity of the CARS signal is determined by the local concentration of the molecular species and therefore, can be used for quantitative analysis of these species . Lipids are rich in C-H stretches and are therefore ideal targets for CARS microscopy. In fact, several studies have investigated CARS for use in the diagnosis of cancer, atherosclerosis and fatty liver disease as well as to examine demyelination processes in neurons *in situ* [414-417]. In cancer diagnostics, CARS has been used to identify circulating cancer cells by their enhanced lipid accumulation, and can highlight tumour margins during surgery, [417-419]. CARS has also been used to identify the localisation of metal oxide and polystyrene nanoparticles within biological tissues [413, 420-422].

Although CARS has been investigated for use in a number of biomedical applications, it has yet to be used to examine surfactant biology and homeostasis. In this study, CARS was used to examine the uptake of Curosurf, a natural derived surfactant replacement therapy, by the RAW264.7 macrophage cell line and to evaluate the effect of surfactant proteins on lipid uptake. CARS was also used to examine the uptake of polystyrene particles of different sizes and surface modifications in this macrophage cell line.

7.2. Methods

7.2.1. Particles

Unlabelled polystyrene particles (100nm and 500nm) with amine functionalised and unmodified surfaces were purchased from Polysciences (Park Scientific, UK). Unlabelled 200nm A-PS, and U-PS particles (Kisker Biotech) were kindly donated by Maurits de Planque. Particles were suspended at a dilution of 1 in 1000 in milliQ water or colourless serum free RPMI with TBS and calcium and analysed using by DLS (Malvern Zetasizer Nano).

7.2.2. RAW264.7 cell preparation for CARS

RAW264.7 cells were routinely sub-cultured in RPMI containing 10% HI FBS and penicillin and streptomycin as described in Chapter 3. Glass cover slips were sterilised with 70% isopropanol and allowed to dry placed in 6 well plates. RAW264.7 cells were then seeded onto the plates at a density of $1x10^6$ cells per well in 3 mL of growth medium and incubated for 24 hours.

7.2.2.1 Lipid uptake

RAW264.7 cells were seeded on glass coverslips as described in section 7.2.2. Curosurf (Chiesi) was suspended in SF RPMI at either 20 or 50 μL / mL concentrations as indicated in the text. Suspensions were vortexed vigorously for 30 seconds to ensure adequate dispersion of lipids within the cell media. Aliquots (1mL) of this suspension were added to the RAW264.7 cells and they were then incubated at 37°C 5% CO_2 in a humidified atmosphere for up to 24 hours as indicated in the text. The cells were then washed twice, fixed in 1% formaldehyde in PBS for 1 hour, stored in PBS then sent to Sumeet Mahajan for CARS analysis.

7.2.2.2 Particle uptake

RAW264.7 cells were seeded on glass coverslips as described in section 7.2.2. Particles were suspended in TBS and calcium and diluted in SF RPMI and vortexed vigorously at a final concentration of 130 μg/mL. The particle suspensions were then incubated with the RAW264.7 cells at 37°C 5% CO_2 in a humidified atmosphere for the indicated time period. The cells were then washed twice in PBS, fixed and sent to Sumeet Mahajan as described in section 7.2.2.1.

7.2.3. CARS laser scanning system

Samples were imaged using CARS and analysed using the MATLAB software by Sumeet Mahajan. The CARS setup was as follows; a Chameleon Ultra titanium-sapphire (Ti:Sa) pulsed femtosecond laser (Coherent) was split into two beams; The pump beam at 835nm, 100 fs pulse and 80MHz repetition rate. The stokes beam was generated by optical parametric generation through an optical parametric oscillator (OPO) (Semi-automatic, APE GmbH, Berlin) which generates photons between 1080nm and 1600nm. The samples were scanned using a home built galvanometer scanner coupled to Nikon Ti-U inverted microscope. Unlabelled lipids and nanoparticles were imaged in RAW264.7 cells at a C-H stretching frequency of 2850 cm^{-1} with the OPO adjusted to 1096nm.

7.3. Results

7.3.1. Analysis of CARS images

In order to quantify lipid and particle uptake CARS images were converted to binary images in MATLAB and the number of pixels counted which exceeded the appropriate threshold (see Figure 7.2). This area was then

compared to the cell area in each field of vision using a second lower threshold.

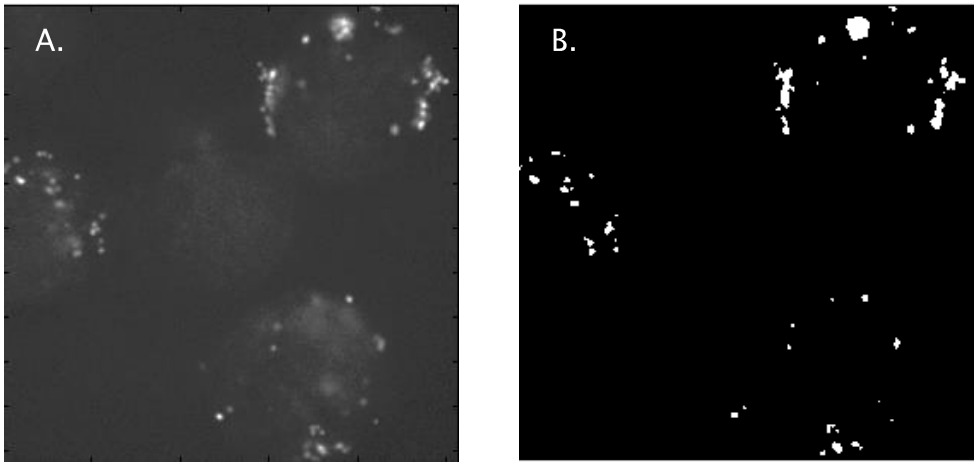

Figure 7.2: Quantification of particle and lipid uptake in RAW264.7 cells. Conversation of A. CARS image to B. binary image for subsequent quantitative analysis using MATLAB software. Positive CARS signal appears white in binary image.

7.3.2. Lipid uptake

The uptake of Curosurf, a natural porcine surfactant therapy used to treat neonatal RDS, was utilised in this study to examine surfactant lipid uptake by the macrophage-like RAW264.7 cells. Preliminary experiments were conducted to determine the appropriate concentration of Curosurf and incubation period to produce a sub-maximal level of lipid uptake.

The cells in the later time point show the lipid dense bodies increased in both size and number compared to the 3 hour time point indicating that the lipid was accumulating within the cells. At 24 hours, the level of lipid uptake by the RAW264.7 cells was slightly increased at the lower concentration of Curosurf (see Figure 7.3C) which may indicate that a maximal level of uptake had been reached for the later time point and highest concentration. In order to further elucidate the time dependency of the lipid uptake within these cells a further study was conducted examining the uptake of 20 μL/mL of Curosurf at incremental time points up to 6 hours. These results, presented in Figure 7.4, show that at time points up to and including 1 hour RAW264.7 cells showed little lipid uptake. At later time points, an increasing number of lipid containing bodies were observed which increased both in number and size over time with a large increase in the total area of lipid within the cells between 2 and 6 hours. Based on the results from these experiments, Curosurf at a concentration of 20 μL/mL for 3 hours was chosen to detect the effect of Surfactant Proteins on lipid uptake in RAW264.7 cells.

A preliminary experiment investigating the role of SP-A on the uptake of Curosurf in RAW264.7 macrophage-like cells was conducted by incubating the cells with 20 μL/mL Curosurf with or without 10 μg/mL nhSP-A for 3 hours. The results, shown in Figure 7.5, show that SP-A resulted in an approximately 3.5 fold increase in lipid uptake in RAW264.7 cells.

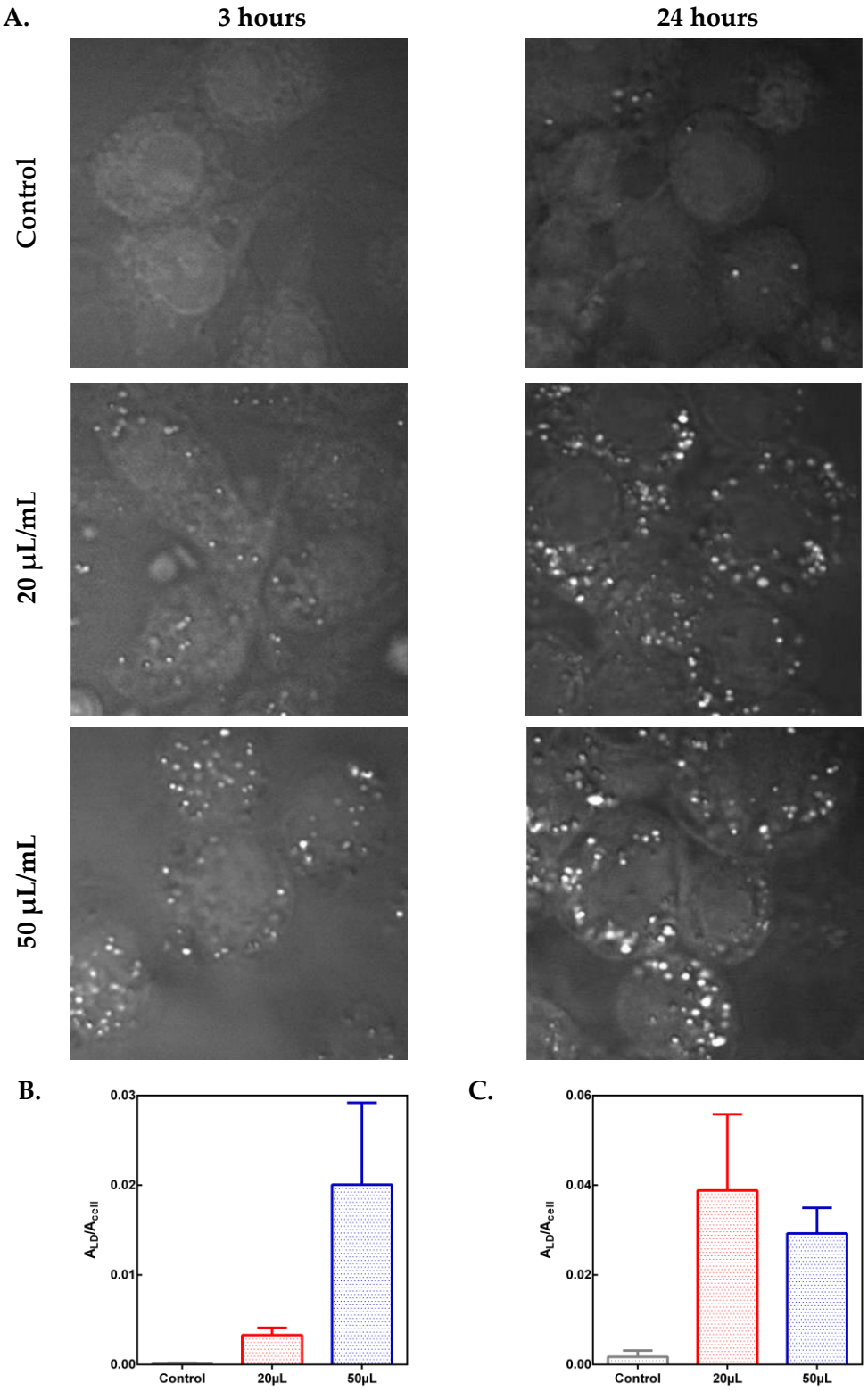

Figure 7.3: Curosurf uptake in RAW264.7 macrophage-like cells. A. CARS images of RAW264.7 macrophage like cells following 3 or 24 hours incubation with different concentrations of Curosurf. **B.** Quantification of Curosurf uptake from CARS images following 3 hours and **C.** 24 hours incubation with RAW264.7 cells. Data is expressed as a ratio of the area of detected lipid within the cell over the total cell area (A_{LD}/A_{cell}) and represents mean ±Stdev from at least 3 images from 1 experiment.

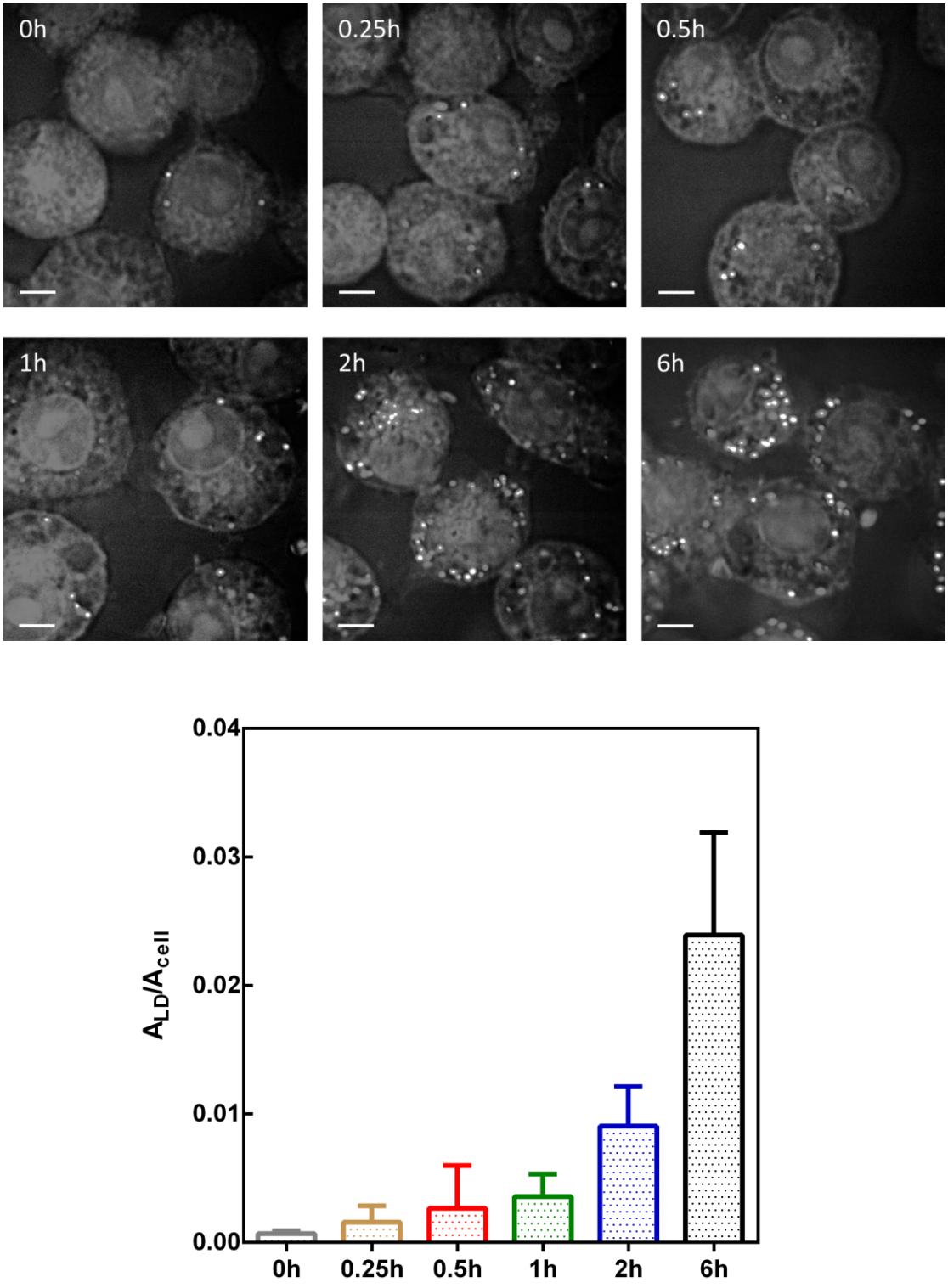

Figure 7.4: Time dependent uptake of Curosurf in RAW264.7 cells. Incubation of RAW264.7 cells with 20μL/mL at incremental time points up to 6 hours. Data is expressed as a ratio of the area of detected lipid within the cell over the total cell area (A_{LD}/A_{cell}) and represents mean ±Stdev from at least 3 images from 1 experiment. Scale bars represent 10μm.

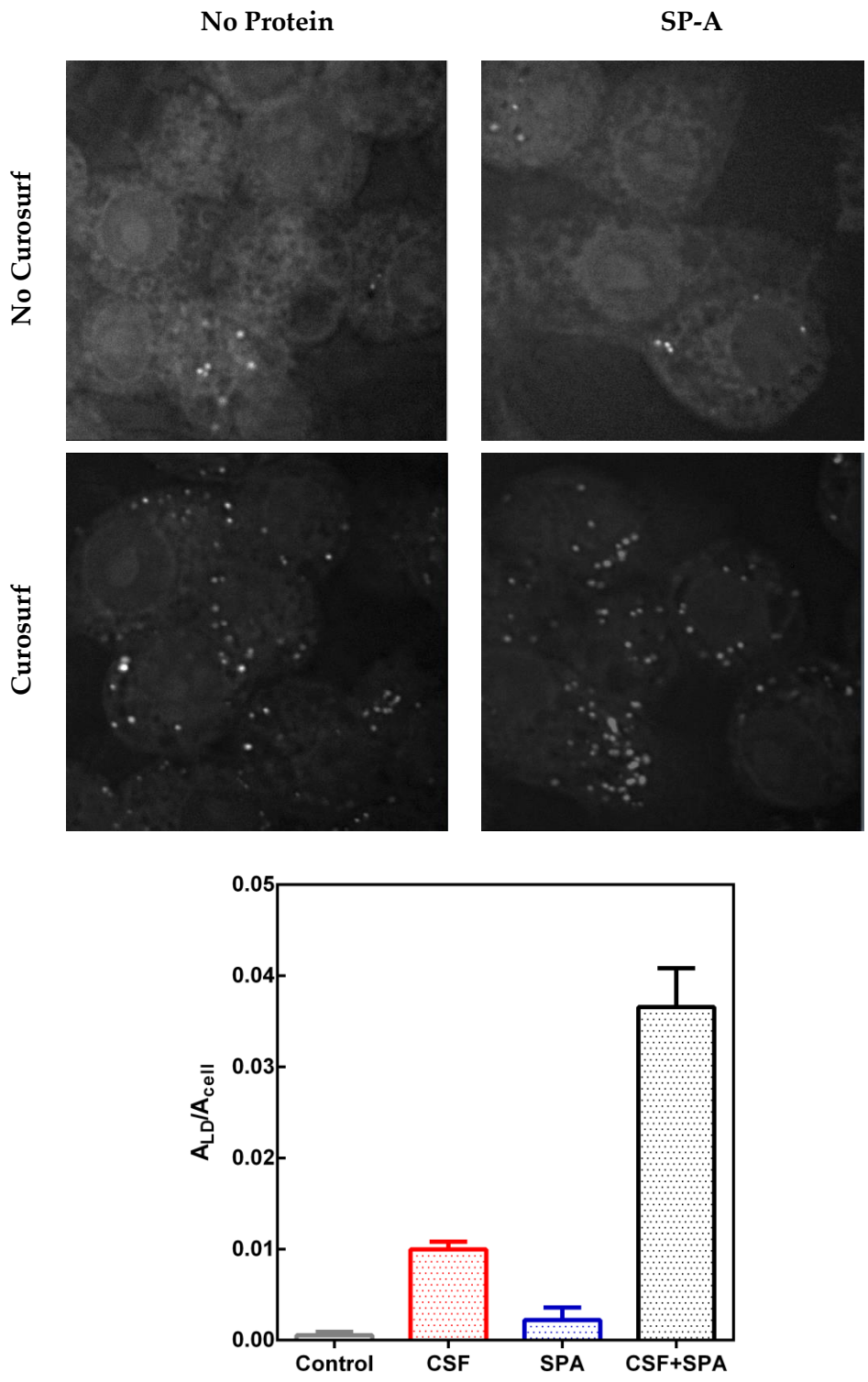

Figure 7.5: Effect of SP-A on the uptake of Curosurf in RAW264.7 cells. A. CARS images of the effect of SP-A on the uptake of Curosurf in RAW264.7 cells following 3 hours incubation. Data is expressed as a ratio of the area of detected lipid within the cell over the total cell area (A_{LD}/A_{cell}) and represents mean ±Stdev from at least 3 images from 1 experiment. Scale bars represent 10μm.

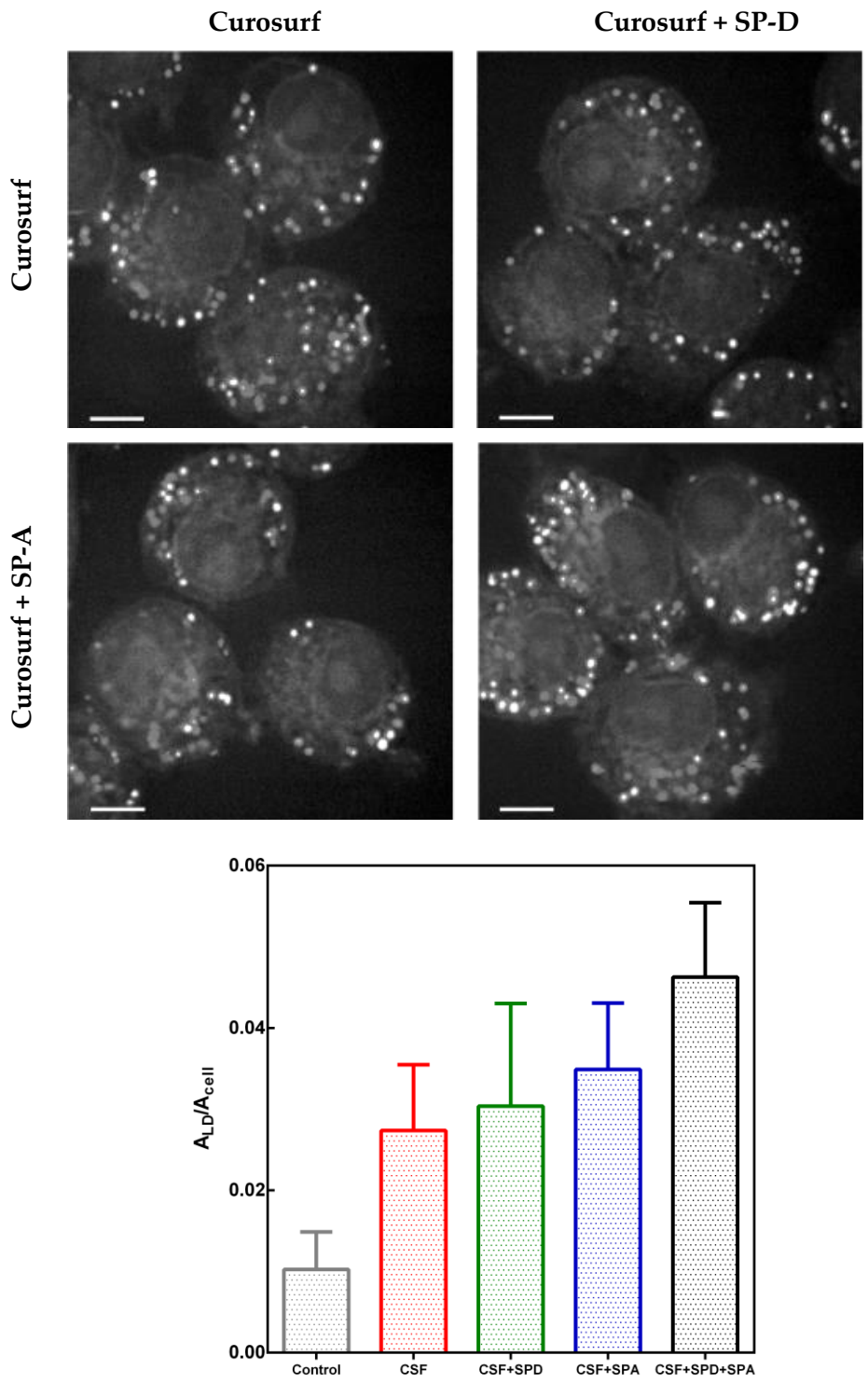

Figure 7.6: Effect of nhSP-A (10µg/mL) and nhSP-D (1µg/mL) on Curosurf (CSF) uptake in RAW264.7 cells following 3 hours incubation. Data is expressed as a ratio of the area of detected lipid within the cell over the total cell area (A_{LD}/A_{cell}) and represents mean ±Stdev from at least 3 images from 1 experiment. Scale bars represent 10µm.

Further experiments were then conducted to determine the effect of SP-A in combination with SP-D on lipid uptake by these macrophages. SP-A and SP-D were incubated with Curosurf at a ratio of 10:1 (w/w) to reflect the higher abundance of SP-A in the lung (see Figure 7.6) [423]. In this experiment, SP-A resulted in a slight increase in Curosurf uptake however, the degree of this enhancement was much less than in the previous experiment. SP-D also resulted in a small increase in the total area of lipid dense bodies within the cells. The co-incubation of SP-A and SP-D at this 10:1 ratio resulted in enhanced lipid uptake over each protein alone.

In order to determine the relative importance of SP-A and SP-D on lipid uptake these proteins were also co-incubated at the reciprocal 1:10 (w/w) concentration ratio. The results, presented in Figure 7.7, show that 1 μg/mL of SP-A or 10 μg/mL SP-D resulted in more than 5 and 3 fold respective increases in the size and number of lipid dense droplets within the RAW264.7 cells over the Curosurf control. When incubated in combination at these concentrations, the level of uptake was similar to that of SP-D alone. In order to determine the significance of these findings further experiments will have to be conducted. Importantly, it should also be noted the high degree of variance in the level of lipid uptake in the absence of protein between these experiments.

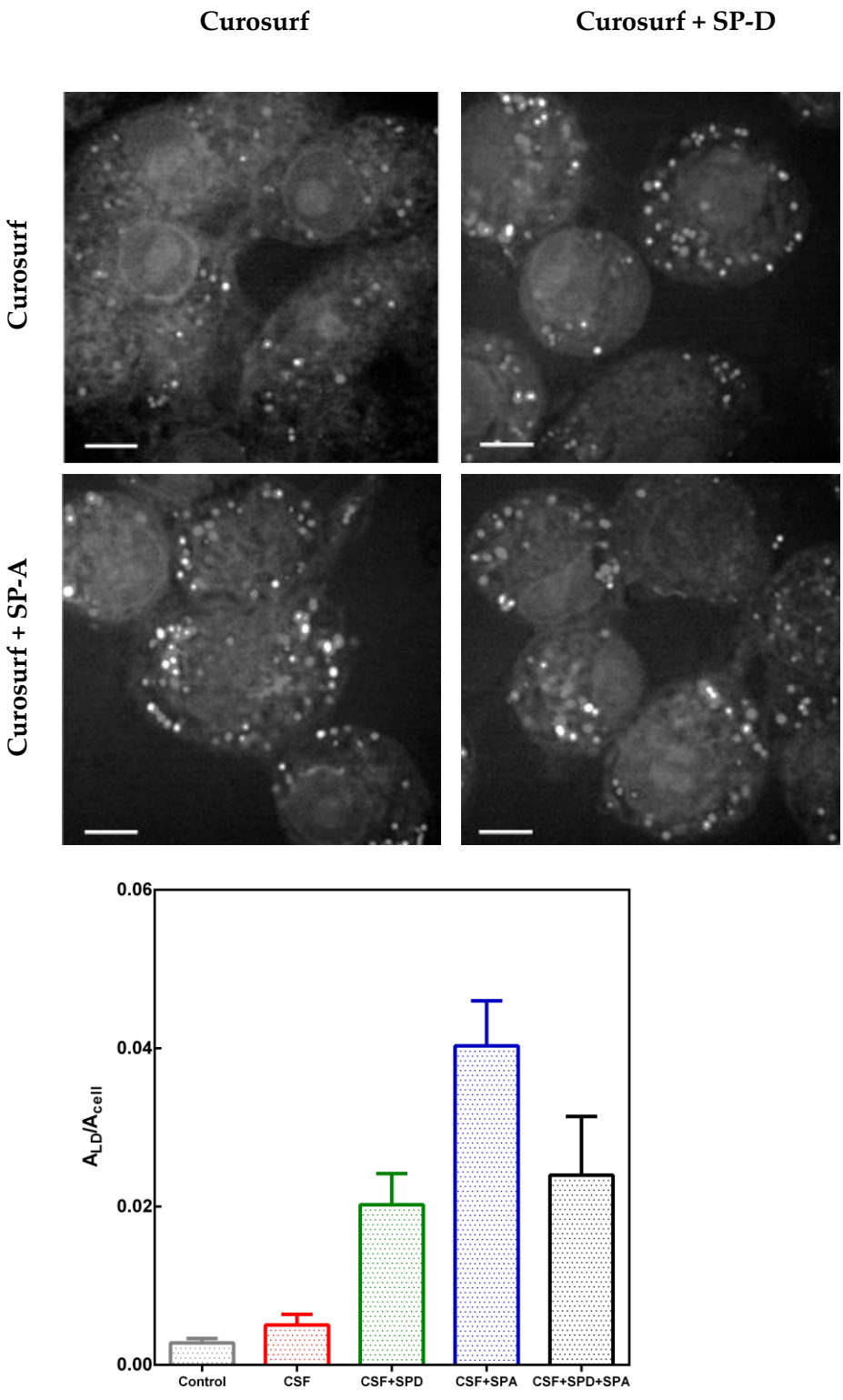

Figure 7.7: Effect of nhSP-A (1µg/mL) and nhSP-D (10µg/mL) on Curosurf uptake in RAW264.7 cells. Data is expressed as a ratio of the area of detected lipid within the cell over the total cell area (A_{LD}/A_{cell}) and represents mean ±Stdev from at least 3 images from 1 experiment. Scale bars represent 10µm.

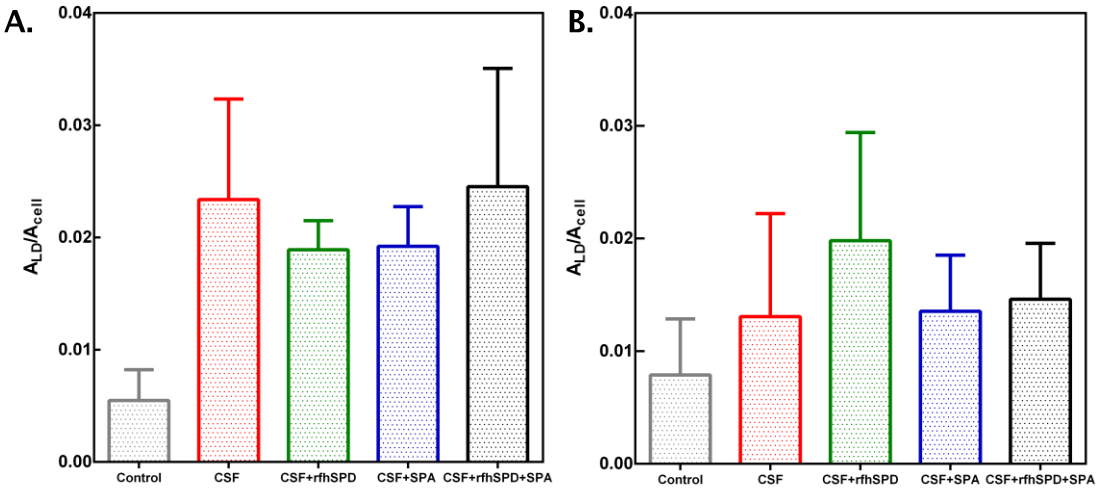

Figure 7.8: Effect of SP-A and rfhSP-D on the uptake of Curosurf (CSF) in RAW264.7 cells. A. Incubation of RAW264.7 cells with 10 μg/mL rfhSP-D and/or 1μg/mL nhSP-A with 20μ/mL Curosurf for 3 hours **B.** Incubation of RAW264.7 cells with 1 μg/mL rfhSP-D and/or 1μg/mL nhSP-A with 20μ/mL Curosurf for 3 hours. Data is expressed as a ratio of the area of detected lipid within the cell over the total cell area (A_{LD}/A_{cell}) and represents mean ±Stdev from at least 3 images from 1 experiment.

The effect of rfhSP-D with and without SP-A was also investigated at 10:1 and 1:1 concentration ratios. The results, presented in Figure 7.8, show that in these experiments 1 μg/mL SP-A either had no effect on Curosurf uptake or resulted in a small reduction in lipid uptake. This is in contrast with the previous experiments, where SP-A tended to result in enhanced lipid uptake. The incubation with 1 μg/mL rfhSP-D resulted in small increase in Curosurf uptake; however, at 10 μg/mL a small reduction in uptake was observed. Interestingly, when SP-A was added to either of these rfhSP-D treatments, lipid uptake returned to the level in the Curosurf control samples.

7.3.3. Particle characterisation

Particle sizes were measured by dynamic light scatter analysis in milliQ water and serum free RPMI media. The results, presented in Table 7.1, show that 100nm U-PS, 200nm A-PS, 200nm U-PS and 500nm A-PS particles

had similar size distributions in both mQ water and SF RPMI with TBS and calcium. The size distribution of 500nm U-PS was slightly increased in SF RPMI compared to mQ water. However, 100nm A-PS particles were highly aggregated in SF RPMI with an average size distribution 10 times greater in the cell media.

Particle	Nominal size (nm)	Size mQH_2O	Size RPMI
A-PS	100	134.4	1343.0
U-PS	100	95.8	95.3
A-PS	200	268.5	270.0
U-PS	200	216.4	213.0
A-PS	500	464.6	447.9
U-PS	500	545.9	865.0

Table 7.1: DLS size measurements of unlabelled polystyrene particles in mQH_2O and SF RPMI with TBS and calcium

7.3.4. Particle uptake

CARS microscopy was also used to study the association of polystyrene particle of different sizes with RAW264.7 cells. The kinetics of this association was examined using 200nm A-PS and U-PS particles over a 2 hour period. The results, shown in Figure 7.9 and Figure 7.10, show that a greater number of 200nm A-PS particles associated with RAW264.7 cells compared to 200nm U-PS particles after at least 1 hour incubation. A-PS association with RAW264.7 cells was dependent on the duration of exposure and continued up to and including the latest (i.e. 2 hour) time point. On the

other hand, the level of U-PS association was similar at each time point over the studied 2 hour time period.

The effect of nhSP-A on the association of 200nm A-PS was also examined following 1 hour incubation with RAW264.7 cells. This time point was chosen as it reflected a sub-maximal level of A-PS association and also the time point used in the flow cytometry experiments in Chapter 4. The incubation of 200nm A-PS with SP-A resulted in 3.4 fold reduction in cellular association of these particles (see Figure 7.11).

The effect of SP-A on 100nm and 500nm A-PS and U-PS association was also examined following 1 hour incubation with RAW264.7 cells. The results, presented in Figure 7.12 and Figure 7.13, show that SP-A had little effect on the total PS area detected following incubation with 100nm or 500nm A-PS. Individual 100nm particles could not be detected using CARS and therefore, only aggregates could be visualised and quantified. Moreover, some of these aggregates appear to be on the outer leaflet of the cell membrane (see Figure 7.12A). A greater number of 100nm A-PS particles appeared to associate with RAW264.7 cells than their 100nm U-PS counterparts. However, there was little difference in particle association between 500nm A-PS and U-PS particles.

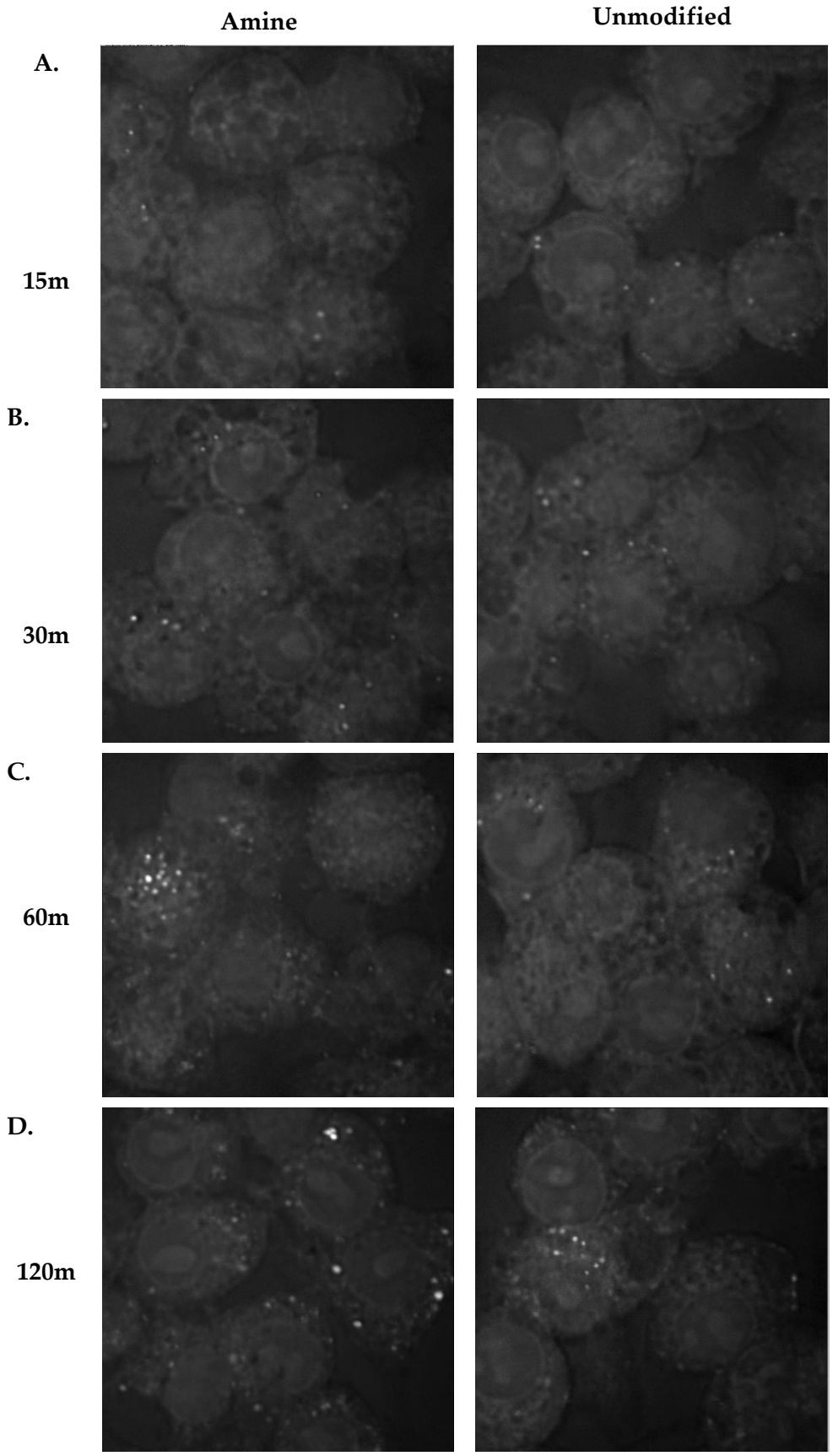

Figure 7.9: Particle association of 200nm A-PS (left panel) and U-PS (right panel) after A. 15, B. 30, C. 60 and D. 120 minute incubation with RAW264.7 cells.

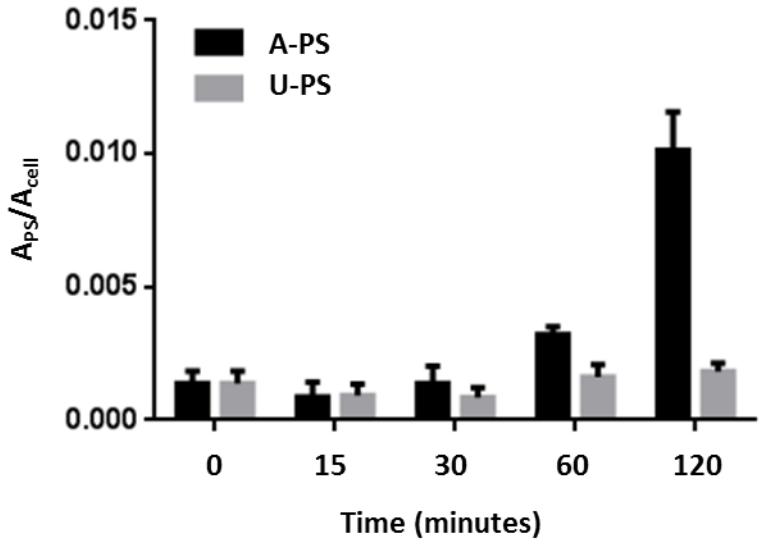

Figure 7.10: Quantification of 200nm A-PS and U-PS association with RAW264.7 cells following incubation for up to 2 hours. Data is expressed as a ratio of the area of polystyrene over the total cell area (A_{PS}/A_{cell}) and represents mean ±Stdev from at least 3 images from 1 experiment.

Individual 500nm particles could clearly be visualised inside the cells (see Figure 7.13A). The incubation of SP-A with both 100nm and 500nm U-PS resulted in approximately 6.1 fold increases in the amount of particles associating with the cells. The micrographs of the U-PS association with RAW264.7 cells, show that U-PS of both sizes are aggregated by SP-A. Some of these aggregates, especially of the larger 500nm particle appeared to be on the outer leaflet of the membrane.

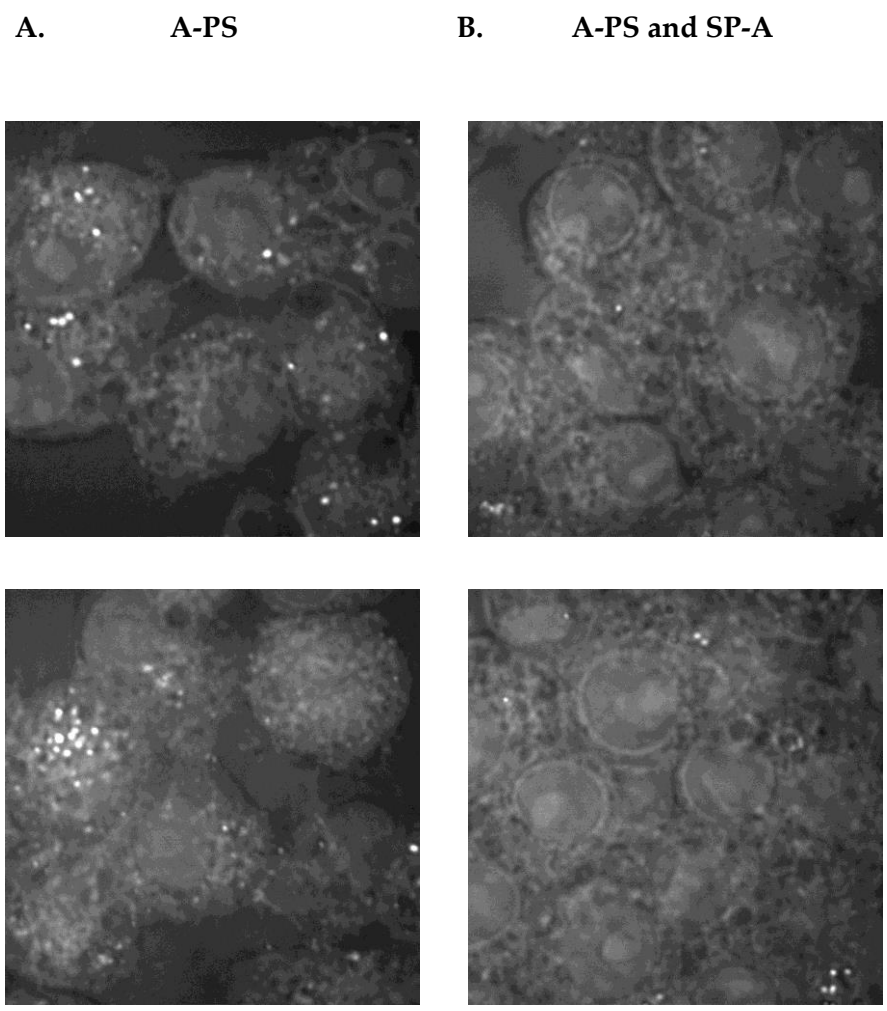

C.

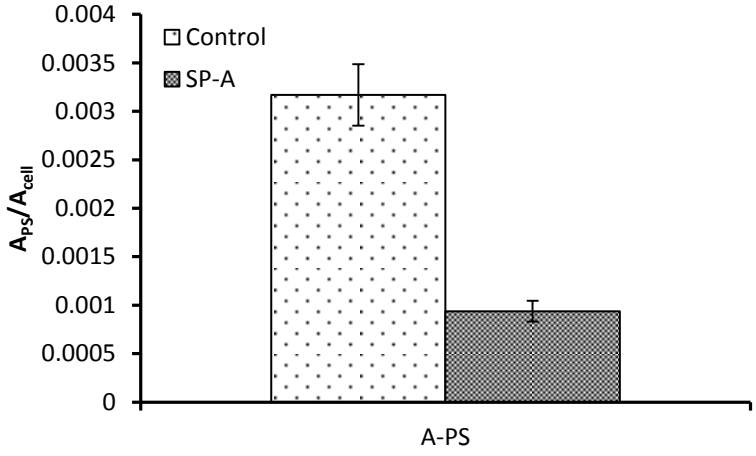

Figure 7.11: Effect of SP-A on the uptake of 200nm A-PS particles in RAW264.7 cells. Data is expressed as a ratio of the area of polystyrene over the total cell area (A_{PS}/A_{cell}) and represents mean ±Stdev from at least 3 images from 1 experiment.

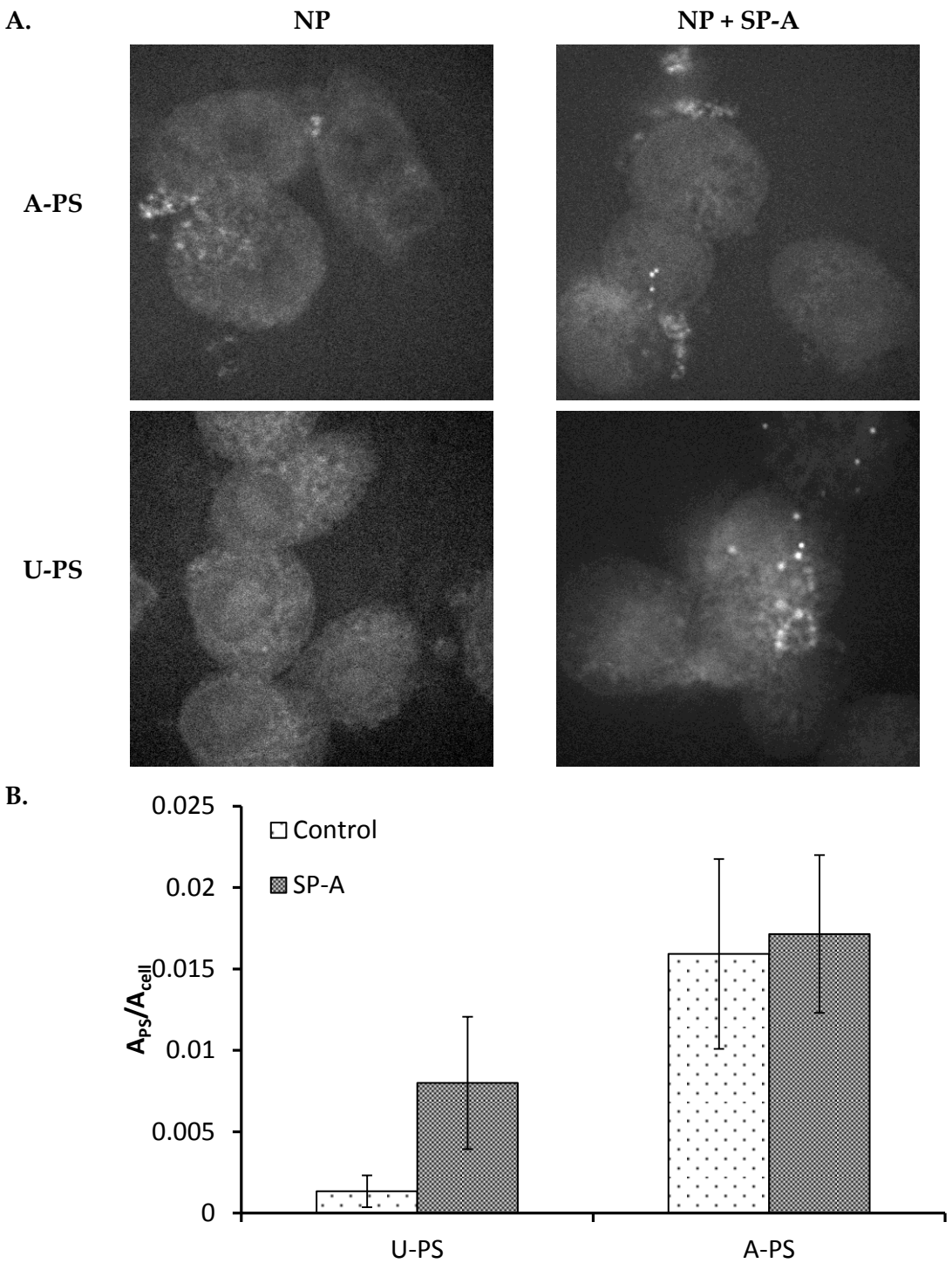

Figure 7.12: Effect of SP-A on the uptake of 100nm A-PS and U-PS in RAW264.7 cells **A.** CARS images of RAW264.7 cells following 1 hour incubation with 100nm A-PS or U-PS with or without SP-A (10 μg/mL). **B**. Quantification of CARS images. A. Data is expressed as a ratio of the area of polystyrene over the total cell area (A_{PS}/A_{cell}) and represents mean ±Stdev from at least 3 images from 1 experiment.

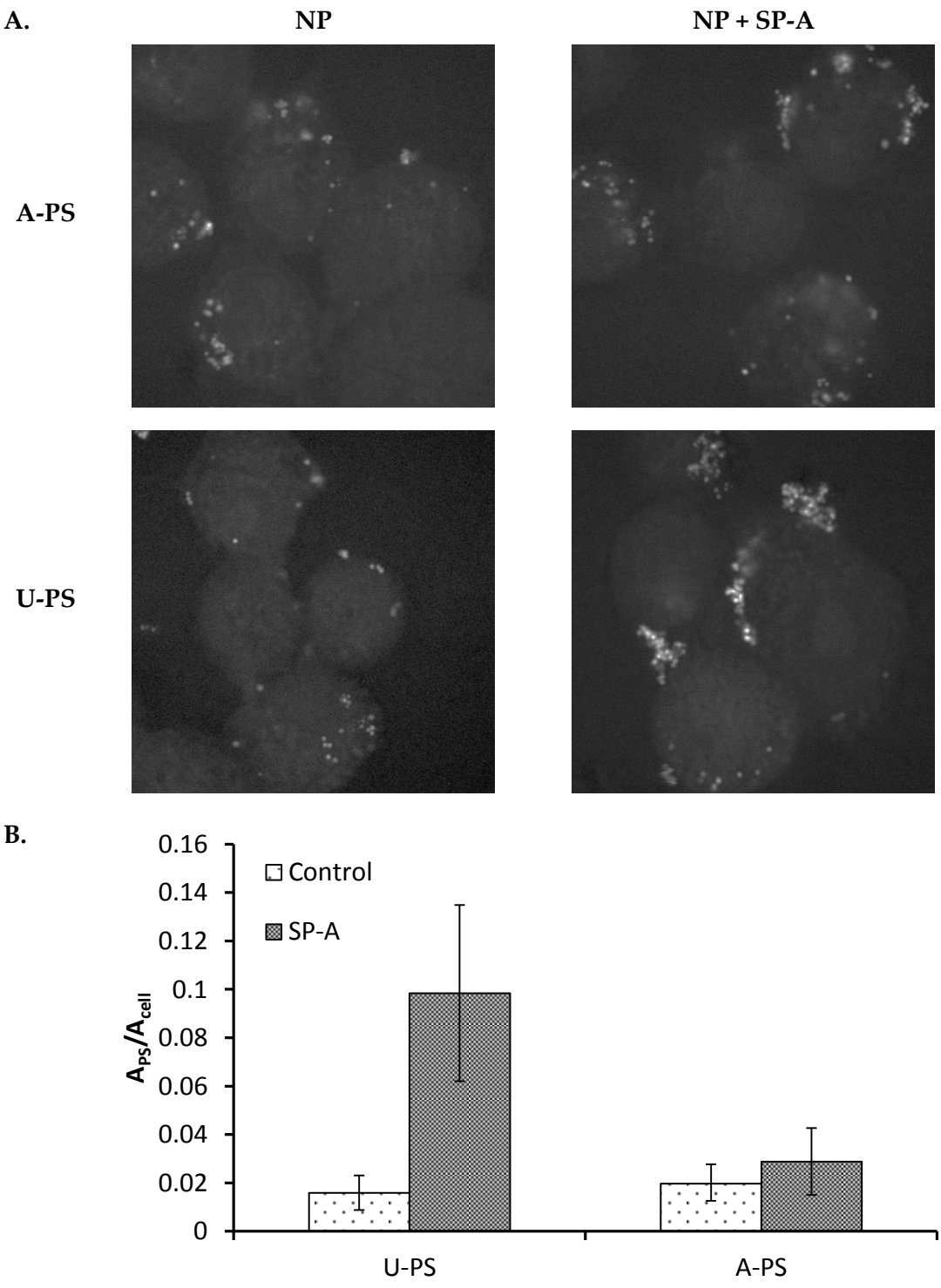

Figure 7.13: Effect of SP-A on 500nm A-PS and U-PS uptake in RAW264.7 cells. **A**. CARS images of RAW264.7 cells following 1 hour incubation with 500nm A-PS or U-PS with or without SP-A (10 μg/mL). **B.** Quantification of CARS images. Data is expressed as a ratio of the area of polystyrene over the total cell area (A_{PS}/A_{cell}) and represents mean ±Stdev from at least 3 images from 1 experiment.

7.4. Discussion

Surfactant levels within the alveolus are regulated by the internalisation of surfactant by ATII cells and alveolar macrophages for recycling and degradation respectively. The internalisation of surfactant lipids by alveolar macrophages therefore, plays an important role in surfactant homeostasis [424]. Curosurf is a natural surfactant therapy derived from the surfactant of pigs and is used to treat neonatal RDS [425]. As a natural surfactant therapy, Curosurf contains surfactant phospholipids and lipids as well as the small hydrophobic lipid associated proteins SP-B and SP-C [284-286]. CARS has been used to monitor lipid involvement in a number of diseases such as multiple sclerosis and cancer [414-417] however, it has yet to be applied to the field of surfactant biology. It was therefore, decided to determine whether CARS could be utilised to monitor surfactant derived lipid accumulation within macrophages. An *in vitro* assay was developed to assess the internalisation of Curosurf by the macrophage-like RAW264.7 cell line. The results show that CARS can detect the accumulation of surfactant lipids within cells in both a time and concentration dependent manner. This indicates that CARS can be used to quantify lipid uptake within these cells. It was therefore, hypothesised that CARS could be used to detect changes in lipid uptake following incubation with SP-A and/or SP-D. A concentration of Curosurf and incubation exposure time point was chosen which yielded a sub-maximal level of lipid uptake. Sub-maximal lipid uptake was required in order to determine any possible modulation in lipid uptake by these surfactant proteins. It has previously been shown that SP-A enhances the uptake of surfactant lipids by macrophages in a time and concentration dependent manner [426]. In the current study, the first preliminary experiment with 10μg/mL SP-A resulted in a 3.5 fold increase in the uptake of

Curosurf into the macrophage like cells. However, in a subsequent experiment a much smaller increase was evident.

SP-A is the most abundant protein in pulmonary surfactant, in BALF the relative proportions of SP-A to SP-D in healthy individuals free of infection has been reported to be between 20:1 to 5:1 [152, 423, 427]. It was therefore decided to examine the effect the co-incubation of SP-A and SP-D at a ratio of 10:1 to represent the enhanced proportion of SP-A found in the lung. The results suggest that when in physiologically relevant proportions (i.e. 10:1 w/w) SP-A and SP-D can act in concert to enhance the uptake of surfactant lipids into these macrophage-like cells. Interestingly, at the reciprocal (i.e. 1:10 w/w) concentrations of SP-A and SP-D there was not an additive effect of SP-A and SP-D on lipid uptake. This indicates the need for SP-A in the uptake of lipids by macrophages. However, due to the high degree of variation in the effect of SP-A on lipid uptake between experiments further experiments will have to be conducted in order to ascertain the statistical and clinical significance of these findings.

CARS is also being investigated by members of this research group into the potential *in vivo* surfactant associated applications. The isolation of alveolar macrophages from wild type and SP-D$^{-/-}$ mice showed enhanced lipid accumulation in the AM of SP-D$^{-/-}$ mice [428] which is consistent with previous reports [132, 429-431]. This shows that CARS could potentially be used to monitor the progression and onset of the emphysema–like phenotype which develops in SP-D deficient mice. CARS could also be used to monitor any changes in lipid accumulation in SP-D deficient mice following therapeutic intervention.

In these experiments, CARS could resolve individual 200nm and 500nm in association with RAW264.7 macrophage-like cells. However, individual

100nm particles were not detectable. In the CARS experiments, SP-A had little effect on the apparent association of 100nm A-PS particles with RAW264.7 cells. This is in contrast with the flow cytometry data which showed that SP-A resulted in a dose dependent reduction in A-PS uptake in these cells. A number of factors could account for these differences, firstly the resolution of the CARS setup means that only aggregated 100nm particles could be detected. Secondly the 100nm A-PS particles self aggregated in the SF RPMI even at room temperature which means that the particles may have been aggregated before the addition of SP-A. In the flow cytometry experiments, the 100nm fluorescent A-PS particles remained relatively monodispersed in TBS with calcium or SF RPMI at room temperature and only aggregated at physiological temperatures (i.e. after the addition of SP-A). Furthermore, the flow cytometry experiments exposed RAW264.7 cells in suspension to the particle-protein dispersions whereas the CARS experiments exposed them following adherence to glass cover slips. In the flow cytometry experiments, trypan blue was to quench the fluorescence from extracellular particles and therefore measured the cellular uptake. However, in the CARS experiments, the ratio of polystyrene over cell area is a measure of total particle association with the cells rather than particle uptake as particles on the outer leaflet of the cell are also included in the analysis. The CARS setup can be modified to obtain simultaneous three dimensional confocal images, allowing the sub cellular localisation of the particles to be determined [413]. This could be investigated further in future experiments.

In the CARS experiments a much higher concentration of particles was used (130 μg/mL) compared to the flow cytometry experiments (6.65 μg/mL). Flow cytometry showed that concentrations of ≥0.156μg/mL of SP-A resulted in significant reductions of 6.65 μg/mL A-PS in RAW264.7 cells giving a minimum effective concentration of SP-A per μg of A-PS as 0.023 μg/ μg. The

CARS experiments used 10 μg/mL of SP-A with 130 μg/mL A-PS which means that theoretically there was sufficient SP-A to reproduce the effect.

Interestingly, the incubation of SP-A with 200nm A-PS particles resulted in a reduction in the association of these particles with RAW264.7 cells. This is in agreement with the flow cytometry data for the 100nm A-PS particles. On the other hand SP-A had little effect on the association of 500nm A-PS particles with RAW264.7 cells. Interestingly, there was also little difference in the association of 500nm A-PS and U-PS whereas A-PS particles of 100nm and 200nm in size associated with RAW264.7 cells to a greater extent than the equivalent U-PS particles. This may be due to enhanced phagocytic uptake of 500nm U-PS particles by RAW264.7 cells compared to the smaller particles. As particle size increases beyond 300nm the contribution of phagocytosis relative to other mechanisms of uptake increases [378, 432]. These experiments will have to be repeated in order to determine their potential statistical and biological significance.

All particles used in the CARS experiments were unlabelled. This was done to ensure that the particles were detected by CARS and not from fluorophore interference as Ramen scattering is weaker than fluorescence [433]. The identification of particles within biological tissues using CARS has been previously described. Gold particles have been visualised inside the hippocampus following intraperitoneal instillation of 17nm particles. The detection of these particles was likely due to accumulation of gold particles in the hippocampus tissue [422]. Titanium dioxide aggregates have also been localised within the gills of fish using CARS microscopy [420, 434] CARS has also been used to monitor the endocytosis of 200nm PS by an epithelial cell line by single particle tracking analysis [421]. These studies demonstrate the potential for CARS to detect particles within biological structures both *in vitro* and *in vivo.* The non-destructive nature of CARS over conventional methods

to visualise unlabelled particle bio-distribution such as TEM provides a number of opportunities. However, these studies, in accordance with the current study have been unable to detect or distinguish single nanoparticles from particle aggregates/clusters.

The detection of unlabelled particles ≥200nm by CARS could enable the *in situ* cellular uptake of particles and monitoring the routes of endocytic uptake. The effect of surfactant proteins on these pathways could also be directly visualised. It would also be interesting to utilise CARS to determine the bio-distribution of inhaled or intranasally instilled particles in extrapulmonary tissues in wild type, SP-A and SP-D deficient mice.

Chapter 8: Summary and Future Work

The overarching hypothesis of this study was that nanoparticles can sequester surfactant proteins A and D in the alveolus, that this sequestration will lead to altered particle clearance by immune cells and, as a consequence, this will lead to a deficiency in these surfactant proteins and enhanced susceptibility to infection.

Firstly, it was demonstrated that the model U-PS and A-PS particles can associate with SP-A and SP-D. These interactions were dependent on the particle surface charge and were independent of the lectin binding domain of the proteins. The interaction of U-PS with SP-A resulted in the formation of a hard corona whereas a soft SP-A corona formed around the A-PS particles. The interaction with A-PS or U-PS with SP-A altered the colloidal stability of these particles at physiological temperatures. This was evidenced by the stabilisation of the self-agglomeration of the A-PS particles and enhanced aggregation of the U-PS particles. Interestingly, although the interaction of SP-A with U-PS particles was calcium independent, calcium greatly enhanced the SP-A mediated aggregation of these particles. In order to investigate the absorption and alterations of colloidal stability further a number of techniques could be employed. Differential sedimentation centrifugation and field flow fractionisation could be used to further elicit the size distributions of these polydispersed samples. The effect of protein absorption on the structure of the protein could also be investigated using circular dichroism and the enthalpy characteristics could be determined by isothermal titration calorimetry. Electron microscopy would support further visualisation of the nanoparticle/protein complexes.

Secondly, the association of SP-A to the A-PS and U-PS particles resulted in altered particle clearance by macrophages. SP-A enhanced the uptake of U-

PS particles by the RAW264.7 macrophage like cells; however, SP-A resulted in a dose dependent reduction in A-PS uptake by RAW264.7 cells, and by the alveolar macrophages from wild type and SP-A deficient mice. Interestingly, A-PS particle uptake was enhanced in the alveolar macrophages of SP-A deficient mice. A-PS particle uptake was reduced in the alveolar macrophages of SP-D deficient compared to wild type mice. Furthermore, the addition of exogenous SP-D resulted in a partial restoration of A-PS uptake. In future *in vitro* studies it would be interesting to investigate the effect of surfactant proteins of different sizes on the uptake into macrophage and epithelial cell lines. Furthermore, the effect of surfactant lipids in these experiments should also be determined. *In vivo* studies could also be conducted to determine the bio- distribution of particles of different sizes and functionalisations in wild type, SP-A deficient, SP-D deficient and SP-A/SP-D double knockout mice.

In order to determine whether nanoparticles could alter the ability of surfactant proteins to neutralise viral infections, *in vitro* infection models first had to be optimised. IAV was chosen as a model viral pathogen as both SP-A and SP-D have been reported to neutralise this virus. TT1, A549 and differentiated THP-1 cells were chosen as the cell lines for these experiments as they represent the predominant cell types found in the alveolar epithelium, namely ATI, ATII and alveolar macrophages. The viral dose was optimised to a sub-maximal infection rate; this viral concentration was used against a range of SP-A and SP-D concentrations to determine the concentration of each protein that resulted in a sub maximal reduction in infection. The protocol to differentiate the monocytic THP-1 cell line into macrophage like cells was also optimised.

Finally, using these models it was demonstrated that nanoparticles can have a biphasic effect on surfactant protein mediated neutralisation. This was evident with a partial loss in surfactant protein mediated neutralisation of

IAV in epithelial cells at low particle concentrations but at higher concentrations an enhancement of surfactant protein mediated IAV neutralisation in some treatment combinations was observed. However, these effects were dependent on the type of particle, particle concentration and cell type in question. U-PS particles resulted in approximately a 50% reduction in the neutralising capacity of SP-D in TT1 cells at a low concentration, whereas at higher concentrations the pre-incubation of SP-D with U-PS and IAV resulted in a dramatic increase in SP-D mediated IAV neutralisation. In A549 cells, U-PS particles resulted in a reduction in the SP-A mediated neutralisation of IAV at low concentrations but an increase in function at higher concentrations. Interestingly, low concentrations of A-PS particles resulted in a reduction in SP-A mediated IAV neutralisation in TT1 cells. However, in A549 cells, low A-PS concentrations resulted in a reduction of SP-D mediated neutralisation of IAV. These experiments demonstrate the need for chronic *in vitro* and *in vivo* exposure systems to determine the effect of nanoparticles on surfactant protein mediated neutralisation of viral infections. *In vivo* experiments would be able to demonstrate whether recovery mechanisms, such as the production of excess SP-A and SP-D, could compensate for the loss of function observed in these experiments. The aggregation kinetics of the IAV, surfactant protein and NP complexes also need to be investigated further.

An assay was also developed to attempt to determine the effect of nanoparticles on the surfactant protein mediated clearance of bacteria. However, this assay proved not to be reliable enough for this purpose as it showed that at low concentrations of the high molecular weight SP-D, an opsonic effect was observed whereas at higher concentrations a reduction in particle clearance was demonstrated. This was shown to be due to the formation of 'super aggregates' at high SP-D concentrations. An LPS

stimulation assay was also developed to determine the biological effect of the rfhSP-D protein on this bacterial product. The results showed that rfhSP-D tended to result in a reduction in the stimulation of macrophages by LPS, as evidenced by a reduction in the production of TNFα and this became more pronounced and significant following 24 hours incubation. This assay could be further developed to determine the effect of nanoparticles on the anti-inflammatory properties of rfhSP-D.

One of the aims of this study was to develop CARS for the detection of unlabelled lipids and nanoparticles *in vitro*. Curosurf, a natural surfactant replacement therapy, was used in this study to examine lipid uptake by macrophages by CARS. This study showed that lipid was internalised in both a time dependent and saturable fashion. Using sub-maximal exposure conditions, initial experiments showed that the incubation of SP-A with Curosurf resulted in increases in lipid uptake. However, as subsequent experiments showed variable results these experiments need to be repeated. The detection of surfactant lipid accumulation in the alveolar macrophages by CARS could be used as a method to detect changes to the pathogenesis of the emphysema like phenotype of the SP-D deficient mouse following therapeutic intervention. The association of different sized polystyrene particles by RAW264.7 cells was also studied by CARS. The results showed that although aggregates of the 100nm particles could be visualised individual particles were not within the resolution of the microscope. 200nm A-PS particles associated with the RAW264.7 cells in a time dependent fashion whereas only a small amount of 200nm U-PS were found to associate with the cells at the time points studied. These experiments need to repeated to confirm the results. Further optimisation of the CARS setup could allow for the three dimensional imaging of the process of particle internalisation *in situ*.

Nanoparticles were shown in this study to modulate the ability of surfactant proteins to neutralise IAV infection *in vitro*. This is the first time this has been reported and could represent an important mechanism through which enhanced exposure to airborne particulates results in the increased incidence and severity of respiratory infections. This opens up interesting lines of enquiry which could be explored through investigations *in vivo* on the effect of nanoparticles on the function of the innate immune defence molecules SP-A and SP-D.

Reference List

1. Bokare, V., K. Murugesan, J.H. Kim, E.J. Kim, and Y.S. Chang, Integrated Hybrid Treatment for the Remediation of 2,3,7,8-Tetrachlorodibenzo-P-Dioxin. The Science of the total environment, 2012. 435-436: 563-6.

2. Tang, H.W., W. Lu, C.M. Che, and K.M. Ng, Gold Nanoparticles and Imaging Mass Spectrometry: Double Imaging of Latent Fingerprints. Anal Chem, 2010. 82: 1589-93.

3. Marangoni, V.S., I.M. Paino, and V. Zucolotto, Synthesis and Characterization of Jacalin-Gold Nanoparticles Conjugates as Specific Markers for Cancer Cells. Colloids and surfaces. B, Biointerfaces, 2013. 112c: 380-386.

4. Hussain, S., J.A.J. Vanoirbeek, K. Luyts, V. De Vooght, E. Verbeken, L.C.J. Thomassen, J.A. Martens, D. Dinsdale, S. Boland, F. Marano, B. Nemery, and P.H.M. Hoet, Lung Exposure to Nanoparticles Modulates an Asthmatic Response in a Mouse Model. European Respiratory Journal, 2011. 37: 299-309.

5. Lanone, S. and J. Boczkowski, Titanium and Gold Nanoparticles in Asthma: The Bad and the Ugly. European Respiratory Journal, 2011. 37: 225-227.

6. Scholars, W.W.I.C.f. The Project on Emerging Nanotechnologies; Www.Nanotechproject.Org. 2011 20/08/2011].

7. Oberdorster, G., E. Oberdorster, and J. Oberdorster, Nanotoxicology: An Emerging Discipline Evolving from Studies of Ultrafine Particles. Environ. Health Perspect., 2005. 113: 823-839.

8. Handy, R., R. Owen, and E. Valsami-Jones, The Ecotoxicology of Nanoparticles and Nanomaterials: Current Status, Knowledge Gaps, Challenges, and Future Needs. Ecotoxicology, 2008. 17: 315-325.

9. (SCENIHR), S.C.o.E.a.N.I.H.R., The Appropraiteness of Existing Methodologies to Assess the Potential Risks Associated with Engineered and Adventitious Products of Nanotechnologies, E.C.H.a.C.P. Directorate-General, Editor. 2006. p. pp79.

10. Demou, E., L. Tran, and C. Housiadas, Effective Biological Dose from Occupational Exposure During Nanoparticle Synthesis, in Inhaled Particles X, L. Kenny, Editor. 2009.

11. Heiss, C., C. Hoffmann, C. Schulte, L. Tietjen, and U. Frank, Authorities Dealing with Reach. Chimia, 2006. 60: 661-668.

12. Oberdorster, G., Z. Sharp, V. Atudorei, A. Elder, R. Gelein, A. Lunts, W. Kreyling, and C. Cox, Extrapulmonary Translocation of Ultrafine Carbon Particles Following Whole-Body Inhalation Exposure of Rats. Journal of Toxicology and Environmental Health-Part A, 2002. 65: 1531-1543.

13. Davies, N.M. and M.R. Feddah, A Novel Method for Assessing Dissolution of Aerosol Inhaler Products. Int J Pharm, 2003. 255: 175-87.

14. Tsuzuki, T., Commercial Scale Production of Inorganic Nanoparticles. International Journal of Nanotechnology, 2009. 6: 567-578.

15. Gehr, P., M. Bachofen, and E.R. Weibel, The Normal Human Lung: Ultrastructure and Morphometric Estimation of Diffusion Capacity. Respiration Physiology, 1978. 32: 121-140.

16. Stone, K.C., R.R. Mercer, P. Gehr, B. Stockstill, and J.D. Crapo, Allometric Relationships of Cell Numbers and Size in the Mammalian Lung. Am. J. Respir. Cell Mol. Biol., 1992. 6: 235-243.

17. Dobbs, L.G., M.D. Johnson, J. Vanderbilt, L. Allen, and R. Gonzalez, The Great Big Alveolar Ti Cell: Evolving Concepts and Paradigms. Cellular physiology and biochemistry : international journal of experimental cellular physiology, biochemistry, and pharmacology, 2010. 25: 55-62.

18. Dobbs, L.G., R. Gonzalez, M.A. Matthay, E.P. Carter, L. Allen, and A.S. Verkman, Highly Water-Permeable Type I Alveolar Epithelial Cells Confer High Water Permeability between the Airspace and Vasculature in Rat Lung. Proc Natl Acad Sci U S A, 1998. 95: 2991-6.

19. Johnson, M.D., J.H. Widdicombe, L. Allen, P. Barbry, and L.G. Dobbs, Alveolar Epithelial Type I Cells Contain Transport Proteins and Transport Sodium, Supporting an Active Role for Type I Cells in Regulation of Lung Liquid Homeostasis. Proceedings of the National Academy of Sciences of the United States of America, 2002. 99: 1966-71.

20. Chen, J., Z. Chen, N.R. Chintagari, M. Bhaskaran, N. Jin, T. Narasaraju, and L. Liu, Alveolar Type I Cells Protect Rat Lung Epithelium from Oxidative Injury. The Journal of physiology, 2006. 572: 625-38.

21. Nord, E.P., S.E. Brown, and E.D. Crandall, Characterization of Na+-H+ Antiport in Type Ii Alveolar Epithelial Cells. The American journal of physiology, 1987. 252: C490-8.

22. Castranova, V., G.S. Jones, J.R. Wright, H.D. Colby, L. Bowman, and P.R. Miles, Transport Properties of Isolated Type Ii Alveolar Epithelial Cells. Am Rev Respir Dis, 1983. 127: S28-33.

23. Danto, S.I., J.M. Shannon, Z. Borok, S.M. Zabski, and E.D. Crandall, Reversible Transdifferentiation of Alveolar Epithelial Cells. Am J Respir Cell Mol Biol, 1995. 12: 497-502.

24. Lu, J.H., H. Wiedemann, U. Holmskov, S. Thiel, R. Timpl, and K.B.M. Reid, Structural Similarity between Lung Surfactant Protein-D and Conglutinin - 2 Distinct, C-Type Lectins Containing Collagen-Like Sequences. European Journal of Biochemistry, 1993. 215: 793-799.

25. Perez-Gil, J., Structure of Pulmonary Surfactant Membranes and Films: The Role of Proteins and Lipid-Protein Interactions. Biochimica Et Biophysica Acta-Biomembranes, 2008. 1778: 1676-1695.

26. Wright, J.R., Pulmonary Surfactant: A Front Line of Lung Host Defense. Journal of Clinical Investigation, 2003. 111: 1453-1455.

27. Waters, P., M. Vaid, U. Kishore, and T. Madan, Lung Surfactant Proteins a and D as Pattern Recognition Proteins, in Target Pattern Recognition in Innate Immunity, U. Kishore, Editor. 2009, Landes BioScience and Springer Science+Business Media: New York. p. 74-97.

28. Ohtani, K., Y. Suzuki, S. Eda, T. Kawai, T. Kase, H. Keshi, Y. Sakai, A. Fukuoh, T. Sakamoto, H. Itabe, T. Suzutani, M. Gasawara, I. Yoshida, and N. Wakamiya, The Membrane-Type Collectin Cl-P1 Is a Scavenger Receptor on Vascular Endothelial Cells. Journal of Biological Chemistry, 2001. 276: 44222-44228.

29. Hansen, S., D. Holm, V. Moeller, L. Vitved, C. Bendixen, K.B. Reid, K. Skjoedt, and U. Holmskov, Cl-46, a Novel Collectin Highly Expressed in Bovine Thymus and Liver. Journal of immunology (Baltimore, Md. : 1950), 2002. 169: 5726-34.

30. Lu, J., S.B. Laursen, S. Thiel, J.C. Jensenius, and K.B. Reid, The Cdna Cloning of Conglutinin and Identification of Liver as a Primary Site of Synthesis of Conglutinin in Members of the Bovidae. The Biochemical journal, 1993. 292 (Pt 1): 157-62.

31. Crouch, E., A. Persson, D. Chang, and J. Heuser, Molecular-Structure of Pulmonary Surfactant Protein-D (Sp-D). Journal of Biological Chemistry, 1994. 269: 17311-17319.

32. Reid, K.B.M., Interactions of Surfactant Protein D with Pathogens, Allergens and Phagocytes. Biochimica Et Biophysica Acta-Molecular Basis of Disease, 1998. 1408: 290-295.

33. Kingma, P.S. and J.A. Whitsett, In Defense of the Lung: Surfactant Protein a and Surfactant Protein D. Current Opinion in Pharmacology, 2006. 6: 277-283.

34. Crouch, E., K. Hartshorn, and I. Ofek, Collectins and Pulmonary Innate Immunity. Immunological Reviews, 2000. 173: 52-65.

35. Clark, H. and K.B.M. Reid, Structural Requirements for Sp-D Function in Vitro and in Vivo: Therapeutic Potential of Recombinant Sp-D. Immunobiology, 2002. 205: 619-631.

36. Clark, H.W., Untapped Therapeutic Potential of Surfactant Proteins: Is There a Case for Recombinant Sp-D Supplementation in Neonatal Lung Disease? Neonatology, 2010. 97: 380-387.

37. Head, J.F., T.R. Mealy, F.X. McCormack, and B.A. Seaton, Crystal Structure of Trimeric Carbohydrate Recognition and Neck Domains of Surfactant Protein A. The Journal of biological chemistry, 2003. 278: 43254-60.

38. Drickamer, K., Engineering Galactose-Binding Activity into a C-Type Mannose-Binding Protein. Nature, 1992. 360: 183-6.

39. Allen, M.J., A. Laederach, P.J. Reilly, and R.J. Mason, Polysaccharide Recognition by Surfactant Protein D: Novel Interactions of a C-Type Lectin with Nonterminal Glucosyl Residues. Biochemistry, 2001. 40: 7789-98.

40. Haurum, J.S., S. Thiel, H.P. Haagsman, S.B. Laursen, B. Larsen, and J.C. Jensenius, Studies on the Carbohydrate-Binding Characteristics of Human Pulmonary Surfactant-Associated Protein a and Comparison with Two Other Collectins: Mannan-Binding Protein and Conglutinin. The Biochemical journal, 1993. 293 (Pt 3): 873-8.

41. Crouch, E.C., K. Smith, B. McDonald, D. Briner, B. Linders, J. McDonald, U. Holmskov, J. Head, and K. Hartshorn, Species Differences in the Carbohydrate Binding Preferences of Surfactant Protein D. Am J Respir Cell Mol Biol, 2006. 35: 84-94.

42. van Eijk, M., M.R. White, E.C. Crouch, J.J. Batenburg, A.B. Vaandrager, L.M. Van Golde, H.P. Haagsman, and K.L. Hartshorn, Porcine Pulmonary Collectins Show Distinct Interactions with Influenza a Viruses: Role of the N-Linked Oligosaccharides in the Carbohydrate Recognition Domain. Journal of immunology (Baltimore, Md. : 1950), 2003. 171: 1431-40.

43. Zhang, P., A. McAlinden, S. Li, T. Schumacher, H. Wang, S. Hu, L. Sandell, and E. Crouch, The Amino-Terminal Heptad Repeats of the Coiled-Coil Neck Domain of Pulmonary Surfactant Protein D Are Necessary for the Assembly of Trimeric Subunits and Dodecamers. The Journal of biological chemistry, 2001. 276: 19862-70.

44. Hakansson, K., N.K. Lim, H.J. Hoppe, and K.B.M. Reid, Crystal Structure of the Trimeric Alpha-Helical Coiled-Coil and the Three Lectin Domains of Human Lung Surfactant Protein D. Structure, 1999. 7: 255-264.

45. Hansen, S. and U. Holmskov, Structural Aspects of Collectins and Receptors for Collectins. Immunobiology, 1998. 199: 165-89.

46. Rust, K., L. Grosso, V. Zhang, D. Chang, A. Persson, W. Longmore, G.Z. Cai, and E. Crouch, Human Surfactant Protein D: Sp-D Contains a C-Type Lectin Carbohydrate Recognition Domain. Arch Biochem Biophys, 1991. 290: 116-26.

47. Lim, B.L., A.C. Willis, K.B. Reid, J. Lu, S.B. Laursen, J.C. Jensenius, and U. Holmskov, Primary Structure of Bovine Collectin-43 (Cl-43). Comparison with Conglutinin and Lung Surfactant Protein-D. The Journal of biological chemistry, 1994. 269: 11820-4.

48. Lu, J.H., A.C. Willis, and K.B.M. Reid, Purification, Characterization and Cdna Cloning of Human Lung Surfactant Protein-D. Biochemical Journal, 1992. 284: 795-802.

49. Crawford, S.W., R.P. Mecham, and H. Sage, Structural Characteristics and Intermolecular Organization of Human Pulmonary-Surfactant-Associated Proteins. The Biochemical journal, 1986. 240: 107-14.

50. Bhattacharyya, S.N. and D.Y. Bell, Characterization of Two Glycoproteins Isolated from Lung Lavage Fluid of Normal Human and from Patients with Two Pulmonary Diseases. Inflammation, 1984. 8: 407-15.

51. Berg, T., R. Leth-Larsen, U. Holmskov, and P. Hojrup, Structural Characterisation of Human Proteinosis Surfactant Protein A. Biochimica et biophysica acta, 2000. 1543: 159-73.

52. Brown-Augsburger, P., K. Hartshorn, D. Chang, K. Rust, C. Fliszar, H.G. Welgus, and E.C. Crouch, Site-Directed Mutagenesis of Cys-15 and Cys-20 of Pulmonary Surfactant Protein D. Expression of a Trimeric Protein with Altered Anti-Viral Properties. The Journal of biological chemistry, 1996. 271: 13724-30.

53. Sanchez-Barbero, F., J. Strassner, R. Garcia-Canero, W. Steinhilber, and C. Casals, Role of the Degree of Oligomerization in the Structure and Function of Human Surfactant Protein A. The Journal of biological chemistry, 2005. 280: 7659-70.

54. Guo, C.J., E.N. Atochina-Vasserman, E. Abramova, J.P. Foley, A. Zaman, E. Crouch, M.F. Beers, R.C. Savani, and A.J. Gow, S-Nitrosylation of Surfactant Protein-D Controls Inflammatory Function. PLoS biology, 2008. 6: e266.

55. Crouch, E., K. Rust, R. Veile, H. Donis-Keller, and L. Grosso, Genomic Organization of Human Surfactant Protein D (Sp-D). Sp-D Is Encoded on Chromosome 10q22.2-23.1. The Journal of biological chemistry, 1993. 268: 2976-83.

56. Hoover, R.R. and J. Floros, Organization of the Human Sp-a and Sp-D Loci at 10q22-Q23. Physical and Radiation Hybrid Mapping Reveal Gene Order and Orientation. Am J Respir Cell Mol Biol, 1998. 18: 353-62.

57. DiAngelo, S., Z. Lin, G. Wang, S. Phillips, M. Ramet, J. Luo, and J. Floros, Novel, Non-Radioactive, Simple and Multiplex Pcr-Crflp Methods for Genotyping Human Sp-a and Sp-D Marker Alleles. Disease markers, 1999. 15: 269-81.

58. Wang, G., C. Myers, A. Mikerov, and J. Floros, Effect of Cysteine 85 on Biochemical Properties and Biological Function of Human Surfactant Protein a Variants. Biochemistry, 2007. 46: 8425-35.

59. Voss, T., K. Melchers, G. Scheirle, and K.P. Schafer, Structural Comparison of Recombinant Pulmonary Surfactant Protein Sp-a Derived from Two Human Coding Sequences: Implications for the Chain Composition of Natural Human Sp-A. Am J Respir Cell Mol Biol, 1991. 4: 88-94.

60. Tagaram, H.R., G. Wang, T.M. Umstead, A.N. Mikerov, N.J. Thomas, G.R. Graff, J.C. Hess, M.J. Thomassen, M.S. Kavuru, D.S. Phelps, and J. Floros, Characterization of a Human Surfactant Protein A1 (Sp-A1) Gene-Specific Antibody; Sp-A1 Content Variation among Individuals of Varying Age and Pulmonary Health. American journal of physiology. Lung cellular and molecular physiology, 2007. 292: L1052-63.

61. Oberley, R.E. and J.M. Snyder, Recombinant Human Sp-A1 and Sp-A2 Proteins Have Different Carbohydrate-Binding Characteristics. American journal of physiology. Lung cellular and molecular physiology, 2003. 284: L871-81.

62. Sanchez-Barbero, F., G. Rivas, W. Steinhilber, and C. Casals, Structural and Functional Differences among Human Surfactant Proteins Sp-A1, Sp-A2 and Co-Expressed Sp-A1/Sp-A2: Role of Supratrimeric Oligomerization. The Biochemical journal, 2007. 406: 479-89.

63. Mikerov, A.N., T.M. Umstead, W. Huang, W. Liu, D.S. Phelps, and J. Floros, Sp-A1 and Sp-A2 Variants Differentially Enhance Association of Pseudomonas Aeruginosa with Rat Alveolar Macrophages. American

journal of physiology. Lung cellular and molecular physiology, 2005. 288: L150-8.

64. Leth-Larsen, R., P. Garred, H. Jensenius, J. Meschi, K. Hartshorn, J. Madsen, I. Tornoe, H.O. Madsen, G. Sorensen, E. Crouch, and U. Holmskov, A Common Polymorphism in the Sftpd Gene Influences Assembly, Function, and Concentration of Surfactant Protein D. Journal of immunology (Baltimore, Md. : 1950), 2005. 174: 1532-8.

65. MacNeill, C., T.M. Umstead, D.S. Phelps, Z. Lin, J. Floros, D.A. Shearer, and J. Weisz, Surfactant Protein a, an Innate Immune Factor, Is Expressed in the Vaginal Mucosa and Is Present in Vaginal Lavage Fluid. Immunology, 2004. 111: 91-99.

66. Madsen, J., I. Tornoe, O. Nielsen, C. Koch, W. Steinhilber, and U. Holmskov, Expression and Localization of Lung Surfactant Protein a in Human Tissues. Am. J. Respir. Cell Mol. Biol., 2003. 29: 591-597.

67. Mo, Y.K., O. Kankavi, P.P. Masci, G.D. Mellick, M.W. Whitehouse, G.M. Boyle, P.G. Parsons, M.S. Roberts, and S.E. Cross, Surfactant Protein Expression in Human Skin: Evidence and Implications. J Invest Dermatol, 2007. 127: 381-386.

68. Kim, J.K., S.S. Kim, K.W. Rha, C.H. Kim, J.H. Cho, C.H. Lee, J.G. Lee, and J.H. Yoon, Expression and Localization of Surfactant Proteins in Human Nasal Epithelium. American journal of physiology. Lung cellular and molecular physiology, 2007. 292: L879-84.

69. Madsen, J., A. Kliem, I. Tornoe, K. Skjodt, C. Koch, and U. Holmskov, Localization of Lung Surfactant Protein D on Mucosal Surfaces in Human Tissues. Journal of immunology (Baltimore, Md. : 1950), 2000. 164: 5866-70.

70. Oberley, R.E., K.L. Goss, D.S. Hoffmann, K.A. Ault, T.L. Neff, K.H. Ramsey, and J.M. Snyder, Regulation of Surfactant Protein D in the Mouse Female Reproductive Tract in Vivo. Molecular human reproduction, 2007. 13: 863-8.

71. Leth-Larsen, R., C. Floridon, O. Nielsen, and U. Holmskov, Surfactant Protein D in the Female Genital Tract. Molecular human reproduction, 2004. 10: 149-54.

72. Crouch, E., K. Hartshorn, T. Horlacher, B. McDonald, K. Smith, T. Cafarella, B. Seaton, P.H. Seeberger, and J. Head, Recognition of Mannosylated Ligands and Influenza a Virus by Human Surfactant Protein D: Contributions of an Extended Site and Residue 343. Biochemistry, 2009. 48: 3335-45.

73. Hartshorn, K.L., Role of Surfactant Protein a and D (Sp-a and Sp-D) in Human Antiviral Host Defense. Frontiers in Bioscience, 2010. 2: 527-46.

74. Hartshorn, K.L., R. Webby, M.R. White, T. Tecle, C. Pan, S. Boucher, R.J. Moreland, E.C. Crouch, and R.K. Scheule, Role of Viral Hemagglutinin Glycosylation in Anti-Influenza Activities of Recombinant Surfactant Protein D. Respiratory Research, 2008. 9: 65.

75. Hall, C.B., Respiratory Syncytial Virus and Parainfluenza Virus. The New England journal of medicine, 2001. 344: 1917-28.

76. Vandini, S., L. Corvaglia, R. Alessandroni, G. Aquilano, C. Marsico, M. Spinelli, M. Lanari, and G. Faldella, Respiratory Syncytial Virus Infection in Infants and Correlation with Meteorological Factors and Air Pollutants. Italian journal of pediatrics, 2013. 39: 1.

77. Tsolia, M.N., D. Kafetzis, K. Danelatou, H. Astral, K. Kallergi, P. Spyridis, and T.E. Karpathios, Epidemiology of Respiratory Syncytial Virus Bronchiolitis in Hospitalized Infants in Greece. European journal of epidemiology, 2003. 18: 55-61.

78. Bamberger, E., I. Srugo, B. Abu Raya, E. Segal, B. Chaim, I. Kassis, A. Kugelman, and D. Miron, What Is the Clinical Relevance of Respiratory Syncytial Virus Bronchiolitis?: Findings from a Multi-Center, Prospective Study. European journal of clinical microbiology & infectious diseases : official publication of the European Society of Clinical Microbiology, 2012. 31: 3323-30.

79. Barr, F.E., H. Pedigo, T.R. Johnson, and V.L. Shepherd, Surfactant Protein-a Enhances Uptake of Respiratory Syncytial Virus by Monocytes and U937 Macrophages. Am J Respir Cell Mol Biol, 2000. 23: 586-92.

80. Hickling, T.P., H. Bright, K. Wing, D. Gower, S.L. Martin, R.B. Sim, and R. Malhotra, A Recombinant Trimeric Surfactant Protein D Carbohydrate Recognition Domain Inhibits Respiratory Syncytial Virus Infection in Vitro and in Vivo. European journal of immunology, 1999. 29: 3478-84.

81. Ghildyal, R., C. Hartley, A. Varrasso, J. Meanger, D.R. Voelker, E.M. Anders, and J. Mills, Surfactant Protein a Binds to the Fusion Glycoprotein of Respiratory Syncytial Virus and Neutralizes Virion Infectivity. The Journal of infectious diseases, 1999. 180: 2009-13.

82. LeVine, A.M., J. Gwozdz, J. Stark, M. Bruno, J. Whitsett, and T. Korfhagen, Surfactant Protein-a Enhances Respiratory Syncytial Virus Clearance in Vivo. The Journal of clinical investigation, 1999. 103: 1015-21.

83. LeVine, A.M., J. Elliott, J.A. Whitsett, A. Srikiatkhachorn, E. Crouch, N. DeSilva, and T. Korfhagen, Surfactant Protein-D Enhances Phagocytosis and Pulmonary Clearance of Respiratory Syncytial Virus. Am J Respir Cell Mol Biol, 2004. 31: 193-9.

84. Kawasaki, Y., K. Endo, K. Suyama, M. Sato, M. Ito, K. Hashimoto, and M. Hosoya, Serum Sp-D Levels as a Biomarker of Lung Injury in Respiratory Syncytial Virus Bronchiolitis. Pediatr Pulmonol, 2011. 46: 18-22.

85. Ampuero, S., V. Luchsinger, L. Tapia, M.A. Palomino, and C.E. Larranaga, Sp-A1, Sp-A2 and Sp-D Gene Polymorphisms in Severe Acute Respiratory Syncytial Infection in Chilean Infants. Infection, genetics and evolution : journal of molecular epidemiology and evolutionary genetics in infectious diseases, 2011. 11: 1368-77.

86. Lahti, M., J. Lofgren, R. Marttila, M. Renko, T. Klaavuniemi, R. Haataja, M. Ramet, and M. Hallman, Surfactant Protein D Gene Polymorphism Associated with Severe Respiratory Syncytial Virus Infection. Pediatric research, 2002. 51: 696-9.

87. Lofgren, J., M. Ramet, M. Renko, R. Marttila, and M. Hallman, Association between Surfactant Protein a Gene Locus and Severe Respiratory Syncytial Virus Infection in Infants. The Journal of infectious diseases, 2002. 185: 283-9.

88. Gaiha, G.D., T. Dong, N. Palaniyar, D.A. Mitchell, K.B. Reid, and H.W. Clark, Surfactant Protein a Binds to Hiv and Inhibits Direct Infection of Cd4+ Cells, but Enhances Dendritic Cell-Mediated Viral Transfer. Journal of immunology (Baltimore, Md. : 1950), 2008. 181: 601-9.

89. Madsen, J., G.D. Gaiha, N. Palaniyar, T. Dong, D.A. Mitchell, and H.W. Clark, Surfactant Protein D Modulates Hiv Infection of Both T-Cells and Dendritic Cells. PLoS One, 2013. 8: e59047.

90. Meschi, J., E.C. Crouch, P. Skolnik, K. Yahya, U. Holmskov, R. Leth-Larsen, I. Tornoe, T. Tecle, M.R. White, and K.L. Hartshorn, Surfactant Protein D Binds to Human Immunodeficiency Virus (Hiv) Envelope Protein Gp120 and Inhibits Hiv Replication. The Journal of general virology, 2005. 86: 3097-107.

91. Martin, W.J., 2nd, J.F. Downing, M.D. Williams, R. Pasula, H.L. Twigg, 3rd, and J.R. Wright, Role of Surfactant Protein a in the Pathogenesis of Tuberculosis in Subjects with Human Immunodeficiency Virus Infection. Proceedings of the Association of American Physicians, 1995. 107: 340-5.

92. Downing, J.F., R. Pasula, J.R. Wright, H.L. Twigg, 3rd, and W.J. Martin, 2nd, Surfactant Protein a Promotes Attachment of Mycobacterium Tuberculosis to Alveolar Macrophages During Infection with Human Immunodeficiency Virus. Proc Natl Acad Sci U S A, 1995. 92: 4848-52.

93. Jacqueline, S.P., K. Ian, P.T. Jon, S. Roberto, M. Jens, and W.C. Howard, Collectin Interactions with Rhinovirus, in A63. New Concepts in the Alveolar Surfactant Structure and Function. American Thoracic Society. p. A1988-A1988.

94. Perino, J., N.M. Thielens, E. Crouch, D. Spehner, J.M. Crance, and A.L. Favier, Protective Effect of Surfactant Protein D in Pulmonary Vaccinia Virus Infection: Implication of A27 Viral Protein. Viruses, 2013. 5: 928-53.

95. Leth-Larsen, R., F. Zhong, V.T. Chow, U. Holmskov, and J. Lu, The Sars Coronavirus Spike Glycoprotein Is Selectively Recognized by Lung

Surfactant Protein D and Activates Macrophages. Immunobiology, 2007. 212: 201-11.

96. van Iwaarden, J.F., J.A. van Strijp, M.J. Ebskamp, A.C. Welmers, J. Verhoef, and L.M. van Golde, Surfactant Protein a Is Opsonin in Phagocytosis of Herpes Simplex Virus Type 1 by Rat Alveolar Macrophages. The American journal of physiology, 1991. 261: L204-9.

97. Deforge, L.E., J.S. Kenney, M.L. Jones, J.S. Warren, and D.G. Remick, Biphasic Production of Il-8 in Lipopolysaccharide (Lps)-Stimulated Human Whole-Blood - Separation of Lps-Stimulated and Cytokine-Stimulated Components Using Antitumor Necrosis Factor and Anti-Il-1 Antibodies. Journal of Immunology, 1992. 148: 2133-2141.

98. Zhang, X., L. Guo, R.D. Collage, J.L. Stripay, A. Tsung, J.S. Lee, and M.R. Rosengart, Calcium/Calmodulin-Dependent Protein Kinase (Camk) I Alpha Mediates the Macrophage Inflammatory Response to Sepsis. Journal of Leukocyte Biology, 2011. 90: 249-261.

99. Sabarirajan, J., P. Vijayaraj, and V. Nachiappan, Induction of Acute Respiratory Distress Syndrome in Rats by Lipopolysaccharide and Its Effect on Oxidative Stress and Antioxidant Status in Lung. Indian Journal of Biochemistry & Biophysics, 2010. 47: 278-284.

100. Wright, S.D., R.A. Ramos, P.S. Tobias, R.J. Ulevitch, and J.C. Mathison, Cd14, a Receptor for Complexes of Lipopolysaccharide (Lps) and Lps Binding-Protein. Science, 1990. 249: 1431-1433.

101. Sano, H., H. Chiba, D. Iwaki, H. Sohma, D.R. Voelker, and Y. Kuroki, Surfactant Proteins a and D Bind Cd14 by Different Mechanisms. Journal of Biological Chemistry, 2000. 275: 22442-22451.

102. Van Iwaarden, J.F., J.C. Pikaar, J. Storm, E. Brouwer, J. Verhoef, R.S. Oosting, L.M.G. Van Golde, and J.A.G. Van Strijp, Binding of Surfactant Protein a to the Lipid a Moiety of Bacterial Lipopolysaccharides. Biochemical Journal, 1994. 303: 407-411.

103. McIntosh, J.C., S. MervinBlake, E. Conner, and J.R. Wright, Surfactant Protein a Protects Growing Cells and Reduces Tnf-Alpha Activity from Lps-Stimulated Macrophages. American Journal of Physiology-Lung Cellular and Molecular Physiology, 1996. 271: L310-L319.

104. Sano, H., H. Sohma, T. Muta, S. Nomura, D.R. Voelker, and Y. Kuroki, Pulmonary Surfactant Protein a Modulates the Cellular Response to Smooth and Rough Lipopolysaccharides by Interaction with Cd14. Journal of Immunology, 1999. 163: 387-395.

105. Stamme, C., M. Muller, L. Hamann, T. Gutsmann, and U. Seydel, Surfactant Protein a Inhibits Lipopolysaccharide-Induced Immune Cell Activation by Preventing the Interaction of Lipopolysaccharide with Lipopolysaccharide-Binding Protein. American Journal of Respiratory Cell and Molecular Biology, 2002. 27: 353-360.

106. Garcia-Verdugo, I., F. Sanchez-Barbero, K. Soldau, P.S. Tobias, and S. Casals, Interaction of Sp-a (Surfactant Protein a) with Bacterial Rough Lipopolysaccharide (Re-Lps), and Effects of Sp-a on the Binding of Re-Lps to Cd14 and Lps-Binding Protein. Biochemical Journal, 2005. 391: 115-124.

107. Kuan, S.F., K. Rust, and E. Crouch, Interactions of Surfactant Protein-D with Bacterial Lipopolysaccharides - Surfactant Protein-D Is an Escherichia-Coli Binding-Protein in Bronchoalveolar Lavage. Journal of Clinical Investigation, 1992. 90: 97-106.

108. Hartshorn, K.L., M.R. White, and E.C. Crouch, Contributions of the N- and C-Terminal Domains of Surfactant Protein D to the Binding, Aggregation, and Phagocytic Uptake of Bacteria. Infection and Immunity, 2002. 70: 6129-6139.

109. Mackay, R.M., M. Deadman, E.R. Moxon, and H. Clark, A Recombinant Fragment of Human Sp-D Promotes Phagocytosis of Haemophilus Influenzae Strains Whose in Vivo Pathogenicity Is Inversely Related to Sp-D Binding. Early Human Development, 2006. 82: 617-617.

110. Sano, H. and Y. Kuroki, The Lung Collectins, Sp-a and Sp-D, Modulate Pulmonary Innate Immunity. Molecular Immunology, 2005. 42: 279-287.

111. Kuzmenko, A.I., H. Wu, and F.X. McCormack, Pulmonary Collectins Selectively Permeabilize Model Bacterial Membranes Containing Rough Lipopolysaccharide. Biochemistry, 2006. 45: 2679-85.

112. Wu, H., A. Kuzmenko, S. Wan, L. Schaffer, A. Weiss, J.H. Fisher, K.S. Kim, and F.X. McCormack, Surfactant Proteins a and D Inhibit the Growth of Gram-Negative Bacteria by Increasing Membrane Permeability. The Journal of clinical investigation, 2003. 111: 1589-602.

113. Canadas, O., I. Garcia-Verdugo, K.M. Keough, and C. Casals, Sp-a Permeabilizes Lipopolysaccharide Membranes by Forming Protein Aggregates That Extract Lipids from the Membrane. Biophys J, 2008. 95: 3287-94.

114. Ariki, S., T. Kojima, S. Gasa, A. Saito, C. Nishitani, M. Takahashi, T. Shimizu, Y. Kurimura, N. Sawada, N. Fujii, and Y. Kuroki, Pulmonary Collectins Play Distinct Roles in Host Defense against Mycobacterium

Avium. Journal of immunology (Baltimore, Md. : 1950), 2011. 187: 2586-94.

115. Raetz, C.R.H. and C. Whitfield, Lipopolysaccharide Endotoxins. Annual Review of Biochemistry, 2002. 71: 635-700.

116. Wang, X. and P.J. Quinn, Lipopolysaccharide: Biosynthetic Pathway and Structure Modification. Progress in Lipid Research, 2010. 49: 97-107.

117. Madan, T., S. Kaur, S. Saxena, M. Singh, U. Kishore, S. Thiel, K.B. Reid, and P.U. Sarma, Role of Collectins in Innate Immunity against Aspergillosis. Medical mycology : official publication of the International Society for Human and Animal Mycology, 2005. 43 Suppl 1: S155-63.

118. Ren, J., Y. Deng, B. Xiao, G. Wang, and Z. Tao, Protective Effects of Exogenous Surfactant Protein a in Allergic Rhinitis: A Mouse Model. The Annals of otology, rhinology, and laryngology, 2013. 122: 240-6.

119. Forbes, L.R. and A. Haczku, Sp-D and Regulation of the Pulmonary Innate Immune System in Allergic Airway Changes. Clinical and experimental allergy : journal of the British Society for Allergy and Clinical Immunology, 2010. 40: 547-62.

120. Schmiedl, A., A. Luhrmann, R. Pabst, and R. Koslowski, Increased Surfactant Protein a and D Expression in Acute Ovalbumin-Induced Allergic Airway Inflammation in Brown Norway Rats. Int Arch Allergy Immunol, 2009. 148: 118-26.

121. Haley, K.J., A. Ciota, J.P. Contreras, M.R. Boothby, D.L. Perkins, and P.W. Finn, Alterations in Lung Collectins in an Adaptive Allergic Immune Response. American journal of physiology. Lung cellular and molecular physiology, 2002. 282: L573-84.

122. Atochina-Vasserman, E.N., C. Winkler, H. Abramova, F. Schaumann, N. Krug, A.J. Gow, M.F. Beers, and J.M. Hohlfeld, Segmental Allergen Challenge Alters Multimeric Structure and Function of Surfactant Protein D in Humans. Am J Respir Crit Care Med, 2011. 183: 856-64.

123. Mahajan, L., T. Madan, N. Kamal, V.K. Singh, R.B. Sim, S.D. Telang, C.N. Ramchand, P. Waters, U. Kishore, and P.U. Sarma, Recombinant Surfactant Protein-D Selectively Increases Apoptosis in Eosinophils of Allergic Asthmatics and Enhances Uptake of Apoptotic Eosinophils by Macrophages. International immunology, 2008. 20: 993-1007.

124. Erpenbeck, V.J., D.C. Malherbe, S. Sommer, A. Schmiedl, W. Steinhilber, A.J. Ghio, N. Krug, J.R. Wright, and J.M. Hohlfeld, Surfactant Protein D Increases Phagocytosis and Aggregation of Pollen-Allergen Starch Granules. American journal of physiology. Lung cellular and molecular physiology, 2005. 288: L692-8.

125. Liu, C.F., Y.L. Chen, C.C. Shieh, C.K. Yu, K.B. Reid, and J.Y. Wang, Therapeutic Effect of Surfactant Protein D in Allergic Inflammation of Mite-Sensitized Mice. Clinical and experimental allergy : journal of the British Society for Allergy and Clinical Immunology, 2005. 35: 515-21.

126. Deng, Y.Q., Z.Z. Tao, Y.G. Kong, B.K. Xiao, S.M. Chen, Y. Xu, Y. Wang, and Q. He, Association between Single Nucleotide Polymorphisms of Surfactant Protein D and Allergic Rhinitis in Chinese Patients. Tissue antigens, 2009. 73: 546-52.

127. Madan, T., Potential of Lung Surfactant Proteins, Sp-a and Sp-D, and Mannan Binding Lectin for Therapy and Genetic Predisposition to Allergic and Invasive Aspergillosis. Recent patents on inflammation & allergy drug discovery, 2007. 1: 183-7.

128. Palaniyar, N., J. Nadesalingam, H. Clark, M.J. Shih, A.W. Dodds, and K.B. Reid, Nucleic Acid Is a Novel Ligand for Innate, Immune Pattern Recognition Collectins Surfactant Proteins a and D and Mannose-Binding Lectin. The Journal of biological chemistry, 2004. 279: 32728-36.

129. Palaniyar, N., J. Nadesalingam, and K.B. Reid, Innate Immune Collectins Bind Nucleic Acids and Enhance DNA Clearance in Vitro. Ann N Y Acad Sci, 2003. 1010: 467-70.

130. Vandivier, R.W., C.A. Ogden, V.A. Fadok, P.R. Hoffmann, K.K. Brown, M. Botto, M.J. Walport, J.H. Fisher, P.M. Henson, and K.E. Greene, Role of Surfactant Proteins a, D, and C1q in the Clearance of Apoptotic Cells in Vivo and in Vitro: Calreticulin and Cd91 as a Common Collectin Receptor Complex. Journal of immunology (Baltimore, Md. : 1950), 2002. 169: 3978-86.

131. Schagat, T.L., J.A. Wofford, and J.R. Wright, Surfactant Protein a Enhances Alveolar Macrophage Phagocytosis of Apoptotic Neutrophils. Journal of immunology (Baltimore, Md. : 1950), 2001. 166: 2727-33.

132. Botas, C., F. Poulain, J. Akiyama, C. Brown, L. Allen, J. Goerke, J. Clements, E. Carlson, A.M. Gillespie, C. Epstein, and S. Hawgood, Altered Surfactant Homeostasis and Alveolar Type Ii Cell Morphology in Mice Lacking Surfactant Protein D. Proceedings of the National Academy of Sciences of the United States of America, 1998. 95: 11869-74.

133. Clark, H., N. Palaniyar, S. Hawgood, and K.B. Reid, A Recombinant Fragment of Human Surfactant Protein D Reduces Alveolar Macrophage Apoptosis and Pro-Inflammatory Cytokines in Mice Developing Pulmonary Emphysema. Ann N Y Acad Sci, 2003. 1010: 113-6.

134. Knudsen, L., M. Ochs, R. Mackay, P. Townsend, R. Deb, C. Muhlfeld, J. Richter, F. Gilbert, S. Hawgood, K. Reid, and H. Clark, Truncated Recombinant Human Sp-D Attenuates Emphysema and Type Ii Cell Changes in Sp-D Deficient Mice. Respir Res, 2007. 8: 70.

135. Ryan, U.S., J.W. Ryan, and D.S. Smith, Alveolar Type Ii Cells: Studies on the Mode of Release of Lamellar Bodies. Tissue & cell, 1975. 7: 587-99.

136. Rooney, S.A., B.A. Page-Roberts, and E.K. Motoyama, Role of Lamellar Inclusions in Surfactant Production: Studies on Phospholipid Composition and Biosynthesis in Rat and Rabbit Lung Subcellular Fractions. Journal of lipid research, 1975. 16: 418-25.

137. Voorhout, W.F., T. Veenendaal, H.P. Haagsman, A.J. Verkleij, L.M. van Golde, and H.J. Geuze, Surfactant Protein a Is Localized at the Corners of the Pulmonary Tubular Myelin Lattice. The journal of histochemistry and cytochemistry : official journal of the Histochemistry Society, 1991. 39: 1331-6.

138. Ikegami, M., T.R. Korfhagen, J.A. Whitsett, M.D. Bruno, S.E. Wert, K. Wada, and A.H. Jobe, Characteristics of Surfactant from Sp-a-Deficient Mice. The American journal of physiology, 1998. 275: L247-54.

139. Pan, T., L.D. Nielsen, M.J. Allen, K.M. Shannon, J.M. Shannon, M. Selman, and R.J. Mason, Serum Sp-D Is a Marker of Lung Injury in Rats. American journal of physiology. Lung cellular and molecular physiology, 2002. 282: L824-32.

140. Kobayashi, H., S. Kanoh, and K. Motoyoshi, Serum Surfactant Protein-a, but Not Surfactant Protein-D or Kl-6, Can Predict Preclinical Lung Damage Induced by Smoking. Biomarkers, 2008. 13: 385-92.

141. Maeda, H., M.Q. Fujita, B.L. Zhu, K. Ishida, L. Quan, S. Oritani, and M. Taniguchi, Pulmonary Surfactant-Associated Protein a as a Marker of Respiratory Distress in Forensic Pathology: Assessment of the Immunohistochemical and Biochemical Findings. Legal medicine (Tokyo, Japan), 2003. 5 Suppl 1: S318-21.

142. Honda, Y., Y. Kuroki, E. Matsuura, H. Nagae, H. Takahashi, T. Akino, and S. Abe, Pulmonary Surfactant Protein D in Sera and Bronchoalveolar Lavage Fluids. Am J Respir Crit Care Med, 1995. 152: 1860-6.

143. Takahashi, H., M. Shiratori, A. Kanai, H. Chiba, Y. Kuroki, and S. Abe, Monitoring Markers of Disease Activity for Interstitial Lung Diseases with Serum Surfactant Proteins a and D. Respirology, 2006. 11 Suppl: S51-4.

144. Olesen, H.V., U. Holmskov, P.O. Schiotz, and G.L. Sorensen, Serum-Surfactant Sp-D Correlates Inversely to Lung Function in Cystic Fibrosis. Journal of cystic fibrosis : official journal of the European Cystic Fibrosis Society, 2010. 9: 257-62.

145. Al-Salmi, Q.A., J.N. Walter, G.N. Colasurdo, M.M. Sockrider, E.O. Smith, H. Takahashi, and L.L. Fan, Serum Kl-6 and Surfactant Proteins a and D in Pediatric Interstitial Lung Disease. Chest, 2005. 127: 403-7.

146. Takahashi, H., T. Fujishima, H. Koba, S. Murakami, K. Kurokawa, Y. Shibuya, M. Shiratori, Y. Kuroki, and S. Abe, Serum Surfactant Proteins a and D as Prognostic Factors in Idiopathic Pulmonary Fibrosis and Their Relationship to Disease Extent. Am J Respir Crit Care Med, 2000. 162: 1109-14.

147. Ju, C.R., W. Liu, and R.C. Chen, Serum Surfactant Protein D: Biomarker of Chronic Obstructive Pulmonary Disease. Disease markers, 2012. 32: 281-7.

148. El-Deek, S.E., H.A. Makhlouf, T.H. Saleem, M.A. Mandour, and N.A. Mohamed, Surfactant Protein D, Soluble Intercellular Adhesion Molecule-1 and High-Sensitivity C-Reactive Protein as Biomarkers of Chronic Obstructive Pulmonary Disease. Medical principles and practice : international journal of the Kuwait University, Health Science Centre, 2013. 22: 469-74.

149. Ozyurek, B.A., S.S. Ulasli, S.S. Bozbas, N. Bayraktar, and S. Akcay, Value of Serum and Induced Sputum Surfactant Protein-D in Chronic Obstructive Pulmonary Disease. Multidisciplinary respiratory medicine, 2013. 8: 36.

150. Winkler, C., E.N. Atochina-Vasserman, O. Holz, M.F. Beers, V.J. Erpenbeck, N. Krug, S. Roepcke, G. Lauer, M. Elmlinger, and J.M. Hohlfeld, Comprehensive Characterisation of Pulmonary and Serum Surfactant Protein D in Copd. Respir Res, 2011. 12: 29.

151. Honda, Y., H. Takahashi, Y. Kuroki, T. Akino, and S. Abe, Decreased Contents of Surfactant Proteins a and D in Bal Fluids of Healthy Smokers. Chest, 1996. 109: 1006-9.

152. Postle, A.D., A. Mander, K.B. Reid, J.Y. Wang, S.M. Wright, M. Moustaki, and J.O. Warner, Deficient Hydrophilic Lung Surfactant Proteins a and D with Normal Surfactant Phospholipid Molecular Species in Cystic Fibrosis. Am J Respir Cell Mol Biol, 1999. 20: 90-8.

153. Noah, T.L., P.C. Murphy, J.J. Alink, M.W. Leigh, W.M. Hull, M.T. Stahlman, and J.A. Whitsett, Bronchoalveolar Lavage Fluid Surfactant Protein-a and Surfactant Protein-D Are Inversely Related to Inflammation in Early Cystic Fibrosis. Am J Respir Crit Care Med, 2003. 168: 685-91.

154. Griese, M., R. Essl, R. Schmidt, E. Rietschel, F. Ratjen, M. Ballmann, and K. Paul, Pulmonary Surfactant, Lung Function, and Endobronchial Inflammation in Cystic Fibrosis. Am J Respir Crit Care Med, 2004. 170: 1000-5.

155. von Bredow, C., A. Wiesener, and M. Griese, Proteolysis of Surfactant Protein D by Cystic Fibrosis Relevant Proteases. Lung, 2003. 181: 79-88.

156. Griese, M., N. Maderlechner, P. Ahrens, and R. Kitz, Surfactant Proteins a and D in Children with Pulmonary Disease Due to Gastroesophageal Reflux. American journal of respiratory and critical care medicine, 2002. 165: 1546-50.

157. Kunitake, R., K. Kuwano, K. Yoshida, T. Maeyama, M. Kawasaki, N. Hagimoto, and N. Hara, Kl-6, Surfactant Protein a and D in Bronchoalveolar Lavage Fluid from Patients with Pulmonary Sarcoidosis. Respiration, 2001. 68: 488-95.

158. Crouch, E., A. Persson, D. Chang, and D. Parghi, Surfactant Protein D. Increased Accumulation in Silica-Induced Pulmonary Lipoproteinosis. The American journal of pathology, 1991. 139: 765-76.

159. Ishii, H., H. Mukae, J. Kadota, H. Kaida, T. Nagata, K. Abe, S. Matsukura, and S. Kohno, High Serum Concentrations of Surfactant Protein a in Usual Interstitial Pneumonia Compared with Non-Specific Interstitial Pneumonia. Thorax, 2003. 58: 52-7.

160. Ishii, T., K. Hagiwara, K. Kamio, S. Ikeda, T. Arai, M.N. Mieno, T. Kumasaka, M. Muramatsu, M. Sawabe, A. Gemma, and K. Kida, Involvement of Surfactant Protein D in Emphysema Revealed by Genetic Association Study. European journal of human genetics : EJHG, 2012. 20: 230-5.

161. Karjalainen, M.K., J.M. Huusko, A. Tuohimaa, A. Luukkonen, R. Haataja, and M. Hallman, A Study of Collectin Genes in Spontaneous Preterm Birth Reveals an Association with a Common Surfactant Protein D Gene Polymorphism. Pediatr Res, 2012. 71: 93-9.

162. Selman, M., H.M. Lin, M. Montano, A.L. Jenkins, A. Estrada, Z. Lin, G. Wang, S.L. DiAngelo, X. Guo, T.M. Umstead, C.M. Lang, A. Pardo, D.S. Phelps, and J. Floros, Surfactant Protein a and B Genetic Variants Predispose to Idiopathic Pulmonary Fibrosis. Human genetics, 2003. 113: 542-50.

163. Jack, D.L., J. Cole, S.C. Naylor, R. Borrow, E.B. Kaczmarski, N.J. Klein, and R.C. Read, Genetic Polymorphism of the Binding Domain of Surfactant Protein-A2 Increases Susceptibility to Meningococcal Disease. Clinical infectious diseases : an official publication of the Infectious Diseases Society of America, 2006. 43: 1426-33.

164. Jiang, F., N.P. Caraway, B. Nebiyou Bekele, H.Z. Zhang, A. Khanna, H. Wang, R. Li, R.L. Fernandez, T.M. Zaidi, D.A. Johnston, and R.L. Katz, Surfactant Protein a Gene Deletion and Prognostics for Patients with Stage I Non-Small Cell Lung Cancer. Clin Cancer Res, 2005. 11: 5417-24.

165. Seifart, C., H.M. Lin, U. Seifart, A. Plagens, S. DiAngelo, P. von Wichert, and J. Floros, Rare Sp-a Alleles and the Sp-A1-6a(4) Allele Associate with Risk for Lung Carcinoma. Clinical genetics, 2005. 68: 128-36.

166. Shijubo, N., Y. Honda, T. Fujishima, H. Takahashi, T. Kodama, Y. Kuroki, T. Akino, and S. Abe, Lung Surfactant Protein-a and Carcinoembryonic Antigen in Pleural Effusions Due to Lung Adenocarcinoma and Malignant Mesothelioma. The European respiratory journal, 1995. 8: 403-6.

167. Griese, M., M. Neumann, T. von Bredow, R. Schmidt, and F. Ratjen, Surfactant in Children with Malignancies, Immunosuppression, Fever and Pulmonary Infiltrates. The European respiratory journal, 2002. 20: 1284-91.

168. D'Ovidio, F., H. Kaneda, C. Chaparro, M. Mura, D. Lederer, S. Di Angelo, H. Takahashi, C. Gutierrez, M. Hutcheon, L.G. Singer, T.K. Waddell, J. Floros, M. Liu, and S. Keshavjee, Pilot Study Exploring Lung Allograft Surfactant Protein a (Sp-a) Expression in Association with Lung Transplant Outcome. American journal of transplantation : official journal of the American Society of Transplantation and the American Society of Transplant Surgeons, 2013.

169. Aramini, B., C. Kim, S. Diangelo, E. Petersen, D.J. Lederer, L. Shah, H. Robbins, J. Floros, S.M. Arcasoy, J.R. Sonett, and F. D'Ovidio, Donor Surfactant Protein D (Sp-D) Polymorphisms Are Associated with Lung Transplant Outcome. American journal of transplantation : official journal of the American Society of Transplantation and the American Society of Transplant Surgeons, 2013. 13: 2130-6.

170. Bejvl, I., L. Weseslindtner, R. Strassl, P. Jaksch, M. Kundi, W. Klepetko, and E. Puchhammer-Stockl, Analysis of Plasma Surfactant Protein D Levels in Lung Transplant Recipients. Transplant infectious disease : an official journal of the Transplantation Society, 2013.

171. Gowdy, K.M., D.M. Cardona, J.L. Nugent, C. Giamberardino, J.M. Thomas, S. Mukherjee, T. Martinu, W.M. Foster, S.E. Plevy, A.M. Pastva, J.R. Wright, and S.M. Palmer, Novel Role for Surfactant Protein a in Gastrointestinal Graft-Versus-Host Disease. Journal of immunology (Baltimore, Md. : 1950), 2012. 188: 4897-905.

172. Palese, P. and M.L. Shaw, Orthomyxoviridae: The Viruses and Their Replication, in Fields Virology 5th Edition, D.M. Knipe and P.M. Howley, Editors. 2007, Lippincott Williams & Wilkins: Philadelphia. p. 1647-1689.

173. Organisation, W.H. Influenza (Seasonal): Fact Sheet Number 211.Http://Www.Who.Int/Mediacentre/Factsheets/Fs211/En/ 2009 20/08/2011].

174. Hardelid, P., R. Pebody, and N. Andrews, Mortality Caused by Influenza and Respiratory Syncytial Virus by Age Group in England and Wales 1999-2010. Influenza and other respiratory viruses, 2013. 7: 35-45.

175. Portela, A. and P. Digard, The Influenza Virus Nucleoprotein: A Multifunctional Rna-Binding Protein Pivotal to Virus Replication. Journal of General Virology, 2002. 83: 723-734.

176. Ruigrok, R.W.H., A. Barge, P. Durrer, J. Brunner, K. Ma, and G.R. Whittaker, Membrane Interaction of Influenza Virus M1 Protein. Virology, 2000. 267: 289-298.

177. Whittaker, G., M. Bui, and A. Helenius, The Role of Nuclear Import and Export in Influenza Virus Infection. Trends in Cell Biology, 1996. 6: 67-71.

178. Sieczkarski, S.B. and G.R. Whittaker, Influenza Virus Can Enter and Infect Cells in the Absence of Clathrin-Mediated Endocytosis. Journal of Virology, 2002. 76: 10455-10464.

179. Zhu, X., W. Yu, R. McBride, Y. Li, L.M. Chen, R.O. Donis, S. Tong, J.C. Paulson, and I.A. Wilson, Hemagglutinin Homologue from H17n10 Bat Influenza Virus Exhibits Divergent Receptor-Binding and Ph-Dependent Fusion Activities. Proc Natl Acad Sci U S A, 2013. 110: 1458-63.

180. Sieczkarski, S.B. and G.R. Whittaker, Characterization of the Host Cell Entry of Filamentous Influenza Virus. Archives of Virology, 2005. 150: 1783-1796.

181. Sidorenko, Y. and U. Reichl, Structured Model of Influenza Virus Replication in Mdck Cells. Biotechnology and Bioengineering, 2004. 88: 1-14.

182. van Eijk, M., M.R. White, J.J. Batenburg, A.B. Vaandrager, L.M.G. van Golde, H.P. Haagsman, and K.L. Hartshorn, Interactions of Influenza a Virus with Sialic Acids Present on Porcine Surfactant Protein D. American Journal of Respiratory Cell and Molecular Biology, 2004. 30: 871-879.

183. Nunes-Correia, I., J. Ramalho-Santos, S. Nir, and M.C.P. de Lima, Interactions of Influenza Virus with Cultured Cells: Detailed Kinetic Modeling of Binding and Endocytosis. Biochemistry, 1999. 38: 1095-1101.

184. Martin, K. and A. Helenius, Transport of Incoming Influenza-Virus Nucleocapsids into the Nucleus. Journal of Virology, 1991. 65: 232-244.

185. Engel, S., S. Scolari, B. Thaa, N. Krebs, T. Korte, A. Herrmann, and M. Veit, Flim-Fret and Frap Reveal Association of Influenza Virus Haemagglutinin with Membrane Rafts. Biochemical Journal, 2010. 425: 567-573.

186. Barman, S., L. Adhikary, Y. Kawaoka, and D.P. Nayak, Influenza a Virus Hemagglutinin Containing Basolateral Localization Signal Does Not Alter the Apical Budding of a Recombinant Influenza a Virus in Polarized Mdck Cells. Virology, 2003. 305: 138-152.

187. Gomez-Puertas, P., C. Albo, E. Perez-Pastrana, A. Vivo, and A. Portela, Influenza Virus Matrix Protein Is the Major Driving Force in Virus Budding. Journal of Virology, 2000. 74: 11538-11547.

188. Korte, T., K. Ludwig, F.P. Booy, R. Blumenthal, and A. Herrmann, Conformational Intermediates and Fusion Activity of Influenza Virus Hemagglutinin. Journal of Virology, 1999. 73: 4567-4574.

189. Bottcher, E., T. Matrosovich, M. Beyerle, H.-D. Klenk, W. Garten, and M. Matrosovich, Proteolytic Activation of Influenza Viruses by Serine Proteases Tmprss2 and Hat from Human Airway Epithelium. Journal of Virology, 2006. 80: 9896-9898.

190. Tecle, T., M.R. White, E.C. Crouch, and K.L. Hartshorn, Inhibition of Influenza Viral Neuraminidase Activity by Collectins. Archives of Virology, 2007. 152: 1731-1742.

191. Benne, C.A., C.A. Kraaijeveld, J.A.G. Vanstrijp, E. Brouwer, M. Harmsen, J. Verhoef, L.M.G. Vangolde, and J.F. Vaniwaarden, Interactions of Surfactant Protein-a with Influenza-a Viruses - Binding and Neutralization. Journal of Infectious Diseases, 1995. 171: 335-341.

192. Anders, E.M., C.A. Hartley, and D.C. Jackson, Bovine and Mouse Serum Beta-Inhibitors of Influenza-a Viruses Are Mannose-Binding Lectins. Proceedings of the National Academy of Sciences of the United States of America, 1990. 87: 4485-4489.

193. Hartley, C.A., D.C. Jackson, and E.M. Anders, 2 Distinct Serum Mannose-Binding Lectins Function as Beta-Inhibitors of Influenza-Virus - Identification of Bovine Serum Beta-Inhibitor as Conglutinin. Journal of Virology, 1992. 66: 4358-4363.

194. Hartley, C.A., P.C. Reading, A.C. Ward, and E.M. Anders, Changes in the Hemagglutinin Molecule of Influenza Type a (H3n2) Virus Associated with Increased Virulence for Mice. Archives of Virology, 1997. 142: 75-88.

195. Li, G., J. Siddiqui, M. Hendry, J. Akiyama, J. Edmondson, C. Brown, L. Allen, S. Levitt, F. Poulain, and S. Hawgood, Surfactant Protein-a-Deficient Mice Display an Exaggerated Early Inflammatory Response to a Beta-Resistant Strain of Influenza a Virus. American Journal of Respiratory Cell and Molecular Biology, 2002. 26: 277-282.

196. Hartshorn, K.L., M.R. White, V. Shepherd, K. Reid, J.C. Jensenius, and E.C. Crouch, Mechanisms of Anti-Influenza Activity of Surfactant Proteins a and D: Comparison with Serum Collectins. American Journal of Physiology, 1997. 273: L1156-L1166.

197. Benne, C.A., B. Benaissa-Trouw, J.A. van Strijp, C.A. Kraaijeveld, and J.F. van Iwaarden, Surfactant Protein a, but Not Surfactant Protein D, Is an Opsonin for Influenza a Virus Phagocytosis by Rat Alveolar Macrophages. Eur J Immunol, 1997. 27: 886-90.

198. White, M., P. Kingma, T. Tecle, N. Kacak, B. Linders, J. Heuser, E. Crouch, and K. Hartshorn, Multimerization of Surfactant Protein D, but Not Its Collagen Domain, Is Required for Antiviral and Opsonic Activities Related to Influenza Virus. Journal of immunology (Baltimore, Md. : 1950), 2008. 181: 7936-43.

199. Ciencewicki, J., K. Gowdy, Q.T. Krantz, W.P. Linak, L. Brighton, M.I. Gilmour, and I. Jaspers, Diesel Exhaust Enhanced Susceptibility to Influenza Infection Is Associated with Decreased Surfactant Protein Expression. Inhalation Toxicology, 2007. 19: 1121-1133.

200. Gowdy, K.M., Q.T. Krantz, C. King, E. Boykin, I. Jaspers, W.P. Linak, and M.I. Gilmour, Role of Oxidative Stress on Diesel-Enhanced Influenza Infection in Mice. Particle and Fibre Toxicology, 2010. 7.

201. Jaspers, I., J. Ciencewicki, W.L. Zhang, M. Brighton, and M. Madden, Diesel Exhaust Particles Enhance Influenza Virus Infections Via Oxidative Stress. Free Radical Biology and Medicine, 2004. 37: S142-S142.

202. Jaspers, I., P.A. Sheridan, W. Zhang, L.E. Brighton, K.D. Chason, X. Hua, and S.L. Tilley, Exacerbation of Allergic Inflammation in Mice Exposed to Diesel Exhaust Particles Prior to Viral Infection. Particle and Fibre Toxicology, 2009. 6.

203. Gerke, A.K., F. Tang, M. Yang, E.D. Foster, J.E. Cavanaugh, and P.M. Polgreen, Predicting Chronic Obstructive Pulmonary Disease Hospitalizations Based on Concurrent Influenza Activity. Copd, 2013. 10: 573-80.

204. Wu, W., K.B. Patel, J.L. Booth, W. Zhang, and J.P. Metcalf, Cigarette Smoke Extract Suppresses the Rig-I-Initiated Innate Immune Response to Influenza Virus in the Human Lung. American Journal of Physiology-Lung Cellular and Molecular Physiology, 2011. 300: L821-L830.

205. Noah, T.L., H. Zhou, J. Monaco, K. Horvath, M. Herbst, and I. Jaspers, Tobacco Smoke Exposure and Altered Nasal Responses to Live

Attenuated Influenza Virus. Environmental Health Perspectives, 2011. 119: 78-83.

206. Liu, S., J. Sun, J. Cai, Z. Miao, M. Lu, S. Qin, X. Wang, H. Lv, Z. Yu, S. Amer, and C. Chai, Epidemiological, Clinical and Viral Characteristics of Fatal Cases of Human Avian Influenza a (H7n9) Virus in Zhejiang Province, China. The Journal of infection, 2013.

207. Xu, C., A.D. Iuliano, M. Chen, P.Y. Cheng, T. Chen, J. Shi, J. Yang, L. Wang, F. Yuan, M.A. Widdowson, and Y. Shu, Characteristics of Hospitalized Cases with Influenza a (H1n1)Pdm09 Infection During First Winter Season of Post-Pandemic in China. PLoS One, 2013. 8: e55016.

208. Bauer, C.M.T., C.C.J. Zavitz, F.M. Botelho, K.N. Lambert, E.G. Brown, K.L. Mossman, J.D. Taylor, and M.R. Staempfli, Treating Viral Exacerbations of Chronic Obstructive Pulmonary Disease: Insights from a Mouse Model of Cigarette Smoke and H1n1 Influenza Infection. Plos One, 2010. 5.

209. Gualano, R.C., M.J. Hansen, R. Vlahos, J.E. Jones, R.A. Park-Jones, G. Deliyannis, S.J. Turner, K.A. Duca, and G.P. Anderson, Cigarette Smoke Worsens Lung Inflammation and Impairs Resolution of Influenza Infection in Mice. Respiratory Research, 2008. 9.

210. Feng, Y., Y. Kong, P.F. Barnes, F.-F. Huang, P. Klucar, X. Wang, B. Samten, M. Sengupta, B. Machona, R. Donis, A.R. Tvinnereim, and H. Shams, Exposure to Cigarette Smoke Inhibits the Pulmonary T-Cell Response to Influenza Virus and Mycobacterium Tuberculosis. Infection and Immunity, 2011. 79: 229-237.

211. Dockery, D.W., C.A. Pope, X.P. Xu, J.D. Spengler, J.H. Ware, M.E. Fay, B.G. Ferris, and F.E. Speizer, An Association between Air-Pollution and

Mortality in 6 United-States Cities. New England Journal of Medicine, 1993. 329: 1753-1759.

212. Krewski, D., R. Burnett, M. Jerrett, C.A. Pope, D. Rainham, E. Calle, G. Thurston, and M. Thun, Mortality and Long-Term Exposure to Ambient Air Pollution: Ongoing Analyses Based on the American Cancer Society Cohort. Journal of Toxicology and Environmental Health-Part a-Current Issues, 2005. 68: 1093-1109.

213. Lin, Y.J., M. Karuppiah, A. Shaw, and G. Gupta, Effect of Simulated Sunlight on Atrazine and Metolachlor Toxicity of Surface Waters. Ecotoxicology and Environmental Safety, 1999. 43: 35-37.

214. Kashima, S., T. Yorifuji, T. Tsuda, J. Ibrahim, and H. Doi, Effects of Traffic-Related Outdoor Air Pollution on Respiratory Illness and Mortality in Children, Taking into Account Indoor Air Pollution, in Indonesia. Journal of Occupational and Environmental Medicine, 2010. 52: 340-345.

215. Stern, G., P. Latzin, M. Roosli, O. Fuchs, E. Proietti, C. Kuehni, and U. Frey, A Prospective Study of the Impact of Air Pollution on Respiratory Symptoms and Infections in Infants. Am J Respir Crit Care Med, 2013. 187: 1341-8.

216. Dominici, F., R.D. Peng, M.L. Bell, L. Pham, A. McDermott, S.L. Zeger, and J.M. Samet, Fine Particulate Air Pollution and Hospital Admission for Cardiovascular and Respiratory Diseases. Jama-Journal of the American Medical Association, 2006. 295: 1127-1134.

217. Jimenez, E., C. Linares, D. Martinez, and J. Diaz, Particulate Air Pollution and Short-Term Mortality Due to Specific Causes among the Elderly in

Madrid (Spain): Seasonal Differences. International journal of environmental health research, 2011. 21: 372-90.

218. Jedrychowski, W.A., F.P. Perera, J.D. Spengler, E. Mroz, L. Stigter, E. Flak, R. Majewska, M. Klimaszewska-Rembiasz, and R. Jacek, Intrauterine Exposure to Fine Particulate Matter as a Risk Factor for Increased Susceptibility to Acute Broncho-Pulmonary Infections in Early Childhood. Int J Hyg Environ Health, 2013. 216: 395-401.

219. Gurley, E.S., N. Homaira, H. Salje, P.K. Ram, R. Haque, W. Petri, J. Bresee, W.J. Moss, P. Breysse, S.P. Luby, and E. Azziz-Baumgartner, Indoor Exposure to Particulate Matter and the Incidence of Acute Lower Respiratory Infections among Children: A Birth Cohort Study in Urban Bangladesh. Indoor Air, 2013.

220. Black, R.E., S.S. Morris, and J. Bryce, Where and Why Are 10 Million Children Dying Every Year? Lancet, 2003. 361: 2226-34.

221. Harrod, K.S., R.J. Jaramillo, C.L. Rosenberger, S.Z. Wang, J.A. Berger, J.D. McDonald, and M.D. Reed, Increased Susceptibility to Rsv Infection by Exposure to Inhaled Diesel Engine Emissions. Am J Respir Cell Mol Biol, 2003. 28: 451-63.

222. Hahon, N., J.A. Booth, F. Green, and T.R. Lewis, Influenza Virus Infection in Mice after Exposure to Coal Dust and Diesel Engine Emissions. Environ Res, 1985. 37: 44-60.

223. Tellabati, A., V.E. Fernandes, F. Teichert, R. Singh, J. Rylance, S. Gordon, P.W. Andrew, and J. Grigg, Acute Exposure of Mice to High-Dose Ultrafine Carbon Black Decreases Susceptibility to Pneumococcal Pneumonia. Part Fibre Toxicol, 2010. 7: 30.

224. Zelikoff, J.T., L.C. Chen, M.D. Cohen, K. Fang, T. Gordon, Y. Li, C. Nadziejko, and R.B. Schlesinger, Effects of Inhaled Ambient Particulate Matter on Pulmonary Antimicrobial Immune Defense. Inhal Toxicol, 2003. 15: 131-50.

225. Oishi, K., Y. Miyamoto, H. Saito, K. Murase, K. Ono, M. Sawada, M. Watanabe, Y. Noguchi, T. Fujiwara, S. Hayashi, and H. Noguchi, In Vivo Imaging of Transplanted Islets Labeled with a Novel Cationic Nanoparticle. PLoS One, 2013. 8: e57046.

226. Patnaik, S. and K.C. Gupta, Novel Polyethylenimine-Derived Nanoparticles for in Vivo Gene Delivery. Expert Opin Drug Deliv, 2013. 10: 215-28.

227. Wang, W., F. Zhou, L. Ge, X. Liu, and F. Kong, Transferrin-Peg-Pe Modified Dexamethasone Conjugated Cationic Lipid Carrier Mediated Gene Delivery System for Tumor-Targeted Transfection. International journal of nanomedicine, 2012. 7: 2513-22.

228. Giri, N., P. Tomar, V.S. Karwasara, R.S. Pandey, and V.K. Dixit, Targeted Novel Surface-Modified Nanoparticles for Interferon Delivery for the Treatment of Hepatitis B. Acta biochimica et biophysica Sinica, 2011. 43: 877-83.

229. Deng, Z., Z. Zhen, X. Hu, S. Wu, Z. Xu, and P.K. Chu, Hollow Chitosan-Silica Nanospheres as Ph-Sensitive Targeted Delivery Carriers in Breast Cancer Therapy. Biomaterials, 2011. 32: 4976-86.

230. Zheng, C., M. Zheng, P. Gong, J. Deng, H. Yi, P. Zhang, Y. Zhang, P. Liu, Y. Ma, and L. Cai, Polypeptide Cationic Micelles Mediated Co-Delivery

of Docetaxel and Sirna for Synergistic Tumor Therapy. Biomaterials, 2013. 34: 3431-8.

231. Zhang, Y., C. Xu, B. Li, and Y. Li, In Situ Growth of Positively-Charged Gold Nanoparticles on Single-Walled Carbon Nanotubes as a Highly Active Peroxidase Mimetic and Its Application in Biosensing. Biosens Bioelectron, 2013. 43: 205-10.

232. Jennings, J., D. Hüglin, J. Mao, and A. MÜHLEBACH, Preparation of Cationic Nanoparticles and Personal Care Compositions Comprising Said Nanoparticles. 2010.

233. Pereda, M.D.C.V., M.A. Polezel, G.C. Dieamant, C. Nogueira, A.G. Marcelino, M.R. Rossan, and S.M.H. Andrade, Sericin Cationic Nanoparticles for Application in Products for Hair and Dyed Hair. 2010.

234. Jennings, J., D. Haglin, J. Mao, and A. Muhlebach, Preparation of Cationic Nanoparticles and Personal Care Compositions Comprising Said Nanoparticles. 2009: US.

235. Salman, H.H.A., A.I. GOÑI, and C.I. ESPARZA, Nanoparticles Comprising a Vegetable Hydrophobic Protein and a Water Miscible Non-Volatile Organic Solvent and Uses Thereof. 2013.

236. Siqueira, N.M., R.V. Contri, K. Paese, R.C. Beck, A.R. Pohlmann, and S.S. Guterres, Innovative Sunscreen Formulation Based on Benzophenone-3-Loaded Chitosan-Coated Polymeric Nanocapsules. Skin Pharmacol Physiol, 2011. 24: 166-74.

237. Clottens, F.L., E.K. Verbeken, M. Demedts, and B. Nemery, Pulmonary Toxicity of Components of Textile Paint Linked to the Ardystil

Syndrome: Intratracheal Administration in Hamsters. Occup Environ Med, 1997. 54: 376-87.

238. Hoet, P.H., L. Gilissen, and B. Nemery, Polyanions Protect against the in Vitro Pulmonary Toxicity of Polycationic Paint Components Associated with the Ardystil Syndrome. Toxicol Appl Pharmacol, 2001. 175: 184-90.

239. Hoet, P.H., L.P. Gilissen, M. Leyva, and B. Nemery, In Vitro Cytotoxicity of Textile Paint Components Linked to the "Ardystil Syndrome". Toxicological sciences : an official journal of the Society of Toxicology, 1999. 52: 209-16.

240. Dombu, C.Y., M. Kroubi, R. Zibouche, R. Matran, and D. Betbeder, Characterization of Endocytosis and Exocytosis of Cationic Nanoparticles in Airway Epithelium Cells. Nanotechnology, 2010. 21: 355102.

241. Yang, S.H., D. Heo, J. Park, S. Na, J.S. Suh, S. Haam, S.W. Park, Y.M. Huh, and J. Yang, Role of Surface Charge in Cytotoxicity of Charged Manganese Ferrite Nanoparticles Towards Macrophages. Nanotechnology, 2012. 23: 505702.

242. Miragoli, M., P. Novak, P. Ruenraroengsak, A.I. Shevchuk, Y.E. Korchev, M.J. Lab, T.D. Tetley, and J. Gorelik, Functional Interaction between Charged Nanoparticles and Cardiac Tissue: A New Paradigm for Cardiac Arrhythmia? Nanomedicine (London, England), 2013. 8: 725-37.

243. Ruenraroengsak, P., P. Novak, D. Berhanu, A.J. Thorley, E. Valsami-Jones, J. Gorelik, Y.E. Korchev, and T.D. Tetley, Respiratory Epithelial Cytotoxicity and Membrane Damage (Holes) Caused by Amine-Modified Nanoparticles. Nanotoxicology, 2012. 6: 94-108.

244. Wang, F., L. Yu, M.P. Monopoli, P. Sandin, E. Mahon, A. Salvati, and K.A. Dawson, The Biomolecular Corona Is Retained During Nanoparticle Uptake and Protects the Cells from the Damage Induced by Cationic Nanoparticles until Degraded in the Lysosomes. Nanomedicine, 2013.

245. Lunov, O., T. Syrovets, C. Loos, G.U. Nienhaus, V. Mailaender, K. Landfester, M. Rouis, and T. Simmet, Amino-Functionalized Polystyrene Nanoparticles Activate the Nlrp3 Inflammasome in Human Macrophages. Acs Nano, 2011. 5: 9648-9657.

246. Xia, T., M. Kovochich, M. Liong, J.I. Zink, and A.E. Nel, Cationic Polystyrene Nanosphere Toxicity Depends on Cell-Specific Endocytic and Mitochondrial Injury Pathways. ACS Nano, 2008. 2: 85-96.

247. Nel, A.E., L. Madler, D. Velegol, T. Xia, E.M.V. Hoek, P. Somasundaran, F. Klaessig, V. Castranova, and M. Thompson, Understanding Biophysicochemical Interactions at the Nano-Bio Interface. Nature Materials, 2009. 8: 543-557.

248. Deng, Z.J., M. Liang, I. Toth, M.J. Monteiro, and R.F. Minchin, Molecular Interaction of Poly(Acrylic Acid) Gold Nanoparticles with Human Fibrinogen. ACS Nano, 2012. 6: 8962-9.

249. Barran-Berdon, A.L., D. Pozzi, G. Caracciolo, A.L. Capriotti, G. Caruso, C. Cavaliere, A. Riccioli, S. Palchetti, and A. Lagana, Time Evolution of Nanoparticle-Protein Corona in Human Plasma: Relevance for Targeted Drug Delivery. Langmuir, 2013. 29: 6485-94.

250. Cedervall, T., I. Lynch, S. Lindman, T. Berggard, E. Thulin, H. Nilsson, K.A. Dawson, and S. Linse, Understanding the Nanoparticle-Protein Corona Using Methods to Quantify Exchange Rates and Affinities of

Proteins for Nanoparticles. Proceedings of the National Academy of Sciences of the United States of America, 2007. 104: 2050-2055.

251. Lundqvist, M., J. Stigler, G. Elia, I. Lynch, T. Cedervall, and K.A. Dawson, Nanoparticle Size and Surface Properties Determine the Protein Corona with Possible Implications for Biological Impacts. Proceedings of the National Academy of Sciences of the United States of America, 2008. 105: 14265-14270.

252. Mahmoudi, M., M.A. Shokrgozar, S. Sardari, M.K. Moghadam, H. Vali, S. Laurent, and P. Stroeve, Irreversible Changes in Protein Conformation Due to Interaction with Superparamagnetic Iron Oxide Nanoparticles. Nanoscale, 2011. 3: 1127-1138.

253. Monopoli, M.P., D. Walczyk, A. Campbell, G. Elia, I. Lynch, F.B. Bombelli, and K.A. Dawson, Physical-Chemical Aspects of Protein Corona: Relevance to in Vitro and in Vivo Biological Impacts of Nanoparticles. Journal of the American Chemical Society, 2011. 133: 2525-2534.

254. Chakraborty, S., P. Joshi, V. Shanker, Z.A. Ansari, S.P. Singh, and P. Chakrabarti, Contrasting Effect of Gold Nanoparticles and Nanorods with Different Surface Modifications on the Structure and Activity of Bovine Serum Albumin. Langmuir, 2011. 27: 7722-7731.

255. Baier, G., C. Costa, A. Zeller, D. Baumann, C. Sayer, P.H.H. Araujo, V. Mailaender, A. Musyanovych, and K. Landfester, Bsa Adsorption on Differently Charged Polystyrene Nanoparticles Using Isothermal Titration Calorimetry and the Influence on Cellular Uptake. Macromolecular Bioscience, 2011. 11: 628-638.

256. Gehr, P., M. Geiser, V.I. Hof, S. Schurch, U. Waber, and M. Baumann, Surfactant and Inhaled Particles in the Conducting Airways - Structural, Stereological, and Biophysical Aspects. Microscopy Research and Technique, 1993. 26: 423-436.

257. Schleh, C., C. Muhlfeld, K. Pulskamp, A. Schmiedl, M. Nassimi, H.D. Lauenstein, A. Braun, N. Krug, V.J. Erpenbeck, and J.M. Hohlfeld, The Effect of Titanium Dioxide Nanoparticles on Pulmonary Surfactant Function and Ultrastructure. Respiratory Research, 2009. 10.

258. Bakshi, M.S., L. Zhao, R. Smith, F. Possmayer, and N.O. Petersen, Metal Nanoparticle Pollutants Interfere with Pulmonary Surfactant Function in Vitro. Biophysical journal, 2008. 94: 855-868.

259. Goerke, J., Pulmonary Surfactant: Functions and Molecular Composition. Biochimica Et Biophysica Acta-Molecular Basis of Disease, 1998. 1408: 79-89.

260. Kendall, M., L. Brown, and K. Trought, Molecular Adsorption at Particle Surfaces: A Pm Toxicity Mediation Mechanism. Inhalation Toxicology, 2004. 16: 99-105.

261. Evora, C., I. Soriano, R.A. Rogers, K.M. Shakesheff, J. Hanes, and R. Langer, Relating the Phagocytosis of Microparticles by Alveolar Macrophages to Surface Chemistry: The Effect of 1,2-Dipalmitoylphosphatidylcholine. Journal of Controlled Release, 1998. 51: 143-152.

262. Kendall, M., Fine Airborne Urban Particles (Pm2.5) Sequester Lung Surfactant and Amino Acids from Human Lung Lavage. Am J Physiol-Lung C, 2007. 293: L1053-L1058.

263. Salvador-Morales, C., P. Townsend, E. Flahaut, C. Venien-Bryan, A. Vlandas, M.L.H. Green, and R.B. Sim, Binding of Pulmonary Surfactant Proteins to Carbon Nanotubes; Potential for Damage to Lung Immune Defense Mechanisms. Carbon, 2007. 45: 607-617.

264. Stringer, B. and L. Kobzik, Alveolar Macrophage Uptake of the Environmental Particulate Titanium Dioxide: Role of Surfactant Components. Am J Respir Cell Mol Biol, 1996. 14: 155-60.

265. Schulze, C., U.F. Schaefer, C.A. Ruge, W. Wohlleben, and C.M. Lehr, Interaction of Metal Oxide Nanoparticles with Lung Surfactant Protein A. European Journal of Pharmaceutics and Biopharmaceutics, 2011. 77: 376-383.

266. Ruge, C.A., J. Kirch, O. Canadas, M. Schneider, J. Perez-Gil, U.F. Schaefer, C. Casals, and C.M. Lehr, Uptake of Nanoparticles by Alveolar Macrophages Is Triggered by Surfactant Protein A. Nanomedicine, 2011. 7: 690-3.

267. Ruge, C.A., U.F. Schaefer, J. Herrmann, J. Kirch, O. Canadas, M. Echaide, J. Perez-Gil, C. Casals, R. Muller, and C.M. Lehr, The Interplay of Lung Surfactant Proteins and Lipids Assimilates the Macrophage Clearance of Nanoparticles. PLoS One, 2012. 7: e40775.

268. Schleh, C., U. Holzwarth, S. Hirn, A. Wenk, F. Simonelli, M. Schaffler, W. Moller, N. Gibson, and W.G. Kreyling, Biodistribution of Inhaled Gold Nanoparticles in Mice and the Influence of Surfactant Protein D. J Aerosol Med Pulm Drug Deliv, 2013. 26: 24-30.

269. Kendall, K., M. Kendall, and F. Rehfeldt, Adhesion of Cells, Viruses and Nanoparticles. Adhesion of Cells, Viruses and Nanoparticles. 2011.

270. Clark, H., N. Palaniyar, P. Strong, J. Edmondson, S. Hawgood, and K.B.M. Reid, Surfactant Protein D Reduces Alveolar Macrophage Apoptosis in Vivo. Journal of Immunology, 2002. 169: 2892-2899.

271. Wright, J.R., Purification of Surfactant Protein a from the Bronchoalveolar Lavage Fluid of Alveolar Proteinosis Patients, J. Madsen, Editor. 2011: Southampton.

272. Strong, P., U. Kishore, C. Morgan, A. Lopez Bernal, M. Singh, and K.B. Reid, A Novel Method of Purifying Lung Surfactant Proteins a and D from the Lung Lavage of Alveolar Proteinosis Patients and from Pooled Amniotic Fluid. J Immunol Methods, 1998. 220: 139-49.

273. Leth-Larsen, R., C. Nordenbaek, I. Tornoe, V. Moeller, A. Schlosser, C. Koch, B. Teisner, P. Junker, and U. Holmskov, Surfactant Protein D (Sp-D) Serum Levels in Patients with Community-Acquired Pneumonia Small Star, Filled. Clinical immunology (Orlando, Fla.), 2003. 108: 29-37.

274. Wright, J.R., R.E. Wager, S. Hawgood, L. Dobbs, and J.A. Clements, Surfactant Apoprotein Mr = 26,000-36,000 Enhances Uptake of Liposomes by Type Ii Cells. The Journal of biological chemistry, 1987. 262: 2888-94.

275. Wang, T., C.A. Lazar, M.C. Fishbein, and J.P. Lynch, 3rd, Pulmonary Alveolar Proteinosis. Seminars in respiratory and critical care medicine, 2012. 33: 498-508.

276. Crouch, E., A. Persson, and D. Chang, Accumulation of Surfactant Protein D in Human Pulmonary Alveolar Proteinosis. The American journal of pathology, 1993. 142: 241-8.

277. Campo, I., Z. Kadija, F. Mariani, E. Paracchini, G. Rodi, F. Mojoli, A. Braschi, and M. Luisetti, Pulmonary Alveolar Proteinosis: Diagnostic and

Therapeutic Challenges. Multidisciplinary respiratory medicine, 2012. 7: 4.

278. Leth-Larsen, R., U. Holmskov, and P. Hojrup, Structural Characterization of Human and Bovine Lung Surfactant Protein D. The Biochemical journal, 1999. 343 Pt 3: 645-52.

279. Mason, R.J., L.D. Nielsen, Y. Kuroki, E. Matsuura, J.H. Freed, and J.M. Shannon, A 50-Kda Variant Form of Human Surfactant Protein D. The European respiratory journal, 1998. 12: 1147-55.

280. Duvoix, A., E. Miranda, J. Perez, G.L. Sorensen, U. Holmskov, B.C. Trapnell, J. Madsen, H.W. Clark, L.D. Edwards, B.E. Miller, R.M. Tal-Singer, and D.A. Lomas, Evaluation of Full-Length, Cleaved and Nitrosylated Serum Surfactant Protein D as Biomarkers for Copd. Copd, 2011. 8: 79-95.

281. Sorensen, G.L., S.V. Hoegh, R. Leth-Larsen, T.H. Thomsen, C. Floridon, K. Smith, K. Kejling, I. Tornoe, E.C. Crouch, and U. Holmskov, Multimeric and Trimeric Subunit Sp-D Are Interconvertible Structures with Distinct Ligand Interaction. Molecular Immunology, 2009. 46: 3060-3069.

282. Altman, M., M. Vanpée, S. Cnattingius, and M. Norman, Neonatal Morbidity in Moderately Preterm Infants: A Swedish National Population-Based Study. The Journal of Pediatrics, 2011. 158: 239-244.e1.

283. Donn, S.M. and J. Dalton, Surfactant Replacement Therapy in the Neonate: Beyond Respiratory Distress Syndrome. Respiratory care, 2009. 54: 1203-8.

284. Halliday, H.L., Controversies: Synthetic or Natural Surfactant. The Case for Natural Surfactant. Journal of perinatal medicine, 1996. 24: 417-26.

285. Walti, H. and M. Monset-Couchard, A Risk-Benefit Assessment of Natural and Synthetic Exogenous Surfactants in the Management of Neonatal Respiratory Distress Syndrome. Drug safety : an international journal of medical toxicology and drug experience, 1998. 18: 321-37.

286. Kresch, M.J. and J.M. Clive, Meta-Analyses of Surfactant Replacement Therapy of Infants with Birth Weights Less Than 2000 Grams. Journal of perinatology : official journal of the California Perinatal Association, 1998. 18: 276-83.

287. Seehase, M., J.J. Collins, E. Kuypers, R.K. Jellema, D.R. Ophelders, O.L. Ospina, J. Perez-Gil, F. Bianco, R. Garzia, R. Razzetti, and B.W. Kramer, New Surfactant with Sp-B and C Analogs Gives Survival Benefit after Inactivation in Preterm Lambs. PLoS One, 2012. 7: e47631.

288. Clark, H. and K. Reid, The Potential of Recombinant Surfactant Protein D Therapy to Reduce Inflammation in Neonatal Chronic Lung Disease, Cystic Fibrosis, and Emphysema. Archives of disease in childhood, 2003. 88: 981-4.

289. Strong, P., P. Townsend, R. Mackay, K.B. Reid, and H.W. Clark, A Recombinant Fragment of Human Sp-D Reduces Allergic Responses in Mice Sensitized to House Dust Mite Allergens. Clinical and experimental immunology, 2003. 134: 181-7.

290. Strong, P., K.B. Reid, and H. Clark, Intranasal Delivery of a Truncated Recombinant Human Sp-D Is Effective at Down-Regulating Allergic Hypersensitivity in Mice Sensitized to Allergens of Aspergillus Fumigatus. Clinical and experimental immunology, 2002. 130: 19-24.

291. Kendall, M., P. Ding, R.M. Mackay, R. Deb, Z. McKenzie, K. Kendall, J. Madsen, and H. Clark, Surfactant Protein D (Sp-D) Alters Cellular Uptake of Particles and Nanoparticles. Nanotoxicology, 2013. 7: 963-73.

292. Jena, P., S. Mohanty, R. Mallick, B. Jacob, and A. Sonawane, Toxicity and Antibacterial Assessment of Chitosan-Coated Silver Nanoparticles on Human Pathogens and Macrophage Cells. International journal of nanomedicine, 2012. 7: 1805-1818.

293. Giard, D.J., S.A. Aaronson, G.J. Todaro, P. Arnstein, J.H. Kersey, H. Dosik, and W.P. Parks, In Vitro Cultivation of Human Tumors: Establishment of Cell Lines Derived from a Series of Solid Tumors. Journal of the National Cancer Institute, 1973. 51: 1417-23.

294. Moschini, E., M. Gualtieri, M. Colombo, U. Fascio, M. Camatini, and P. Mantecca, The Modality of Cell-Particle Interactions Drives the Toxicity of Nanosized Cuo and Tio2 in Human Alveolar Epithelial Cells. Toxicol Lett, 2013. 222: 102-16.

295. Okoturo-Evans, O., A. Dybowska, E. Valsami-Jones, J. Cupitt, M. Gierula, A.R. Boobis, and R.J. Edwards, Elucidation of Toxicity Pathways in Lung Epithelial Cells Induced by Silicon Dioxide Nanoparticles. PloS one, 2013. 8: e72363.

296. Paranjpe, M., V. Neuhaus, J.H. Finke, C. Richter, T. Gothsch, A. Kwade, S. Buttgenbach, A. Braun, and C.C. Muller-Goymann, In Vitro and Ex Vivo Toxicological Testing of Sildenafil-Loaded Solid Lipid Nanoparticles. Inhal Toxicol, 2013. 25: 536-43.

297. Hartshorn, K.L., M.R. White, T. Tecle, G. Sorensen, U. Holmskov, and E.C. Crouch, Viral Aggregating and Opsonizing Activity in Collectin

Trimers. American Journal of Physiology-Lung Cellular and Molecular Physiology, 2010. 298: L79-L88.

298. Gref, R., M. Luck, P. Quellec, M. Marchand, E. Dellacherie, S. Harnisch, T. Blunk, and R.H. Muller, 'Stealth' Corona-Core Nanoparticles Surface Modified by Polyethylene Glycol (Peg): Influences of the Corona (Peg Chain Length and Surface Density) and of the Core Composition on Phagocytic Uptake and Plasma Protein Adsorption. Colloids and surfaces. B, Biointerfaces, 2000. 18: 301-313.

299. Lesniak, A., A. Campbell, M.P. Monopoli, I. Lynch, A. Salvati, and K.A. Dawson, Serum Heat Inactivation Affects Protein Corona Composition and Nanoparticle Uptake. Biomaterials, 2010. 31: 9511-8.

300. Lesniak, A., F. Fenaroli, M.P. Monopoli, C. Aberg, K.A. Dawson, and A. Salvati, Effects of the Presence or Absence of a Protein Corona on Silica Nanoparticle Uptake and Impact on Cells. ACS Nano, 2012. 6: 5845-57.

301. Sampson, J.R., S. Jones, S. Dolwani, and J.P. Cheadle, Mutyh (Myh) and Colorectal Cancer. Biochemical Society Transactions, 2005. 33: 679-683.

302. Kendall, M., P. Ding, and K. Kendall, Particle and Nanoparticle Interactions with Fibrinogen: The Importance of Aggregation in Nanotoxicology. Nanotoxicology, 2011. 5: 55-65.

303. Polysciences, I. Technical Data Sheet 788: Polybead Microspheres. 2013.

304. Ruano, M.L., I. Garcia-Verdugo, E. Miguel, J. Perez-Gil, and C. Casals, Self-Aggregation of Surfactant Protein A. Biochemistry, 2000. 39: 6529-37.

305. Liu, X., N. Huang, H. Li, Q. Jin, and J. Ji, Surface and Size Effects on Cell Interaction of Gold Nanoparticles with Both Phagocytic and Nonphagocytic Cells. Langmuir, 2013. 29: 9138-48.

306. Jones, L., P.W. Atkins, and P.W.C. Atkins, Chemistry : Molecules, Matter, and Change. 4th ed. / Loretta Jones, Peter Atkins. ed. 2000, New York: W. H. Freeman ; Basingstoke : Macmillan. 1 v. (various pagings).

307. Kendall, M., Zeta Potentials of Amine Functionalised Polystyrene Particles, Z. Mckenzie, Editor. 2011: Birmingham, UK. p. Personal Communication.

308. van der Maaden, K., K. Sliedregt, A. Kros, W. Jiskoot, and J. Bouwstra, Fluorescent Nanoparticle Adhesion Assay: A Novel Method for Surface Pka Determination of Self-Assembled Monolayers on Silicon Surfaces. Langmuir, 2012. 28: 3403-11.

309. Vezenov, D.V., A. Noy, L.F. Rozsnyai, and C.M. Lieber, Force Titrations and Ionization State Sensitive Imaging of Functional Groups in Aqueous Solutions by Chemical Force Microscopy. Journal of the American Chemical Society, 1997. 119: 2006-2015.

310. Chiu, C.C., P.B. Moore, W. Shinoda, and S.O. Nielsen, Size-Dependent Hydrophobic to Hydrophilic Transition for Nanoparticles: A Molecular Dynamics Study. The Journal of chemical physics, 2009. 131: 244706.

311. Caspi, A., O. Yeger, I. Grosheva, A.D. Bershadsky, and M. Elbaum, A New Dimension in Retrograde Flow: Centripetal Movement of Engulfed Particles. Biophysical journal, 2001. 81: 1990-2000.

312. Townsend, J.P., Personal Communication: Gel Electrophoresis of Rfhsp-D, Z.A. McKenzie, Editor. 2011: Southampton.

313. Wangoo, N., C. Raman Suri, and G. Shekhawat, Interaction of Gold Nanoparticles with Protein: A Spectroscopic Study to Monitor Protein Conformational Changes. Applied Physics Letters, 2008: 133104-1-3.

314. Liu, W., J. Rose, S. Plantevin, M. Auffan, J.Y. Bottero, and C. Vidaud, Protein Corona Formation for Nanomaterials and Proteins of a Similar Size: Hard or Soft Corona? Nanoscale, 2013. 5: 1658-68.

315. Wells, M.A., A. Abid, I.M. Kennedy, and A.I. Barakat, Serum Proteins Prevent Aggregation of Fe2o3 and Zno Nanoparticles. Nanotoxicology, 2012. 6: 837-46.

316. Mosmann, T., Rapid Colorimetric Assay for Cellular Growth and Survival: Application to Proliferation and Cytotoxicity Assays. Journal of Immunological Methods, 1983. 65: 55-63.

317. Kroll, A., M.H. Pillukat, D. Hahn, and J. Schnekenburger, Interference of Engineered Nanoparticles with in Vitro Toxicity Assays. Arch Toxicol, 2012. 86: 1123-36.

318. Holder, A.L., R. Goth-Goldstein, D. Lucas, and C.P. Koshland, Particle-Induced Artifacts in the Mtt and Ldh Viability Assays. Chemical research in toxicology, 2012. 25: 1885-92.

319. Guadagnini, R., B. Halamoda Kenzaoui, L. Cartwright, G. Pojana, Z. Magdolenova, D. Bilanicova, M. Saunders, L. Juillerat, A. Marcomini, A. Huk, M. Dusinska, L.M. Fjellsbo, F. Marano, and S. Boland, Toxicity Screenings of Nanomaterials: Challenges Due to Interference with Assay Processes and Components of Classic in Vitro Tests. Nanotoxicology, 2013.

320. Bhattacharjee, S., L.H. de Haan, N.M. Evers, X. Jiang, A.T. Marcelis, H. Zuilhof, I.M. Rietjens, and G.M. Alink, Role of Surface Charge and Oxidative Stress in Cytotoxicity of Organic Monolayer-Coated Silicon Nanoparticles Towards Macrophage Nr8383 Cells. Part Fibre Toxicol, 2010. 7: 25.

321. Ruizendaal, L., S. Bhattacharjee, K. Pournazari, M. Rosso-Vasic, L.H.J. de Haan, G.M. Alink, A.T.M. Marcelis, and H. Zuilhof, Synthesis and Cytotoxicity of Silicon Nanoparticles with Covalently Attached Organic Monolayers. Nanotoxicology, 2009. 3: 339-347.

322. Oh, W.K., S. Kim, M. Choi, C. Kim, Y.S. Jeong, B.R. Cho, J.S. Hahn, and J. Jang, Cellular Uptake, Cytotoxicity, and Innate Immune Response of Silica-Titania Hollow Nanoparticles Based on Size and Surface Functionality. ACS Nano, 2010. 4: 5301-13.

323. Xia, T., M. Kovochich, J. Brant, M. Hotze, J. Sempf, T. Oberley, C. Sioutas, J.I. Yeh, M.R. Wiesner, and A.E. Nel, Comparison of the Abilities of Ambient and Manufactured Nanoparticles to Induce Cellular Toxicity According to an Oxidative Stress Paradigm. Nano Lett, 2006. 6: 1794-807.

324. Kemp, S.J., A.J. Thorley, J. Gorelik, M.J. Seckl, M.J. O'Hare, A. Arcaro, Y. Korchev, P. Goldstraw, and T.D. Tetley, Immortalization of Human Alveolar Epithelial Cells to Investigate Nanoparticle Uptake. American Journal of Respiratory Cell and Molecular Biology, 2008. 39: 591-597.

325. Hartshorn, K.L., M. Collamer, M. Auerbach, J.B. Myers, N. Pavlotsky, and A.I. Tauber, Effects of Influenza-a Virus on Human Neutrophil Calcium-Metabolism. Journal of Immunology, 1988. 141: 1295-1301.

326. Hartshorn, K.L., E.C. Crouch, M.R. White, P. Eggleton, A.I. Tauber, D. Chang, and K. Sastry, Evidence for a Protective Role of Pulmonary Surfactant Protein D (Sp-D) against Influenza a Viruses. The Journal of clinical investigation, 1994. 94: 311-9.

327. Killian, M., Hemagglutination Assay for the Avian Influenza Virus, in Avian Influenza Virus, E. Spackman, Editor. 2008, Humana Press. p. 47-52.

328. Tanya, V.N. and G.R. Scott, Viral Haemagglutination of Glutaraldehyde-Fixed Sheep Erythrocytes. Revue d'elevage et de medecine veterinaire des pays tropicaux, 1994. 47: 283-4.

329. Hoeve, M.A., A.A. Nash, D. Jackson, R.E. Randall, and I. Dransfield, Influenza Virus a Infection of Human Monocyte and Macrophage Subpopulations Reveals Increased Susceptibility Associated with Cell Differentiation. PLoS One, 2012. 7: e29443.

330. Cline, T.D., E.A. Karlsson, B.J. Seufzer, and S. Schultz-Cherry, The Hemagglutinin Protein of Highly Pathogenic H5n1 Influenza Viruses Overcomes an Early Block in the Replication Cycle to Promote Productive Replication in Macrophages. J Virol, 2013. 87: 1411-9.

331. Kilbourne, E.D., Influenza Pandemics of the 20th Century. Emerging Infectious Diseases, 2006. 12: 9-14.

332. Levine, R.J., R.M. Moore, G.D. McLaren, W.F. Barthel, and P.J. Landrigan, Occupational Lead-Poisoning, Animal Deaths, and Environmental Contamination at a Scrap Smelter. American Journal of Public Health, 1976. 66: 548-552.

333. Hartshorn, K., D. Chang, K. Rust, M. White, J. Heuser, and E. Crouch, Interactions of Recombinant Human Pulmonary Surfactant Protein D and Sp-D Multimers with Influenza A. American Journal of Physiology-Lung Cellular and Molecular Physiology, 1996. 271: L753-L762.

334. McCormack, F.X., H.M. Calvert, P.A. Watson, D.L. Smith, R.J. Mason, and D.R. Voelker, The Structure and Function of Surfactant Protein A. Hydroxyproline- and Carbohydrate-Deficient Mutant Proteins. The Journal of biological chemistry, 1994. 269: 5833-41.

335. Berg, J., J. Tymoczko, and L. Stryer, Biochemistry: 5th Edition. 2002, New York, USA: W H Freeman. pp974.

336. Hawgood, S., C. Brown, J. Edmondson, A. Stumbaugh, L. Allen, J. Goerke, H. Clark, and F. Poulain, Pulmonary Collectins Modulate Strain-Specific Influenza a Virus Infection and Host Responses. Journal of Virology, 2004. 78: 8565-8572.

337. Thiel, J.F. and K.O. Smith, Fluorescent Focus Assay of Viruses on Cell Monolayers in Plastic Petri Plates. Proceedings of the Society for Experimental Biology and Medicine. Society for Experimental Biology and Medicine (New York, N.Y.), 1967. 125: 892-5.

338. Bodewes, R., N.J. Nieuwkoop, R.J. Verburgh, R.A. Fouchier, A.D. Osterhaus, and G.F. Rimmelzwaan, Use of Influenza a Viruses Expressing Reporter Genes to Assess the Frequency of Double Infections in Vitro. The Journal of general virology, 2012. 93: 1645-8.

339. Li, D., R. Saito, Y. Suzuki, I. Sato, H. Zaraket, C. Dapat, I.M. Caperig-Dapat, and H. Suzuki, In Vivo and in Vitro Alterations in Influenza a/H3n2 Virus M2 and Hemagglutinin Genes: Effect of Passage in Mdck-Siat1 Cells and Conventional Mdck Cells. J Clin Microbiol, 2009. 47: 466-8.

340. Ottmann, M., M.B. Duchamp, J.S. Casalegno, E. Frobert, V. Moules, O. Ferraris, M. Valette, V. Escuret, and B. Lina, Novel Influenza a(H1n1)

2009 in Vitro Reassortant Viruses with Oseltamivir Resistance. Antiviral therapy, 2010. 15: 721-6.

341. Swain, R.J., S.J. Kemp, P. Goldstraw, T.D. Tetley, and M.M. Stevens, Assessment of Cell Line Models of Primary Human Cells by Raman Spectral Phenotyping. Biophys J, 2010. 98: 1703-11.

342. Mason, R.J. and M.C. Williams, Phospholipid Composition and Ultrastructure of A549 Cells and Other Cultured Pulmonary Epithelial Cells of Presumed Type Ii Cell Origin. Biochimica et biophysica acta, 1980. 617: 36-50.

343. Foster, K.A., C.G. Oster, M.M. Mayer, M.L. Avery, and K.L. Audus, Characterization of the A549 Cell Line as a Type Ii Pulmonary Epithelial Cell Model for Drug Metabolism. Exp Cell Res, 1998. 243: 359-66.

344. Shapiro, D.L., L.L. Nardone, S.A. Rooney, E.K. Motoyama, and J.L. Munoz, Phospholipid Biosynthesis and Secretion by a Cell Line (A549) Which Resembles Type Ii Aleveolar Epithelial Cells. Biochimica et biophysica acta, 1978. 530: 197-207.

345. Tsuchiya, S., M. Yamabe, Y. Yamaguchi, Y. Kobayashi, T. Konno, and K. Tada, Establishment and Characterization of a Human Acute Monocytic Leukemia Cell Line (Thp-1). International journal of cancer. Journal international du cancer, 1980. 26: 171-6.

346. Schwende, H., E. Fitzke, P. Ambs, and P. Dieter, Differences in the State of Differentiation of Thp-1 Cells Induced by Phorbol Ester and 1,25-Dihydroxyvitamin D3. J Leukoc Biol, 1996. 59: 555-61.

347. Daigneault, M., J.A. Preston, H.M. Marriott, M.K. Whyte, and D.H. Dockrell, The Identification of Markers of Macrophage Differentiation in

Pma-Stimulated Thp-1 Cells and Monocyte-Derived Macrophages. PLoS One, 2010. 5: e8668.

348. Traore, K., M.A. Trush, M. George Jr, E.W. Spannhake, W. Anderson, and A. Asseffa, Signal Transduction of Phorbol 12-Myristate 13-Acetate (Pma)-Induced Growth Inhibition of Human Monocytic Leukemia Thp-1 Cells Is Reactive Oxygen Dependent. Leukemia Research, 2005. 29: 863-879.

349. Takashiba, S., T.E. Van Dyke, S. Amar, Y. Murayama, A.W. Soskolne, and L. Shapira, Differentiation of Monocytes to Macrophages Primes Cells for Lipopolysaccharide Stimulation Via Accumulation of Cytoplasmic Nuclear Factor Kappab. Infect Immun, 1999. 67: 5573-8.

350. Park, E.K., H.S. Jung, H.I. Yang, M.C. Yoo, C. Kim, and K.S. Kim, Optimized Thp-1 Differentiation Is Required for the Detection of Responses to Weak Stimuli. Inflammation research : official journal of the European Histamine Research Society ... [et al.], 2007. 56: 45-50.

351. Martin, T.R., S.M. Mongovin, P.S. Tobias, J.C. Mathison, A.M. Moriarty, D.J. Leturcq, and R.J. Ulevitch, The Cd14 Differentiation Antigen Mediates the Development of Endotoxin Responsiveness During Differentiation of Mononuclear Phagocytes. J Leukoc Biol, 1994. 56: 1-9.

352. Tate, M.D., D.L. Pickett, N. van Rooijen, A.G. Brooks, and P.C. Reading, Critical Role of Airway Macrophages in Modulating Disease Severity During Influenza Virus Infection of Mice. J Virol, 2010. 84: 7569-80.

353. Friesenhagen, J., Y. Boergeling, E. Hrincius, S. Ludwig, J. Roth, and D. Viemann, Highly Pathogenic Avian Influenza Viruses Inhibit Effective

Immune Responses of Human Blood-Derived Macrophages. J Leukoc Biol, 2012. 92: 11-20.

354. Yu, W.C., R.W. Chan, J. Wang, E.A. Travanty, J.M. Nicholls, J.S. Peiris, R.J. Mason, and M.C. Chan, Viral Replication and Innate Host Responses in Primary Human Alveolar Epithelial Cells and Alveolar Macrophages Infected with Influenza H5n1 and H1n1 Viruses. J Virol, 2011. 85: 6844-55.

355. Chan, R.W., C.Y. Leung, J.M. Nicholls, J.S. Peiris, and M.C. Chan, Proinflammatory Cytokine Response and Viral Replication in Mouse Bone Marrow Derived Macrophages Infected with Influenza H1n1 and H5n1 Viruses. PLoS One, 2012. 7: e51057.

356. Gonzalez, L., M. Lukamowicz-Rajska, L.C. Thomassen, C.E. Kirschhock, L. Leyns, D. Lison, J.A. Martens, A. Elhajouiji, and M. Kirsch-Volders, Co-Assessment of Cell Cycle and Micronucleus Frequencies Demonstrates the Influence of Serum on the in Vitro Genotoxic Response to Amorphous Monodisperse Silica Nanoparticles of Varying Sizes. Nanotoxicology, 2013.

357. Grabowski, N., H. Hillaireau, J. Vergnaud, L.A. Santiago, S. Kerdine-Romer, M. Pallardy, N. Tsapis, and E. Fattal, Toxicity of Surface-Modified Plga Nanoparticles toward Lung Alveolar Epithelial Cells. Int J Pharm, 2013. 454: 686-94.

358. Wu, H., H. Zhuzhu, X. Li, Z. Li, W. Zheng, T. Chen, B. Yu, and K.H. Wong, Induction of Apoptosis and Cell Cycle Arrest in A549 Human Lung Adenocarcinoma Cells by Surface Encapping Selenium Nanoparticles: An Effect Enhanced by Polysaccharides-Protein Complexes from Polyporus Rhinocerus. J Agric Food Chem, 2013.

359. Hartshorn, K.L., M.R. White, T. Tecle, I. Tornoe, G.L. Sorensen, E.C. Crouch, and U. Holmskov, Reduced Influenza Viral Neutralizing Activity of Natural Human Trimers of Surfactant Protein D. Respir Res, 2007. 8: 9.

360. Jiang, R.D., H. Shen, and Y.J. Piao, The Morphometrical Analysis on the Ultrastructure of A549 Cells. Romanian journal of morphology and embryology = Revue roumaine de morphologie et embryologie, 2010. 51: 663-7.

361. Kalina, M., F.X. McCormack, H. Crowley, D.R. Voelker, and R.J. Mason, Internalization of Surfactant Protein a (Sp-a) into Lamellar Bodies of Rat Alveolar Type Ii Cells in Vitro. The journal of histochemistry and cytochemistry : official journal of the Histochemistry Society, 1993. 41: 57-70.

362. Stevens, P.A., H. Wissel, S. Zastrow, D. Sieger, and K.P. Zimmer, Surfactant Protein a and Lipid Are Internalized Via the Coated-Pit Pathway by Type Ii Pneumocytes. American journal of physiology. Lung cellular and molecular physiology, 2001. 280: L141-51.

363. Schumann, C., S. Schubbe, C. Cavelius, and A. Kraegeloh, A Correlative Approach at Characterizing Nanoparticle Mobility and Interactions after Cellular Uptake. Journal of biophotonics, 2012. 5: 117-27.

364. Swain, R.J., S.J. Kemp, P. Goldstraw, T.D. Tetley, and M.M. Stevens, Spectral Monitoring of Surfactant Clearance During Alveolar Epithelial Type Ii Cell Differentiation. Biophysical Journal, 2008. 95: 5978-5987.

365. He, C., Y. Hu, L. Yin, C. Tang, and C. Yin, Effects of Particle Size and Surface Charge on Cellular Uptake and Biodistribution of Polymeric Nanoparticles. Biomaterials, 2010. 31: 3657-3666.

366. Vijayakumar, S. and S. Ganesan, Gold Nanoparticles as an Hiv Entry Inhibitor. Current HIV research, 2012. 10: 643-6.

367. Kosmider, B., E.M. Messier, W.J. Janssen, P. Nahreini, J. Wang, K.L. Hartshorn, and R.J. Mason, Nrf2 Protects Human Alveolar Epithelial Cells against Injury Induced by Influenza a Virus. Respir Res, 2012. 13: 43.

368. Geiler, J., M. Michaelis, P. Sithisarn, and J. Cinatl, Jr., Comparison of Pro-Inflammatory Cytokine Expression and Cellular Signal Transduction in Human Macrophages Infected with Different Influenza a Viruses. Medical microbiology and immunology, 2011. 200: 53-60.

369. Lowy, R.J. and D.S. Dimitrov, Characterization of Influenza Virus-Induced Death of J774.1 Macrophages. Experimental cell research, 1997. 234: 249-58.

370. Nunes-Correia, I., A. Eulalio, S. Nir, and M.C.P. De Lima, Caveolae as an Additional Route for Influenza Virus Endocytosis in Mdck Cells. Cellular & Molecular Biology Letters, 2004. 9: 47-60.

371. de Vries, E., D.M. Tscherne, M.J. Wienholts, V. Cobos-Jimenez, F. Scholte, A. Garcia-Sastre, P.J. Rottier, and C.A. de Haan, Dissection of the Influenza a Virus Endocytic Routes Reveals Macropinocytosis as an Alternative Entry Pathway. PLoS pathogens, 2011. 7: e1001329.

372. Bawa, R., S.Y. Fung, A. Shiozaki, H. Yang, G. Zheng, S. Keshavjee, and M. Liu, Self-Assembling Peptide-Based Nanoparticles Enhance Cellular

Delivery of the Hydrophobic Anticancer Drug Ellipticine through Caveolae-Dependent Endocytosis. Nanomedicine, 2012. 8: 647-54.

373. Ekkapongpisit, M., A. Giovia, C. Follo, G. Caputo, and C. Isidoro, Biocompatibility, Endocytosis, and Intracellular Trafficking of Mesoporous Silica and Polystyrene Nanoparticles in Ovarian Cancer Cells: Effects of Size and Surface Charge Groups. International journal of nanomedicine, 2012. 7: 4147-58.

374. Kim, J.S., T.J. Yoon, K.N. Yu, M.S. Noh, M. Woo, B.G. Kim, K.H. Lee, B.H. Sohn, S.B. Park, J.K. Lee, and M.H. Cho, Cellular Uptake of Magnetic Nanoparticle Is Mediated through Energy-Dependent Endocytosis in A549 Cells. Journal of veterinary science, 2006. 7: 321-6.

375. Stearns, R.C., J.D. Paulauskis, and J.J. Godleski, Endocytosis of Ultrafine Particles by A549 Cells. Am. J. Respir. Cell Mol. Biol., 2001. 24: 108-115.

376. dos Santos, T., J. Varela, I. Lynch, A. Salvati, and K.A. Dawson, Effects of Transport Inhibitors on the Cellular Uptake of Carboxylated Polystyrene Nanoparticles in Different Cell Lines. PLoS One, 2011. 6: e24438.

377. Pacheco, P., D. White, and T. Sulchek, Effects of Microparticle Size and Fc Density on Macrophage Phagocytosis. PLoS One, 2013. 8: e60989.

378. Li, F., A. Zhu, X. Song, L. Ji, and J. Wang, The Internalization of Fluorescence-Labeled Pla Nanoparticles by Macrophages. Int J Pharm, 2013. 453: 506-13.

379. Gonzalez, O., R.L. Smith, and S.B. Goodman, Effect of Size, Concentration, Surface Area, and Volume of Polymethylmethacrylate Particles on Human Macrophages in Vitro. J Biomed Mater Res, 1996. 30: 463-73.

380. Cannon, G.J. and J.A. Swanson, The Macrophage Capacity for Phagocytosis. J Cell Sci, 1992. 101 (Pt 4): 907-13.

381. Champion, J.A., A. Walker, and S. Mitragotri, Role of Particle Size in Phagocytosis of Polymeric Microspheres. Pharm Res, 2008. 25: 1815-21.

382. Parton, R.G., Caveolae and Caveolins. Current Opinion in Cell Biology, 1996. 8: 542-548.

383. Campbell, L., A.J. Hollins, A. Al-Eid, G.R. Newman, C. von Ruhland, and M. Gumbleton, Caveolin-1 Expression and Caveolae Biogenesis During Cell Transdifferentiation in Lung Alveolar Epithelial Primary Cultures. Biochemical and Biophysical Research Communications, 1999. 262: 744-751.

384. Mo, Y. and L.Y. Lim, Mechanistic Study of the Uptake of Wheat Germ Agglutinin-Conjugated Plga Nanoparticles by A549 Cells. J Pharm Sci, 2004. 93: 20-8.

385. Perumal, O.P., R. Inapagolla, S. Kannan, and R.M. Kannan, The Effect of Surface Functionality on Cellular Trafficking of Dendrimers. Biomaterials, 2008. 29: 3469-76.

386. Rejman, J., V. Oberle, I.S. Zuhorn, and D. Hoekstra, Size-Dependent Internalization of Particles Via the Pathways of Clathrin- and Caveolae-Mediated Endocytosis. The Biochemical journal, 2004. 377: 159-69.

387. McAuley, J.L., M.D. Tate, C.J. MacKenzie-Kludas, A. Pinar, W. Zeng, A. Stutz, E. Latz, L.E. Brown, and A. Mansell, Activation of the Nlrp3 Inflammasome by Iav Virulence Protein Pb1-F2 Contributes to Severe Pathophysiology and Disease. PLoS pathogens, 2013. 9: e1003392.

388. Cilloniz, C., K. Shinya, X. Peng, M.J. Korth, S.C. Proll, L.D. Aicher, V.S. Carter, J.H. Chang, D. Kobasa, F. Feldmann, J.E. Strong, H. Feldmann, Y. Kawaoka, and M.G. Katze, Lethal Influenza Virus Infection in Macaques Is Associated with Early Dysregulation of Inflammatory Related Genes. PLoS pathogens, 2009. 5: e1000604.

389. Yazdi, A.S., G. Guarda, N. Riteau, S.K. Drexler, A. Tardivel, I. Couillin, and J. Tschopp, Nanoparticles Activate the Nlr Pyrin Domain Containing 3 (Nlrp3) Inflammasome and Cause Pulmonary Inflammation through Release of Il-1alpha and Il-1beta. Proc Natl Acad Sci U S A, 2010. 107: 19449-54.

390. Frohlich, E., C. Meindl, E. Roblegg, A. Griesbacher, and T.R. Pieber, Cytotoxity of Nanoparticles Is Influenced by Size, Proliferation and Embryonic Origin of the Cells Used for Testing. Nanotoxicology, 2012. 6: 424-39.

391. Roblegg, E., E. Frohlich, C. Meindl, B. Teubl, M. Zaversky, and A. Zimmer, Evaluation of a Physiological in Vitro System to Study the Transport of Nanoparticles through the Buccal Mucosa. Nanotoxicology, 2012. 6: 399-413.

392. Wang, X.Z., Y. Yang, R.F. Li, C. McGuinnes, J. Adamson, I.L. Megson, and K. Donaldson, Principal Component and Causal Analysis of Structural and Acute in Vitro Toxicity Data for Nanoparticles. Nanotoxicology, 2013.

393. Bexiga, M.G., J.A. Varela, F. Wang, F. Fenaroli, A. Salvati, I. Lynch, J.C. Simpson, and K.A. Dawson, Cationic Nanoparticles Induce Caspase 3-, 7- and 9-Mediated Cytotoxicity in a Human Astrocytoma Cell Line. Nanotoxicology, 2011. 5: 557-67.

394. Lei, M., H. Jiao, T. Liu, L. Du, Y. Cheng, D. Zhang, Y. Hao, C. Man, and F. Wang, Sirna Targeting Mcd14 Inhibits Tnf-Alpha, Mip-2, and Il-6 Secretion and No Production from Lps-Induced Raw264.7 Cells. Applied Microbiology and Biotechnology, 2011. 92: 115-124.

395. Hartshorn, K.L., E. Crouch, M.R. White, M.L. Colamussi, A. Kakkanatt, B. Tauber, V. Shepherd, and K.N. Sastry, Pulmonary Surfactant Proteins a and D Enhance Neutrophil Uptake of Bacteria. The American journal of physiology, 1998. 274: L958-69.

396. Yamazoe, M., C. Nishitani, M. Takahashi, T. Katoh, S. Ariki, T. Shimizu, H. Mitsuzawa, K. Sawada, D.R. Voelker, H. Takahashi, and Y. Kuroki, Pulmonary Surfactant Protein D Inhibits Lipopolysaccharide (Lps)-Induced Inflammatory Cell Responses by Altering Lps Binding to Its Receptors. Journal of Biological Chemistry, 2008. 283: 35878-35888.

397. Zelikoff, J.T., K.R. Schermerhorn, K.J. Fang, M.D. Cohen, and R.B. Schlesinger, A Role for Associated Transition Metals in the Immunotoxicity of Inhaled Ambient Particulate Matter. Environ. Health Perspect., 2002. 110: 871-875.

398. Lundborg, M., S.E. Dahlen, U. Johard, P. Gerde, C. Jarstrand, P. Camner, and L. Lastbom, Aggregates of Ultrafine Particles Impair Phagocytosis of Microorganisms by Human Alveolar Macrophages. Environmental research, 2006. 100: 197-204.

399. Lundborg, M., U. Johard, L. Lastbom, P. Gerde, and P. Camner, Human Alveolar Macrophage Phagocytic Function Is Impaired by Aggregates of Ultrafine Carbon Particles. Environmental research, 2001. 86: 244-53.

400. Renwick, L.C., K. Donaldson, and A. Clouter, Impairment of Alveolar Macrophage Phagocytosis by Ultrafine Particles. Toxicol Appl Pharmacol, 2001. 172: 119-27.

401. Pikaar, J.C., W.F. Voorhout, L.M. van Golde, J. Verhoef, J.A. Van Strijp, and J.F. van Iwaarden, Opsonic Activities of Surfactant Proteins a and D in Phagocytosis of Gram-Negative Bacteria by Alveolar Macrophages. Journal of Infectious Diseases, 1995. 172: 481-9.

402. Wang, H., J. Head, P. Kosma, H. Brade, S. Muller-Loennies, S. Sheikh, B. McDonald, K. Smith, T. Cafarella, B. Seaton, and E. Crouch, Recognition of Heptoses and the Inner Core of Bacterial Lipopolysaccharides by Surfactant Protein D. Biochemistry, 2008. 47: 710-20.

403. Eda, S., Y. Suzuki, T. Kawai, K. Ohtani, T. Kase, Y. Fujinaga, T. Sakamoto, T. Kurimura, and N. Wakamiya, Structure of a Truncated Human Surfactant Protein D Is Less Effective in Agglutinating Bacteria Than the Native Structure and Fails to Inhibit Haemagglutination by Influenza a Virus. The Biochemical journal, 1997. 323 (Pt 2): 393-9.

404. Jansky, L., P. Reymanova, and J. Kopecky, Dynamics of Cytokine Production in Human Peripheral Blood Mononuclear Cells Stimulated by Lps or Infected by Borrelia. Physiological research / Academia Scientiarum Bohemoslovaca, 2003. 52: 593-8.

405. Kishore, U., J.Y. Wang, H.J. Hoppe, and K.B. Reid, The Alpha-Helical Neck Region of Human Lung Surfactant Protein D Is Essential for the Binding of the Carbohydrate Recognition Domains to Lipopolysaccharides and Phospholipids. The Biochemical journal, 1996. 318 (Pt 2): 505-11.

406. Mullen, A., C.E. Loscher, and H.M. Roche, Anti-Inflammatory Effects of Epa and Dha Are Dependent Upon Time and Dose-Response Elements Associated with Lps Stimulation in Thp-1-Derived Macrophages. The Journal of nutritional biochemistry, 2010. 21: 444-50.

407. Garrelds, I.M., P.T. van Hal, R.C. Haakmat, H.C. Hoogsteden, P.R. Saxena, and F.J. Zijlstra, Time Dependent Production of Cytokines and Eicosanoids by Human Monocytic Leukaemia U937 Cells; Effects of Glucocorticosteroids. Mediators of inflammation, 1999. 8: 229-35.

408. Ohki, K., F. Amano, S. Yamamoto, and O. Kohashi, Suppressive Effects of Serum on the Lps-Induced Production of Nitric Oxide and Tnf-Alpha by a Macrophage-Like Cell Line, Wehi-3, Are Dependent on the Structure of Polysaccharide Chains in Lps. Immunology and cell biology, 1999. 77: 143-52.

409. Wang, M., Y. Zhang, Y. Chen, L. Zhang, X. Lu, and Z. Chen, Mannan-Binding Lectin Regulates Dendritic Cell Maturation and Cytokine Production Induced by Lipopolysaccharide. BMC immunology, 2011. 12: 1.

410. Wright, J.R., D.F. Zlogar, J.C. Taylor, T.M. Zlogar, and C.I. Restrepo, Effects of Endotoxin on Surfactant Protein a and D Stimulation of No Production by Alveolar Macrophages. The American journal of physiology, 1999. 276: L650-8.

411. Maker, P.D. and R.W. Terhune, Study of Optical Effects Due to an Induced Polarization Third Order in the Electric Field Strength. Physical Review, 1965. 137: A801-A818.

412. Duncan, M.D., J. Reintjes, and T.J. Manuccia, Scanning Coherent Anti-Stokes Raman Microscope. Optics letters, 1982. 7: 350-2.

413. Zumbusch, A., G.R. Holtom, and X.S. Xie, Three-Dimensional Vibrational Imaging by Coherent Anti-Stokes Raman Scattering. Physical Review Letters, 1999. 82: 4142-4145.

414. Wu, Y.M., H.C. Chen, W.T. Chang, J.W. Jhan, H.L. Lin, and I. Liau, Quantitative Assessment of Hepatic Fat of Intact Liver Tissues with Coherent Anti-Stokes Raman Scattering Microscopy. Analytical chemistry, 2009. 81: 1496-504.

415. Kim, S.H., E.S. Lee, J.Y. Lee, E.S. Lee, B.S. Lee, J.E. Park, and D.W. Moon, Multiplex Coherent Anti-Stokes Raman Spectroscopy Images Intact Atheromatous Lesions and Concomitantly Identifies Distinct Chemical Profiles of Atherosclerotic Lipids. Circ Res, 2010. 106: 1332-41.

416. Le, T.T., I.M. Langohr, M.J. Locker, M. Sturek, and J.X. Cheng, Label-Free Molecular Imaging of Atherosclerotic Lesions Using Multimodal Nonlinear Optical Microscopy. Journal of biomedical optics, 2007. 12: 054007.

417. Mitra, R., O. Chao, Y. Urasaki, O.B. Goodman, and T.T. Le, Detection of Lipid-Rich Prostate Circulating Tumour Cells with Coherent Anti-Stokes Raman Scattering Microscopy. BMC cancer, 2012. 12: 540.

418. Yang, Y., F. Li, L. Gao, Z. Wang, M.J. Thrall, S.S. Shen, K.K. Wong, and S.T. Wong, Differential Diagnosis of Breast Cancer Using Quantitative, Label-Free and Molecular Vibrational Imaging. Biomedical optics express, 2011. 2: 2160-74.

419. Gao, L., H. Zhou, M.J. Thrall, F. Li, Y. Yang, Z. Wang, P. Luo, K.K. Wong, G.S. Palapattu, and S.T. Wong, Label-Free High-Resolution Imaging of

Prostate Glands and Cavernous Nerves Using Coherent Anti-Stokes Raman Scattering Microscopy. Biomedical optics express, 2011. 2: 915-26.

420. Moger, J., B.D. Johnston, and C.R. Tyler, Imaging Metal Oxide Nanoparticles in Biological Structures with Cars Microscopy. Optics express, 2008. 16: 3408-19.

421. Tong, L., Y. Lu, R.J. Lee, and J.X. Cheng, Imaging Receptor-Mediated Endocytosis with a Polymeric Nanoparticle-Based Coherent Anti-Stokes Raman Scattering Probe. The journal of physical chemistry. B, 2007. 111: 9980-5.

422. Chen, Y.S., Y.C. Hung, L.W. Lin, I. Liau, M.Y. Hong, and G.S. Huang, Size-Dependent Impairment of Cognition in Mice Caused by the Injection of Gold Nanoparticles. Nanotechnology, 2010. 21: 485102.

423. Greene, K.E., J.R. Wright, K.P. Steinberg, J.T. Ruzinski, E. Caldwell, W.B. Wong, W. Hull, J.A. Whitsett, T. Akino, Y. Kuroki, H. Nagae, L.D. Hudson, and T.R. Martin, Serial Changes in Surfactant-Associated Proteins in Lung and Serum before and after Onset of Ards. Am J Respir Crit Care Med, 1999. 160: 1843-50.

424. Poelma, D.L., L.J. Zimmermann, H.H. Scholten, B. Lachmann, and J.F. van Iwaarden, In Vivo and in Vitro Uptake of Surfactant Lipids by Alveolar Type Ii Cells and Macrophages. American journal of physiology. Lung cellular and molecular physiology, 2002. 283: L648-54.

425. Dizdar, E.A., F.N. Sari, C. Aydemir, S.S. Oguz, O. Erdeve, N. Uras, and U. Dilmen, A Randomized, Controlled Trial of Poractant Alfa Versus Beractant in the Treatment of Preterm Infants with Respiratory Distress Syndrome. American journal of perinatology, 2012. 29: 95-100.

426. Wright, J.R. and D.C. Youmans, Degradation of Surfactant Lipids and Surfactant Protein a by Alveolar Macrophages in Vitro. The American journal of physiology, 1995. 268: L772-80.

427. Kerr, M.H. and J.Y. Paton, Surfactant Protein Levels in Severe Respiratory Syncytial Virus Infection. American Journal of Respiratory and Critical Care Medicine, 1999. 159: 1115-1118.

428. Madsen, J. and S. Mahajan, Lipid Accumulation in the Alveolar Macrophages of Sp-D Deficient Mice (Unpublished Data). 2013.

429. Stidsen, J.V., R. Khorooshi, M.K. Rahbek, K.L. Kirketerp-Moller, P.B. Hansen, P. Bie, K. Kejling, S. Mandrup, S. Hawgood, O. Nielsen, C.H. Nielsen, T. Owens, U. Holmskov, and G.L. Sorensen, Surfactant Protein D Deficiency in Mice Is Associated with Hyperphagia, Altered Fat Deposition, Insulin Resistance, and Increased Basal Endotoxemia. PLoS One, 2012. 7: e35066.

430. Yoshida, M. and J.A. Whitsett, Alveolar Macrophages and Emphysema in Surfactant Protein-D-Deficient Mice. Respirology, 2006. 11 Suppl: S37-40.

431. Knudsen, L., K. Wucherpfennig, R.M. MacKay, P. Townsend, C. Muhlfeld, J. Richter, S. Hawgood, K. Reid, H. Clark, and M. Ochs, A Recombinant Fragment of Human Surfactant Protein D Lacking the Short Collagen-Like Stalk Fails to Correct Morphological Alterations in Lungs of Sp-D Deficient Mice. Anatomical Record-Advances in Integrative Anatomy and Evolutionary Biology, 2009. 292: 183-189.

432. Pratten, M.K. and J.B. Lloyd, Pinocytosis and Phagocytosis: The Effect of Size of a Particulate Substrate on Its Mode of Capture by Rat Peritoneal

Macrophages Cultured in Vitro. Biochimica et biophysica acta, 1986. 881: 307-13.

433. Dutta, P.K., J.R. Nestor, and T.G. Spiro, Resonance Coherent Anti-Stokes Raman Scattering Spectra of Fluorescent Biological Chromophores: Vibrational Evidence for Hydrogen Bonding of Flavin to Glucose Oxidase and for Rapid Solvent Exchange. Proc Natl Acad Sci U S A, 1977. 74: 4146-9.

434. Johnston, B.D., T.M. Scown, J. Moger, S.A. Cumberland, M. Baalousha, K. Linge, R. van Aerle, K. Jarvis, J.R. Lead, and C.R. Tyler, Bioavailability of Nanoscale Metal Oxides Tio(2), Ceo(2), and Zno to Fish. Environmental science & technology, 2010. 44: 1144-51.